



**HAL**  
open science

# Role of selective autophagy receptors in MHC-II-restricted antigen presentation and their hijacking by viruses to escape T cell immunity

Gabriela Sarango

► **To cite this version:**

Gabriela Sarango. Role of selective autophagy receptors in MHC-II-restricted antigen presentation and their hijacking by viruses to escape T cell immunity. Adaptive immunology. Université Paris-Saclay, 2023. English. NNT : 2023UPASQ006 . tel-04370241

**HAL Id: tel-04370241**

**<https://theses.hal.science/tel-04370241>**

Submitted on 3 Jan 2024

**HAL** is a multi-disciplinary open access archive for the deposit and dissemination of scientific research documents, whether they are published or not. The documents may come from teaching and research institutions in France or abroad, or from public or private research centers.

L'archive ouverte pluridisciplinaire **HAL**, est destinée au dépôt et à la diffusion de documents scientifiques de niveau recherche, publiés ou non, émanant des établissements d'enseignement et de recherche français ou étrangers, des laboratoires publics ou privés.

# Role of selective autophagy receptors in MHC-II-restricted antigen presentation and their hijacking by viruses to escape T cell immunity

*Rôle des récepteurs de l'autophagie sélective dans la présentation des antigènes par les molécules du CMH-II, et leur détournement par les virus pour échapper à l'immunité médiée par les cellules T*

## Thèse de doctorat de l'université Paris-Saclay

École doctorale n°569, innovation thérapeutique : du fondamental à l'appliqué (ITFA)  
Spécialité de doctorat : Microbiologie  
Graduate School : Sciences de la vie et de la santé. Référent : Faculté de pharmacie

Thèse préparée dans l'unité de recherche  
**Institut de Biologie Intégrative de la cellule** (Université Paris-Saclay, CEA, CNRS),  
sous la direction d'**Arnaud Moris**, DR

Thèse soutenue à Gif-sur-Yvette, le 16 mars 2023, par

**Gabriela SARANGO**

## Composition du Jury

Membres du jury avec voix délibérative

<b>Géraldine SCHLECHT-LOUF</b> Professeure, Université Paris Saclay	Présidente
<b>Lucile ESPERT</b> CR, Université de Montpellier, CNRS	Rapportrice et Examinatrice
<b>Jean-François FONTENEAU</b> CR, Inserm	Rapporteur et Examinateur
<b>Lisa CHAKRABARTI</b> DR, Institut Pasteur	Examinatrice

**Titre :** Rôle des récepteurs de l'autophagie sélective dans la présentation des antigènes par les molécules du CMH-II, et leur détournement par les virus pour échapper à l'immunité médiée par les cellules T.

**Mots clés :** Autophagie, virus, antigènes, CMH-II, lymphocytes, CD4.

**Résumé :** Les lymphocytes T CD4+ jouent un rôle important dans l'immunité antivirale. Ils reconnaissent des peptides présentés par les molécules du complexe majeur d'histocompatibilité de classe II (CMH-II) dans les cellules présentatrices d'antigènes (CPA).

L'autophagie participe à la dégradation d'antigènes cellulaires et est souvent ciblée par les virus. Ici, nous étudions le rôle des récepteurs de l'autophagie sélective (RAS) dans la présentation d'antigènes viraux par le CMH-II. Nous montrons que TAX1BP1 impacte la présentation de peptides par le CMH-II aux lymphocytes T CD4+.

En utilisant la protéine Tax du virus T-lymphotrope humain de type 1 (HTLV-1), nous étudions le détournement des RAS pour échapper à l'immunité antivirale. Nous montrons que le recrutement via l'ubiquitination d'OPTN par Tax est nécessaire pour inhiber la présentation d'un antigène viral par le CMH-II. Dans l'ensemble, nous montrons que TAX1BP1 joue un rôle important dans la présentation d'antigènes par le CMH-II et proposons OPTN comme une cible de HTLV-1 pour échapper à la réponse T.

**Title :** Role of selective autophagy receptors in MHC-II-restricted antigen presentation and their hijacking by viruses to escape T cell immunity.

**Keywords :** Autophagy, viruses, antigens, MHC-II, lymphocytes, CD4.

**Abstract :** CD4+ T cells play an important role in antiviral immunity. They are activated by virus-derived peptides presented by the major histocompatibility complex class-II (MHC-II) molecules in antigen presenting cells (APC). Autophagy contributes to the processing of cellular antigens and is often targeted by viruses. We first asked whether selective autophagy receptors (SARs) play a role in MHC-II viral antigen presentation. We show that TAX1BP1 strongly influences the loading and presentation of peptides by MHC-II molecules to

CD4+T cells. We then used Human T-cell leukemia virus type 1 (HTLV-1) Tax protein, known to recruit TAX1BP1, OPTN and p62 to ask whether viruses target SARs to escape antiviral immunity. We show that the recruitment of OPTN by Tax is required to inhibit MHC-II-restricted viral antigen presentation and CD4+T cell activation. Altogether, we show that TAX1BP1 plays an important role in MHC-II antigen presentation and put forward OPTN as an HTLV-1 target to escape T cell immunity.

## Acknowledgements

I would like to thank the members of the jury for evaluating my work as well as for their advice to improve this manuscript.

A special thanks to Dr. Chloé Journo for her goodwill all along our collaboration during my thesis and for accepting the invitation to my defense.

I would also like to thank Dr. Bénédicte Manoury for receiving me in her laboratory. It was a very rewarding experience, in which I learned a lot.

I thank my thesis director for the opportunity to join the lab, to attend great scientific conferences over the years and for his patience in correcting this manuscript.

I thank of course Audrey for introducing me to the "Herpes cluster" as a young M2 student, I would not have imagined back then that I would spend 4 years in the team, with everything that that entailed. This leads me to thank my lab colleagues for very fun, piggy and intense years (we did move twice) during which I learned more than just science. A very special thanks to Marion, Eva and Guillaume for the great TPs in which we taught students to use their brains and so much more; and to Anita for all the existential talks in the L2. I am also beyond grateful for the time spent with Cecilia in the lab, for her mentorship and good spirits; I would need an entire manuscript to transcribe all our anecdotes and am excited to begin a new scientific adventure together.

To the I2BC coupains (Lisa, Adri, Emilie, Maxime, Benjamin, Benoit, Kenza and so many others), a big thanks for all the fun aperos with pétanque and loup-garou.

I also thank my friends, from school and university who are always there unconditionally for drinks, bowling, rugby or just to talk (la chicas guapas, Sylvio, Sebo, Julito, Estella, Marie, Antho, Stef, Céline, Emile) even when we are miles apart.

I thank Tim for his patience, kindness and support during all these years, you have helped me live through this ordeal. A special thanks to the Ray family and their kind support as well.

I will finish of course, by thanking my family for all of their support. To my parents who made coming to France possible and always encouraged me to accomplish my goals. I also thank them for all the travelling, which definitely made the thesis more bearable. To my sisters and their spouses for all the talks, the fun and the traveling as well. To my uncles in Hawai for their amazing support and advice, can't wait to fly there again, I will hopefully take the right flight this time. Finally, to my uncle and aunt in Paris, who have helped me in so many ways, I will be forever grateful.







## Table of content

<b>Table of figures</b> .....	9
<b>Acronyms</b> .....	11
<b>Overview</b> .....	12
<b>Introduction</b> .....	13
<b>I. Selective autophagy receptors</b> .....	13
A. Characteristics of selective autophagy receptors (SARs) .....	14
1. p62/SQSTM1 and the identification of the LC3-Interacting Region (LIR) .....	14
2. Next to BRCA1 gene (NBR1) protein.....	15
3. CALCOCO family proteins: CALCOCO1, NDP52 and TAX1BP1.....	16
4. Optineurin (OPTN) .....	18
5. Toll-like interacting protein (Tollip) .....	19
B. Pathways of selective autophagy.....	19
1. Aggrephagy.....	19
2. Mitophagy.....	20
3. Xenophagy.....	21
C. Cargo-SAR-mediated recruitment of the autophagy machinery.....	23
1. The autophagy pathway.....	23
a) <i>Initiation</i> .....	24
b) <i>Elongation</i> .....	24
c) <i>Maturation</i> .....	25
2. How SARs recruit the autophagy core machinery.....	26
D. Other roles of SARs in the cell.....	28
1. Role of SARs in the internalization of transferrin receptor.....	28
2. Role of SARs in vesicle trafficking and maturation.....	28
3. Role of SARs in the NF- $\kappa$ B signaling pathway.....	29
<b>II. MHC-restricted antigen presentation pathways</b> .....	32
A. The human Major Histocompatibility Complex.....	32
1. Major Histocompatibility Complex Class I (MHC-I) .....	33
2. Major Histocompatibility Complex Class II (MHC-II) .....	34
B. Antigen presentation by MHC-I molecules.....	35
1. Endogenous antigen presentation by MHC-I molecules.....	35
a) <i>The role of the proteasome</i> .....	35
b) <i>The proteasome substrates</i> .....	37
c) <i>Peptide transport to the ER and loading on MHC-I molecules</i> .....	37
2. Exogenous antigen presentation by MHC-I molecules.....	39
a) <i>Cytosolic pathway</i> .....	39
b) <i>Vacuolar pathway</i> .....	39
C. Antigen presentation by MHC-II molecules.....	40
1. Expression of MHC-II molecules and control by CIITA.....	40
2. MHC-II antigen presentation route.....	40



a) ER assembly of MHC-II molecules.....	40
b) Traffic of $\alpha\beta$ -li complexes.....	42
c) Antigen loading in the MIIC.....	43
d) Traffic of MHC-II $\alpha\beta$ -peptide complexes to the cell membrane.....	45
3. What becomes of surface MHC-II molecules.....	48
4. Regulation of li and antigen processing.....	50
a) Lysosomal cathepsins.....	50
b) Regulation of processing activity.....	51
D. Pathways of antigen delivery to the MIIC.....	52
1. Endocytosis.....	52
2. Phagocytosis.....	52
3. Macropinocytosis.....	53
4. MHC-II recycling.....	53
5. Role of autophagosomes.....	53
6. The role of LC3 associated phagocytosis (LAP) .....	54
7. The role of chaperone-mediated autophagy (CMA) .....	56
8. Bona fide cytosolic processing.....	56
9. Regulation by Heat Shock Protein 90 (Hsp90) .....	56
<b>III. Viruses and immunity: interaction with selective autophagy receptors</b>	
<b>and the MHC-II pathway.....</b>	<b>58</b>
A. Viral manipulation of MHC-II-restricted antigen presentation.....	58
1. Targeting CIITA function.....	58
2. Targeting invariant chain (li) function.....	60
3. Targeting MHC-II molecules.....	61
4. Targeting degradation pathways.....	62
5. TCR recognition inhibition.....	63
B. Viral interaction with selective autophagy receptors.....	64
1. Exploiting SAR function to promote viral replication.....	64
2. Inhibiting SAR function to escape cell intrinsic antiviral immunity.....	65
3. SAR targeting by viruses to modulate innate immune signaling.....	66
C. Human T cell leukemia virus type 1.....	67
1. HTLV-1 viral cycle.....	67
2. Tax modulation of the NF- $\kappa$ b signaling pathway.....	70
3. Anti-HTLV-1 T cell responses.....	73
4. Tax modulation of autophagy.....	74
<b>Scientific context and thesis objectives.....</b>	<b>77</b>
<b>Results project 1.....</b>	<b>78</b>
<b>Results project 2.....</b>	<b>106</b>
<b>Discussion and perspectives.....</b>	<b>167</b>
<b>References.....</b>	<b>152</b>
<b>Appendix.....</b>	<b>188</b>

## Table of figures

### Introduction

Figure 1: Structure of p62/SQSTM1.....	15
Figure 2: Structure of NBR1.....	16
Figure 3: Structure of CALCOCO family proteins.....	17
Figure 4: Structure of Optineurin.....	18
Figure 5: Figure 5. Structure of Toll-like interacting protein.....	19
Figure 6: PINK and Parkin mediate mitophagy.....	21
Figure 7: NDP52-mediated xenophagy.....	22
Figure 8: Steps of autophagosome formation.....	25
Figure 9: SARs promote autophagosome maturation.....	26
Figure 10: SARs promote endosome maturation.....	29
Figure 11: Schematic representation of the role of SARs in the NF- $\kappa$ B signaling pathway .....	30
Figure 12: Schematic representation of the MHC loci on chromosome 6.....	32
Figure 13: Schematic representation of the structure of MHC-I molecules.....	33
Figure 14: Schematic representation of the MHC-II peptide-binding groove.....	35
Figure 15: The constitutive proteasome and the immunoproteasome. ....	36
Figure 16: The MHC-I antigen presentation pathway.....	38
Figure 17: The different domains on the Ii invariant chain.....	41
Figure 18: The MHC-II antigen presentation pathway.....	42
Figure 19: The processing of Ii by lysosomal proteases .....	44
Figure 20: Tubulation of multivesicular MIICs during DC maturation.....	46
Figure 21: Transport of $\alpha\beta$ -peptide complexes to the cell membrane.....	47
Figure 22: The role of ubiquitination in MHC-II degradation.....	49
Figure 23: LC3-associated phagocytosis improves MHC-II-restricted antigen presentation .....	55
Figure 24: Induction of MHC class II gene expression by interferon- $\gamma$ .....	59
Figure 25: Viruses target the MHC-II antigen presentation pathway.....	64
Figure 26: 25 Viral strategies to target SARs.....	65
Figure 27: Major steps of HTLV-1 replication cycle.....	68

Figure 28: Structure of the HTLV-1 proviral genome and gene product key functions.....69

Figure 29: Domains of Tax for interactions and post-translational modifications.....70

Figure 30: Tax-induced relocalization.....72

Figure 31: Tax-induced autophagy modulation.....75

## **Discussion and Perspectives**

Figure 32: Model of the impact of TAX1BP1 silencing on MHC-II endogenous antigen presentation..160

## Acronyms

APC: Antigen presenting cell	MIIC: MHC-II loading compartment
ATG: Autophagy related genes	MTOC: Microtubule organizing center
BCR: B cell receptor	mTOR: Mammalian target of rapamycin
CD: Cluster of differentiation	NBR1: Next to BRCA1 gene
CMA: Chaperon mediated autophagy	NF- $\kappa$ B: Nuclear factor kappa light chain enhancer
CIITA: Class II Major Histocompatibility Complex Transactivator	OPTN: Optineurin
DC: Dendritic cell	PE: Phosphatidylethanolamine
EBV: Epstein-Barr virus	PI3K: phosphatidylinositol 3-kinase
ER: Endoplasmic reticulum	PBMC: Peripheral blood mononuclear cell
HA: Hemagglutinin	RSV: Respiratory syncytial virus
HLA: Human leucocyte antigen	SAR: Selective autophagy receptor
HTLV: Human T-cell lymphotropic virus	SCV: Salmonella-containing vacuole
HCMV: Human Cytomegalovirus	TAX1BP1: Tax-1 binding protein
HIV: Human immunodeficiency virus	Tollip: Toll-like receptor
HSV: Herpes Simplex virus	TCR: T cell receptor
IFN: Interferon	TM: Transmembrane domain
IL: Interleukin	TLR: Toll like receptor
ILV: Intra-luminal vesicle	Ub: Ubiquitin
IRF3: Interferon regulatory factor 3	UBA: Ubiquitin associated domain
KSHV: Kaposi Sarcoma-associated Herpesvirus	UPS: Ubiquitin proteasome system
LIR: LC3-interacting region	ZF: Zinc finger domain
LAP: LC3-associated phagocytosis	ULK: Unc-51-like kinase
LPS: Lipopolysaccharide	UBD: Ubiquitin binding domain
MEV: Measles virus	WB: Western Blot
MHC: Major Histocompatibility Complex	

## Overview

CD4<sup>+</sup>T cells play a key role in the establishment of adaptive immunity. Their activation relies on the recognition of antigenic peptides derived from pathogens and/or tumors presented by the Major Histocompatibility Complex II (MHC-II) at the surface of antigen presenting cells (APC). Antigens can be derived from external sources through endocytosis, resulting in exogenous antigen presentation, or they can derive from neosynthesized proteins, resulting in endogenous antigen presentation. The mechanisms of routing and loading of endogenous antigens on MHC-II molecules remain poorly characterized. Defining them will allow a better understanding of the mechanisms driving antiviral immunity.

Several groups have demonstrated that autophagy plays a role in generating MHC-II-restricted antigens. Autophagy is a lysosomal degradation process essential for maintaining cellular homeostasis. This pathway plays an important role in several physiological functions and its deregulation is associated with many pathologies. Autophagy also plays a role in infectious contexts by promoting intracellular pathogen destruction and participating in innate and adaptive immune responses. Thus, numerous viruses have evolved strategies to modulate autophagy to their benefit.

Prior to my arrival in the laboratory, my team showed that targeting an antigen to autophagosomes enhanced the capacity of APCs to activate antigen-specific CD4<sup>+</sup>T cells. Autophagy is now progressively regarded as a selective process and, therefore, selective autophagy receptors could play a role in MHC-II antigen presentation. Nevertheless, very few antigens have been described as being degraded in an autophagy-dependent manner and the molecular links between autophagy and MHC-II antigen presentation remain poorly characterized.

In this manuscript, I will first introduce the different selective autophagy receptors (SARs), their role and the pathways in which they are implicated and how they recruit the autophagy machinery. In the second part of the introduction, I will describe the MHC antigen presentation pathways, with a focus on MHC-II. I will finally present different strategies used by viruses to escape MHC-II-restricted antigen presentation and to target SARs to their benefit. I will then focus on HTLV-1 and its oncoprotein Tax known to target SARs to modulate innate immunity. These elements will allow me to introduce the results of my thesis work, presented in a second part in the form of two articles. Finally, the last part of this manuscript will be devoted to the discussion and perspectives of this work.

# Introduction

## I. Selective autophagy receptors

Maintaining cellular homeostasis requires the elimination of unwanted or damaged cellular components in a controlled fashion. Autophagy was discovered in the 1960s and described as a non-selective pathway targeting cytosolic proteins for lysosomal degradation as a response to amino acid starvation<sup>1,2</sup>. We can distinguish three types of autophagy: macroautophagy, microautophagy and chaperone-mediated autophagy (CMA). Hereafter, we will use autophagy to designate macroautophagy and will not describe the two other pathways in detail. Autophagy is a conserved degradation process consisting of the formation of double-membrane vesicles, autophagosomes, around a cargo. Autophagosomes fuse with lysosomes to deliver their cargo to degradation by enzymes, allowing disassembly and recycling of its constituents. The process is regulated by a set of Autophagy-related genes (ATG)<sup>3</sup>.

At the turn of the 21st century, Daniel Klionsky's team discovered specialized adaptor proteins delivering specific cargos to autophagosomes whilst working on the biosynthetic cytoplasm-to-vacuole targeting pathway, a selective autophagy-like process in yeast<sup>4</sup>. They showed that the transport of several vacuolar hydrolases from the cytoplasm, where they are synthesized, to the vacuole relies on the same set of ATG genes as starvation-induced autophagy. In mammals, the characterization of the selective autophagy machinery was led by the identification of p62/SQSTM1 (hereafter referred as p62), responsible for the degradation of aggregated proteins. Peroxisomes and mitochondria were the first large substrates shown to be selectively degraded by autophagy, which led to the description of respective degradation processes as pexophagy and mitophagy<sup>5,6</sup>. Selective autophagy allows the discrimination of specific content targeted to autophagosomes (bacteria, damaged organelles, aggregated proteins, etc) leading to the exclusion of other fractions of the cytoplasm<sup>7</sup>. Different receptors, named selective autophagy receptors (SARs), specifically recognize and bind relevant cargos whilst recruiting LC3/GABARAP proteins and the rest of the ATG core machinery<sup>8,9</sup>. Different pathways of selective autophagy exist and are named in relation to their targeted cellular material: protein aggregates (aggrephagy), pathogens (xenophagy), damaged mitochondria

(mitophagy), ER (ER-phagy), lysosomes (lysophagy), ribosomes (ribophagy) amongst others. In this first part of the introduction, I will present the SAR family proteins and the pathways in which they are involved. I will then explain how SARs link their cargo to the core ATG machinery. Finally, I will show how SARs can play different roles in the cell, including cell trafficking and cell signaling, adding to their role as autophagy receptors.

## **A. Characteristics of selective autophagy receptors (SARs)**

SARs emerged by convergent evolution and subsequent duplication events<sup>10</sup>. Ubiquitination is the most characterized modification that mediates cargo recognition by SARs<sup>11</sup>. The most characterized mammal SARs are the SQSTM1-like receptor (SLR) family proteins<sup>12</sup> consisting of p62/Sequestosome-1 (SQSTM1), Next to BRCA1 gene (NBR1), Optineurin (OPTN), Toll-like interacting protein (Tollip) and two CALCOCO family proteins: Tax-1 binding protein (TAX1BP1) and Nuclear dot protein 52 (NDP52).

### **1. p62 and the identification of the LC3-Interacting Region (LIR)**

Work on the protein aggregation pathway allowed the identification of the selective autophagy machinery in mammalian cells and, more particularly, allowed the identification of the first SAR. The ubiquitin-binding protein p62 was described as a cargo-sequestering component of ubiquitin-positive protein aggregates through its ubiquitin binding domain (UBA)<sup>13-16</sup> and capable of oligomerizing via its N-terminal Phox and Bem1p (PB1) domain<sup>17,18</sup> (Figure 1). The Johansen group showed that p62 by itself forms protein aggregates, later degraded in the lysosome, and demonstrated that ubiquitinated cargo recruits p62 whose oligomerization is required for efficient cargo degradation, complying with the earlier definition of autophagy receptors for degradation<sup>19</sup>. In 2007, they showed a direct interaction between p62 and LC3/GABARAP proteins, constituents of autophagosomes. By means of a p62 construct, they described the peptide found within the SAR that determines the interaction with LC3 and the subsequent integration into autophagosomes and trafficking to lysosomes. This constitutes the first mapping of the LC3-interacting region (LIR)<sup>20</sup>(Figure 1), today considered a major defining feature of SARs.



**Figure 1. Structure of p62/SQSTM1<sup>21</sup>(adapted from White *et al.*, 2023).** N-terminal PB1 domain mediates its interaction with itself and other PB1 domain-containing proteins; ZZ-type zinc finger (ZF) domain binds N-terminal arginine moieties and RNA; TB is the tumor necrosis factor receptor associated factor 6 (TRAF6)-binding domain; LIR is the LC3-Interacting Region; KIR is the Kelch-like ECH-associated protein 1 (Keap1)-interacting region; and UBA is the C-terminal ubiquitin-binding domain.

The LIR domain has since been described as a linear sequence of a core consensus of amino acids W/F/YXXL/I/V (X is any amino acid) which adopts an extended  $\beta$ -stranded conformation and forms a parallel  $\beta$ -sheet with the  $\beta$ -strand 2 of LC3. W/F/Y and L/I/V amino acids are each located in and interact with two hydrophobic pockets HP1 and HP2 forming the LIR docking site (LDS) on LC3, exploited by the majority of SARs<sup>22</sup>. The residues at positions X-1 to X-3 immediately N-terminal to the core LIR are often negatively charged, enhancing the affinity of the LIR with LC3, and the phosphorylation of amino acids within LIR or flanking this region can overall regulate the affinity of SARs to LC3 proteins<sup>23-25</sup>.

In addition to the LIR, binding ubiquitin is also an important trait that defines SARs. Oligomerized p62 forms bodies containing ubiquitinated cargo bound by the UBA domain of p62. This binding is regulated by phosphorylation of the UBA region<sup>26,27</sup>. Mutations in the UBA region of p62 are associated with Paget's disease of bone, showing the importance of p62 in aggrephagy *in vivo*<sup>28,29</sup>.

## 2. Next to BRCA1 gene (NBR1) protein

In 2009, the p62 homolog Next to BRCA1 gene (NBR1) was identified as a SAR containing a ubiquitin-binding (UBA) domain and a LIR required for its degradation via autophagy<sup>30</sup>. NBR1 and p62 interact with each other via their respective PB1 domains<sup>17</sup>. NBR1 binds and co-localizes with p62 in p62 bodies, playing a major role in aggrephagy<sup>30</sup>. Although they are organized in a similar way, NBR1 is twice the size of p62 and contains additional coiled-coil domains responsible for its dimerization and an additional amphipathic  $\alpha$ -helical J (JUBA) domain that binds lipid membranes<sup>31</sup> (Figure 2). The interaction with membranes via the JUBA domain is critical in the removal of surplus peroxisomes by autophagy<sup>32</sup>.





**Figure 2. Structure of NBR1<sup>9</sup> (adapted from Johansen & Lamark, 2011).** N-terminal PB1 domain mediates its interaction with itself and other PB1 domain-containing proteins; ZZ-type zinc finger (ZF) domain binds N-terminal arginine moieties and RNA; coiled-coil (CC) domains mediate its dimerization; LIR is the LC3-Interacting Region; J (JUBA) domain binds lipid membranes and UBA is the C-terminal ubiquitin-binding domain.

### 3. CALCOCO family proteins: CALCOCO1, NDP52 and TAX1BP1

By the time p62 and NBR1 had been described as SARs, it was clear that ubiquitin was a common “eat-me” signal present on several types of cargos (aggregated proteins, peroxisomes) and other potential cargos such as bacteria, ribosomes and depolarized mitochondria<sup>33,34</sup>.

Studies on cytoplasmic *Salmonella* revealed a role for TANK Binding Protein 1 (TBK1) adaptor nuclear dot protein 52 kDa (NDP52) in TBK1-regulated autophagy of the intracellular bacterium and described NDP52 as a xenophagy SAR<sup>35</sup>. A few years later, whilst studying TBK1 addiction in KRAS-driven cancer cells, Newman *et al.* investigated the role of TBK1-mediated autophagy in the regulation of NF- $\kappa$ B signaling given the need of cancer cells for constitutive autophagy, TBK1 and NF- $\kappa$ B activity. In the study, the team explored Tax-1-binding protein (TAX1BP1), a homolog of NDP52 and capable of interacting with TBK1, as a potential SAR. They showed that a chloroquine treatment stabilizes TAX1BP1, which in turn co-localizes with LC3-positive vesicles and possesses a non-canonical LIR, thus suggesting TAX1BP1 as a SAR<sup>36</sup>. In 2015, Tumbarello *et al.* showed that TAX1BP1 is also required for efficient clearance of *Salmonella*<sup>37</sup>. NDP52 and TAX1BP1, also known as calcium binding and coiled-coil domain 2 (CALCOCO2) and calcium binding and coiled-coil domain 3 (CALCOCO3) - respectively, constitute the small CALCOCO protein family along with calcium binding and coiled-coil domain 1 (CALCOCO1) described as implicated in ER-phagy and Golgi-phagy<sup>38,39</sup>. Although belonging to the same family as NDP52 and TAX1BP1, CALCOCO1 is not considered an SLR due to its lack of ubiquitin-binding domains. The CALCOCO family proteins share well-conserved domains composed of an N-terminal SKIP carboxyl homology (SKICH) domain, central coiled-coil regions (CC), a non-canonical LIR named cLIR motive region<sup>40</sup> between the SKICH domain and the CC domain and C-terminal ubiquitin binding zinc fingers (ZF) (Figure 3).

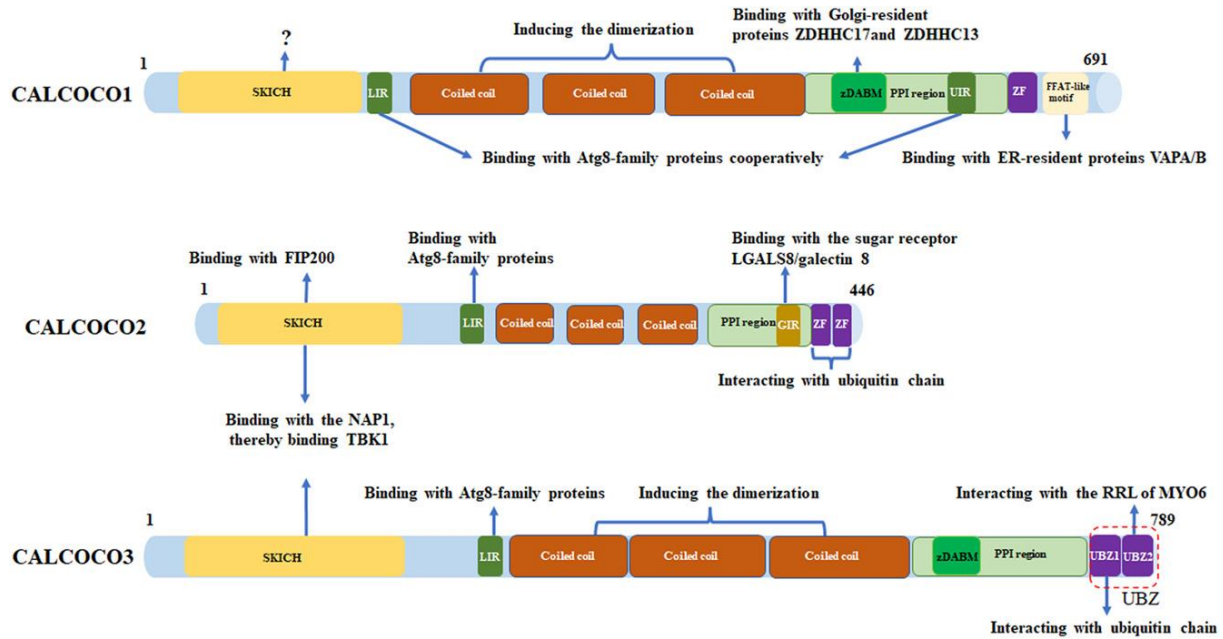


**Figure 3. Structure of CALCOCO family proteins<sup>39</sup> (adapted from Chen *et al.*, 2022).** CALCOCO family proteins contain the SKICH domain, a conserved LIR motive (LVV), coiled-coil regions (CC), and zinc finger domains (ZF). Notably, CALCOCO1 possesses a two phenylalanines (FF) in an acidic tract (FFAT) -like motive and a zDABC ankyrin repeat-binding motive (zDABM). CALCOCO2 contains a dynamic unconventional zinc-finger (ZF1) and a C2H2-type zinc-finger (ZF2), while CALCOCO3 possesses two canonic C2H2-type ZF.

CALCOCO1 possesses also a ubiquitin-interacting motive (UIM)-like- docking site (UDS) - interacting region (UIR) recognized by the UDS region on LC3 molecules<sup>546</sup>. The UIR motive cooperates with LIR to bind LC3<sup>38</sup>. Other domains allow the interaction with ER membranes and Golgi proteins (FFAT-like motive and zDABM) (Figure 3). Although TAX1BP1 also presents a zDABM motive that allows interaction with Golgi-resident proteins<sup>41</sup>, a role of TAX1BP1 in Golgi-phagy is still unknown. In contrast to CALCOCO1, which only has one ZF domain, NDP52 and TAX1BP1 have two C-terminal ZF domains. NDP52 contains an unconventional zinc-finger (ZF1) and a C2H2-type zinc-finger (ZF2), but there is no direct coupling between them<sup>42</sup>. TAX1BP1 possesses two unique ubiquitin- binding C2H2-type zinc fingers (UBZ), UBZ1, and UBZ2. These two ZFs are directly coupled with each other through a unique Trp-residue<sup>43</sup> (Figure 3). Both ZF domains in NDP52 and TAX1BP1 serve as ubiquitin-binding domains that recognize ubiquitinated intracellular bacteria and therefore promote xenophagy<sup>37,44</sup>. The ZF domains are also involved in the binding to the motor protein myosin VI that mediates autophagosome maturation<sup>45</sup> in the case of NDP52 and TAX1BP1; the role of the ZF domain on CALCOCO1 remains unclear. NDP52 contains also a GIR domain that recognizes Galectin-8

accumulated on damaged *Salmonella*-containing vacuoles (SCVs) or any other damaged endosome or lysosome in the cytosol<sup>46</sup>.

#### 4. Optineurin (OPTN)

An additional ubiquitin-binding SAR involved in xenophagy was described in 2011: Optineurin (OPTN). It contains several oligomerization-prone coiled-coil domains, a short linear LIR, and a C-terminal ubiquitin-binding domains in ABIN proteins and NEMO (UBAN) region and ZF domains (Figure 4).



**Figure 4. Structure of Optineurin<sup>10</sup> (adapted from Randow & Youle, 2014).** Coiled-coil (CC) regions mediate oligomerization, LIR mediates LC3/GABARAP interaction, UBAN mediates interaction with signaling molecules and ubiquitin, ZnF mediates interaction with ubiquitin.

OPTN is found enriched in various pathological inclusions, including Lewy bodies in Parkinson disease and its mutations are associated with amyotrophic lateral sclerosis (ALS) and glaucoma<sup>47</sup>. In order to clear cytoplasmic *Salmonella*, the phosphorylation of its LIR motive (S177) and UBAN domain (S473) by TBK1 are essential<sup>24,48-50</sup>. The phosphorylation of the LIR following the recruitment of OPTN strongly increases its affinity to LC3 and polyubiquitin. This SAR plays overall an important role in mitophagy, xenophagy and aggrephagy.

#### 5. Toll-like interacting protein (Tollip)

In 2014, Stefan Jentsch at the Max Planck Institute identified protein Cue5 containing an N-terminal ubiquitin-binding Coupling of ubiquitin conjugation to ER degradation (CUE) domain<sup>51</sup> and a C-terminal AIM (yeast equivalent of LIR) as a SAR for ubiquitinated proteins in *Saccharomyces cerevisiae*<sup>52</sup>. CUE domains are named for the yeast Cue1p protein, which recruits the ubiquitin-conjugating enzyme Ubc7p to the ER, where it is essential for misfolded protein degradation<sup>53</sup>. Cue5 is capable of self-interacting and participates in the selective degradation of the proteasome (proteaphagy) after its inactivation<sup>54</sup>. Its human counterpart was Tollip, previously implicated in innate immunity and protein trafficking<sup>55</sup> as well as in MHC-II molecule trafficking<sup>56</sup>. Tollip has a C-terminal CUE domain preceded by the PI3P-binding C2 domain (Figure 5). The interaction with ubiquitin interferes with the PI3P binding, which has unknown consequences for the SAR function of Tollip<sup>57</sup>. Tollip has two putative LIRs included in C2 that

are required for clearing mutant huntingtin<sup>52</sup>. The presence of putative LIR domains and the binding to ubiquitin makes Tollip a SAR.

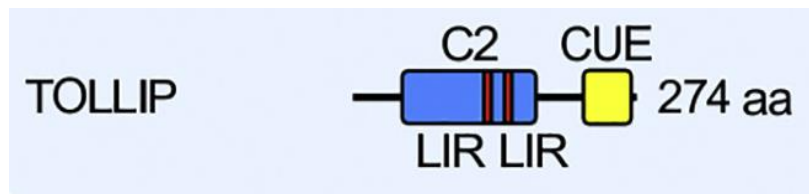


**Figure 5. Structure of Toll-like interacting protein (adapted from Kirkin & Rogov, 2019).** C2 domain mediates binding to PI3P, two putative LIR domain mediate recruitment of ATG machinery; CUE domain mediates binding to ubiquitin.

## B. Pathways of selective autophagy

As mentioned previously, several pathways of selective autophagy exist that target pathogens, damaged organelles or aggregated proteins. Here, I will focus on aggrephagy, xenophagy and mitophagy given their role in innate immunity and their possible link to antigen processing.

### 1. Aggrephagy

Protein aggregation is generated because of improper folding or misfolding caused by mutations, incomplete translation, abnormal post-translational modifications and oxidative stress<sup>58</sup>. In addition to molecular chaperones and the ubiquitin-proteasome system (UPS), a type of selective autophagy can eliminate protein aggregation, aggrephagy<sup>59</sup>. Aggrephagy is mediated by several SARs including Tollip, p62, NBR1, OPTN and TAX1BP1<sup>30,48,60,61,551</sup>. SARs recognize ubiquitinated aggregated proteins and, along with adaptor protein Histone Deacetylase 6 (HDAC6), form an aggresome to which the autophagy machinery is recruited<sup>9</sup>. Both p62 and HDAC6 seem to have a preference for K63-linked polyubiquitin chains<sup>62</sup> and the addition of K63-linked Ub chains has been reported to correlate with the clearance of protein inclusions by autophagy<sup>63</sup>. HDAC6 mediates transport, via dynein molecular motors, of smaller Ub-containing aggregates to the microtubule-organizing center (MTOC) region where the aggresome is formed, usually encaged by intermediate filaments<sup>64-66</sup>. HDAC6 may also be important for the transport of the autophagy machinery to the aggresomes<sup>65</sup>. The presence of p62 is a common feature of most cytoplasmic and nuclear protein aggregates found in human diseases<sup>67</sup>. A specific protein other than p62 induces most pathological aggregates and the recruitment of p62 is a later event induced by the ubiquitination of the aggregates. p62 is not

required for the formation of polyglutamine inclusions of Huntington's disease<sup>68</sup> and the presence of p62 in aggregates is thought to reflect a role of p62 in autophagic degradation. Interestingly, Sarraf et al. reported that the loss of TAX1BP1 leads to a decreased ability to target protein aggregates for degradation when compared to the loss of other SARs, including p62. In addition, they showed that overexpressing TAX1BP1 promotes aggregate clearance and rescues cell viability after exposure to proteotoxic stress. Unlike its homolog NDP52, TAX1BP1 is strongly expressed in the brain (human and murine), thus suggesting that SARs present spatial and functional specificities at a tissue level<sup>551</sup>.

In DCs, inflammation can increase the proportion of Defective Ribosomal Products (DRiPs)<sup>69</sup>. DRiPs can be found in DC aggresome-like induced structures (DALIS)<sup>70</sup>. During maturation of DCs and murine macrophage cell lines, protein synthesis and DRiP degradation are finely regulated<sup>71,72</sup>. The protein chaperones Hsc/Hsp70 recognize and bind newly synthesized DRiPs to allow DALIS formation after their ubiquitination<sup>73</sup>. DALIS formation is believed to promote antigen presentation. In the late stages of maturation, accumulated DALIS are bound to degradation by the proteasome or by selective autophagy mediated by p62 and the chaperones BAG1 and BAG3.

## 2. Mitophagy

Mitophagy designates the specific degradation of mitochondria via autophagy. Damaged mitochondria are culled in several cell types to maintain quality control because excess mitochondrial damage can perturb cellular homeostasis and must therefore be eliminated rapidly<sup>74</sup>. Mitophagy is also involved in innate immunity, cell differentiation, cell death, cancer and neurodegenerative diseases<sup>75</sup>.

In mammalian cells, the mitochondrial kinase, PINK1, is stabilized in the outer mitochondrial membrane (OMM) of depolarized mitochondria where it subsequently recruits and activates E3 ubiquitin ligase Parkin and phosphorylates ubiquitin residues<sup>76-78</sup>. Parkin is mutated in familial cases of Parkinson's disease<sup>79</sup>. Parkin then ubiquitinates proteins on the outer membrane of mitochondria<sup>80,81</sup> (Figure 6). In a HeLa cell model genetically edited to knock out five SARs TAX1BP1, NDP52, NBR1, p62 and OPTN (penta KO), Lazarou *et al.* showed that ectopic expression of NDP52 and OPTN and to a lesser extent TAX1BP1 rescued mitophagy<sup>82</sup>. In the same study, neither NDP52 nor OPTN single KO caused a defect in mitophagy, whereas NDP52/OPTN DKO and, to a greater extent, NDP52/OPTN/TAX1BP1 TKO inhibited mitophagy.

These results suggest that NDP52, OPTN and TAX1BP1 play redundant roles in mitophagy and this is not the case for p62, NBR1 and Tollip. Interestingly, the unaltered mitophagy observed in OPTN single KO contrasts with a report indicating loss of mitophagy using RNAi-mediated knockdown of OPTN in HeLa cells<sup>83</sup>. This could be explained by the redundant roles of NDP52 and TAX1BP1 not being efficiently set in motion in a transitory RNAi-mediated silencing of OPTN.

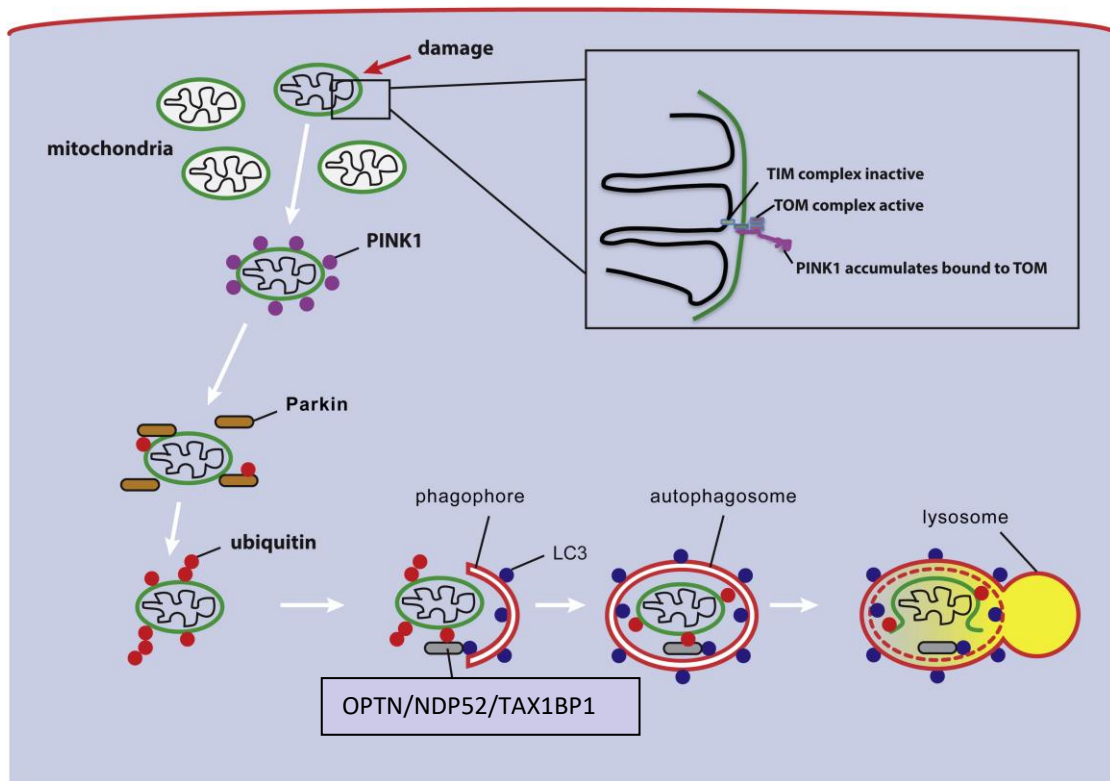


**Figure 6. PINK and Parkin mediate mitophagy<sup>10</sup>(adapted from Randow & Youle, 2014).** When a mitochondrion loses membrane potential or accumulates misfolded proteins, PINK1 accumulates on the outer mitochondrial membrane. The PINK1 kinase recruits Parkin to mitochondria from the cytosol and activates the E3 ligase to ubiquitinate outer mitochondrial membranes. These ubiquitinated proteins act as “eat-me” signals for SARs that signal autophagy.

Ubiquitin motives also recruit myosin VI to damaged mitochondria. The PINK1-Parkin mitophagy pathway mediated by OPTN seems to be involved in numerous neurodegenerative diseases such as Alzheimer’s disease and has been shown to play a role in diabetic neuropathies<sup>84</sup>.

### 3. Xenophagy

Xenophagy designates the selective degradation of foreign organisms by autophagy. This pathway is mobilized in the innate immune response to control infections by intracellular

pathogens like bacteria or viruses. It is a fundamental host cell response to invasion by a variety of intracellular bacteria including *Shigella flexneri*, *Listeria monocytogenes* and *Salmonella Typhimurium*<sup>85-87</sup>. During a bacterial infection, cells coat bacteria with polyubiquitin<sup>33</sup>, this constitutes an “eat-me” signal. In 2009, Felix Randow’s group described the SAR NDP52, to be associated with ubiquitin-coated *Salmonella enterica* via its ubiquitin-binding domain and to mediate its degradation via autophagy through its LIR domain<sup>35</sup> (Figure 7). p62, OPTN and TAX1BP1 have also been described as playing a role in restricting *Salmonella*<sup>37,88,89</sup>. Upon generation of a breach in endosomal compartments, galectins accumulate and recognize glycans that are present abundantly in post-Golgi compartments and are lacking in the cytosol<sup>46</sup>. Accumulation of galectin-8 around endosomes breached by *S. typhimurium* provides another “eat me” signal for NDP52 to target bacteria to the autophagy machinery<sup>46</sup> (Figure 7). Recently, Tollip was found to be recruited to group A Streptococcus-containing vacuoles prior to bacterial escape to the cytosol. Interestingly, Tollip knockout prevented the recruitment of other SARs such as NBR1, TAX1BP1, and NDP52 to bacteria-containing autophagosomes leading to prolonged bacterial survival. Tollip was also shown to be required for the recruitment of galectin-1 and -7 to bacteria-containing autophagosomes<sup>90</sup>.

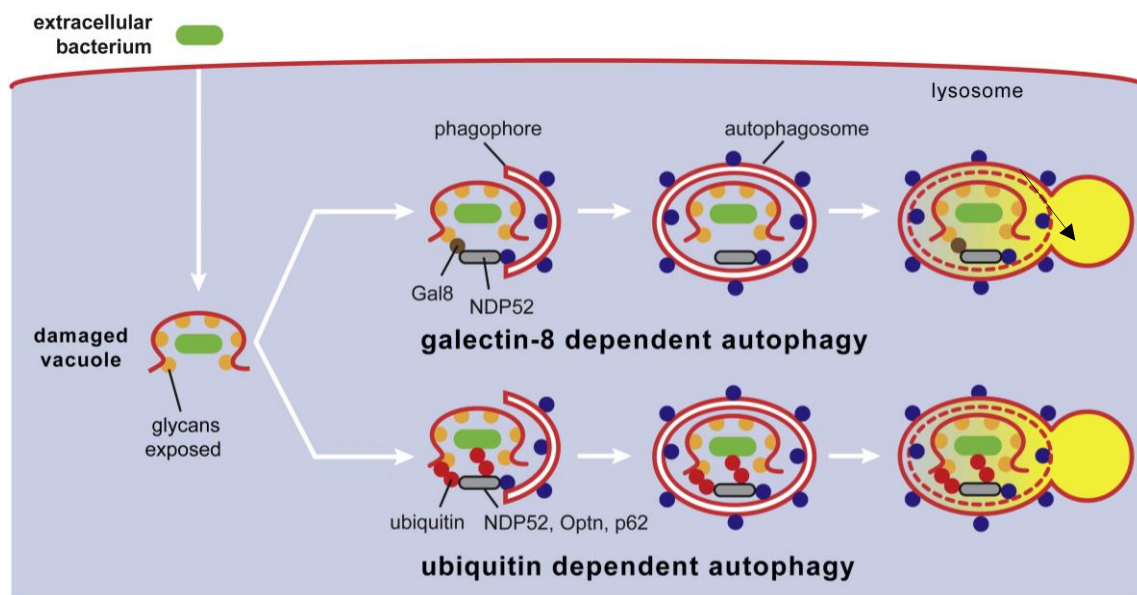


**Figure 7. NDP52-mediated xenophagy<sup>10</sup> (adapted from Randow & Youle, 2014).** On damaged vacuoles, exposure of otherwise hidden glycans recruits the danger receptor galectin-8, whose accumulation provides an “eat-me” signal for SAR NDP52, inducing autophagy. The ubiquitin coat deposited around cytosol-exposed bacteria (which may still be in association with vacuolar membrane remnants) serves as an alternative “eat-me” signal for SARs (NDP52, OPTN, p62), thereby inducing autophagy.

As seen previously, SARs are implicated in different types of selective autophagy by acting in a combined, redundant or specific manner, this constitutes an important level of complexity in the autophagic pathway. Furthermore, the existence of canonical and non-canonical LIRs adds on to the complexity and selectivity of the process by suggesting that specific cargos can be bound by SARs and be targeted to what could constitute specific subsets of autophagosomes given the diversity of LC3/GABARAP proteins. In addition, before being described as SARs, these different molecules were initially characterized as mainly scaffold proteins implicated in different signaling pathways. These include, for instance, the TBK1-mediated NF- $\kappa$ B signaling pathway (we will see these roles more in detail in the last part of this chapter) known to be implicated in both innate and adaptive immune responses<sup>91,92</sup>. In the next part, I will detail the mechanisms of autophagosome formation led by cargo-SAR complexes in order to show the interplay between autophagy and immunity and understand how SARs could participate in antigen degradation in autolysosomes.

### **C. Cargo-SAR-mediated recruitment of the autophagy machinery**

It is important to note that other pathways of autophagy (other than macroautophagy) exist: microautophagy and chaperone-mediated autophagy (CMA). CMA is a selective process in which single proteins are recognized as unfolded/ misfolded when exposing a KFERQ-like pentapeptide motive recognized by heat shock cognate protein of 70 kDa (Hsc70)<sup>93</sup>. This pathway has been shown to play a role in MHC-II antigen presentation<sup>94,95</sup>. Microautophagy can be both unselective and selective and involves the direct engulfment of cytoplasmic material by lysosomes or endosomes, either by invagination or by membrane protrusions<sup>96,97</sup>. In this part, I will describe the cargo-SAR-mediated recruitment of the macroautophagy machinery as a way to explore the mechanisms potentially delivering antigens to autophagosomes for subsequent MHC-II antigen presentation.

#### **1. The autophagy pathway**

In a simplified way, we can subdivide the process of recruitment of the autophagy machinery and the formation of autophagosomes until their maturation in three stages: initiation, elongation and maturation.



### a) *Initiation*

This stage corresponds to the recruitment and activation of different protein complexes that allow the formation of the phagophore. The transmission of these signals occurs near the ER membranes<sup>98</sup> where the nucleation of the insulation membrane will take place. Two complexes work together to induce autophagy: the class III PI3K complex and the ULK complex.

The master cell growth regulator serine/threonine kinase mammalian Target of Rapamycin (mTOR), formed by two sub-complexes mTORC1 and mTORC2, is a downstream effector of the PI3K-Akt signaling pathway. In basal conditions, mTORC1 is bound to phosphorylated Unc-51-like kinase 1 and 2 (ULK1/2) forming an inactive complex. Upon nutrient deprivation, mTORC1 and ULK1/2 are dephosphorylated followed by the release of ULK1/2. ULK1/2 auto phosphorylate and phosphorylate Atg13 and focal adhesion kinase family interacting protein of 200 kD (FIP200) and form a complex along with and Atg101. The ULK complex (ULK1/2:Atg13:FIP200 and Atg101) and Atg9, a transmembrane protein essential for autophagy and delivering membranes, are independently recruited to the initiation site. The ULK kinase activity recruits the lipid kinase (PI3K) complex VPS34 (formed of vacuolar protein sorting 34 (VPS34), Beclin-1 and vacuolar protein sorting 15 (VPS15)) that produces membrane patches rich in phosphatidylinositol 3-phosphate (PI3P) at the site of nucleation<sup>99</sup> (Figure 8). The origin of this phosphatidylinositol-2-phosphate-rich (PI3P) membrane is to this day controversial. In fact, *de novo* synthesis is not required and instead this membrane finds its origin in preexisting organelle membranes. The endoplasmic reticulum<sup>98,100,101</sup>, mitochondria<sup>102</sup>, the plasma membrane<sup>103</sup> and the Golgi apparatus<sup>104</sup> are potential sources for the formation of the phagophore. PI3P allows the recruitment of effector proteins such as DFCP1 and WIPI that participate in phagophore elongation.

### b) *Elongation*

The elongation and ultimate closure of the phagophore relies on the conjugation of two ubiquitin-like proteins, Atg12 and LC3, to Atg5 and the lipid phosphatidyl ethanolamine (PE), respectively<sup>105</sup> (Figure 8). To catalyze LC3 lipidation on glycine 120, the Atg12-Atg5 conjugate associates with Atg16 into an E3-like enzyme complex, whose localization, together with more upstream components, specifies the site of autophagosome biogenesis. While yeasts encode only a single Atg8 gene, humans harbor six orthologs that cluster into the LC3 and GABARAP subfamilies<sup>7</sup>. Membrane-associated LC3/GABARAP provide docking sites for receptors that deliver specific cargos to phagophores during selective autophagy<sup>8,9</sup>.

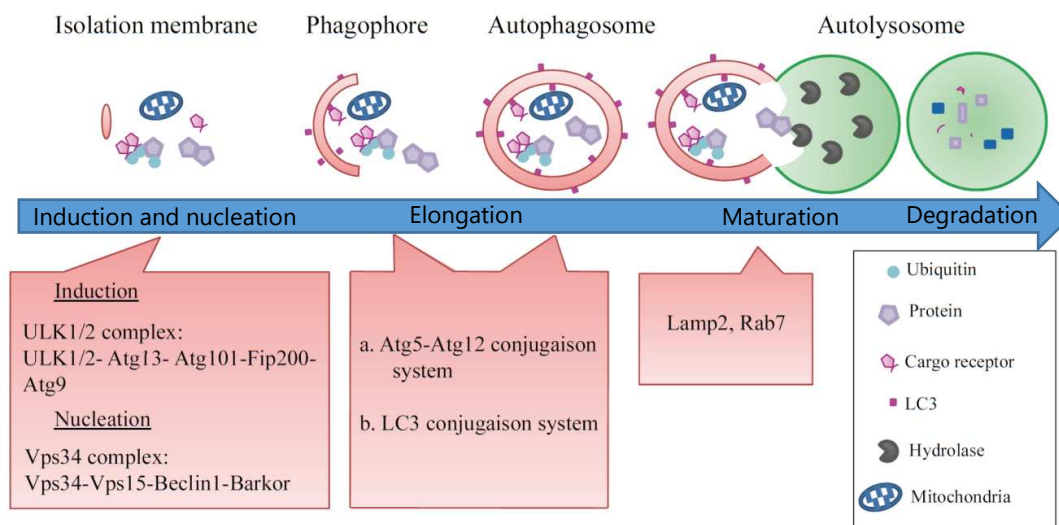


**Figure 8. Steps of autophagosome formation<sup>106</sup> (adapted from Trocoli & Djavaheri-Mergny).** Autophagy consists of three major steps: initiation, elongation and maturation. Initiation corresponds to the induction and nucleation of the phagophore. The phagophore elongates to form a double membrane vesicle, the autophagosome. Maturation corresponds to the fusion of the phagophore with endosomes and lysosomes to form the autolysosome where the content is degraded.

### c) *Maturation*

The last step of the process is autophagosome maturation, which allows degrading their content after fusion with lysosomes. The VPS34 complex associates with the protein UVRAG (UV-radiation resistance associated gene) via its interaction with Beclin-1 and forms a complex that contributes to autophagosome maturation<sup>99</sup>. However, UVRAG associated with VPS34 complex can also bind Rubicon and this interaction suppresses vesicular transport and inhibits autophagosome maturation<sup>107,108</sup>. Rab7, belonging to the Ras GTPase protein family, plays a key role in autophagosome fusion with lysosomes<sup>109,110</sup> and Rab11 is necessary for the fusion of autophagosomes with late endosomes in response to nutrient deprivation<sup>111</sup> (Figure 8).

The fusion of autophagosomes to endolysosomal compartments also requires other tethering proteins such as VAMP7 and VAMP8 belonging to the SNARE family<sup>112</sup> and proteins from the ESCRT complex that are implicated in endosome traffic and endosome biogenesis<sup>113</sup>.

Tumbarello *et al.* showed that NDP52, OPTN and TAX1BP1 act as a bridge between the external membranes of autophagosomes, via their LIR motive, and Tom-1-expressing endosomes<sup>45,114</sup>. This occurs through the interaction of the SARs with Myosin VI (MyoVI) via their ubiquitin-binding regions<sup>45,115,116</sup> (Figure 9). MyoVI is capable of interacting with ESCRT protein Tom-1

expressed at the surface of endosomes, allowing the delivery of endocytic cargo to autophagosomes, which is necessary for their subsequent maturation and fusion with lysosomes. In addition, NDP52 was shown to target intracellular bacteria to autophagosomes and to singularly ensure pathogen degradation by regulating bacteria-containing autophagosome maturation and promoting xenophagy<sup>547</sup>. The ability of certain SARs to link endocytic vesicles to autophagosomes could confer them a role in antigen delivery to MHC-II loading compartments, described as endolysosomal vesicles (I will describe them more in detail in the second part of the introduction).

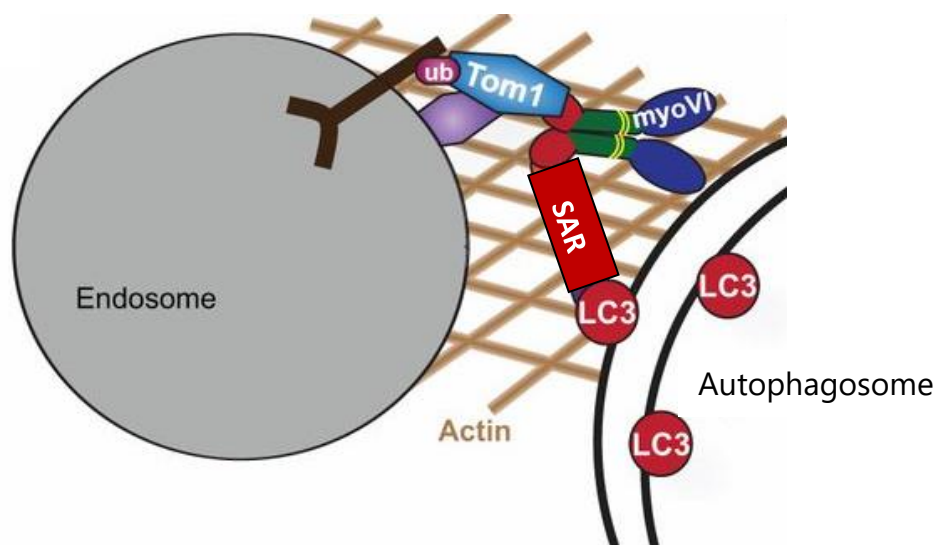


**Figure 9. SARs promote autophagosome maturation (adapted from Tumbarello *et al.*, 2013).** OPTN, NDP52 and TAX1BP1 interact with autophagosomes through their LIR domain and with Myosin VI (MyoVI) through their ubiquitin-binding domains. Myo VI interacts with Tom-1-expressing endosomal vesicles by binding to Tom-1. OPTN, NDP52 and TAX1BP1 link autophagosomes to endosomal vesicles and promote autophagosome maturation.

## 2. How SARs recruit the autophagy core machinery

Once SARs have bound to their target, it is important to then induce the formation of an autophagosome around it in order to isolate the target from the rest of the cytoplasm and ensure its proper degradation. Selective autophagy relies on the docking of the cargo to the phagophore but also on the upstream autophagy core machinery to initiate phagophore formation<sup>82,117,118</sup>.

The LIR motive is essential for targeting the cargo to the forming phagophore. Efficient docking of the cargo is believed to rely on multiple LC3/GABARAP-SAR interactions<sup>119,120</sup> thus the phagophore may grow along the selected cargo, as opposed to bulk non-selective autophagy. This process requires a certain level of SAR multivalence. p62 uses its PB1 domain to oligomerize and concert the formation of an isolation membrane with the ubiquitinated cargo<sup>120</sup>. How other SARs achieve this is still unknown, although it may involve additional LIR motives and protein-protein interaction structures such as coiled-coil domains present in TAX1BP1 and NDP52<sup>121</sup>.

Several studies suggest that SARs directly recruit FIP200 to the cargo. Indeed, Vargas *et al.* showed that NDP52 uses its SKICH domain to interact directly with FIP200. They showed that locating NDP52 ectopically on mitochondria or peroxisomes is sufficient to initiate selective autophagy and activating the ULK complex in a FIP200-dependent manner and this pathway is facilitated by TBK1 interaction with NDP52<sup>122</sup>. The SKICH domain of TAX1BP1 similarly binds to FIP200<sup>123</sup>. In addition, p62 was also shown to bind the C-terminal Atg11 homology region of FIP200 through its newly defined FIP200-interacting region (FIR). This interaction recruits the ULK complex to induce phagophore formation *in situ* at the cargo site<sup>124</sup>.

Components of the ULK complex contain LIR motives and can interact with LC3/GABARAP proteins<sup>125-127</sup>. LC3/GABARAP and FIP200 may therefore play a redundant role. How FIP200 engages the VPS34 complex in selective autophagy remains poorly characterized. Birgisdottir *et al.* showed that sub-units of the VPS34 complex also contain LIRs and preferentially interact with GABARAP proteins. They showed that these interactions stabilize the association of the ULK complex with the phagophore and that disrupting the interactions of LC3/GABARAP with Atg14 (Atg14 is in the VPS34 complex) led to defective mitophagy<sup>128</sup>. This suggests that LC3/GABARAP proteins act as scaffold proteins in the interplay of the different protein complexes. Considering that some SARs only bind to a subset of LC3/GABARAP proteins (e.g. NDP52), the involvement of a specific SAR could modulate the signaling pathway by specifically recruiting the different actors.

Another way in which SARs could recruit the autophagy core machinery is via their interaction with Tripartite motive (TRIM) proteins involved in “precision autophagy”. More than 80 TRIM proteins have been identified in humans and are implicated in different cellular processes. The term “precision autophagy” is due to a specific feature of TRIM proteins, which is the ability to

act as autophagy receptor regulators. This means that TRIMs can directly bind cargos and act as platforms for assembly of the autophagy machinery, such as Beclin-1 and the ULK complex<sup>548, 549</sup>. Certain TRIM proteins have been reported as binding SARs such as p62<sup>548</sup>, making this a means for SARs to recruit the autophagy machinery as well as highly selective cargos (not depending on ubiquitin or galectin) to forming autophagosomes. Interestingly, TRIM5 binds to the HIV-1 capsid protein<sup>550</sup> and contributes to its delivery to autophagic degradation. The binding of viral proteins by TRIM proteins could be a way to deliver antigens to autophagosomes for further MHC-II antigen presentation.

#### **D. Other roles of SARs in the cell**

SARs have different functions outside their role in autophagy. Here I will summarize some relevant functions whose study complements the works of my thesis.

##### **1. Role of SARs in the internalization of transferrin receptor**

OPTN is also a binding partner of transferrin receptor implicated in transferrin-mediated uptake and endocytosis. An overexpression of OPTN was shown to decrease transferrin uptake<sup>129</sup> by inducing the clustering of transferrin receptor molecules to perinuclear foci containing OPTN. This caused less availability of transferrin receptors at the surface of the cell and showed how OPTN participates in the regulation of this transferrin clathrin-mediated endocytosis<sup>130</sup>.

##### **2. Role of SARs in vesicle trafficking and maturation**

The SARs TAX1BP1, Tollip and p62 have an additional role in endosome trafficking maturation. Via their UBD, they participate in the retention of early endosomes at the perinuclear ER membrane. Deubiquitination of p62 releases the early endosomes from the ER/nuclear membrane and promotes their release and subsequent maturation into late endosomes<sup>131</sup>. This feature of SARs could be linked to the trafficking of MHC-II loading compartments (MIIC) since they are endolysosomal vesicles trafficking from the ER to the cell membrane in a regulated manner (Figure 10).

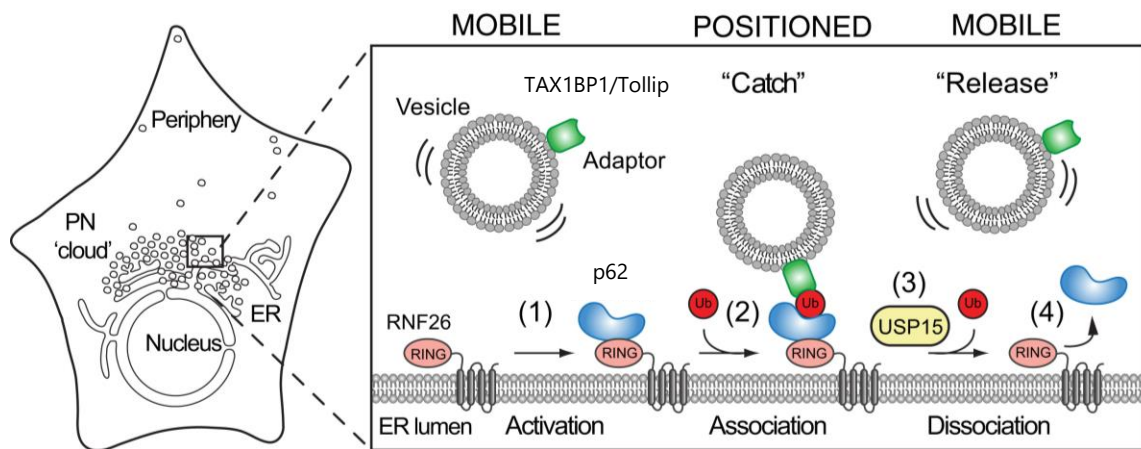


**Figure 10. SARs promote endosome maturation<sup>131</sup> (adapted from Jongsma *et al.*, 2016).** The ER-located E3 ubiquitin ligase RNF26 employs p62 to capture TAX1BP1 and Tollip to retain vesicles in the perinuclear cloud. Action of DUB USP15 releases the vesicles in the cytoplasm. The opposite effects of RNF26 and USP15 draw the endosomal system's architecture and orchestrate vesicle maturation and cargo trafficking in space and time.

### 3. Role of SARs in the NF- $\kappa$ B signaling pathway

A tight regulation of both autophagy and the NF- $\kappa$ B signaling pathway is necessary to maintain cellular homeostasis. A deregulation of either one of these pathways is often associated with cancer development and other pathologies<sup>132</sup>. Autophagy is involved in numerous cellular functions regulated by NF- $\kappa$ B such as cell survival, senescence, inflammation and immunity. With several common upstream signals, these two pathways coexist in a complex interplay.

The NF- $\kappa$ B family of transcription factors regulates the expression of several target genes by dimerizing and binding to specific DNA sequences on their promoters called  $\kappa$ B sites. The NF- $\kappa$ B dimers are retained in the cytoplasm as latent complexes binding a member of the inhibitor of NF- $\kappa$ B I $\kappa$ B protein family<sup>133</sup>. Two different pathways can promote NF- $\kappa$ B activation: canonical and non-canonical. In both pathways, activation is mediated by the phosphorylation of the I $\kappa$ B kinase (IKK) complex formed by both the catalytic kinases IKK $\alpha$  and IKK $\beta$  and the regulatory protein NEMO (IKK $\gamma$ ) or by IKK $\alpha$  homo-dimers<sup>106</sup>. The NF- $\kappa$ B pathway regulates both innate and adaptive immune responses and is activated rapidly in response to a wide range of stimuli, all converging in the activation of IKK. IKK then phosphorylates I $\kappa$ B that is then ubiquitinated and targeted for degradation by the proteasome, thereby releasing NF- $\kappa$ B dimers from the

cytoplasmic NF- $\kappa$ B-I $\kappa$ B complex and allowing them to translocate to the nucleus. In a normal context, NF- $\kappa$ B activation is transient and feedback loops that terminate the activation are established. Repressors like A20 mediate the K63-deubiquitination and inactivation of signaling molecules that are required for NF- $\kappa$ B activation<sup>134,135</sup> and to this end, they cooperate with ubiquitin-binding proteins such as the SAR TAX1BP1<sup>136</sup>. TAX1BP1 is also known as T6BP (TRAF6 binding protein) since it was identified as binding to ubiquitinated TNF-receptor-associated factor 6 (TRAF6) through its ubiquitin binding domain (UBZ2) and binding to K63-ubiquitinated receptor-interacting serine/threonine kinase (RIP). Both TRAF6 and RIP are found upstream of the activation of IKK<sup>137</sup>. Therefore, a model was proposed in which TAX1BP1 functions as a ubiquitin-binding adaptor protein that recruits A20 to the signaling proteins TRAF6 and RIP1 leading to their deubiquitination and disruption of IL-1- and TNF-induced NF- $\kappa$ B signaling<sup>138,139</sup>. Another model suggested, by studying TAX1BP1 deficient cells<sup>140</sup>, that A20 can also inhibit NF- $\kappa$ B signaling by being recruited by TAX1BP1 to E2 conjugating enzymes (UBC13, UBC5c) and inducing their K48-ubiquitylation and proteasomal degradation thus disrupting the binding of E3 ubiquitin ligases (TRAF6, TRAF2, cIAP1) and abolishing the recruitment of downstream kinase complexes<sup>139</sup> (Figure 11).

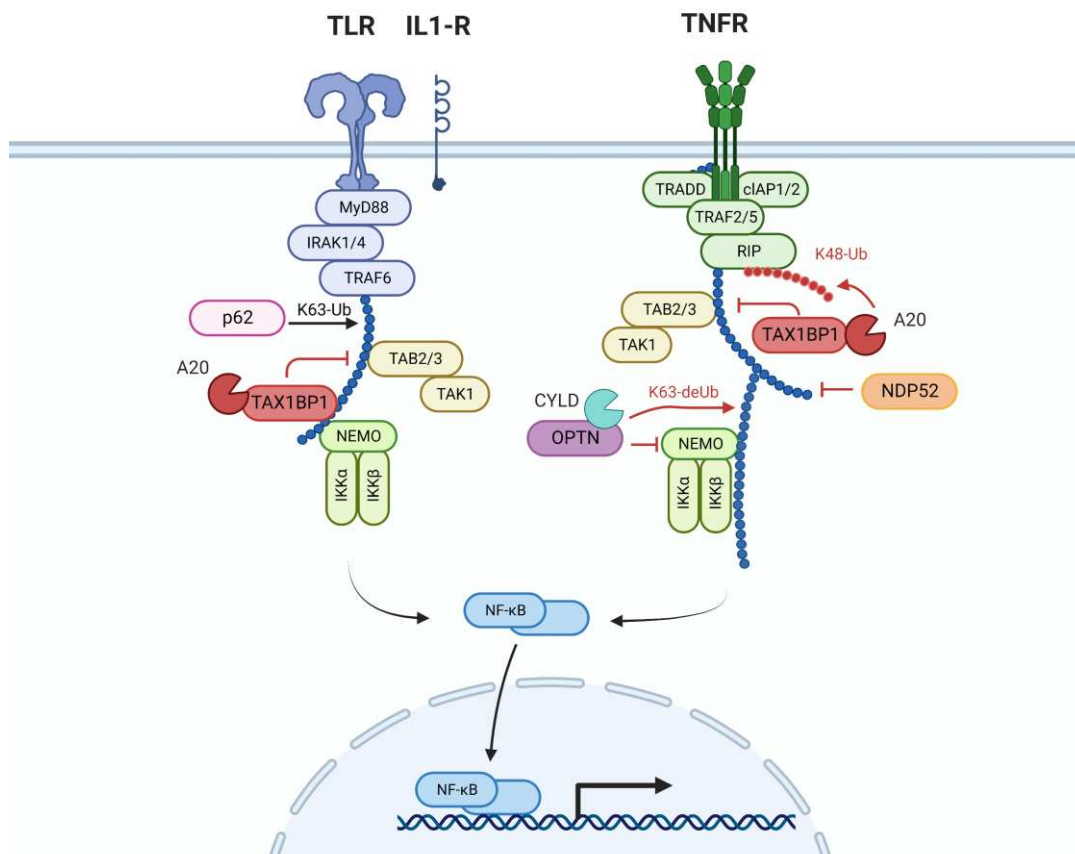


**Figure 11. Schematic representation of the role of SARs in the NF- $\kappa$ B signaling pathway.** TAX1BP1 recognizes ubiquitinated (K63-Ub) TRAF6 and RIP and recruits A20. A20 can induce the deubiquitination (K63-deUb) of TRAF6 and RIP as well as the K48-ubiquitination of RIP and further proteasomal degradation. OPTN recruits CYLD to K63-ubiquitinated RIP, which induces its deubiquitination. NDP52 also inhibits RIP K63-ubiquitination. TAX1BP1, OPTN and NDP52 negatively regulate the NF- $\kappa$ B signaling pathway by abolishing the recruitment of downstream protein complexes. On the other hand, p62 promotes TRFA6 K63-ubiquitination and the activation of the NF- $\kappa$ B signaling pathway.

Another SAR involved in the NF- $\kappa$ B signaling pathway is OPTN, also known as NRP (NEMO-related protein)<sup>141</sup>. OPTN competes with NEMO (NF- $\kappa$ B Essential Modulator) to bind ubiquitinated RIP (Ub-RIP) necessary for TNF $\alpha$ -induced NF- $\kappa$ B activation and recruits the deubiquitinase CYLD to Ub-RIP causing the blockage of the downstream reaction in the NF- $\kappa$ B pathway which results in apoptosis<sup>130</sup>. In fact, OPTN participates in a retro feedback loop involving TNF $\alpha$  and NF- $\kappa$ B activation<sup>142</sup> (Figure 11).

Finally, p62 and NDP52 are also involved in the NF- $\kappa$ B signaling pathway. p62 has been reported to be involved in the K63-polyubiquitination of TRAF6 necessary for NF- $\kappa$ B activation<sup>143</sup>. In addition, through the use of ubiquitination mutants and overexpression of NDP52, Miyashita *et al.*, showed that NDP52 is a negative regulator of the NF- $\kappa$ B signaling pathway<sup>144</sup> (Figure 11).

Overall, SARs serve an important function in regulating selective autophagy of proteins, invading microorganisms and damaged organelles that could compromise cell homeostasis and survival. Moreover, they also play a significant and much broader role as scaffold proteins in vesicle trafficking and cell signaling pathways, which makes them ideal targets for viruses and other pathogens to disrupt the cell machinery. Given their role in specific targeting, autophagosome generation and maturation as well as in vesicle trafficking, SARs could very well play a part in antigen degradation and delivery to MHC-II-containing compartments for antigen presentation.

In the second part of this work, I will overview the MHC-II antigen presentation pathway that occurs inside membranes and vesicles of different nature in antigen presenting cells (APC) and relies on the cell traffic machinery.



## II. MHC-restricted antigen presentation pathways

Antigen presentation by major histocompatibility complex (MHC) molecules is fundamental for the establishment of adaptive immunity. Prior to being presented, antigenic peptides must be generated from proteins that either are products of the cell's translation machinery or have passed through the endolysosomal degradative system. MHC-peptide complexes interact with T lymphocyte receptors (TCR), which leads these cells to mount specific immune responses. In this part, I will present the different characteristics of the MHC molecules as well as the different mechanisms of antigen presentation. We will then focus on MHC class II (MHC-II) antigen presentation, the aim of my thesis being to understand further the mechanisms of endogenous antigen presentation by MHC-II molecules.

### A. The human Major Histocompatibility Complex

The human Major Histocompatibility Complex (MHC) molecules are part of the Human Leucocyte Antigen (HLA) system. The HLA name was originally given because these antigens were first described after leukocyte-agglutinating antibodies were observed in the serum of transfused patients<sup>145</sup>. This system is composed of a complex set of genes located on chromosome 6. The genetic loci historically involved in the rejection of foreign organs are known as the MHC and are the most polymorphic genetic system in vertebrates (Figure 12). At the molecular level, MHC molecules are surface glycoproteins, divided into class I and class II, that present self- and foreign antigens and participate in regulating immune responses.

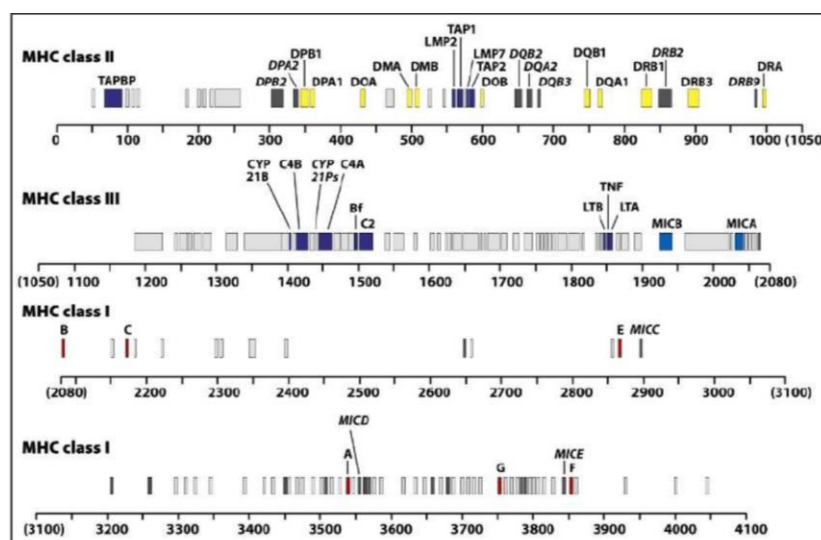


**Figure 12. Schematic representation of the MHC loci on chromosome 6.** The class I and II regions encode the different proteins involved in MHC-I (red) and MHC-II antigen presentation (yellow corresponds to genes and grey corresponds to pseudo genes). The class III region does not encode any HLA molecules but contains genes encoding complement components (dark blue) and cytokines involved in immune responses.

## 1. Major Histocompatibility Complex Class I (MHC-I)

Human MHC-I molecules are expressed by most nucleated cells and are encoded by three genes termed: HLA-A, -B, -C, all highly polymorphic (Figure 12).

MHC-I molecules are immunoglobulin-type protein complexes resulting from the association of an invariant  $\beta_2m$  microglobulin sub-unit and a heavy  $\alpha$  chain to which 8 to 10 amino acid long peptides will bind. The  $\alpha$  chain is divided into three domains: the conserved  $\alpha_3$  domain containing the C-terminal transmembrane region and the  $\alpha_1$  and  $\alpha_2$  domains. The  $\alpha_1$  and  $\alpha_2$  domains form a structure consisting of a platform of eight antiparallel  $\beta$  strands and two antiparallel  $\alpha$  helices on top. The groove formed by the two  $\alpha$  helices and the  $\beta$  strand platform is the peptide-binding groove for antigenic peptides. Two binding pockets within the peptide binding groove of the MHC-I molecule determine the peptide repertoire binding to a given HLA allele. The binding of a peptide and the  $\beta_2$  sub-unit are necessary for MHC-I molecule stabilization and migration to the cell membrane.

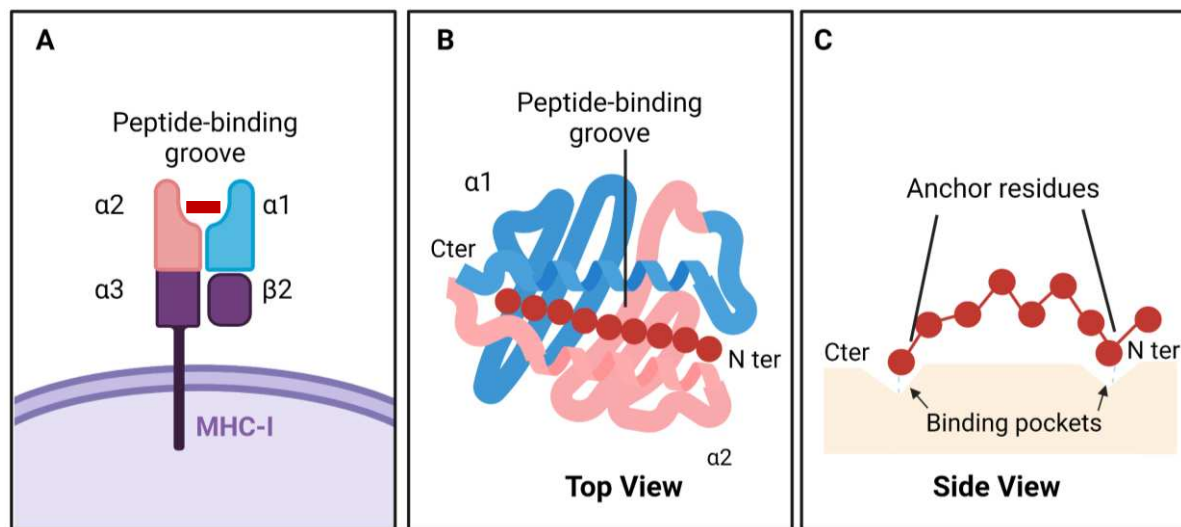


**Figure 13. Schematic representation of the structure of MHC-I molecules.** (A) MHC-I-peptide complex constituted by the two sub-units  $\alpha_1$  and  $\alpha_2$  harboring the peptide groove, the  $\alpha_3$  sub-unit and the  $\beta_2m$  sub-unit (B) and (C) Top and side views of the peptide binding groove with two anchoring residues binding pockets formed by the  $\alpha_1$  and  $\alpha_2$  sub-units.

Polymorphism of the  $\alpha$  chain is reflected on the variability of amino acid sequences of the  $\alpha 1$  and  $\alpha 2$  sub-domains, which control the nature of the peptide binding groove and determine the antigenic specificities of the MHC-I molecules. Peptide binding depends on specific anchor residues that interact with the binding pockets in the groove and on the interactions between the residues of adjacent amino acids and the  $\alpha$  helices surrounding them (Figure 13). Therefore, the nature of the peptide sequence will determine its capacity to bind to a given MHC-I allele.

## 2. Major Histocompatibility Complex Class II (MHC-II)

The HLA class II loci encode for three variable MHC-II surface molecules HLA-DP, HLA-DQ and HLA-DR and two non-variable molecules HLA-DM and HLA-DO. MHC-II molecules are heterodimeric glycoprotein complexes composed of an  $\alpha$  chain and a  $\beta$  chain non-covalently bound, each chain is divided into two sub-domains 1 and 2 (Figure 14). For HLA-DP and HLA-DQ molecules, a single gene encodes each  $\alpha$  and  $\beta$  chain (DPA1 and DPB1 and DQA1 and DQB1, respectively) (Figure 12). In the case of HLA-DR molecules, one gene encodes the  $\alpha$  chain (DRA) and one or two genes encode the  $\beta$  chain (DRB1 and or DRB3) (Figure 12). Polymorphic residues are mainly found in the  $\beta$  chains of the three MHC-II molecules<sup>146</sup>.

MHC-II molecules anchor to the cell membrane through their C-terminal region (Figure 14, panel A). The peptide-binding groove formed by the  $\alpha 1$  and  $\beta 1$  sub-domains consists of two  $\alpha$  helices on a  $\beta$ -pleated sheet platform, and the peptide sits between the helices as in MHC-I molecules<sup>147,148</sup>. The conformation of the peptide-binding groove allows the binding of peptides ranging from 12 to 25 amino acids in length, longer than MHC-I peptides (Figure 14 panel B).

The nine amino acid core has 3 to 4 MHC-II anchor residues. The peptides adopt a stretched polyproline conformation in which some amino acid side chains, including the anchor residues, point toward the peptide-binding groove and some residues are exposed and potentially constitute T cell receptor (TCR) contact sites<sup>149</sup>. Similar to MHC-I molecules, the binding of the peptide depends on interactions between the backbone with the  $\alpha$  helices and on various interactions between the MHC-II anchor residues and the binding pockets (Figure 14). Polymorphism is translated in the diversity of the binding pockets, resulting in different pockets accepting different peptide anchor residues. Therefore, different peptides bind to different alleles<sup>150</sup>.

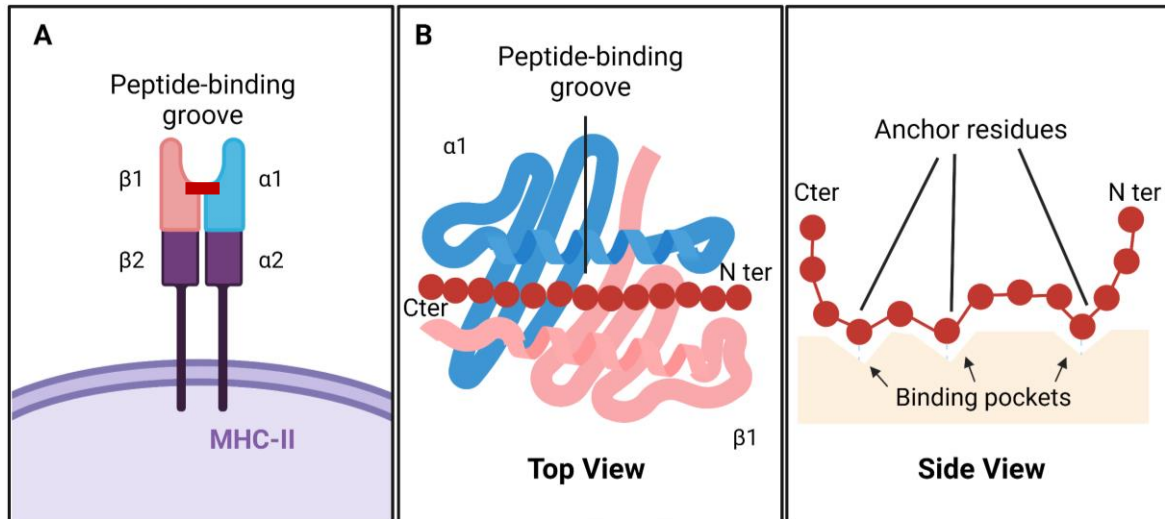


**Figure 14. Schematic representation of the MHC-II peptide-binding groove.** (A) MHC-II-peptide complex constituted by a heterodimer of  $\alpha$  and  $\beta$  chains each composed of two sub-units, the  $\alpha 1$  and  $\beta 1$  sub-units harboring the peptide. (B) Top and side views of the peptide binding groove with three anchoring residues binding pockets formed by the  $\alpha 1$  and  $\beta 1$  sub-units.

I will now proceed to briefly describe the MHC-I antigen presentation pathway with a focus on endogenous presentation since there might be a cross talk with MHC-II-restricted antigen presentation, the subject of my thesis work.

## B. Antigen presentation by MHC-I molecules

MHC-I molecules present peptides derived from endogenous sources such as neosynthesized viral proteins or cytosolic and nuclear cellular proteins. They can also present peptides derived from exogenous sources such as pathogens or cancer cells. The peptide-loaded MHC-I molecules expressed at the cell surface are recognized by the TCR of  $CD8^+$  cytotoxic lymphocytes allowing a rapid detection of tumor or infected cells.

### 1. Endogenous antigen presentation by MHC-I molecules

Historically, MHC-I molecules are known to present endogenous peptides derived from cytosolic or nuclear proteins. The generation of MHC-I endogenous peptides is dependent on protein synthesis and the Ubiquitin-proteasome System (UPS) to degrade them.

#### a) *The role of the proteasome*

MHC-I endogenous antigen presentation begins when proteins are recognized and degraded by the UPS<sup>151</sup>. The UPS ensures protein degradation via two successive steps. First, the substrate is tagged by covalent attachment of multiple ubiquitin molecules, and then the tagged protein

is degraded by the proteasome with release of free and reusable ubiquitin<sup>152</sup>. There is a distinction between the constitutive proteasome, ubiquitously expressed in every cell, and the immunoproteasome, more active and expressed in professional antigen presenting cells (pAPC) upon IFN $\gamma$  and TNF induction<sup>153</sup>. The constitutive proteasome 26S is composed of a 20S subunit, ensuring the proteolytic activity of the complex, and a 19S subunit that recognizes ubiquitinated proteins to be translocated to the 20S subunit<sup>154</sup> (Figure 15). The constitutive proteasome generates peptides containing an acid C terminal end that prevents them from properly binding MHC-I molecules<sup>155,156</sup>. Immunoproteasomes contain replacements for the three catalytic subunits of standard proteasomes: LMP2, LMP7 and LMP10, which generate peptides with a hydrophobic or basic C-terminal increasing their affinity to MHC-I molecules<sup>157</sup> (Figure 15). Modifying these three catalytic subunits affects the MHC-I peptide repertoire and antiviral CD8<sup>+</sup>T cell responses<sup>158,159</sup>.

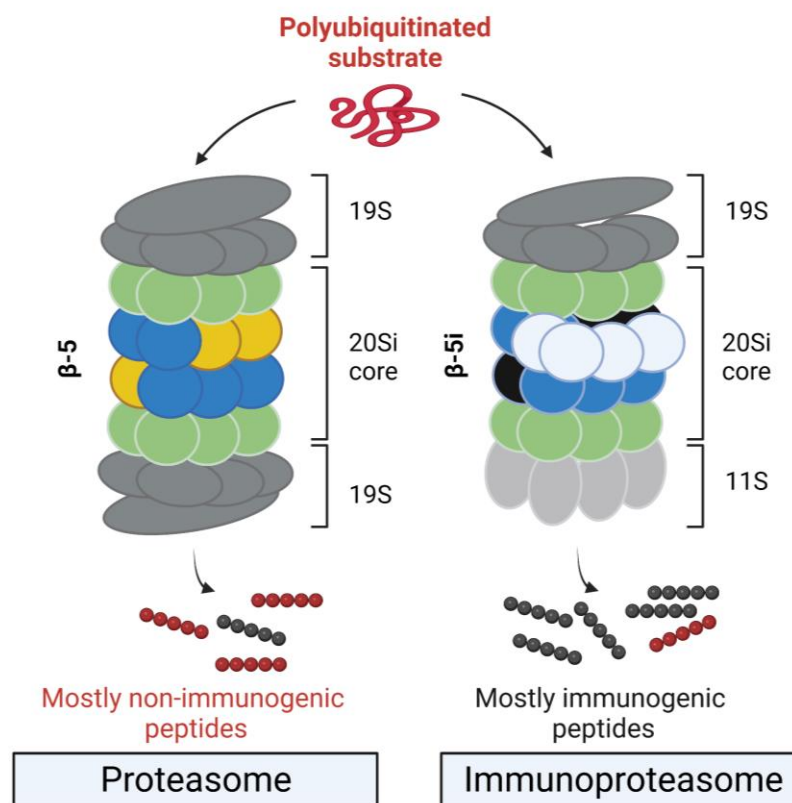


**Figure 15. The constitutive proteasome and the immunoproteasome.** The constitutive proteasome 26S is composed of a 20S sub-unit and two 19S sub-units. The 20S sub-unit, composed of four heptameric rings containing catalytically active  $\beta$ -sub-units, ensures the proteolytic activity of the complex and the 19S sub-units recognize and target ubiquitinated proteins for degradation. In the immunoproteasome, three catalytic  $\beta$ -sub-units are modified, improving its capacity to generate high affinity MHC-I restricted peptides.

b) *The proteasome substrates*

The generation of peptides presented by MHC-I molecules depends, on the one hand, on protein degradation by the UPS and, on the other hand, on ribosomal translation and protein synthesis<sup>151,160</sup>. Inhibiting protein synthesis or proteasome degradation drastically decreases MHC-I-restricted antigen presentation<sup>161–163</sup>. The source of MHC-I peptides can be short-lived proteins (degraded in less than 10 min) or long-lived peptides (degraded on average in 24h)<sup>164–168</sup>, the preferred source is still a matter of debate<sup>169</sup>. Amongst the short-lived proteins, we can distinguish mature and functional proteins from the products of transcription or translation errors, in which case they are called Defective Ribosomal Products (DRiPs)<sup>165,166,168,170</sup>. The existence of DRiPs was first suggested to explain kinetic observations of virus-infected cells that were recognized by antigen-specific CD8<sup>+</sup> cytotoxic T cells soon after infection, long before the source proteins could be detected<sup>164,171</sup>. Although it was first suggested that DRiPs derived from deliberate premature termination or nascent-chain misfolding, the definition has broadened to include defective polypeptides emerging from alternative or defective mRNAs<sup>172</sup>, ribosomal frame shifting<sup>173,174</sup>, downstream initiation on bona fide mRNAs<sup>175</sup> and other transcription errors<sup>176</sup>.

c) *Peptide transport to the ER and loading on MHC-I molecules*

The peptides are transported from the cytosol to the ER lumen, by the ATP-binding transporter associated with antigen processing (TAP). TAP allows the translocation of peptides ranging from 8 to 40 amino acids but favors peptides between 8 and 12. Cells deficient of either of the TAP subunits (TAP1 or TAP2) do not form MHC-I-peptide complexes because there is no peptide translocation to the ER<sup>154</sup>. The ER aminopeptidase associated with antigen processing (ERAAP) as well as its human homologs ERAP1 and ERAP2 shorten long peptides on their N-terminal end to obtain an optimal length to bind to MHC-I molecules thus making ERAAP crucial to form stable MHC-I-peptide complexes<sup>177–180</sup>.

The nascent heavy  $\alpha$  MHC-I chain is anchored to the ER membrane during translation and is then N-glycosylated and stabilized by the chaperone Calnexin (CANX) until the incorporation of the  $\beta$ 2m subunit when CANX is exchanged with another chaperone Calreticulin (CRT)<sup>181</sup> (Figure 16). The protein ERp57 then binds the MHC-I- $\beta$ 2m complexes and stabilizes them. Tapasin (Tsn) binds to ERp57 and, along with MHC-I- $\beta$ 2m and TAP, form the peptide-loading complex (PLC)<sup>154</sup> (Figure 16). The PLC orchestrates stringent peptide proofreading and quality control processes; in fact, Tsn selects high-affinity peptides by creating an energy barrier

through a widening of the peptide groove and promotes the exchange of intermediate- and low-affinity peptides for high-affinity epitopes<sup>182</sup>. The structural homolog of Tsn, TAP-binding protein-related (TAPBPR), also recognizes peptide-receptive MHC-I in the ER and catalyzes peptide proofreading thus altering the MHC-I peptidome<sup>183</sup>. Peptide proofreading and proper MHC-I-peptide assembly is coupled to glycan processing of MHC-I molecules in the ER<sup>184</sup>. The stable MHC-I-peptide complexes then leave the PLC and are transported to the Golgi apparatus and then to the cell surface where they interact with CD8<sup>+</sup>T cells (Figure 16).

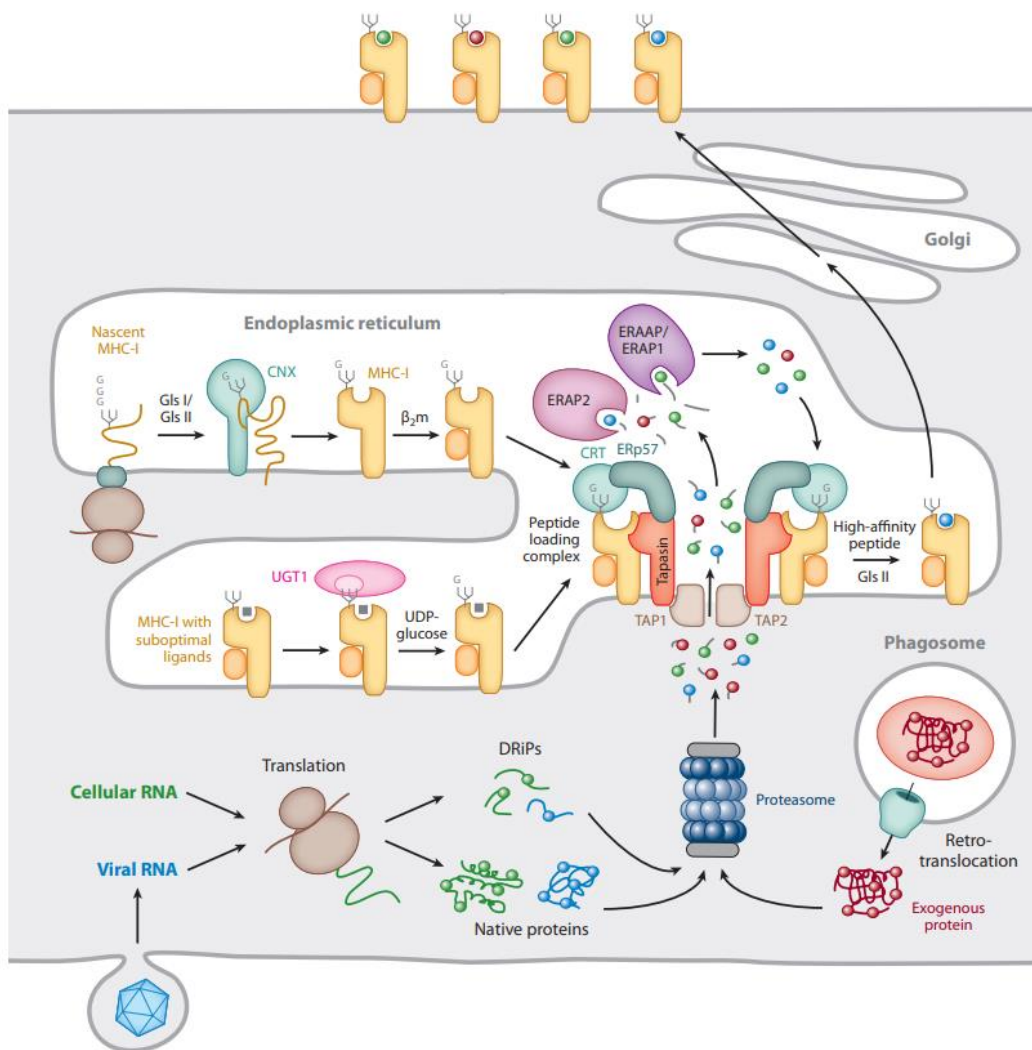


**Figure 16. The MHC-I antigen presentation pathway<sup>154</sup> (adapted from Blum *et al.*, 2013).** Peptides derived from cellular translation, viral protein translation or non-functional peptides called DRiPs and degraded by the proteasome are translocated to the ER by the transporter TAP. The peptides are loaded directly on MHC-I molecules or shortened by ERAAP/ERAP1 or ERAP2 before loading. The MHC-I-peptide complexes are released by the PLC and transported to the plasma membrane to interact with CD8<sup>+</sup>T lymphocytes.

## 2. Exogenous antigen presentation by MHC-I molecules

APCs can process and present antigenic peptides derived from phagocytosed external sources on MHC-I molecules (virus-infected cells, pathogens and tumoral cells). The antigens can also be routed into phagosomes in a surface receptor-mediated manner. This antigen presentation pathway is named cross-presentation and plays a role in CD8<sup>+</sup>T cell cytotoxic response initiation<sup>185</sup>. There are two main mechanisms of cross-presentation: the cytosolic pathway and the vacuolar pathway.

### a) *Cytosolic pathway*

This pathway is modulated by surface receptors recognizing danger patterns on APCs. During HIV infection, the type-C lectin DC-SIGN captures viral particles by binding the envelope protein gp120 and promotes CD4<sup>+</sup>T cell trans-infection<sup>186,187</sup>. Although the transport mechanisms remain poorly understood, the cytosolic pathway can be TAP- and proteasome-dependent. It is suggested that the ER-associated (ERAD) translocation machinery is recruited to phagosomes and helps translocating the exogenous antigens to the cytosol and then the proteasome to generate MHC-I peptides<sup>188</sup>. Traffic regulator proteins, such as Sec22b, regulate the traffic of the PLC from the ER to phagosomes. Peptide loading could overall happen in both ER and phagosomes since both resident aminopeptidases seem implicated in peptide generation<sup>189,190</sup> (Figure 16).

### b) *Vacuolar pathway*

Upon phagocytosis of a pathogen, antigenic peptides can be directly generated or pre-processed by cathepsins<sup>191</sup>. MHC-I molecules and the PLC can be already present in phagosomes and thus peptide loading can occur on site<sup>192</sup>. MHC-I molecules could also be recycled from the cell surface<sup>193,194</sup>. This pathway is resistant to proteasome inhibitors but sensitive to inhibitors of lysosomal proteolysis, particularly cathepsin S inhibitors, confirming that both antigen processing and loading on MHC-I molecules occurs inside phagosomes in a proteasome- and TAP-independent manner<sup>185</sup> (Figure 16).



## C. Antigen presentation by MHC-II molecules

MHC-II molecules are historically known to present antigens derived from external sources (exogenous presentation), such as internalized pathogens, to CD4<sup>+</sup>T cells but they can also present antigens derived from internal sources (endogenous presentation) such as cytosolic and nuclear proteins or neosynthesized viral proteins. I will proceed to describe the trafficking of MHC-II molecules, the different mechanisms participating in the generation of peptides as well as the different possible sources.

### 1. Expression of MHC-II molecules and control by CIITA

The expression of MHC-II molecules is constitutive in APCs and controlled by the Class II Major Histocompatibility Complex Transactivator CIITA<sup>195-197</sup>. The CREB-NFY-RFX complex recruits CIITA on the conserved regions X1, X2 and Y of the « X box region » upstream of the Class II locus promoter<sup>198</sup>. Expressing CIITA alone is sufficient to induce the expression of MHC-II molecules in any cell type<sup>199</sup>. CIITA expression is inducible by IFN $\gamma$  and other inflammatory signals<sup>195,200</sup> and also regulates the expression of genes encoding proteins involved in MHC-II antigen presentation such as the invariant chain Ii (CD74) and the chaperones HLA-DM and HLA-DO<sup>199</sup>. The differential activation of certain promoters and isoforms of CIITA in a cell-specific manner finely tune the expression of the MHC-II locus<sup>200-202</sup>.

### 2. MHC-II antigen presentation route

#### a) ER assembly of MHC-II molecules

MHC-II  $\alpha$  and  $\beta$  glycoproteins are synthesized and assembled in the ER where they interact with different chaperones such as CANX and the invariant chain Ii (Figure 18). The ER chaperone CANX associates rapidly with newly synthesized MHC-II  $\alpha$  and  $\beta$  chains and with Ii trimers. A combination of pulse-chase and cross-linking experiments showed that this association with CANX endures until the formation of a nonameric complex composed of a trimer of Ii and three  $\alpha\beta$  heterodimers<sup>203</sup> and that CANX only dissociates once the  $\alpha\beta$ -Ii complex is addressed out of the ER<sup>204</sup>. This suggests that CANX plays a key role in the assembly process of the nonamer. Nevertheless, it was later shown that inhibiting the Ii-CANX interaction does not prevent  $\alpha\beta$ -Ii nonamers from forming but enhances Ii pre-endosomal degradation; thus suggesting CANX is not absolutely required for nonamer formation but rather retains Ii and  $\alpha$  and  $\beta$  chains in the ER to inhibit their degradation<sup>205</sup>. Unlike the GRP94 and ERp72 ER chaperones that only interact

with MHC-II molecules, CANX is the only one that can also interact with the invariant chain li and thus with the three elements of the  $\alpha\beta$ -li complexes<sup>206,207</sup>.

The invariant chain li is a non-polymorphic transmembrane glycoprotein that acts as a chaperone promoting the assembly  $\alpha\beta$ -li nonamers. In addition, li protects the peptide-binding groove on MHC-II molecules via its CLIP domain<sup>208-210</sup>, thus preventing the binding of low affinity peptides to MHC-II molecules in the ER or to intact polypeptides also present in the ER<sup>210,211</sup>. The invariant chain is composed of a 30 residue cytoplasmic tail at its N-terminal region, a transmembrane domain between residues 30 and 60; and a C-terminal ER luminal domain<sup>212-214</sup> (Figure 17). Remarkably, the cytoplasmic region contains a di-leucine-targeting motive that directs  $\alpha\beta$ -li complexes into the endocytic pathway from the trans-Golgi network or via rapid internalization from the cell membrane<sup>212,215,216</sup> and a di-arginine ER retention motive (RXR) involved in li trimerization<sup>217</sup> (Figure 17). Thereafter, li plays a dual role in MHC-II biology, directing MHC-II molecule trafficking through its cytosolic tail and protecting the peptide-binding groove from low-affinity peptide binding with its CLIP domain (Figure 18). Four isoforms of li have been described in humans and are named based on their molecular weight: p33, p35, p41 and p43; p33 being the prototypic and most abundantly expressed<sup>218</sup>. p35 and p43 are N-terminally extended due to the use of an alternative upstream start codon while p41 and p43 both contain an additional luminal domain due to alternative splicing<sup>219</sup>.

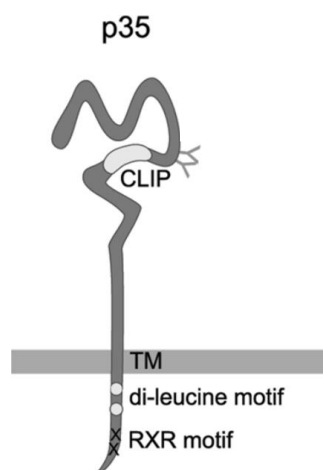


**Figure 17. The different domains on the li invariant chain<sup>217</sup> (adapted from Cloutier *et al.*, 2021).**

The 30-residue N-terminal cytoplasmic tail contains a di-leucine-targeting motive that directs MHC-II complexes into the endocytic pathway and a di-arginine (RXR) motive involved in li trimerization. The transmembrane domain (TM) allows anchoring to cytosolic membranes. The C-terminal ER lumen domain contains the peptide CLIP that ultimately stabilizes MHC-II molecules before its exchange with high-affinity peptides.

b) *Traffic of  $\alpha\beta$ -li complexes*

The di-leucine motive that targets  $\alpha\beta$ -li complexes to the endocytic pathway allows the interaction of li with clathrin adaptors AP-1 and AP-2<sup>220,221</sup>. AP-1 is an adaptor of the trans-Golgi network and AP-2 a cell membrane adaptor. ER-exiting  $\alpha\beta$ -li complexes can follow two routes: traffic to the plasma membrane and then rapidly re-internalize in the endocytic pathway<sup>216</sup> via AP-2 or traffic directly to the MHC-II loading compartment (MIIC) via the trans-Golgi network<sup>203</sup> in an AP-1-dependent manner (Figure 18). AP-2 endocytosis is preferentially observed in B cells, immature dendritic cells (DC) and Hela cells<sup>222</sup>, whereas in mature DCs MHC-II molecules traffic directly to the MIIC<sup>223</sup>.

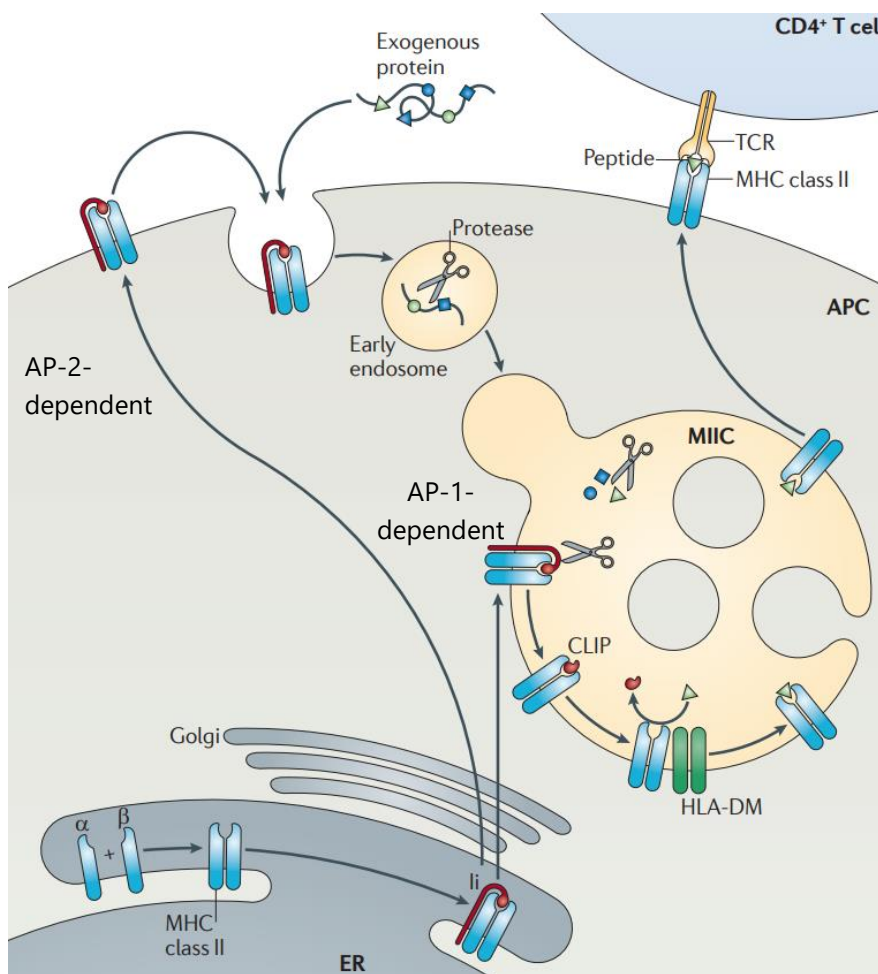


**Figure 18. The MHC-II antigen presentation pathway<sup>153</sup> (adapted from Neeffjes *et al.*, 2011).** The  $\alpha\beta$ -li complexes are synthesized in the ER and then traffic through the trans-Golgi network to join the plasma membrane.  $\alpha\beta$ -li complexes can traffic to the plasma membrane and then rapidly re-internalize in the endocytic pathway in an AP-2-dependent manner to reach the MHC-II loading compartment (MIIC) or they can traffic directly to the MIIC in an AP-1-dependent manner. In the MIIC, li is degraded by vesicular proteases. CLIP is liberated from the peptide-binding groove by the chaperone HLA-DM. The newly formed  $\alpha\beta$ -peptide complexes are then transported to the plasma membrane where they interact with the TCR of CD4<sup>+</sup>T cells.

### c) *Antigen loading in the MIIC*

The MIIC was first described as a late endosome-like acidic compartment presenting a multivesicular (MVB) or multilamellar morphology when visualized by electron microscopy<sup>224</sup> (Figure 18). This compartment assembles MHC-II molecules, the chaperone HLA-DM (Figure 18) and lysosomal cathepsins such as B and S responsible for the generation of antigenic peptides<sup>225,226</sup>. Conventional late-endosome markers and tetraspanin markers also serve to characterize the MIIC: Lamp-1, CD63 and CD82. Tetraspanins are believed to facilitate the interaction between HLA-DM and MHC-II molecules<sup>227</sup>. According to the cell type, the MIIC seems to have a different morphology: MVB, late endosome, multilamellar or a combination of these<sup>228</sup>, which would reflect the maturation state of the MIIC<sup>153</sup>. Regions of the MIIC membrane invaginate to form intraluminal vesicles (ILVs) where MHC-II molecules and HLA-DM are incorporated<sup>229</sup>.

Once the  $\alpha\beta$ -I $\alpha$  complex arrives in the MIIC, due to acidification of the endolysosomal compartments, I $\alpha$  is progressively cleaved by pH-dependent cathepsins. I $\alpha$  is ultimately fully degraded with the exception of a fragment of around three kDa named CLIP embedded in the peptide-binding groove of MHC-II molecules<sup>230</sup> (Figure 19). CLIP is then in turn exchanged with high affinity peptides in the MHC-II peptide-binding groove<sup>208,231,232</sup> (Figure 18).

The processing of I $\alpha$  critically determines the timing and location of MHC-II-restricted peptide loading. Asparagine endopeptidase (AEP) has been described as the first cathepsin to process I $\alpha$ <sup>233</sup>. Cathepsins B, L and S are believed to play a major role in the last steps of I $\alpha$  degradation<sup>234,235</sup>. Cathepsin S plays a major role in I $\alpha$  processing in professional APCs *in vivo*<sup>236-238</sup> and *in vitro*<sup>239,240</sup> (Figure 19). Cath S also regulates I $\alpha$  processing in human CD4<sup>+</sup>T cells expressing HLA-DR<sup>241</sup>. Cathepsin L plays an important role in the final processing steps of I $\alpha$  in thymic epithelial cells and participates in the selection of CD4<sup>+</sup>T cells<sup>235</sup>. Moreover, I $\alpha$  p41 isoform contains a motive recognized by cathepsin L<sup>242,243</sup> that stabilizes its mature form, blocking its activity<sup>244,245</sup>. This suggests that the processing of the invariant chain can regulate cathepsin activity.

The implication of each cathepsin in I $\alpha$  processing and thus MHC-II trafficking through the endosomal route can vary according to the type of APC<sup>246,247</sup>. I $\alpha$  proteolysis steps are coordinated by HLA-DM and cathepsins and generate several maturation cleavage

intermediates: the 22-kDa Lip fragment visible after treatment with protease inhibitor leupeptin; and the 10-kDa Slip fragment that will be later cleaved to become CLIP (Figure 19).

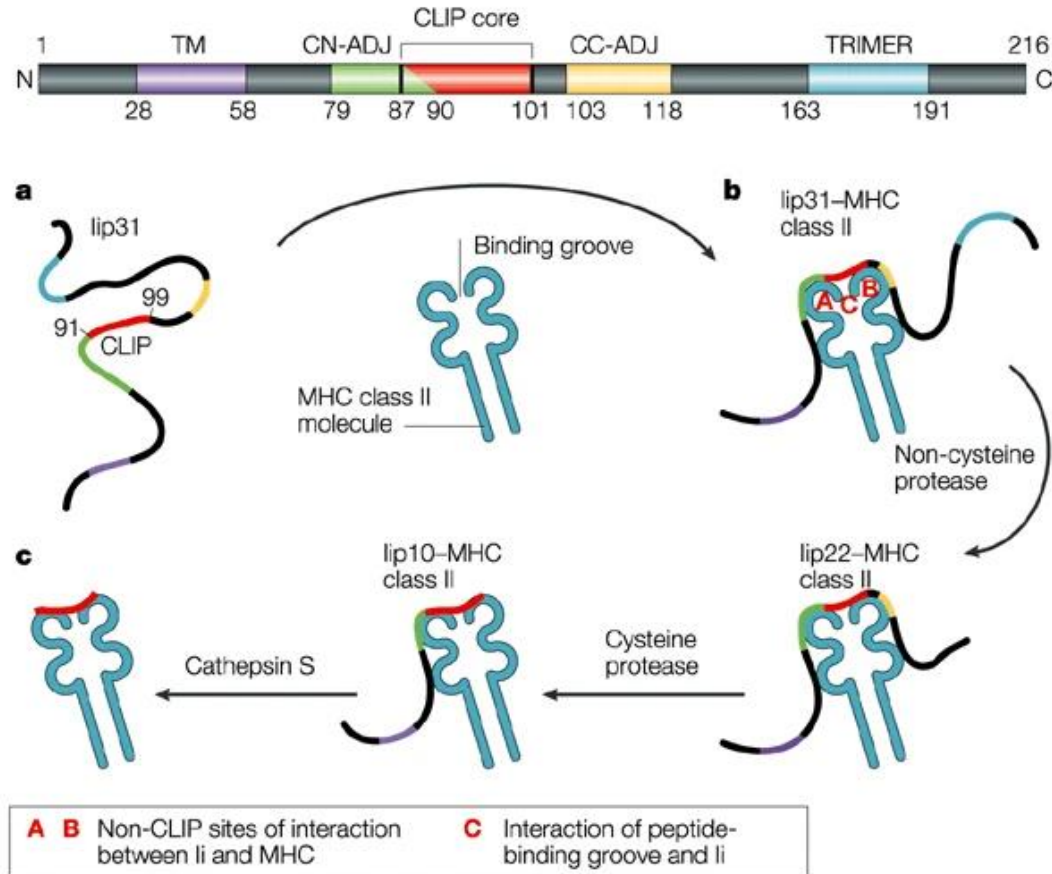


**Figure 19. The processing of Ii by lysosomal proteases<sup>248</sup> (adapted from Sercarz & Maverakis, 2003).** The processing of the Ii invariant chain is regulated by lysosomal proteases. Stepwise processing of Ii, several of its functional sites of interaction with MHC class II molecules are indicated: TM, transmembrane; CLIP, class II-associated Ii peptide; CN-ADJ, CLIP amino-terminal adjacent peptide; CC-ADJ, CLIP carboxy-terminal adjacent peptide; TRIMER, trimerization domain. (a) and (b), sites A and B on the MHC-II molecule present areas that have a binding affinity for regions of Ii; site C is the peptide binding groove binding the CLIP peptide. After arrival in vesicular compartments, there is a stepwise reduction of the flanking ends of Ii until final cleavage by cathepsin S produces  $\alpha\beta$ -CLIP. (c), subsequently, HLA-DM molecules catalyze the removal of CLIP and its exchange with high affinity peptides.

The CLIP region plays an essential role in the chaperone functions of Ii<sup>209,249</sup> and inhibits the binding of low affinity peptides on MHC-II molecules<sup>250,251</sup>. The presence of CLIP in the binding groove suffices to ensure trafficking of MHC-II molecules<sup>252</sup>. HLA-DM plays the role of a chaperone that lightly modifies the MHC-II peptide-binding groove and is also a versatile

peptide editor that selects high-stability  $\alpha\beta$ -peptide complexes by kinetic proofreading before these complexes are presented to T cells<sup>253</sup>. HLA-DM exchanges CLIP with high affinity peptides<sup>254,255</sup> (Figure 18). The role of HLA-DM<sup>256</sup> was discovered in mutant APC cell lines that showed an impairment in the presentation of peptides derived from internalized proteins. When the MHC-II immunopeptidome (peptide repertoire presented by MHC-II molecules at a specific time point) was analyzed, it contained numerous CLIP peptides associated to Ii, showing an impairment of CLIP exchange for high affinity peptides on MHC-II molecules in the absence of HLA-DM<sup>257-259</sup>. HLA-DM also stabilizes unbound "empty" MHC-II molecules and regulates their maturation<sup>260</sup>. In the absence of HLA-DM, a failed peptide-editing process leads to the appearance of MHC-II-peptide complexes that are structurally immature in vesicles and at the plasma membrane<sup>259</sup>. Interestingly, in cells not expressing Ii (hence not expressing CLIP) an aberrant HLA-DM-HLA-DR association and HLA-DM retention in the ER was observed showing a possible role of Ii in maintaining the function of HLA-DM<sup>261</sup>.

Human B-lymphocytes, certain subtypes of DCs and thymic epithelial cells<sup>262</sup> express the chaperone HLA-DO, a negative regulator of HLA-DM<sup>263</sup>. HLA-DO-dependent inhibition of HLA-DM is high in naïve B cells and immature DCs. This could be explained by a more tolerogenic immunopeptidome (less HLA-DM activity and broader peptide repertoire) in naïve APCs versus a more immunity-induced immunopeptidome (more HLA-DM activity thus more high-stability peptides) in mature APCs<sup>223</sup>. Alvaro-Benito *et al.* showed, by an immunopeptidomics approach, that different levels of HLA-DM affect the HLA-DR immunopeptidome in a quantitative and qualitative manner<sup>264-266</sup>, thus highlighting the importance of HLA-DM activity in the MHC-II immunopeptidome.

*d) Traffic of MHC-II $\alpha\beta$ -peptide complexes to the cell membrane*

After Ii degradation,  $\alpha\beta$ -peptide complexes are transported from proteolytic endosomal/lysosomal MIIC compartments to the cell surface where they interact with CD4<sup>+</sup>T cells (Figure 18). This occurs by direct transport and fusion of the MIIC with the plasma membrane<sup>267</sup> or via an intermediary tubular step, which is the case for activated DC's<sup>268</sup> (Figure 20). The mechanism by which MIICs fusion with the plasma membrane remain unclear<sup>153</sup> but have been studied further in mature DCs. In mature DCs, membrane-bound proteins such as MHC-II, HLA-DM and tetraspanins are transferred from ILVs to the surface membrane of the MIIC that fuses with the plasma membrane<sup>269</sup>.

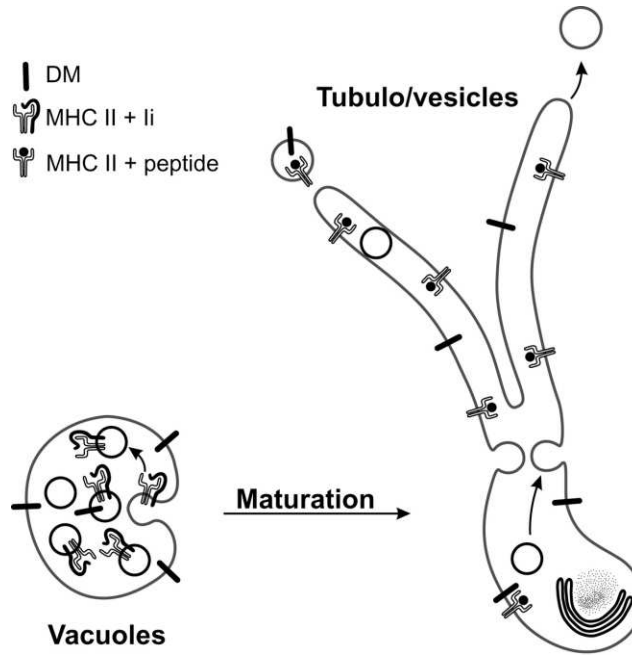


**Figure 20. Tubulation of multivesicular MIICs during DC maturation<sup>268</sup> (adapted from Kleijmeer *et al.*, 2001).** Upon stimulation, MIICs in DCs undergo a dramatic shape change from vacuolar to tubular, most likely by fusion of the MIIC internal membrane vesicles with the limiting membrane. This implies that MHC II-rich internal membranes stored in the lumen of the MIIC relocate to the limiting membrane, allowing egress of MHC II from these tubules to the plasma membrane. The final transport step to the cell surface is probably mediated by transport vesicles, which bud from the tubular MIICs and non-selectively incorporate MHC II molecules. Because of MHC II translocation to the DM-rich limiting membrane, contact between DM and MHC II is increased, which may facilitate peptide loading and editing during maturation.

Both direct and tubular transport mechanisms imply vesicle movement in a bidirectional manner along microtubules and the actin-myosin cytoskeleton.

In B-lymphocytes, the inhibition of Myosin II affects cell-surface expression levels of MHC-II molecules and the targeting of BCR-antigen complexes into lysosomes and thus the antigen processing and formation of  $\alpha\beta$ -peptide complexes<sup>270</sup>. In a genome-wide multidimensional RNAi screening, Paul *et al.* identified the motor Myosin 1E as being recruited by the effector protein ARD7EP controlled by GTPase ARL14/ARF7; and controlling the movement of MHC-II vesicles along the actin cytoskeleton in human DCs<sup>271</sup> (Figure 21). It would be relevant to study the role of Myosin VI in MIIC traffic given its essential role in the transport and steady-state localization of vesicles and organelles, in the dynamic remodeling of the plasma membrane and its role on exocytosis and secretion<sup>272,273</sup>.

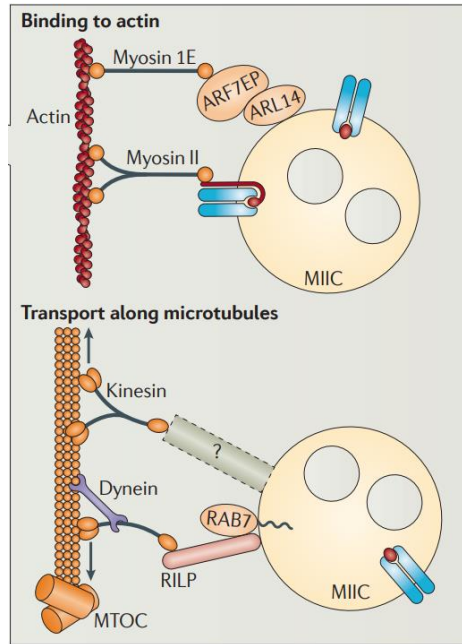


**Figure 21. Transport of  $\alpha\beta$ -peptide complexes to the cell membrane<sup>153</sup> (adapted from Neefjes *et al.*, 2011).** The MIIC is transported to the plasma membrane via the actin-myosin cytoskeleton or along the microtubules: by the ARL14/ARF7EP complex and Myosins 1E and II, or by Rab7 and the dynein-kinesin cytoskeleton, respectively.

The MIIC can also traffic along microtubules motored by kinesin motors in the direction of the plasma membrane and by dynein motors in the direction of the nucleus<sup>274</sup> (Figure 21). The small GTPase Rab7, found on late endosome vesicles, may accomplish this bidirectional movement of the MIIC. Rab7 on the MIIC forms a complex with RILP, ORP1L and  $\beta$ III spectrin to interact with Dynein and Kinesin and regulate vesicle movement<sup>275</sup>.

A fraction of  $\alpha\beta$ -peptide complexes acquires a stable conformation resistant to dissociation by SDS. Several teams have used SDS stable MHC-II  $\alpha\beta$  dimer detection as a marker of maturation of MHC-II molecules<sup>276-278</sup>. Mature  $\alpha\beta$ -peptide complexes can be found in micro domains known as lipid rafts at the surface of APCs<sup>279</sup> along with HLA-DM and other markers such as CD82 and CD86<sup>280</sup>. These micro domains serve the purpose of clustering and favoring antigen presentation to CD4<sup>+</sup>T cells<sup>279,281</sup>.

Unlike HLA-DM and Ii, MHC-II molecules do not have an internalization sequence in their cytoplasmic region. Therefore, the turnover of MHC-II molecules is ensured by their ubiquitination.



### 3. What becomes of surface MHC-II molecules

Once at the plasma membrane, MHC-II molecules recycle to early endosomes and back to the plasma membrane. This was shown by the presentation of antigenic epitopes that only require unfolding and limited proteolysis and do not require li-dependent MHC-II transport<sup>282</sup>.

Ubiquitination seems to play a role in  $\alpha\beta$ -peptide complex degradation<sup>283,284</sup>. MHC-II molecules can be ubiquitinated on a single lysine at position 225 in the cytoplasmic domain of the  $\beta$ -chain<sup>283</sup>. Membrane-Associated RING-CH-domain containing (MARCH) E3 ubiquitin ligases are a family of E3 ubiquitin ligases that participate in the ubiquitination of MHC-II molecules, in particular MARCH-I in B cells and DCs<sup>284-286</sup>. Ubiquitination of MHC-II molecules could play a role in recycling MHC-II molecules to the endosomal pathway<sup>153,287</sup>.

In immature DCs, there is a rapid turnover of MHC-II molecules<sup>288</sup> (Figure 22). Upon DC activation, this turnover is strongly decreased and the half-life of  $\alpha\beta$ -peptide complexes is increased<sup>289</sup>. Results from MARCH-I KO and K255R ubiquitination-mutant mice demonstrated that MARCH-I regulates MHC-II surface expression by ubiquitinating MHC-II molecules<sup>287</sup>. Moreover, DC activation induces a decrease of MHC-II ubiquitination<sup>287</sup> (Figure 22). In fact, MARCH-I mRNA expression is rapidly downregulated following DC activation. Furthermore, MARCH-I has a short half-life and is regulated by auto-ubiquitination, which explains that the termination of March-I mRNA expression leads to a rapid drop in March-I protein levels<sup>290</sup>. Inhibiting lysosomal proteolysis delays March-I-induced MHC-II degradation, which suggests that ubiquitinated MHC-II is degraded in late endosomes/lysosomes. The expression of CD83 on mature DCs inhibits MARCH-I and promotes surface expression of CD86 and MHC-II molecules<sup>291</sup>. Both CD83 and MARCH-I are found in early and recycling endosomes where MHC-II ubiquitination is thought to occur<sup>56</sup>.

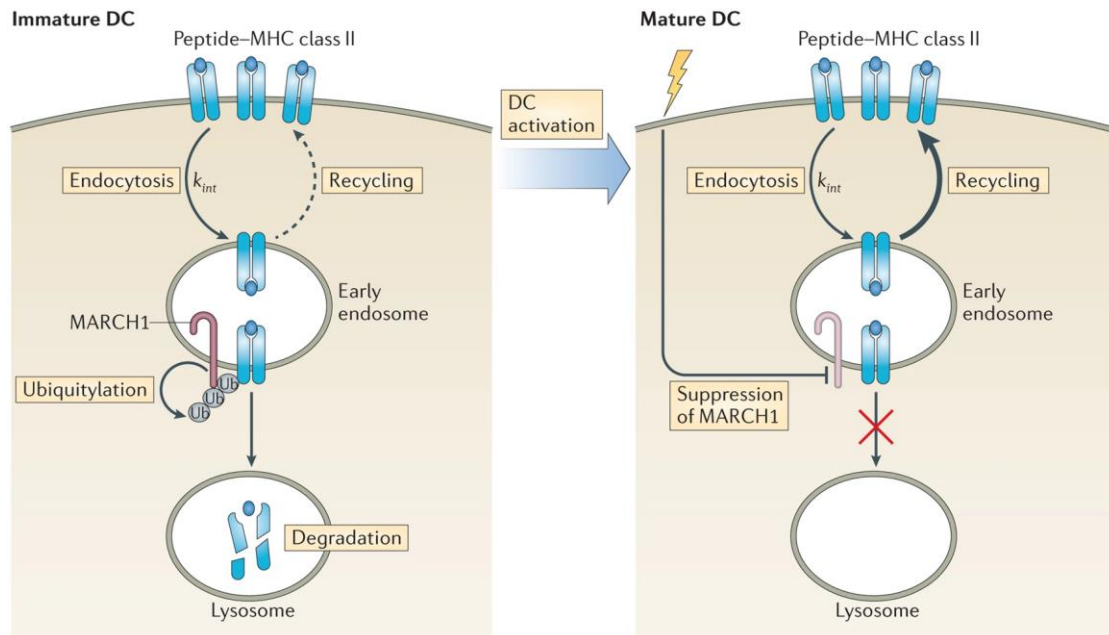


**Figure 22. The role of ubiquitination in MHC-II degradation<sup>56</sup> (adapted from Roche & Furuta, 2015).** In immature and mature DCs, surface  $\alpha\beta$ -peptide complexes are recycled in early endosomes. MARCH-I ubiquitinates MHC-II molecules to target them to lysosomal degradation. Upon DC maturation, MARCH-I expression is inhibited, which prevents MHC-II ubiquitination and subsequent degradation. Recycling to the cell membrane is then favored.

Anti-inflammatory cytokine IL-10 up-regulates MARCH-I expression and MHC-II ubiquitination<sup>292</sup>, which reduces MHC-II molecule survival<sup>284,285,287</sup>. Although MARCH-I is also expressed by resting B cells and macrophages, it remains to be determined whether activation of these cells also suppresses MARCH-I. In B cells, MHC-II molecules are also ubiquitinated but do not seem to accumulate in lysosomes. Recent data suggests that different ubiquitin chain lengths in B cells and DCs may affect MHC class II localization. In DCs, MHC-II molecules contain longer ubiquitin chains that preferentially target them to late endolysosomal compartments, whereas in B cells MHC-II molecules contain short ubiquitin chains that target them to early endosomes<sup>293</sup>. Overall, in DCs and B cells, MARCH-I regulates MHC-II ubiquitination and survival but the role of MHC-II ubiquitination in internalization kinetics remains controversial<sup>290</sup>. Interestingly, in mice bearing mutant MHC-II molecules unable to be ubiquitinated, efficiency of antigen presentation of a model ovalbumin-derived antigen to appropriately specific T cells remained unaffected. In addition, the animals present normal CD4<sup>+</sup>T cell populations and are

capable of generating antigen-specific antibodies in response to model antigens and viral infection. Thus, these results suggest that MHC-II trafficking via ubiquitination might not be essential for the function of MHC-II molecules in antigen presentation or antibody production<sup>294</sup>. It is suggested that before incorporation into ILVs, ubiquitin may be removed and recycled by deubiquitinating enzymes<sup>295</sup>.

In HeLa-CIITA cells, Tollip reduces the expression of MARCH-I and enhances the expression of MHC-II molecules. Tollip and MARCH-I compete to interact with MHC-II molecules<sup>296</sup>. This underlines the importance of ubiquitination in the regulation of MHC-II expression in APCs. Whether other SARs might also regulate MHC-II ubiquitination is unknown.

#### 4. Regulation of Ii and antigen processing

##### a) *Lysosomal cathepsins*

Antigen and invariant chain Ii processing are important determinants of the quality and the magnitude of CD4<sup>+</sup>T cell responses<sup>297,298</sup>. The processing of Ii mainly takes place in the MIIC, although it can also take place in the different compartments along the endo/lysosomal pathway<sup>299</sup>. Antigen processing takes place in numerous low-pH vesicles as we have mentioned in the previous paragraph. A balanced proteolytic environment is necessary for adequate antigen processing to generate MHC-II ligands ranging from 12 to 25 amino acids in length<sup>299,300</sup>.

As already discussed, late endosome-like compartments with an acidic pH, such as the MIIC, contain endo/lysosomal proteases that generate antigenic peptides; amongst these proteases, we find different families of cathepsins. These include cysteine proteases (B, C, F, H, K, L, O, S, V, X, W and AEP), serine proteases (A and G), aspartate proteases (D and E) and an IFN $\gamma$ -inducible lysosomal thiol reductase GILT/IFI30 which does not cleave proteins but reduces disulfide bonds making the proteins better substrates for cathepsins<sup>301</sup>. The protease nomenclature designates the amino acid of the protease active site that catalyzes hydrolysis of the substrate. Some exclusive roles in antigen generation have been defined for cathepsins; nevertheless, these proteases seem to have also redundant functions in acidic vesicles<sup>299</sup>. In fact, the processing machinery for MHC-II peptides varies between immune cell types and this includes the expression of different proteases. Therefore, the kinetics and efficiency of antigen fragmentation may differ from one cell type to another<sup>302,303</sup>.

### b) *Regulation of processing activity*

Several factors influence and regulate the activity of the processing enzymes found in the MHC-II pathway. Among these factors, there is vesicular pH, endogenous inhibitors, activators and chaperones.

Some lysosomal proteases arrive in the endocytic compartments as preforms or zymogens and require a low pH and/or other protease precursors (or themselves) to remove their propeptide by proteolysis<sup>304</sup>. This is the case for cathepsin L, which cleaves itself into a 30 kDa active form and requires AEP to attain a two-chain form. Another example is the regulation by GILT of cathepsin B expression in B cells<sup>299</sup>. Interestingly, Trombetta *et al.* showed that DC maturation induced the activation of the vacuolar proton pump V-ATPase, enhancing lysosomal acidification. Acidification enhanced efficient proteolysis in mature DCs that were, in turn, more capable of degrading internalized antigens<sup>305</sup>. Although proteases cleave antigens, thus generating peptides, proteolysis can also be responsible for peptide destruction in lysosomes. Epitope stability is dependent on the type of antigen and its sensitivity to proteolysis, therefore a regulated proteolysis can favor antigen presentation in APCs<sup>302</sup>. Stable epitopes, resistant to proteolysis, can be more immunogenic and favor CD4<sup>+</sup>T cell activation *in vivo*<sup>306</sup>.

One of the major regulators of cathepsin activity are cystatins. These are high-affinity inhibitors expressed ubiquitously in nucleated cells and regulate cathepsin activity<sup>246</sup>. Cystatin C was shown to regulate cathepsin S activity in DCs. Maturation of DCs was accompanied by a decrease in cystatin C expression levels and a modification of its localization in relation to cathepsins S and L<sup>307</sup>.

Ii fragment p41, characterized by the presence of an additional segment with significant homology to thyroglobulin type 1 domains, inhibits cysteine cathepsins<sup>242</sup>. This fragment inhibits cathepsins L, V, K and F, and to a lesser extent cathepsin S by structurally mimicking the N-terminal region of cystatins. Thus, Ii itself can modulate cathepsin activity in acidified vesicles and potentially play a role in MHC-II antigen presentation<sup>299</sup>.

Overall, the regulation of cathepsins S and L is essential for Ii processing and antigen presentation in APCs since these proteases do not seem to play redundant roles in B cells, DCs or thymic epithelial cells<sup>236,238,308</sup>. In addition, cathepsin B has been described as playing a role in MHC-II-restricted antigen presentation<sup>308</sup>. Nevertheless, testing non-redundancy of cathepsins is still a complex task due to the lack of specific, non-broad, inhibitors available.

## D. Pathways of antigen delivery to the MHC

It is historically admitted that peptides presented by MHC-II molecules are exclusively derived from extracellular antigenic sources (bacteria, fungi) phagocytosed by APCs. However, since the end of the 1980s, it became evident that MHC-II molecules could also present peptides derived from endogenous sources. Several studies showed that peptides derived from endogenous (synthesized by the cell) self and viral antigens (from MeV, HIV, influenza, vaccinia virus, EBV) can be presented to MHC-II molecules to activate CD4<sup>+</sup>T cells<sup>309-314</sup>.

Here, I will highlight how different degradation pathways can converge in the generation of peptides to be loaded on and presented by MHC-II molecules.

### 1. Endocytosis

In endocytosis, receptor-ligand complexes, membrane proteins and soluble macromolecules are internalized. Enhanced antigen presentation by MHC-II molecules has been observed following antigen uptake via several receptors that cluster in clathrin-coated domains, including Fc receptors, C-type lectin family receptors, as well as mannose and transferrin receptors<sup>315-318</sup>. B cells with antigen-specific B Cell Receptors (BCR) are more efficient in processing and presenting antigens to cognate T cells than B cells with BCRs specific for an irrelevant antigen<sup>319</sup>. They rely mostly on BCR-mediated endocytosis<sup>320</sup> and can only internalize extracellular antigens by fluid phase endocytosis when present at high concentrations. The binding of antigens on lectin DEC205, expressed by DCs and B cells, potentiates antigen-specific CD4<sup>+</sup>T cell activation *in vivo* and *in vitro*<sup>317,321</sup>. In HIV-1 infection, DC-SIGN captures viral particles and promotes MHC-II viral antigen presentation to virus-specific CD4<sup>+</sup>T cells<sup>318</sup>.

### 2. Phagocytosis

Phagocytosis consists of the capture of pathogens at the plasma membrane into a microenvironment containing reactive oxygen species (ROS), proteases and anti-microbial agents. It is an essential mechanism of foreign antigen uptake by DCs and macrophages *in vivo*<sup>322,323</sup> that can also be mediated by receptors such as C-type lectins, Fc receptors and complement receptors. This process requires large amounts of membranes to capture the cargo into phagosomes that later fuse with endosomes and lysosomes to constitute phagolysosomes<sup>324</sup>.

### 3. Macropinocytosis

Macropinocytosis is a non-selective process in which large portions of extracellular material are captured by membrane ruffling. This pathway exists in DCs, B cells and macrophages although it is believed to be a major mechanism of antigen uptake by DCs and the main mode of entry of viruses such as adenovirus type 3 and herpes simplex virus<sup>325</sup>. Vesicle maturation drives an increase in luminal acidification and fusion with TGN-derived vesicles delivering enzymes that promote antigen denaturation and proteolysis. Lowering the temperature from 37°C to 18°C has been shown to block the maturation step and also disrupts the presentation of several exogenous antigens by MHC-II molecules<sup>326</sup>.

For endocytosis and macropinocytosis, early endosomes and macropinosomes fuse with the external membrane of the MIIC to deliver antigens. In the case of phagosomes, antigen delivery to the MIIC is still unclear and it is possible that the MHC-II loading machinery is present in those compartments<sup>56</sup>.

### 4. MHC-II recycling

Pinet *et al.* reported on an HLA-DR-restricted influenza hemagglutinin (HA) epitope whose presentation from input virus did not require li or MHC-II synthesis. They showed that antigen presentation was abrogated when the cytoplasmic tails of HLA-DR were truncated, which prevented their internalization<sup>327</sup>. In addition, the Eisenlohr group showed that the presentation of an acidification-sensitive influenza antigen by B cells was inhibited upon treatment with primaquine, a compound that prevents recycling of surface molecules. Moreover, the use of brefeldin A, which inhibits the exit of proteins from the endoplasmic reticulum, did not abrogate the presentation of the same antigen, thus confirming that no nascent MHC-II molecules were required<sup>328</sup>.

### 5. Role of autophagosomes

Analysis of experiments involving the elution of peptides presented by MHC-II molecules (ligandome) showed that a fraction of the peptides derives from nuclear and cytosolic proteins<sup>156,329-331</sup>. In fact, upon APC starvation-induced autophagy there is an increase in MHC-II presentation of certain cytosolic antigens<sup>332</sup>.

In cells infected by Epstein Barr virus (EBV), the Münz laboratory detected the nuclear antigen EBNA1 in autophagosomes and showed that silencing the autophagy protein Atg12 partially inhibited the presentation of an EBNA1-derived epitope by MHC-II molecules<sup>333</sup>. Also in EBV-

infected cells, Leung *et al.* studied three EBNA1-derived epitopes, two weakly presented to CD4<sup>+</sup>T cells and one not presented. Amongst the two, one was processed through autophagy and the other one processed through another endogenous route. They showed that when EBNA1 is expressed in the cytoplasm, all three studied epitopes were presented more efficiently to CD4<sup>+</sup>T cells via autophagy<sup>334</sup>. Münz's team also reported that LC3-containing autophagosomes could fuse to the MIIC<sup>335</sup> and that coupling a cytosolic antigen to the autophagy protein LC3 allows its targeting to autophagosomes inducing MHC-II presentation of this antigen. Other evidence that autophagy plays a role in MHC-II antigen presentation comes from *in vitro* studies using APCs transfected with cDNAs encoding tumor antigens targeted to autophagosomes<sup>336</sup>. In 2016, my laboratory showed that targeting an HIV-gag antigen to autophagosomes via fusion to LC3 induced an increase in the activation of gag-specific CD4<sup>+</sup>T cells by DCs<sup>337</sup>.

Altogether, these experiments connect autophagy to the endogenous MHC-II-restricted antigen presentation pathway.

Autophagy is also implicated in MHC-II presentation of exogenous antigens from HSV-1 and HSV-2 and HIV<sup>338,339</sup>. In mice, in cells deficient for Atg5, anti-HSV-1-specific CD4<sup>+</sup>T cell response drastically diminished and the mice died after infection by HSV-2. In fact, in these cells the absence of Atg5 seems to affect the fusion of autophagosomes to lysosomes and therefore proper antigen degradation.

Autophagy also plays a role in the delivery of antigens derived from nuclear or cytosolic citrullinated proteins to MHC-II molecules<sup>340,341</sup>. In fact, peptides containing citrullinated residues are a unique set of antigens and this could be relevant in the autoimmune disease context since autoantibodies against citrullinated proteins can be found abundantly in rheumatoid arthritis<sup>299</sup>.

#### 6. The role of LC3-associated phagocytosis (LAP)

MHC-II antigens can be degraded in LAPosomes generated through LC3-associated phagocytosis (LAP). LAPosomes are single membrane vesicles (instead of the characteristic double membrane of autophagosomes) decorated with LC3 on their cytosolic side<sup>342</sup>. Extracellular material is phagocytosed, engaging different receptors, such as Toll-like receptor 2 (TLR2), TLR4, antibody Fc receptors, type-C lectins or the apoptosis-related receptor TIM4<sup>343</sup>.

This pathway depends on VPS34 and LC3/Atg8 complexes but does not require the ULK complex unlike canonical autophagy<sup>344</sup>. VPS34 induces PI3P marks on the phagosomal membrane, which allows the recruitment of NADPH oxidase 2 (NOX2). NOX2 generates reactive oxygen species (ROS) required for LAP and induces an oxidative burst<sup>345</sup>. Atg16L1-mediated recruitment of Atg5 and Atg12 then allows LC3/Atg8 conjugation to the cytosolic side of phagosomes. LC3 tags are only removed prior to LAPosome fusion with lysosomes and the MIIC<sup>342,346</sup> (Figure 23). The binding of the phagocytosis receptor Dectin-1 to sugar moieties present on the membrane of parasites such as *Candida Albicans* induces LAP and improves MHC-II antigen presentation of parasite-derived antigens<sup>293</sup>. Romao *et al.* showed, in human monocyte-derived macrophages, that LAPosomes store antigens for prolonged processing and improve MHC-II-restricted fungus-derived antigen presentation<sup>346</sup>. Experiments on mice with Atg5 deficiency showed that LAP also affects autoantigen processing and MHC-II-restricted presentation to autoreactive CD4<sup>+</sup>T cells<sup>347</sup>. In addition, Frédéric Gros's team showed that BCR polarization, crucial for antigen presentation, is Atg5-dependent and relies on the Beclin-1-PI3K pathway but does not depend on ULK-dependent signaling. This suggests that BCR trafficking occurs in vesicles that may resemble LAPosomes<sup>348</sup>.

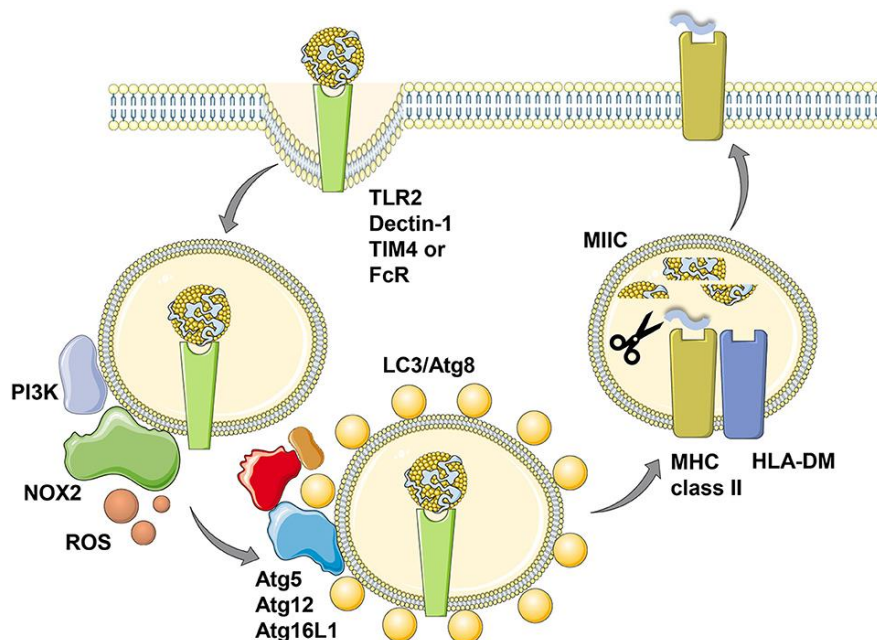


**Figure 23. LC3-associated phagocytosis (LAP) improves MHC-II-restricted antigen presentation<sup>349</sup> (adapted from Müntz, 2018).** Phagocytosis mediated by Toll-like receptor 2 (TLR2), Dectin-1, T-cell immunoglobulin and mucin domain-containing molecule 4 (TIM4) or antibody Fc receptors (FcR) leads to LC3 conjugation to the phagosomal membrane forming a LAPosome. Presumably, prior to LC3 conjugation, PI3 kinase modifies the membrane to recruit NADPH oxidase 2 (NOX2), whose reactive oxygen species (ROS) production is required for LAP. The cargo contained in the LAPosome is then more efficiently processed for MHC-II antigen presentation when delivered to the MIIC.



Therefore, LAP vesicles constitute appropriate compartments where pathogens are sensed and can deliver antigens to MHC-II-enriched compartments for antigen presentation.

#### 7. The role of chaperone-mediated autophagy (CMA)

In CMA, proteins containing the peptide sequence KFERQ motive are transferred from the cytoplasm to lysosomes in a lysosome-associated membrane protein-2a (LAMP-2a)-dependent manner<sup>350</sup>. Within the lumen of the lysosome, Hsc70 protects peptides from degradation by binding and delivering them to MHC class II molecules for presentation<sup>351</sup>. In a human B cell line expressing a model cytosolic glutamate decarboxylase (GAD) antigen, peptides derived from GAD degradation are processed and presented by MHC-II molecules in a LAMP-2a-dependent manner<sup>94</sup>. Overexpressing LAMP-2a or Hsc70 in these cells increases the loading of a GAD-derived epitope on MHC-II molecules and potentiates CD4<sup>+</sup>T cell activation. Under nutritional stress, Hsc70 plays a key role in MHC-II antigen presentation by selectively regulating endocytosis and autophagy in B cells<sup>351</sup>. More recently, Blum's team showed that LAMP-2c, a LAMP-2 isoform, modulates the expression of several cytoplasmic proteins targeted for degradation by CMA, diminishing peptide translocation in B cells. This inhibition of CMA affected MHC-II-restricted antigen presentation of cytoplasmic antigens<sup>352</sup>.

#### 8. Bona fide cytosolic processing

The main path of cytosolic degradation is the proteasome, well known for generating peptides conveyed via the transporter TAP for MHC-I antigen presentation. Nevertheless, the proteasome can also serve to generate MHC-II-restricted epitopes. By tracking the presentation of a minigene-encoded peptide derived from influenza HA, the Long laboratory showed that MHC-II presentation was reduced in the absence of TAP<sup>353</sup>. Furthermore, the Eisenlohr group has demonstrated with several epitopes that highly specific proteasome inhibition abrogates *in vitro* presentation from endogenous sources of influenza virus proteins<sup>282,354,355</sup>. Remarkably, they find that proteasome-dependent epitopes drive an important part of the CD4<sup>+</sup>T cell response to influenza. TAP can be located at the membrane of phagosomes and endosomes and could participate in MHC-II antigen loading in these compartments upon MHC-II recycling.

#### 9. Regulation by Heat Shock Protein 90 (Hsp90)

Hsp90 seems to play an important role in the presentation of model and tumor antigens by MHC-II molecules. Rajagopal *et al.* showed that overexpressing Hsp90 enhanced the levels of

SDS-stable  $\alpha\beta$ -peptide complexes, which correlated with enhanced MHC-II-restricted antigen presentation. In addition, treatment of mouse APCs with an Hsp90 inhibitor abrogated MHC-II-mediated presentation of endocytosed and cytosolic proteins as well as synthetic peptides to specific T cells<sup>356</sup>. Houlihan *et al.* demonstrated the role of Hsp90 in the presentation of select antigens to MHC-II molecules<sup>357</sup>. Moreover, in a melanoma cell line expressing the NY-ESO-1 epitope, its processing was shown to be independent of CMA, autophagy and TAP but dependent on the proteasome and endolysosomal proteases. The presentation of the epitope was dependent on endosomal proteases and chaperoning by the cytosolic Hsp90, believed to translocate antigenic peptides between the cytoplasm and endosomes/lysosomes in a process similar to CMA<sup>358</sup>.

To conclude, exogenous and endogenous antigens can be delivered to the MHC-II through several pathways. The quality of the T cell responses can be dependent on the antigen itself and its localization in the cell (e.g. Autophagosomes). In addition, antigen degradation pathways can also be cell-specific. For several pathways, the mechanisms involved in antigen delivery to the MHC-II remain to be further elucidated. It is important to investigate the mechanisms leading to MHC-II antigen presentation given its importance in eliciting CD4<sup>+</sup>T cell activation and thus modulating adaptive immunity. Moreover, understanding these mechanisms can confer a better insight on how pathogens are sensed and subsequently eliminated and, as importantly, on how pathogens can modulate the cell machinery to evade immune responses.

### **III. Viruses and immunity: interaction with selective autophagy receptors and the MHC-II pathway**

Recognition of peptides bound to MHC-II molecules by CD4<sup>+</sup>T cells and their subsequent activation is a major step in the orchestration of adaptive immune responses. During viral infections, CD4<sup>+</sup>T cells play an essential role as helpers of CD8<sup>+</sup>T cells leading the CTL response. More recently, CD4<sup>+</sup>T cells have been shown to exert a cytotoxic activity of their own. Therefore, many viruses have evolved numerous mechanisms to escape helper CD4<sup>+</sup>T cell recognition, thus to block and avoid MHC-II antigen presentation and escape antiviral immunity altogether.

In this part, I will show how viruses can manipulate the MHC-II antigen presentation pathways and SARs to their benefit. Finally, I will focus on HTLV-1, the immune responses elicited by the virus and more specifically the transactivator Tax, which recruits SARs to modulate innate immune responses.

#### **A. Viral manipulation of MHC-II-restricted antigen presentation**

I have previously detailed the MHC-II antigen presentation pathway. Here, I will present different mechanisms that viruses employ to manipulate this antigen presentation pathway.

##### **1. Targeting CIITA function**

The transcription of the HLA-II locus is highly dependent on CIITA expression. CIITA is constitutively expressed in professional APCs, such as DCs, B cells and macrophages and in thymic epithelial cells (TECs) and activated T cells. In other cells, such as keratinocytes, fibroblasts and epithelial cells, IFN- $\gamma$  induces CIITA expression and thus MHC-II expression<sup>56,202,359</sup>. Several viruses have developed different mechanisms to inhibit constitutive and IFN- $\gamma$  –induced CIITA expression, both leading to a downregulation of MHC-II molecules.

Two of the four promoters regulating CIITA gene expression contain regulatory elements that are targets of the signal transducer and activator of transcription 1 (STAT1), major regulator of the Jak-STAT signaling pathway<sup>360-362</sup>. IFN- $\gamma$  induces the dimerization of cytoplasmic STAT1, which then relocates to the nucleus and binds to CIITA promoters as well as other IFN-induced genes<sup>363</sup> (Figure 24).

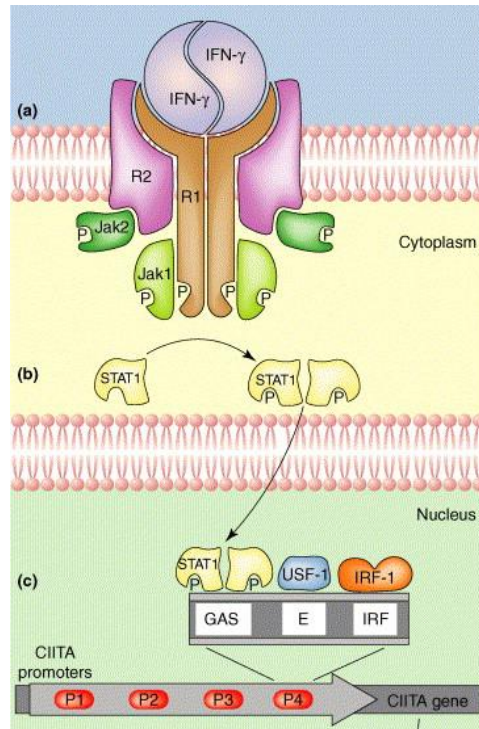


**Figure 24. Induction of MHC class II gene expression by interferon- $\gamma$ <sup>362</sup> (adapted from Hegde *et al.*, 2003).** (a) Binding of IFN- $\gamma$  promotes homodimerization of IFN- $\gamma$  receptor R1 subunits and recruitment of R2 subunits. This results in the approximation and phosphorylation (P) of Jak1 and Jak2. (P)Jak1 phosphorylates R1, which becomes a docking site for the signal transducer and activator of transcription 1 (STAT1). Jak2 then phosphorylates STAT1. (b) (P)STAT1 homodimerizes and translocates to the nucleus to activate transcription of IFN- $\gamma$ -induced genes, including the gene encoding the class II transactivator (CIITA). (c) Each CIITA promoter contains three regulatory elements: (1) a g-activation sequence (GAS) box, (2) an E box, and (3) an IFN responsive factor (IRF) box. These elements are cooperatively bound by basal and IFN-inducible transcription factors.

The Jak-STAT pathway can be a target for viruses to prevent IFN- $\gamma$ -induced CIITA transcription. Varicella Zoster Virus (VZV) can prevent the IFN- $\gamma$ -induced CIITA expression in human foreskin fibroblasts and inhibit the expression of MHC-II molecules<sup>364</sup>. Likewise, adenovirus (Ad) E1A protein binds STAT1 inhibiting its function whilst decreasing its levels in the cells<sup>365</sup>. E1A also inhibits transcription of IFN- $\gamma$  receptor subunit R2 and overall inhibits transcription of CIITA<sup>360,361,366</sup>. Furthermore, HCMV can also induce the degradation of Jak2 and repress IFN- $\gamma$ -induced CIITA transcription<sup>367,368</sup> (Figure 25). Overall, viral targeting of the Jak-STAT signaling pathway certainly plays a broader role since CIITA is not the only gene targeted by IFN that will play an antiviral role<sup>362</sup>.

Several herpesviruses have been shown to inhibit CIITA function. BZLF1, the master regulator of EBV lytic cycle, can bind the CIITA promoter and inhibit its transcription and further

constitutive expression<sup>369,370</sup>. LMP2A, also an EBV protein, can indirectly downregulate CIITA by inhibiting (via the activation of the PI3K/Akt signaling pathway) the two transcription factors E47 and PU.1 positively regulating the P3 CIITA promoter in B cells. LMP2A downregulates CIITA, MHC-II and Ii expressions<sup>371</sup>. Kaposi's Sarcoma-Associated Herpesvirus (KSHV) encodes for latency associated nuclear antigen (LANA). LANA interacts directly with IRF-4, an activator of both the P3 and P4 CIITA promoters, and blocks the DNA-binding ability of IRF-4 on both promoters thus suppressing CIITA transcription to evade MHC-II antigen presentation<sup>372,373</sup>. The protein vIRF3, also from KSHV, can also downregulate CIITA transcription and modulate MHC-II expression and antigen presentation<sup>374,375</sup>.

HCMV has also been shown to reduce CIITA transcript levels in mature Langerhans cells in a mechanism that remains to be elucidated<sup>376</sup>.

Furthermore, HIV transcriptional transactivator (Tat) protein competes with CIITA for the binding of cyclin T1, a binding necessary for productive transcription of the HLA-II locus<sup>377</sup>.

## 2. Targeting invariant chain (Ii) function

The invariant chain Ii is involved in the trafficking of MHC-II molecules and plays an important role in peptide loading in the MIIC and endolysosomal vesicles<sup>378,379</sup>. It is hence a common target of viruses to modulate MHC-II antigen presentation.

Neumann *et al.* showed an 80% reduction in Ii expression levels after 64h of Herpes Simplex Virus 1 (HSV-1) infection in B cells but no impact on HLA-DR or HLA-DM expression levels. Moreover, the amount of SDS-stable of  $\alpha\beta$ -peptide complexes was highly reduced upon infection, thus suggesting that HSV-1 infection induces Ii degradation and impairs peptide loading and subsequent MHC-II antigen presentation<sup>380</sup> (Figure 25).

Distinct from its previously mentioned role on CIITA, EBV-encoded BZLF1 downregulates Ii in a yet unknown post-transcriptional manner and evades CD4<sup>+</sup>T cell recognition<sup>381</sup>. Vaccinia virus (VACV) has also been shown to inhibit MHC-II antigen presentation<sup>382-384</sup>, in part through Ii downregulation<sup>385</sup>. In fact, the virulent factor A35, localized in endosomes, is believed to modulate the exchange of CLIP for antigenic peptides<sup>386,387</sup>.

In addition to modulating Ii expression levels, the HCMV-encoded US3 protein binds MHC-II  $\alpha\beta$  dimers and decreases their affinity for Ii, thus partially abrogating MHC-II expression at the cell surface and preventing CD4<sup>+</sup>T cell activation<sup>362</sup>.

Finally, HIV Nef protein upregulates Ii and surface-expressed  $\alpha\beta$ -Ii complexes (immature MHC-II molecules). This interferes with  $\alpha\beta$ -peptide complex formation and presentation at the cell surface<sup>388,389</sup>.

### 3. Targeting MHC-II molecules

MHC-II  $\alpha\beta$  dimers and their correct folding, assembly and trafficking are essential for proper MHC-II-restricted antigen presentation. Viruses have evolved to target these different aspects (Figure 25).

Tomazin *et al.* reported that HCMV-US2 causes the rapid proteasome-mediated degradation of the  $\alpha$  subunits of both DR and DM, without affecting  $\beta$  subunits, and inhibits the presentation of exogenous antigens to CD4<sup>+</sup>T cells<sup>390</sup>. US3, another HCMV-encoded protein, was shown to block exogenous MHC-II antigen presentation. In fact, US3 binds to  $\alpha\beta$  dimers in the ER preventing their association with Ii, thus leading to their mislocalization and delay in reaching the MIIC where fewer  $\alpha\beta$ -peptide complexes are formed<sup>391</sup>.

The use of a mutant HCMV lacking pp65 prevented the accumulation and degradation of HLA-DR in vacuoles or lysosomes near the nucleus, usually observed upon HCMV infection, thus suggesting that pp65 also participates in the degradation of HLA-DR<sup>392</sup>. Similarly, EBV late lytic protein BDLF3 was shown to induce MHC-II ubiquitination and subsequent proteasomal degradation of surface MHC-II molecules. BDLF3 enhances the internalization of surface MHC-II molecules and delays their rate of appearance at the plasma membrane<sup>393</sup>. In the study, the authors discuss the recruitment of MARCH proteins by BDLF3 but underline that no protein is known to induce ubiquitination of MHC-II and this without affecting other surface markers.

Koch's team identified, using a bioinformatics approach, a sequence in HSV-1-gB identical to the highly conserved HLA-DR binding motive in human Ii. The sequence identity was confirmed experimentally by the association of gB with different HLA-DR allotypes<sup>394</sup>. Using an HSV-1 infected B cell model, they showed that gB can also bind HLA-DM independently of HLA-DR. In addition, the team showed that gB can compete with Ii for binding to MHC-II

heterodimers<sup>380</sup>. Both gB-associated HLA-DR and HLA-DM heterodimers can be exported from the ER to Golgi compartments. Nevertheless, the association of HLA-DR with gB changes the intracellular localization of HLA-DR, thus reducing its expression at the cell surface. Overall, the binding of gB to MHC-II molecules inhibits peptide loading and prevents the presentation of viral peptides.

HIV-Nef also affects MHC-II proteins, reducing endogenous HA-derived peptide presentation to CD4<sup>+</sup>T cells. In HeLa cells expressing CIITA and Nef, cells express 50% less surface mature MHC-II molecules than control cells and express, in contrast, more  $\alpha\beta$ -li complexes at the surface<sup>388</sup>.

Other mechanisms of viral targeting of MHC-II molecules include the arrest of global host protein synthesis. Following entry into lytic cycle (alpha- and gamma-herpesviruses are concerned); virus host shutoff (vhs) genes are expressed decreasing cellular mRNA half-life and diminishing MHC-II antigen presentation pathways by limiting the availability of newly synthesized MHC molecules<sup>395</sup>.

#### 4. Targeting degradation pathways

Certain viruses induce cellular IL-10 or express viral IL-10 homologs. Remarkably, both decrease cell-surface MHC-II molecule expression (Figure 25) and increase the pH of the MIIC, inhibiting cathepsin activity and therefore reducing the generation of antigenic peptides<sup>362</sup>.

HSV-1 ICP34.5 targets directly Beclin-1 to block autophagy<sup>396</sup> and is also described as interacting with TBK1<sup>397</sup>. TBK1 is a necessary factor for autophagic maturation and can phosphorylate the selective autophagy receptors p62 and OPTN to regulate cargo recruitment into phagophores for degradation<sup>398</sup>.

Finally, Gannagé *et al.* showed that influenza A virus, an important human pathogen, causes the accumulation of autophagosomes in infected cells by blocking their fusion with lysosomes. The matrix protein 2 (M2) is necessary for this inhibition of autophagosome degradation and was shown to interact with Beclin-1, known to facilitate autophagosome fusion with lysosomes. The team suggests that trapping viral antigens in autophagosomes might prevent their degradation for direct presentation on MHC molecules in an M2-dependent manner<sup>399</sup>.

Several HIV-1 proteins target autophagy to protect the virus from degradation. This is the case for Vif, Vpr and Nef. Vif binds LC3B and inhibits autophagy<sup>400</sup>. Vpr decreases the expression levels of LC3B and Beclin-1 and an autophagy-related protein BNIP and Nef counteracts autophagy at late stages of infection also by interacting with regulatory factor Beclin-1<sup>401,402</sup>.

Limiting autophagy pathways could limit antigen presentation by preventing the delivery of viral peptides to the MHC molecules.

### 5. TCR recognition inhibition

In addition to targeting different intracellular actors of the MHC-II antigen presentation pathway, viruses have evolved to modulate MHC-II antigen presentation even after the  $\alpha\beta$ -peptide complexes have reached the cell surface (Figure 25).

The EBV lytic phase protein gp42 can bind to MHC-II molecules at the cell surface. More particularly gp42 binds the  $\beta$ -chain on a domain that participates in the formation of peptide binding pockets<sup>403</sup>. Crystal structure studies revealed that gp42 sterically competes with cognate TCR binding<sup>404,405</sup> thus, by physically preventing  $\alpha\beta$ -peptide-TCR interactions, gp42 decreases CD4<sup>+</sup>T cell activation<sup>406</sup>.

More recently, research on poxviruses revealed that the virulence factor B22 is necessary and sufficient for inhibition of CD4<sup>+</sup>T cell responses. B22 is located on the cell surface of APCs and affects TCR signaling, leading the authors to suggest that B22 engages an inhibitory co-receptor<sup>407</sup>.



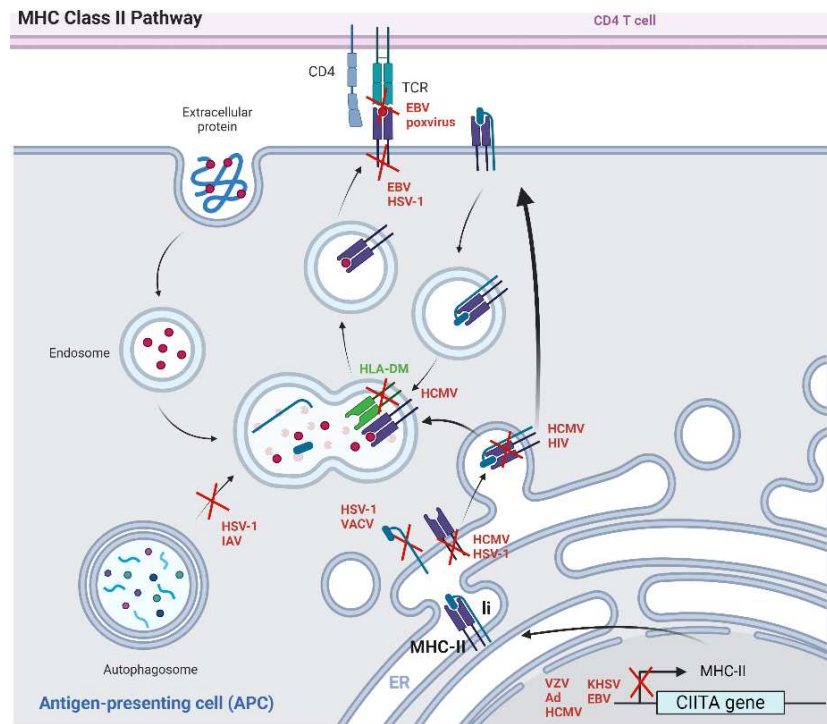


**Figure 25. Viruses target the MHC-II antigen presentation pathway.** Viruses can target the different stages of the MHC-II antigen presentation pathway: CIITA transcription and expression of MHC-II molecules,  $\alpha\beta$ -li complexes and their expression at the cell surface; HLA-DM interaction with MHC-II molecules and the exchange of CLIP for high affinity peptides, the delivery of autophagosome content to the MIIC, mature MHC-II molecule expression at the cell surface, interaction with TCR and antigen presentation to CD4<sup>+</sup>T cells.

## B. Viral interaction with selective autophagy receptors

Amongst the several cellular factors targeted by viruses, we will focus on SARs. As we have seen in the first part of the introduction, SARs play an important role in the clearance of pathogens including viruses (Virophagy) and act as scaffold proteins involved in innate immunity signaling pathway.

### 1. Exploiting SAR function to promote viral replication

Viruses can also take advantage of the host cell selective autophagy machinery to promote their replication.

Measles Virus (MeV) benefits from inducing a complete autophagic flux to improve its replication<sup>408</sup>. More specifically, SARs TAX1BP1 and NDP52 were identified as essential for autophagy-mediated viral maturation by means of the interactions of TAX1BP1 with MeV-N protein and NDP52 with MeV-C and MeV-V. Petkova *et al.* showed that silencing TAX1BP1 and NDP52 strongly reduced the ability of MeV to produce infectious particles in infected cells; this was not the case when silencing other SARs like p62 or OPTN. Moreover, treating infected cells

with non-specific autophagosome maturation blocking agents did not have a comparable impact in virus replication compared to TAX1BP1 and NDP52 individual silencing. In addition, concomitant silencing decreased MeV replication even further than individual SAR silencing. The authors concluded that TAX1BP1 and NDP52 could regulate the maturation of distinct types of autophagosomes, both required for optimal MeV replication. How MeV distinguishes different autophagosomes, mechanisms potentially involving N, C or V proteins, is still unclear<sup>409</sup>.

## 2. Inhibiting SAR function to escape cell intrinsic antiviral immunity

Viruses can target SARs that play a role in selective autophagy of viral components; this process is known as virophagy<sup>410</sup>. In fact, one strategy to resist virophagy involves the cleavage of SARs by viral proteases<sup>411</sup>. Coxsackievirus B3 (CVB3)-encoded proteases 2A and 3C cleave p62, NBR1 and NDP52<sup>412,413</sup> (Figure 26). NDP52 and p62 are known to target ubiquitinated VP1 capsid component for degradation<sup>414</sup>. Other viruses such as Enterovirus D68 (EV-D68), rhinovirus 1A (RV1A) and poliovirus 1 (PV) also encode for proteases that are able to cleave p62 (Figure 26) and other components that allow fusion of autophagosomes to lysosomes to prevent degradation of viruses and promote viral replication and exit from the cell<sup>415</sup>.

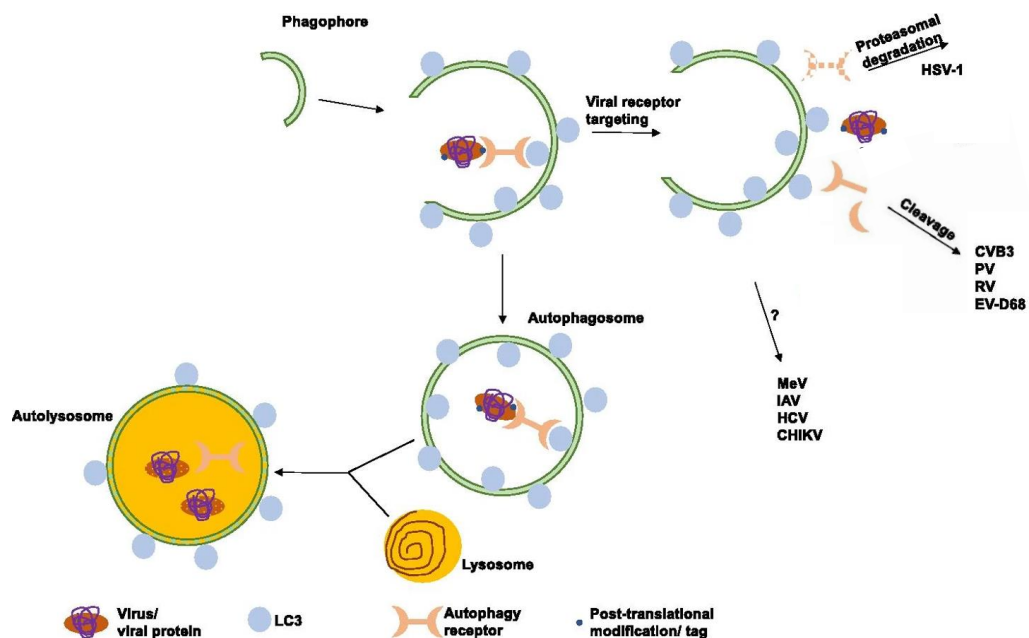


**Figure 26. Viral strategies to target SARs<sup>101</sup> (adapted from Ylä-Anttila, 2021).** Targeting for proteasomal degradation, herpes simplex virus type 1 (HSV-1); Epstein–Barr virus (EBV), classical swine fever virus (CSFV); proteolytic cleavage, coxsackievirus B3 (CVB3), poliovirus (PV), rhinovirus (RV), enterovirus D68 (EV-D68); binding and/or unknown mechanism, measles virus (MeV), influenza A virus (IAV), hepatitis C virus (HCV), chikungunya virus (CHIKV).

Other viruses like HSV-1 can also inactivate SARs by targeting them to proteasomal degradation. Waisner and Kalamvoki showed that ICP0, an early phase protein, is involved in high levels of ubiquitination of OPTN and p62 leading to their proteasomal degradation. By overexpressing p62, they restricted early HSV-1 growth (Figure 26). Although the type and mechanisms of antiviral functions involving p62 and OPTN remain unknown, they do not exclude that other SARs might follow the same fate given their multiple roles in an outside selective autophagy<sup>416</sup>.

### 3. SAR targeting by viruses to modulate innate immune signaling

By means of a yeast two-hybrid approach, Leymarie *et al.* identified influenza A virus (IAV) protein PB1-F2 as an interactor of NDP52. PB1-F2 is well known for enhancing the host pro-inflammatory response induced by IAV infection in lung epithelial cells. The team showed, using an NF- $\kappa$ B-luciferase reporter construct, that overexpressing NDP52 and PB1-F2 highly potentiates the NF- $\kappa$ B activity mediated by Mitochondrial Antiviral Signaling (MAVS) protein. In addition, silencing NDP52 reduced TBK1-mediated IFN-stimulated response element (ISRE) activity, thus suggesting that the interaction of PB1-F2 with NDP52 is involved in the pathological process induced by IAV<sup>417</sup>.

To avoid hyperactivation of IFN responses that could trigger severe immunopathology, several SARs are reported to mediate selective degradation of the key signal components at each level of the IFN signaling pathway<sup>418-422</sup>. Several viruses promote the autophagic degradation of adaptor proteins in the IFN pathway to block signal amplification. IAV H7N9 PB1 protein recruits host E3 ligase RNF5 to induce K27-linked ubiquitination of MAVS at its Lys362 and Lys461, which will subsequently be recognized by NBR1 and lead to its autophagic degradation. The PB1 protein-mediated degradation of MAVS decreases RIG-I-MAVS IFN signaling and enhances H7N9 infection<sup>423</sup>. SARS-CoV-2 helicase NSP13 can promote the autophagic degradation of TBK1, central kinase in the IFN pathway, in cooperation with p62 thus inhibiting IFN production<sup>424</sup>.

Overall, viruses are capable of targeting SARs either to diminish their function in antiviral selective autophagy or to hijack other functions they accomplish, such as autophagosome maturation or innate immune signaling.

To conclude this chapter, I will center on the Human T-cell Leukemia Virus type 1 (HTLV-1). I will briefly describe its viral cycle; the T cell responses elicited by the virus and will then focus on the oncoprotein Tax. Tax is known to recruit SARs to subvert the NF- $\kappa$ B signaling pathway.

### **C. Human T cell leukemia virus type 1**

In 1980, Human T-cell leukemia virus type 1 (HTLV-1) was the first oncogenic human retrovirus discovered<sup>425</sup>. It is the etiologic agent of Adult T-cell Leukemia (ATL)<sup>426</sup> and various neurological pathologies, primarily HTLV-Associated Myelopathy/ Tropical Spastic Paraparesis (HAM/TSP). It is estimated that between five to ten million people are infected worldwide, most of them residing in Japan and the Caribbean Basin<sup>427</sup>. Approximately, 2%-6% of infected individuals acquire ATL or HAM/TSP.

#### **1. HTLV-1 viral cycle**

HTLV-1 is an enveloped virus, approximately 100 nm in diameter, containing a single stranded positive sense RNA genome. The inner virion envelope membrane contains the viral matrix protein (MA), which encloses the viral capsid (CA) carrying two identical strands of the genomic RNA as well as functional protease (Pro), integrase (IN), and reverse transcriptase (RT) enzymes<sup>428</sup>.

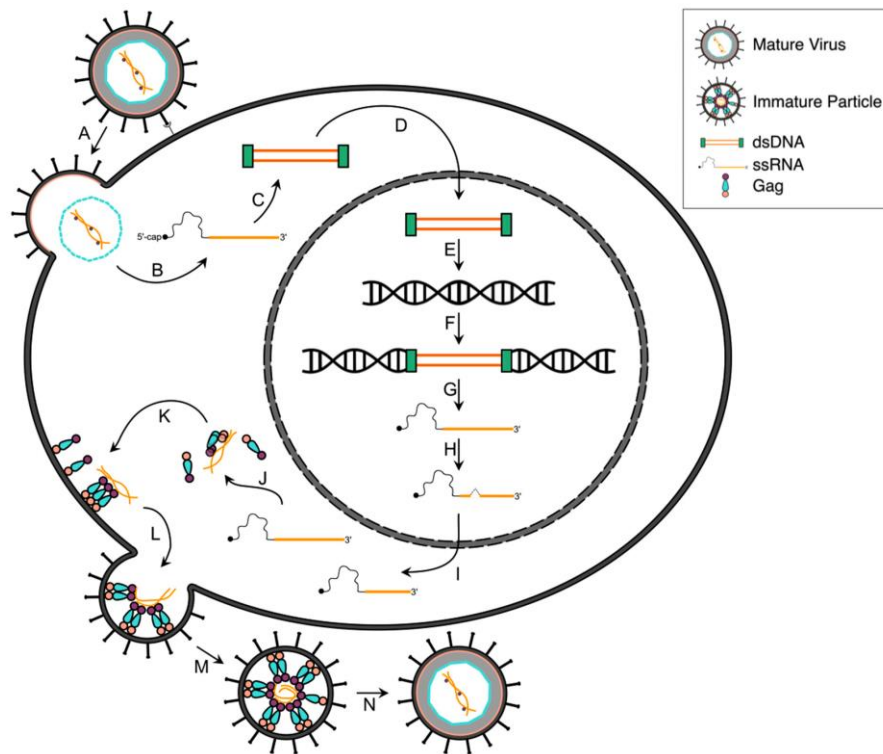


**Figure 27. Major steps of HTLV-1 replication cycle<sup>429</sup> (adapted from Martin *et al.*, 2016).** (A) Following fusion, the viral core containing the viral genomic RNA (gRNA) is delivered into the cytoplasm (B), and during and/or following entry the gRNA genome undergoes reverse transcription to convert the gRNA into double stranded DNA (dsDNA) (C). The dsDNA is transported to the nucleus (D) and is integrated into the host genome; (E,F). The provirus is transcribed by cellular RNA polymerase II (G), as well as post-translationally modified (H). Both full-length and spliced viral mRNAs are exported from the nucleus to the cytoplasm (I). The viral proteins are then translated by the host cell translation machinery (J), and the Gag, Gag-Pol and Env proteins transported to the plasma membrane (PM) along with two copies of the gRNA genome (K). These viral proteins and gRNA assemble at a virus budding site along the PM to form an immature virus particle (L). The budding particle releases from the cell surface (M), and undergoes a maturation process through the action of the viral protease, which cleaves the viral polyproteins to form an infectious, mature virus particle (N).

CD4<sup>+</sup>T cells are the primary targets of HTLV-1 infection but the virus can also infect other cell types, such as CD8<sup>+</sup>T cells, B cells, monocytes, epithelial cells or DCs<sup>430–433</sup>. HTLV-1 is able to interact with this variety of cells because it binds to three widely distributed cellular surface receptors: glucose transporter (GLUT1), heparin sulfate proteoglycan (HSPG) and VEGF-165 receptor neuropilin-1 (NRP-1)<sup>429</sup>. Viral entry into the cytoplasm occurs by membrane fusion through the interaction of HTLV-1 Env protein with HSPG, NRP-1 and GLUT1 (Figure 27). The RT reverse transcribes the viral RNA into double stranded DNA, then transported to the nucleus to be integrated into the host chromosome forming the provirus<sup>434,435</sup> (Figure 27).

The long terminal repeats (LTR) of the provirus contain the promoter and enhancer elements necessary to initiate RNA transcription. The retroviral plus strand genome encodes structural proteins Gag (capsid, nucleocapsid, matrix), Pro, polymerase (Pol) and Env<sup>436–438</sup> and regulatory and accessory proteins, such as Tax and Rex (Figure 28). Only one protein is encoded by the minus strand genome, originating from the 3' LTR, HTLV-1 bZIP factor (HBZ)<sup>439</sup>. HBZ is involved in viral transcriptional regulation and cell proliferation<sup>440</sup> (Figure 28).

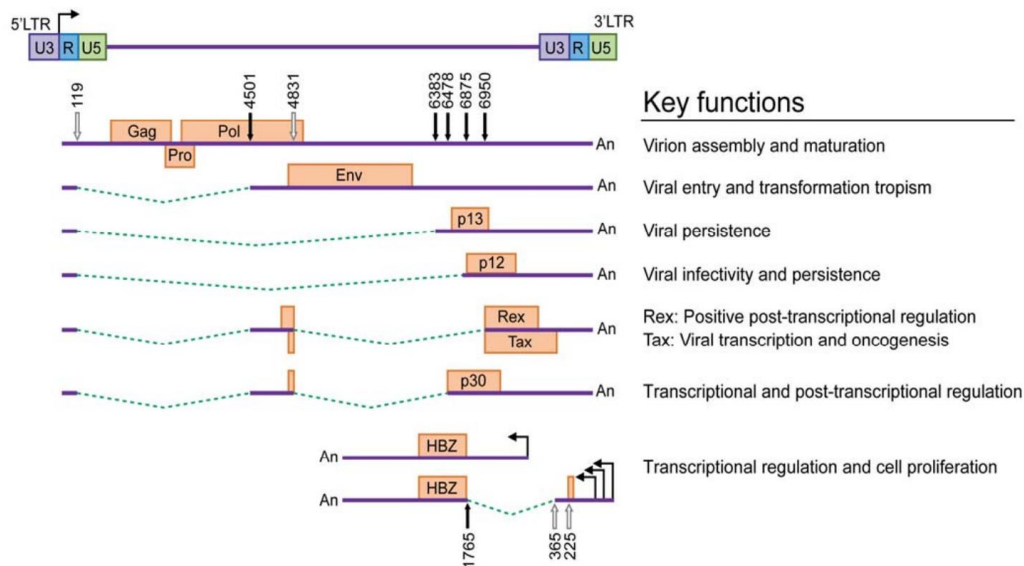


**Figure 28. Structure of the HTLV-1 proviral genome and gene product key functions<sup>428</sup> (adapted from Kannian & Green, 2010).** The proviral DNA with the LTRs, and the unspliced, singly spliced and doubly spliced mRNA transcripts are shown. The names of the gene transcripts and the key functions associated to the proteins are given.

Tax is the transactivator gene. It increases the rate of viral transcription<sup>441–443</sup> and regulates the transcription of multiple cellular genes involved in cell proliferation, differentiation, cycle control and DNA repair<sup>444–448</sup>.

Tax was shown to be an oncogenic protein in Tax transgenic mice that developed different tumors according to the promoter used to drive Tax expression<sup>449,450</sup> and is necessary for HTLV-1 transformation of T cells<sup>451–454</sup>.

Viral particles form after Gag traffics from the cytoplasm to the plasma membrane in what is still an unknown mechanism. The nucleocapsid protein as well as the matrix protein both bind viral RNA. It is still unclear how viral mRNA reaches the membrane and budding sites. HTLV-1 full-length viral RNA could diffuse through the cytoplasm to reach the membrane, but it could also bind to Gag before reaching the membrane<sup>429</sup>.

Gag interacts with the viral genomic RNA (gRNA), with the membrane and with other Gag proteins. All these interactions are required for the assembly and budding of viral particles<sup>455</sup>. Budding sites are determined by the interactions between the matrix and membrane lipid rafts<sup>456,457</sup>. The budding results in the release of immature viral particles<sup>458</sup> in which the viral protease cleaves Gag and Pol polyproteins shortly after the release<sup>459</sup>.

HTLV-1 virions are poorly infectious and cell-mediated infection is much more efficient<sup>460</sup>. A virological synapse by cell-cell contact is formed by productively infected HTLV-1+ cells with uninfected T cells mediated by interactions between ICAM-1 and LFA-1 adhesion molecules<sup>461,462</sup>. The virological synapse ensures the spread of HTLV-1 core complexes and the HTLV-1 genome.

## 2. Tax modulation of the NF- $\kappa$ B signaling pathway

Tax protein is composed of 353 amino acids (40 kDa) and contains several domains that mediate interactions with many cellular proteins<sup>463</sup> (Figure 29). Tax localizes in different compartments of the cell: cytosol, nucleus, Golgi apparatus and endoplasmic reticulum (ER) for dedicated functions that benefit viral replication and persistence. The presence of a nuclear localization sequence (NLS) and a nuclear export sequence (NES) allows the shuttling between these different cellular compartments<sup>464</sup>. Tax can also be secreted to the extracellular environment where it can contribute to inflammation and pathogenesis<sup>465</sup>.

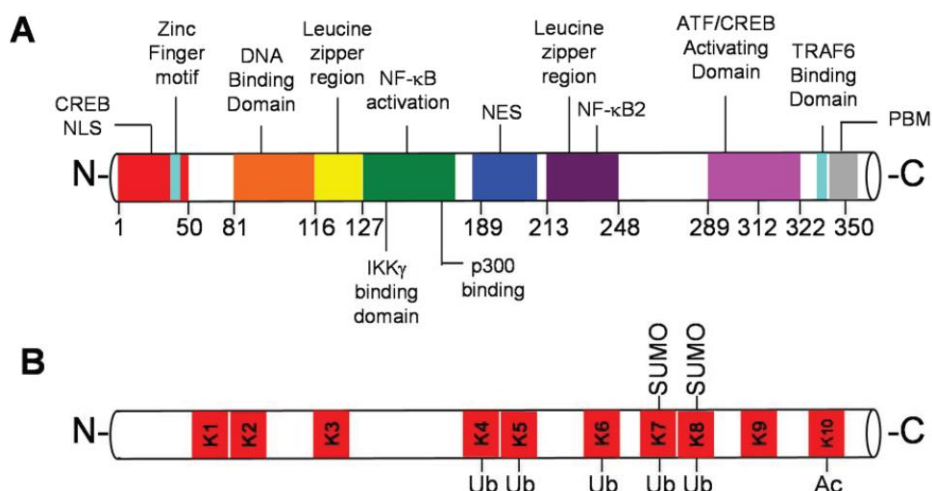


**Figure 29. Domains of Tax for interactions and post-translational modifications<sup>466</sup> (adapted from Lavorgna and Harhaj, 2014).** (A) Schematic representation of Tax protein-protein interaction domains and other motives regulating Tax function. (B) Schematic representation of known ubiquitination (Ub), SUMOylation (SUMO) and acetylation (Ac) sites in Tax.

Tax ensures multiple functions and regulates different cellular signaling pathways such as AP-1, NFAT, CREB and NF- $\kappa$ B<sup>467,468</sup> (Figure 29). One of the major cellular targets is the transcription factor NF- $\kappa$ B, modulated by Tax in the cytoplasm and cis-Golgi, whereas the regulation of viral gene expression occurs in the nucleus.

Tax interacts with specific components of the canonical and non-canonical NF- $\kappa$ B pathways to drive the proliferation, survival and transformation of HTLV-1-infected T cells. The canonical NF- $\kappa$ B signaling pathway is induced upon stimulation by pro-inflammatory cytokines, such as TNF $\alpha$ , IL-1b and IL-6, pathogen-associated molecular patterns (PAMPs) from viruses and bacteria and agonists for the B or T cell antigen receptors. The non-canonical NF- $\kappa$ B signaling pathway is induced by a subset of TNF family members such as B cell activating factor (BAFF), lymphotoxin $\beta$ -(LT $\beta$ ) and CD40L<sup>466</sup>. Thus, each pathway contains its own receptors, molecules and generated responses<sup>469</sup>. Tax constitutively activates both pathways<sup>470,471</sup> by interacting with the NEMO subunit of the IKK complex and persistently activating it<sup>472-474</sup>. Upon IKK activation, IKK $\beta$  phosphorylates and triggers the degradation of I $\kappa$ B $\alpha$  and I $\kappa$ B $\beta$  followed by the nuclear translocation of RelA/p50 dimers<sup>475</sup>. Robek and Ratner showed that a Tax mutant unable to activate IKK, and hence NF- $\kappa$ B, is unable to induce cell proliferation and immortalization of T cells<sup>452</sup>. The activation of the non-canonical pathway occurs by interaction of Tax with IKK $\gamma$ /NEMO and p100 to induce its proteasome-mediated processing<sup>476</sup>.

Consistent with many viral infections, HTLV-1 takes advantage of the host cell machinery including the autophagic machinery and post-translational modifications (PTM).

Tax is subjected to multiple PTMs such as ubiquitination, SUMOylation, phosphorylation and acetylation. To note, Tax has 10 lysine (K) residues (K1 to K10) of which K4 through K10 are the main targets of both monoubiquitination and polyubiquitination<sup>477-479</sup> (Figure 29). Tax ubiquitination, by E2 enzyme Ubc13, is largely composed of K63-linked polyubiquitin chains. K63-linked polyubiquitin was found to regulate Tax stability and to be required for its interaction with NEMO and NF- $\kappa$ B activation<sup>138</sup>. Therefore, the recruitment of IKK and subsequent NF- $\kappa$ B persistent activation occurs in a macromolecular IKK signalosome based on ubiquitin-dependent interactions (Figure 30). Tax has also been shown to activate IKK in Golgi-associated lipid raft microdomains (LRD) as well as near the centrosome<sup>480,481</sup>. Tax thus appears to use the Golgi as a specific platform for IKK activation.



In addition, Journo *et al.* showed that K63-linked polyubiquitinated Tax recruits NEMO-related protein (NRP)/Optineurin (OPTN) and Tax-1 Binding Protein (TAX1BP1) to perinuclear Golgi structures, and the recruitment of SARS is required to induce sustained NF- $\kappa$ B activation<sup>482</sup> (Figure 30). It is therefore likely that Tax recruits SARs to the IKK signalosome.

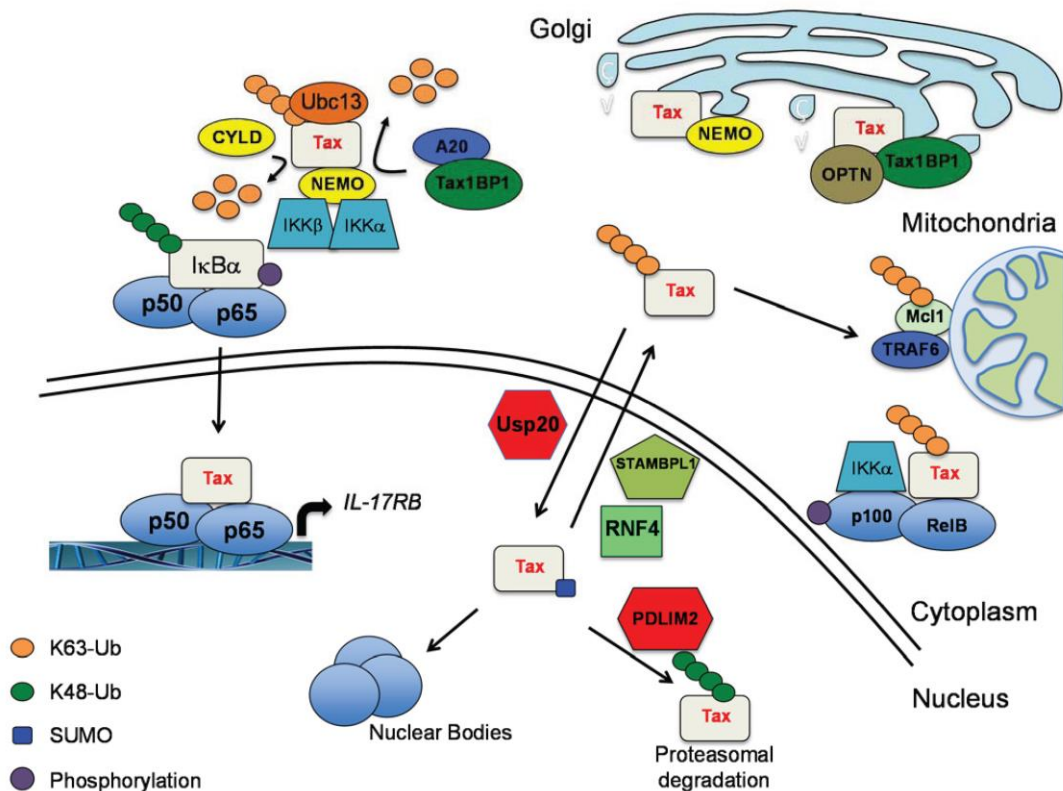


**Figure 30. Tax-induced relocalization<sup>466</sup> (adapted from Lavorgna and Harhaj, 2014).** Relocalization and activation of canonical and non-canonical NF- $\kappa$ B signaling pathways. Tax relocates NEMO, OPTN and TAX1BP1 to perinuclear Golgi structures to induce sustained activation of the NF- $\kappa$ B signaling pathway.

Historically, TAX1BP1 was identified in a yeast two-hybrid screen as an interactant of Tax named TXBP151<sup>483,484</sup>. TAX1BP1 is involved in the recruitment of the deubiquitinase A20 and the negative control of TNF $\alpha$ , IL-1- and LPS-mediated NF- $\kappa$ B activation<sup>138,485</sup>. In addition to TAX1BP1, A20 is also dependent on other co-factors including the E3 ligases RNF11 and Itch that assemble to form the A20-ubiquitin-editing complex, upon induction<sup>486,487</sup>. Tax prevents the assembly of the A20 complex by blocking IKK $\alpha$ -mediated phosphorylation of TAX1BP1<sup>488</sup> and relocates TAX1BP1 to inactivate the A20 complex by impairing interactions between members of the complex<sup>486</sup>. Tax inactivation of A20 alleviates the negative feedback control of

NF- $\kappa$ B and facilitates persistent NF- $\kappa$ B signaling that drives cell transformation. Recently, Schwob *et al.* showed that Tax also recruits p62 via polyubiquitin chains to the peri-Golgian Tax-induced Signalosome, where the other SARs are recruited, and potentiates sustained NF- $\kappa$ B activation<sup>489</sup>.

### 3. Anti-HTLV-1 T cell responses

CD4<sup>+</sup>T cells are the major targets of HTLV-1 chronic infection. The establishment of a chronic infection suggests that HTLV-1 manipulates the immune responses normally initiated upon primo-infection. As we have seen previously, the effect of Tax on the NF- $\kappa$ B signaling pathway is an important factor in the establishment of chronicity. In addition, during the chronic phase of infection, disruption of the equilibrium between viral replication and HTLV-1-specific T cell responses (reflected by an increase in the proviral load (PVL)) is an important determinant of disease progression<sup>490</sup>. Strong HTLV-1-specific CD8<sup>+</sup>T cytotoxic T cell (CTL)<sup>491,492</sup> and CD4<sup>+</sup> helper T cell<sup>493,494</sup> responses are observed in the blood of HTLV-1-infected individuals, and *ex vivo*, Tax-specific CTL from patients have been shown to kill Tax-expressing autologous cells<sup>430</sup>. Surprisingly, there is no clear correlation between the magnitude of T cell responses and the PVL<sup>495</sup>. It seems that the quality, rather than the magnitude of HTLV-1-specific T cell responses, might allow chronicity and determine the disease outcome. Resistance to disease progression has been associated with protective HLA alleles, such as HLA-A\*02 or -Cw\*08<sup>496-498</sup> whereas disease susceptibility has been associated with HLA-B\*5401 or HLA-DRB1\*0101<sup>497,498</sup>. Compared to healthy carriers of the virus, HAM/TSP patients exhibit an HTLV-1-specific CTL compartment with compromised expression of stimulatory molecules and lower degranulation capacity<sup>499</sup>. Comparing the frequency and lytic activity of HTLV-1-specific CTLs in fresh unstimulated PBMCs of patients, Kattan *et al.* also concluded that the efficient control of HTLV-1 *in vivo* depends on the CTL lytic efficiency<sup>500</sup>. An inverse correlation<sup>501</sup> between the PVL and the expression of exhaustion markers (PD-1) by Tax-specific CTLs has been reported, further highlighting that the quality of CTL responses is critical for clinical evolution. Interestingly, a strong negative correlation has been observed between the frequency of CD4<sup>+</sup>FoxP3<sup>+</sup> T<sub>regs</sub> and the CTL activity in HTLV-1-infected individuals<sup>502</sup>, indicating that the quality of CD4<sup>+</sup>T cell responses might be one of the largest single determinants of the quality of the HTLV-1-specific CTL responses.

Remarkably, myeloid cells<sup>503-505</sup> and HTLV-1-specific T cells from infected individuals show compromised phenotypes and functions, strongly suggesting that the establishment of a chronic infection, and the subsequent development of diseases, may be primed by an early defect in the initiation of immune responses to the virus. In addition, as mentioned above, HTLV-1 infection is often associated with a higher susceptibility to opportunistic infections<sup>506</sup>, indicating immune dysfunctions that may not be restricted to HTLV-1-specific responses, but whose origin remains largely unclear. As APCs, DCs dictate the quality of T cell responses, through the kinetics and amount of antigens presented, but also the engagement of co-stimulatory or co-inhibitory signals and the cytokine environment. Several groups have documented the productive *in vitro* infection of myeloid DCs and of monocyte-derived DCs (MDDCs)<sup>504,505,507-509</sup>. Very little is known about the capacity of HTLV-1-infected DCs to prime efficient T cell responses. Several studies have shown that blood DCs from HTLV-1-infected patients<sup>433,503,504</sup> and DCs from uninfected individuals, exposed *in vitro* to HTLV-1<sup>510</sup>, induce an abnormal proliferation of autologous T cells, with a more pronounced influence on CD4<sup>+</sup>T cell stimulation<sup>504</sup>. Specifically, MDDCs from ATL patients have altered capacities to stimulate the proliferation of allogenic T cells in mixed lymphocyte reactions, independent of antigen recognition<sup>505,511</sup>. Exposure of MDDCs to recombinant Tax increased the expression of activation and maturation markers<sup>512</sup>, the secretion of pro-inflammatory cytokines<sup>513</sup>, and the induction of antigen-independent T-cell proliferation<sup>513</sup>, in an NF-κB-dependent manner. This suggests that, as in CD4<sup>+</sup>T cells, Tax modulates NF-κB with a potential effect on antigen presentation and activation of CD4<sup>+</sup>T cells. However, the detailed signaling properties of Tax in DCs remain to be investigated.

#### 4. Tax modulation of autophagy

HTLV-1 has also been shown to promote autophagy via IKK activation, supporting the proliferation and survival of HTLV-1 transformed cell lines<sup>514</sup>. This capacity to increase autophagosomes depends on the capacity of Tax to activate the NF-κB pathway<sup>515</sup>. In fact, Tax recruits Beclin-1 and Bif-1 to LRDs, inducing the recruitment of all the elements for autophagosomes biogenesis (Figure 31). The IKK signalosome is necessary in this Tax-mediated autophagy dysregulation since Tax does not localize in the Golgi-associated LRDs in absence of IKKγ/NEMO and depletion or impairment of any IKK complex member prevents Beclin-1 and Bif-1 recruitment<sup>514</sup>. Golgi-associated LRDs seem to function as platforms where

Tax engages the NF- $\kappa$ B and autophagy pathways by the local interaction of Tax, Beclin-1, SARs and the IKK complex<sup>469</sup> (Figure 31).

The Tax-mediated deregulation of autophagy is completed on the final steps of autophagosome maturation. Tang *et al.* showed that Tax inhibits autophagosome-lysosome fusion. Interestingly, treatment with bafilomycin A improves Tax stability suggesting that Tax could be degraded into lysosomes via the autophagy pathway. The team then showed that Tax inhibits the fusion of these degrading vesicles. Therefore, Tax interferes with the autophagy pathway by generating autophagosome accumulation but impeding their maturation and thus preventing its own degradation<sup>515</sup>.

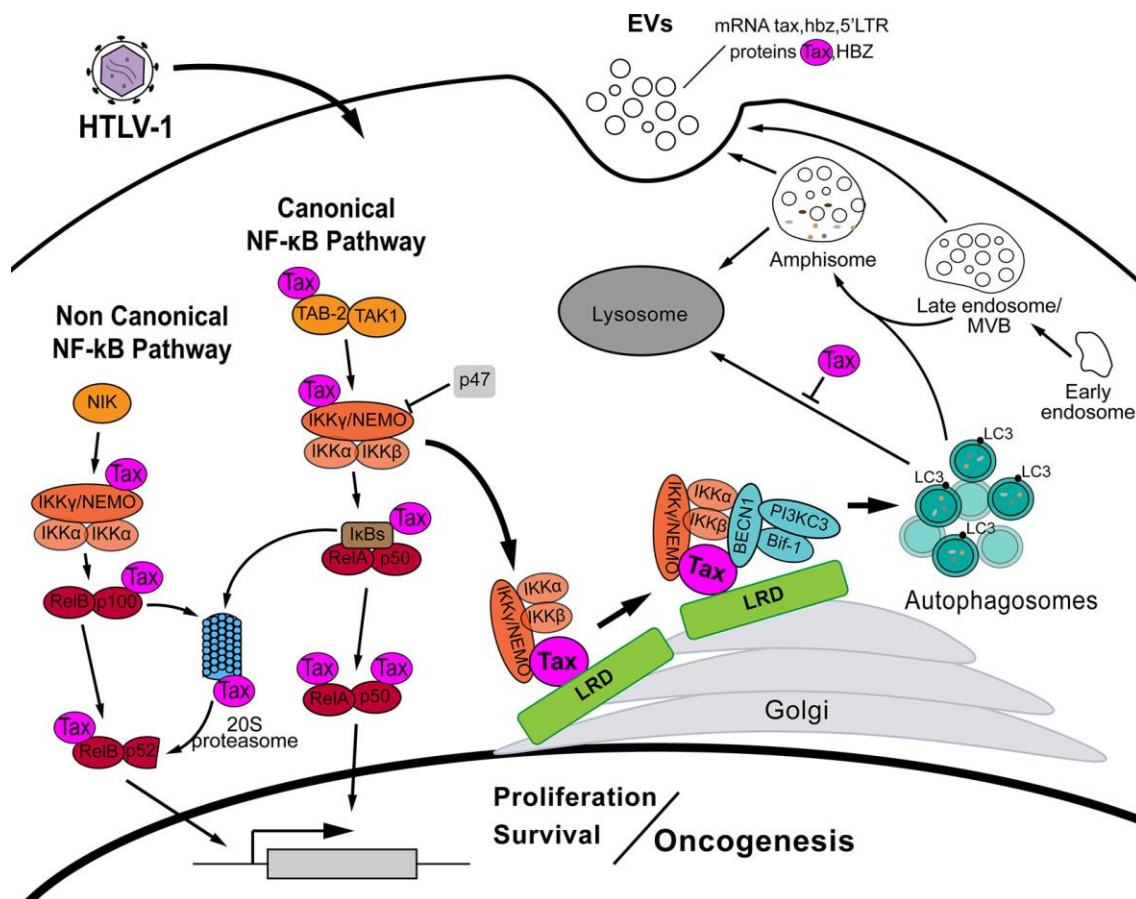


**Figure 31. Tax-induced autophagy modulation<sup>469</sup> (adapted from Ducasa *et al.*, 2021).** Tax interferes at several steps of both canonical and noncanonical NF- $\kappa$ B pathway to induce cellular transformation. By interaction with IKK $\gamma$ /NEMO, Tax recruits and activates the IKK complex in Golgi-associated lipid raft domains (LRDs). After IKK activation, Tax recruits the autophagy proteins Beclin-1 (BECN1), Bif-1 and the PI3KC3 complex through its direct interaction with BECN1, which in turn binds also with IKK $\alpha$ , IKK $\beta$ . Tax deregulates the autophagy pathway fostering autophagosome biogenesis whilst blocking the autophagosome-lysosome fusion. Autophagosome accumulation enhances HTLV-1 replication.

Taken together, it appears that Tax utilizes the Golgi-located Signalosome, and possibly other cytoplasmic substructures, as a specific platform for IKK activation and modulation of the NF- $\kappa$ B and autophagy pathways.

Tax relocation of SARs could also have other effects, for example in vesicle trafficking, given the diverse roles played by SARs described in the first part of this introduction. The blockage of autophagosome maturation by Tax could also have an impact on antigen processing, especially considering that Tax not only infects CD4<sup>+</sup>T lymphocytes but also infects DCs.

In conclusion, we have seen that viruses have developed numerous mechanisms allowing them to target and escape the different pathways of MHC-II-restricted antigen presentation and CD4<sup>+</sup>T cell activation. SARs seem to be at the crossroads of immune sensing. Indeed, their modulation can play a role not only in antigen processing, but also in antiviral intrinsic immunity, innate immune signaling pathways and can be subverted for viral profit. In the first part of my PhD, together with my team, we recently showed that TAX1BP1, amongst the SARs recruited by Tax to induce NF- $\kappa$ B activation, is a key player in MHC-II antigen presentation. One of the main questions raised was whether TAX1BP1 and other SARs might be viral targets to escape MHC-II-mediated antiviral immunity.

## Scientific context and thesis objectives

Several groups have shown the contribution of the different forms of selective autophagy, such as CMA, in antigen processing and MHC-II-restricted antigen presentation. My team is interested in the interplays between autophagy and antiviral immunity.

Following the demonstration by the laboratory that targeting the HIV antigen gag to autophagosomes induced a more potent activation of gag-specific CD4<sup>+</sup>T cells than the one elicited by the native antigen, the team decided to focus on the role of selective autophagy receptors (SARs) in MHC-II-restricted viral antigen presentation.

When I arrived in the laboratory, the team had shown that silencing the expression of TAX1BP1 affected viral antigen presentation and virus-specific CD4<sup>+</sup>T cell activation in model APCs. In the same functional screen, they had silenced other SARs as well but this had no impact on MHC-II antigen presentation. In addition, they had analyzed the MHC-II peptide repertoire in the absence of TAX1BP1 and observed a drastic effect on the quantity and the quality of the peptides presented compared to cells expressing TAX1BP1.

The objective of the first part of my thesis was to characterize the mechanisms underlying the effect of TAX1BP1 silencing on MHC-II-restricted antigen presentation. To this end, I aimed at studying the biology and kinetics of different elements of the MHC-II antigen presentation pathway in the absence of TAX1BP1. In addition, I aimed at characterizing novel interactants of TAX1BP1 and their role in MHC-II-restricted antigen presentation to get a better insight on the mechanisms governing the effect of TAX1BP1 silencing on MHC-II antigen presentation.

After describing TAX1BP1 as a key player in MHC-II antigen presentation, I then sought to study whether viral proteins might target SARs, amongst them TAX1BP1, to escape MHC-II antigen presentation and thus antiviral immunity.

The objective of the second part of my thesis was to use HTLV-1 Tax oncoprotein, known to target SARs including TAX1BP1, as a tool to assess the impact of SAR hijacking on MHC-II antigen presentation. To this end, I aimed at studying the effect of Tax expression on MHC-II-restricted viral antigen presentation as well as on the biology and kinetics of the MHC-II antigen presentation pathway including the MHC-II immunopeptidome. In addition, I aimed at evaluating the role of different SARs in the effect of Tax expression on MHC-II viral antigen presentation.

## Project 1: article published in EMBO Reports in 2022

To study the role of selective autophagy receptors (SARs) in MHC-II-restricted antigen presentation, we performed a functional siRNA screen of NDP52, TAX1BP1, OPTN and p62 in our model HeLa-CIITA cells. We observed that only the silencing of TAX1BP1 affected the presentation of the HIV gag antigen fused to LC3 (gag-LC3) to CD4<sup>+</sup>T cells and induced a decrease of CD4<sup>+</sup>T cell activation. Remarkably, TAX1BP1 also affected the presentation of the native gag antigen and the mutant form of gag-LC3 (G120A), which cannot be included in autophagosomes. To determine whether the absence of TAX1BP1 might influence MHC-II kinetics, we assessed the internalization of mature MHC-II-complexes as well as their surface expression and found no significant effect of TAX1BP1 silencing on MHC-II internalization kinetics. Given these results, we then asked whether TAX1BP1 silencing might affect the stability of MHC-II-peptide complexes. In fact, a fraction of peptide-loaded MHC-II heterodimers adopts a stable conformation resistant to dissociation by SDS at room temperature but not at 95°C<sup>276</sup>. I found that SDS-stable complexes were greatly reduced in the absence of TAX1BP1.

The nature of the peptides presented can influence the quality of MHC-II-peptide complexes<sup>56</sup>. We therefore analyzed the global peptide repertoire (immunopeptidome) presented by MHC-II molecules in cells silenced or expressing TAX1BP1 and found that TAX1BP1 expression has a strong influence on the peptide repertoire, the relative abundance, and the relative affinity of epitopes presented by MHC-II molecules. These results could explain the effect of TAX1BP1 silencing on viral antigen presentation and CD4<sup>+</sup>T cell activation; and show a broad role of TAX1BP1 on the MHC-II immunopeptidome. In order to understand the effect of TAX1BP1 on the peptide repertoire, we asked whether TAX1BP1 might play a role in the intracellular trafficking of MHC-II molecules prior to reaching the plasma membrane. To this end, using confocal microscopy, I evaluated the effect of TAX1BP1 silencing on the subcellular localization of MHC-II molecules together with other markers of the MHC-II loading compartment (MIIC), such as HLA-DM, and markers of endo-lysosomal vesicles. Of note, HLA-DM is a chaperone involved in MHC-II peptide loading<sup>257</sup>. Combined together, MHC-II, HLA-DM and endo-lysosomal markers serve to identify the MIIC. Strikingly, MHC-II positive vesicles localized closer to the nucleus in cells silenced for TAX1BP1. I observed a similar strong relocalization of HLA-DM and the different endo-lysosomal markers we assessed. Therefore, TAX1BP1 influences the

positioning of the MIIC. The relocalization of the MIIC towards the nucleus, in the absence of TAX1BP1, could partially account for the defect of MHC-II maturation and could sustain the dramatic changes in the global MHC-II peptide repertoire. The invariant chain Ii (CD74) is essential for the trafficking and maturation of MHC-II molecules<sup>208,212,215,516</sup>. In the MIIC, Ii degradation is also strictly regulated to ensure appropriate loading of MHC-II molecules with high-affinity peptides<sup>233,236</sup>. I therefore assessed the effect of TAX1BP1 silencing on Ii expression. Remarkably, the absence of TAX1BP1 induces an exacerbated Ii degradation. I could recover Ii expression upon treatment with chloroquine, suggesting that Ii is degraded in acidified vesicles in the absence of TAX1BP1. Ii has been shown to influence both the cellular trafficking and the immunopeptidome of MHC-II molecules<sup>265</sup>, therefore the exacerbated degradation of Ii could explain the strong influence of TAX1BP1 silencing on the MHC-II immunopeptidome in our model.





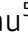







To decipher the mechanism by which T6BP influences MHC-II-restricted endogenous antigen presentation, we decided to define the interactome of T6BP in HeLa-CIITA cells. We used a plasmid encoding GFP-TAX1BP1 and performed a large-scale immunoprecipitation (IP) using GFP as a tag. We used as negative control the same plasmid encoding GFP. We identified a novel partner of TAX1BP1, the ER chaperone Calnexin (CANX). We focused on this protein because of its known interaction with Ii<sup>204</sup>. I confirmed TAXBP1 interaction with CANX in our model APCs and in model DCs and B cells and showed that CANX interacts with TAX1BP1 through its cytosolic tail. In addition, I showed that silencing CANX recapitulates Ii exacerbated degradation and MHC-II antigen presentation and subsequent CD4<sup>+</sup>T cell activation decrease. The same effects observed upon TAX1BP1 silencing. We suggest that TAX1BP1 silencing affects CANX functions resulting in Ii degradation and aberrant MHC-II peptide loading and antigen presentation to CD4<sup>+</sup>T cells.

Overall, we demonstrate that TAX1BP1 regulates de loading and presentation of endogenous viral antigens by MHC-II molecules, with a direct effect on CD4<sup>+</sup>T cell activation. We provide evidence that TAX1BP1 regulates CANX functions, which include the stabilization of Ii. Nonetheless, we believe that TAX1BP1 might also influence MHC-II-restricted antigen presentation through the regulation of the trafficking of MHC-II-loading compartments and more globally of acidified vesicular compartments.





# The Autophagy Receptor TAX1BP1 (T6BP) improves antigen presentation by MHC-II molecules

Gabriela Sarango<sup>1,2,†</sup> , Clémence Richetta<sup>2,3,†</sup>, Mathias Pereira<sup>1,2,†</sup> , Anita Kumari<sup>1,2</sup> , Michael Ghosh<sup>4</sup> , Lisa Bertrand<sup>1,2</sup> , Cédric Pionneau<sup>5</sup> , Morgane Le Gall<sup>6</sup> , Sylvie Grégoire<sup>1,2</sup>, Raphaël Jeger-Madiot<sup>2,‡</sup>, Elina Rosoy<sup>2</sup>, Frédéric Subra<sup>3</sup>, Olivier Delelis<sup>3</sup>, Mathias Faure<sup>7,8</sup> , Audrey Esclatine<sup>1</sup>, Stéphanie Graff-Dubois<sup>2,‡</sup> , Stefan Stevanović<sup>4</sup> , Bénédicte Manoury<sup>9,\*</sup> , Bertha Cecilia Ramirez<sup>1,2</sup>  & Arnaud Moris<sup>1,2,\*\*</sup> 

## Abstract

CD4<sup>+</sup> T lymphocytes play a major role in the establishment and maintenance of immunity. They are activated by antigenic peptides derived from extracellular or newly synthesized (endogenous) proteins presented by the MHC-II molecules. The pathways leading to endogenous MHC-II presentation remain poorly characterized. We demonstrate here that the autophagy receptor, T6BP, influences both autophagy-dependent and -independent endogenous presentation of HIV- and HCMV-derived peptides. By studying the immunopeptidome of MHC-II molecules, we show that T6BP affects both the quantity and quality of peptides presented. T6BP silencing induces the mislocalization of the MHC-II-loading compartments and rapid degradation of the invariant chain (CD74) without altering the expression and internalization kinetics of MHC-II molecules. Defining the interactome of T6BP, we identify calnexin as a T6BP partner. We show that the calnexin cytosolic tail is required for this interaction. Remarkably, calnexin silencing replicates the functional consequences of T6BP silencing: decreased CD4<sup>+</sup> T cell activation and exacerbated CD74 degradation. Altogether, we unravel T6BP as a key player of the MHC-II-restricted endogenous presentation pathway, and we propose one potential mechanism of action.

**Keywords** calnexin; CD4<sup>+</sup> T cell activation; interactome; immunopeptidome; virus

**Subject Categories** Autophagy & Cell Death; Immunology; Signal Transduction

**DOI** 10.15252/embr.202255470 | Received 23 May 2022 | Revised 16 September 2022 | Accepted 23 September 2022

**EMBO Reports (2022) e55470**

## Introduction

CD4<sup>+</sup> helper T cells that orchestrate adaptive immune responses recognize pathogen- or tumor-derived peptides presented by the major histocompatibility complex class II (MHC-II) molecules. MHC-II molecules are expressed by professional antigen-presenting cells (APC) such as B cells, macrophages and dendritic cells (DC), thymic epithelial cells (TEC), and by nonprofessional APCs in inflammatory conditions (Roche & Furuta, 2015; Wijdeven *et al.*, 2018). The MHC-II transactivator, CIITA, governs the transcription of the MHC-II locus that includes genes encoding for the  $\alpha$ - and  $\beta$ -chains of MHC-II molecules, the invariant chain (called Ii or CD74), and the chaperon proteins HLA-DM/HLA-DO (Reith *et al.*, 2005). The transmembrane  $\alpha$ - and  $\beta$ -chains are assembled within the endoplasmic reticulum (ER), where they associate with CD74 leading to the formation of nonameric  $\alpha\beta$ -CD74 complexes that traffic into late endo-lysosomal compartments named MIIC (Bakke & Dobberstein, 1990; Lotteau *et al.*, 1990; Neeffjes *et al.*, 1990; Roche *et al.*, 1991). In the MIIC, CD74 is progressively cleaved by vesicular proteases (Riese *et al.*, 1996; Nakagawa *et al.*, 1998; Shi *et al.*, 2000; Manoury

1 Université Paris-Saclay, CEA, CNRS, Institute for Integrative Biology of the Cell (I2BC), Gif-sur-Yvette, France

2 Sorbonne Université, INSERM, CNRS, Center for Immunology and Microbial Infections (CIMI-Paris), Paris, France

3 LBPA, ENS-Paris Saclay, CNRS UMR8113, Université Paris Saclay, Gif-sur-Yvette, France

4 Department of Immunology, Institute for Cell Biology, University of Tübingen, Tübingen, Germany

5 Sorbonne Université, INSERM, UMS Production et Analyse de Données en Sciences de la vie et en Santé, PASS, Plateforme Post-génomique de la Pitié Salpêtrière, Paris, France

6 3P5 proteom<sup>2</sup>IC facility, Université de Paris, Institut Cochin, INSERM U1016, CNRS-UMR 8104, Paris, France

7 CIRI, Centre International de Recherche en Infectiologie, Université de Lyon, Inserm U1111, Université Claude Bernard Lyon 1, CNRS, UMR5308, ENS de Lyon, Lyon, France

8 Equipe Labellisée par la Fondation pour la Recherche Médicale, FRM

9 Institut Necker Enfants Malades, INSERM U1151-CNRS UMR 8253, Faculté de médecine Necker, Université de Paris, Paris, France

\*Corresponding author. Tel: +33 140615382; E-mail: benedicte.manoury@inserm.fr

\*\*Corresponding author. Tel: +33 169826294; E-mail: arnaud.moris@i2bc.paris-saclay.fr

†These authors contributed equally to this work

‡Present address: Sorbonne Université, INSERM U959, Immunology-Immunopathology-Immunotherapy (i3), Paris, France

et al, 2003), leaving a residual MHC-II-associated Ii peptide (CLIP) that occupies the peptide binding groove (Roche & Cresswell, 1991; Bijlmakers et al, 1994; Busch et al, 1996). HLA-DM then facilitates the exchange of the CLIP fragments with high-affinity peptides generated from pathogen- or tumor-derived antigens (Morris et al, 1994; Sanderson et al, 1994; Denzin & Cresswell, 1995). MHC-II molecules are then transported to the plasma membrane to expose antigenic peptides to CD4<sup>+</sup> T cells (Thibodeau et al, 2019).

MHC-II molecules present peptides derived from extra- and intracellular sources of antigens, so-called exogenous and endogenous presentation, respectively (Watts, 2004; Veerappan Ganesan & Eisenlohr, 2017). Extracellular antigens are captured and internalized into APCs by various means including macropinocytosis, phagocytosis, or receptor-mediated endocytosis (Roche & Furuta, 2015). Antigens are then delivered to the MIIC where they are progressively degraded by endo-lysosomal proteases such as cathepsins (Watts, 2004), into peptides (or epitopes) ranging from 12 to 25 amino acids in length, that can be loaded on nascent MHC-II molecules (Rudensky et al, 1991; Unanue et al, 2016). Epitopes from extracellular antigens can also bind, in early endosomes, to recycling MHC-II molecules (Pinet et al, 1995; Sinnathamby & Eisenlohr, 2003). The endogenous pathway relies on protein antigen synthesis by virus-infected (Jacobson et al, 1988; Sekaly et al, 1988; Eisenlohr & Hackett, 1989; Jaraquemada et al, 1990; Nuchtern et al, 1990; Thiele et al, 2015) or tumor cells (Tsuji et al, 2012). Some early *in vitro* studies showed that neosynthesized self-epitopes are displayed, after lysosomal proteolysis, by MHC-II molecules leading to CD4<sup>+</sup> T cell activation (Bikoff & Birshstein, 1986; Rudensky & Yurin, 1989; Weiss & Bogen, 1989). More recently, it was shown that the initiation of CD4<sup>+</sup> T cell responses to *influenza virus* is mainly driven by epitopes derived from the processing of intracellular antigens within APCs (Miller et al, 2015). However, the pathways leading to the loading of MHC-II molecules with endogenous antigens remain poorly characterized. Components of the MHC class I (MHC-I) processing pathway such as proteasome have been implicated (Lich et al, 2000; Tewari et al, 2005). One unresolved issue is how cytosolic antigens are transported into MHC-II-enriched compartments (Dani et al, 2004; Crotzer & Blum, 2008). For some specific epitopes but not others, the transporter associated with antigen presentation of MHC-I molecules (TAP) has been linked with the delivery of endogenous peptides on MHC-II molecules (Malnati et al, 1992; Tewari et al, 2005). In fact, depending on the cellular localization, the trafficking, and the nature of the antigen itself, different pathways might be involved in the degradation and delivery of endogenous antigens to MHC-II loading compartments (Mukherjee et al, 2001; Tewari et al, 2005; Leung, 2015).

The pathways of autophagy contribute to the processing of MHC-II-restricted endogenous antigens. The receptor of chaperone-mediated autophagy, LAMP-2A, has been shown to facilitate the presentation of a cytosolic self-antigen by MHC-II molecules (Zhou et al, 2005). The analysis of the MHC-II immunopeptidome revealed that macroautophagy (herein referred to as autophagy) also contributes to the processing of cytoplasmic and nuclear antigens (Dengiel et al, 2005). Autophagy is a self-eating cellular degradation pathway, in which double-membrane autophagosomes deliver their cytoplasmic constituents for lysosomal degradation (Kirkin, 2020). Using various models, several labs established that autophagy

participates, in TECs, in the generation of MHC-II-restricted endogenous epitopes and strongly influences the thymic selection of autoreactive CD4<sup>+</sup> T cells (Aichinger et al, 2013; Schuster et al, 2015). Other evidence that autophagy plays a role in endogenous antigen presentation comes from *in vitro* studies using APCs transfected with mRNAs encoding tumor antigens (Dorfel et al, 2005) or cDNAs encoding tumor or viral antigens targeted to autophagosomes (Schmid et al, 2007; Jin et al, 2014; Coulon et al, 2016; Fonteneau et al, 2016). Targeting antigens to autophagosomes through the fusion to LC3, an autophagy effector that incorporates into and participates in the elongation of autophagosomes enhances the capacity of APCs to activate antigen-specific CD4<sup>+</sup> T cells (Coulon et al, 2016). However, overall, there are few examples where endogenous degradation of native tumors or viral antigens has been shown to be dependent on autophagy (Paludan et al, 2005; Leung, 2015). In fact, autophagy effectors may directly or indirectly affect the presentation of MHC-II-restricted antigens (Fletcher et al, 2018) by regulating, for instance, the delivery of proteases into the MIIC (Lee et al, 2010). Thereafter, autophagy also contributes to the exogenous presentation of viral and bacterial antigens (Jagannath et al, 2009; Blanchet et al, 2010). The molecular links between autophagy and MHC-II-restricted antigen presentation, in particular the mechanisms allowing the delivery of autophagy-degraded antigens to the MIIC, are poorly defined.

A growing body of evidence indicates that autophagosomes selectively target their cargos while excluding the rest of the cytoplasmic content (Kirkin, 2020). Several forms of selective autophagy exist, depending on the substrate, but all rely on the so-called autophagy receptors (ARs) that include: Nuclear Dot Protein 52 (NDP52), Optineurin (OPTN), Sequestosome-1 / p62, Next to BRCA1 gene protein-1 (NBR1) and TAX1-binding protein-1 also called TRAF6-binding protein (TAX1BP1/T6BP) (Kirkin & Rogov, 2019). ARs contain ubiquitin (Ub) and LC3-binding domains that allow, on the one hand, binding to ubiquitinated proteins and, on the other hand, their targeting into autophagosomes through interaction with LC3 on the internal membranes of forming autophagosomes (Kirkin & Rogov, 2019). As such, ARs are involved in multiple cellular processes including selective degradation of incoming bacteria and of damaged mitochondria, processes called xenophagy (Tumbarello et al, 2015) and mitophagy (Randow & Youle, 2014), respectively. In addition to their role in selective autophagy, T6BP, NDP52, and OPTN are required for the maturation of autophagosomes (Tumbarello et al, 2012). Thanks to the binding to myosin-VI, these ARs bridge autophagosomes to Tom-1-expressing endosomes and lysosomes, thus facilitating their fusion (Sahlender et al, 2005; Morriswood et al, 2007; Tumbarello et al, 2012). T6BP, OPTN, and NDP52, by promoting autophagosome maturation (Verlhac et al, 2015), are essential for the degradation of *Salmonella typhimurium* (Thurston et al, 2009; Wild et al, 2011; Lin et al, 2019). Remarkably, T6BP, NDP52, and p62 were also shown to orchestrate the maturation of early endosomes into late endosomes (Jongsma et al, 2016). This process also involves the Ub-binding domain of these receptors (Jongsma et al, 2016). Therefore, ARs exert multiple redundant but also exclusive roles in selective autophagy and in the traffic and maturation of vesicles such as autophagosomes and endosomes.

Here, we hypothesize that ARs may contribute at various, so far unknown, levels to MHC-II-restricted viral antigen presentation. We

show that silencing of NDP52, OPTN, and p62 in model APCs does not significantly affect the presentation of an autophagy-dependent antigen to CD4<sup>+</sup> T cells. By contrast, T6BP influences both autophagy-dependent and -independent endogenous viral, as well as cellular, antigen processing and presentation by MHC-II molecules. In fact, the action of T6BP is not limited to viral antigens since the global repertoire of peptides presented by MHC-II molecules (immunopeptidome) is dramatically changed upon T6BP silencing. We show that T6BP silencing does not perturb the global cell-surface expression nor internalization kinetics of MHC-II molecules. However, it induces significant relocalization of the MIIC closer to the nucleus and the generation of unstable MHC-II-peptide complexes. Importantly, we demonstrate that the absence of T6BP expression induces a strong and rapid degradation of the invariant chain CD74, which directly influences the quality of the peptide repertoire loaded on MHC-II molecules. Finally, to get a hint on possible mechanisms, we defined the interactome of T6BP and identified novel protein partners that potentially participate in the T6BP-mediated regulation of the MHC-II peptide loading process. Among them, we identified the ER chaperone calnexin (CANX). We show that T6BP binds the cytoplasmic tail of CANX known to regulate its ER functions. Finally, we provide the direct demonstration that silencing CANX also induces CD74 degradation and decreases the capacity of model APCs to activate CD4<sup>+</sup> T cells. Altogether, this study unravels a new role for T6BP as a key player in MHC-II-restricted antigen presentation, and in CD4<sup>+</sup> T cell immunity.

## Results

### T6BP silencing influences endogenous viral antigen presentation and CD4<sup>+</sup> T cell activation

Owing to their functions in selective autophagy and in the maturation of autophagosomes, we focused our work on NDP52, OPTN, and T6BP asking whether these ARs might be involved in endogenous antigen presentation by MHC-II molecules and subsequent activation of CD4<sup>+</sup> T cells. To this end, HeLa cells modified to express CIITA (HeLa-CIITA) were silenced for the expression of ARs using siRNAs targeting NDP52, OPTN, and T6BP and evaluated for their capacity to activate CD4<sup>+</sup> T cell clones (Fig 1A). An siRNA targeting p62 was also included as this AR plays, in multiple models, a dominant role in selective autophagy but does not participate in the maturation of autophagosomes (Tumbarello *et al*, 2012). 24 h post-siRNA transfection HeLa-CIITA cells were transfected with a plasmid encoding HIV Gag protein fused to LC3. This Gag-LC3 fusion enables specific targeting of Gag into autophagosomes and enhances HIV-specific T cell activation in an autophagy-dependent manner (Coulon *et al*, 2016). 48 h post-siRNA treatment (24 h post-DNA transfection), we analyzed by flow cytometry the percentages of living and of Gag-positive (Gag<sup>+</sup>) cells, using viability dye and Gag intracellular staining, respectively (Appendix Fig S1A). In all tested conditions, the levels of Gag<sup>+</sup> cells were similar and the sequential transfections (siRNA and cDNA) had no significant influence on cell viability (Appendix Fig S1B and C). The silencing of AR expression was also analyzed by Western Blot (WB). As compared to the control siRNA (CTRL), all siRNAs led to a marked decrease in AR expression (Fig 1B). HeLa-CIITA cells were then co-cultured with

Gag-specific CD4<sup>+</sup> T cells that we previously isolated and characterized (Moris *et al*, 2006). These Gag-specific CD4<sup>+</sup> T cell clones recognize HIV-infected cells (Moris *et al*, 2006; Coulon *et al*, 2016). CD4<sup>+</sup> T cell activation was monitored using IFN $\gamma$ -ELISPOT (Fig 1C). Cells transfected with CTRL, NDP52, OPTN, or p62 targeting siRNAs led to similar levels of CD4<sup>+</sup> T cell activation (Fig 1C, right and left panel). By contrast, T6BP silencing greatly decreased the activation of Gag-specific T cells (Fig 1C, left panel). On average, T6BP silencing led to a 75% decrease in Gag-specific CD4<sup>+</sup> T cell activation (Fig 1C, right panel).

We next analyzed the effect of T6BP silencing on autophagy-independent endogenous viral antigen processing and presentation by MHC-II molecules. As previously, HeLa-CIITA cells were first transfected with CTRL- or T6BP-targeting siRNAs (siCTRL and siT6BP, respectively), then transfected with various plasmids encoding Gag, Gag-LC3<sub>G120A</sub>, or Gag-LC3, and co-cultured with the Gag-specific CD4<sup>+</sup> T cells (Fig 1D). Importantly, in our previous work we demonstrated that newly synthesized Gag is processed in an autophagy-independent manner both in monocyte-derived DCs (MDDCs) and in HeLa-CIITA cells (Coulon *et al*, 2016). This was shown by using productively infected MDDCs and Gag-cDNA-transfected HeLa-CIITA cells treated with various drugs influencing autophagy (e.g., 3-MA, Spautin-1, and Torin-1), shRNA targeting LC3 or overexpressing a trans-dominant mutant of Atg4B (Atg4BC74A), which blocks the formation of autophagosomes. Using the same tools, we also showed that the fusion with LC3 (Gag-LC3) targets Gag to autophagosome-mediated degradation leading to an enhancement of CD4<sup>+</sup> T cell activation. Gag-LC3<sub>G120A</sub> was also used as a negative control for autophagy-dependent degradation, as the G120A mutation in the C-terminus of LC3 abolishes the lipidation and incorporation of LC3 in the nascent membranes of autophagosomes, thus preventing Gag targeting into autophagosomes. Finally, we showed that upon Gag-LC3<sub>G120A</sub>-transfection, Gag antigens are processed in an autophagy-independent manner (Coulon *et al*, 2016). 24 h post-transfection and prior co-culture with the CD4<sup>+</sup> T cells, the percentage of Gag<sup>+</sup> cells, Gag expression levels and the cell viability were similar in all tested conditions (Appendix Fig S1C). As previously, T6BP silencing strongly decreased the capacity of HeLa-CIITA cells expressing Gag-LC3 to activate the Gag-specific T cells (Fig 1D, left panel). However, we observed that the effect of T6BP silencing was not limited to Gag-LC3 as the capacity of HeLa-CIITA expressing Gag- or Gag-LC3<sub>G120A</sub> to activate the CD4<sup>+</sup> T cell clones, was also reduced in siT6BP-treated cells (Fig 1D, left panel). Importantly, T6BP silencing did not interfere with the ability of HeLa-CIITA cells to present the cognate peptide recognized by Gag-specific T cells when the peptide was added exogenously (Fig 1D, right panel). These results suggest that T6BP silencing influences the generation of Gag-, Gag-LC3- and Gag-LC3<sub>G120A</sub>-derived endogenous epitopes and their subsequent presentation by MHC-II molecules to Gag-specific CD4<sup>+</sup> T cells but does not affect the presentation of exogenous peptides by MHC-II molecules. Note that we obtained similar results with several siRNAs targeting different exons and introns of T6BP mRNA. We then sought to extend these observations to additional viral antigens. To this end, HeLa-CIITA cells treated with siCTRL or siT6BP were transfected with a plasmid encoding the immunodominant pp65 HCMV antigen and co-cultured with a pp65-specific CD4<sup>+</sup> T cell line (Fig 1A and E). Remarkably, T6BP silencing also led to a

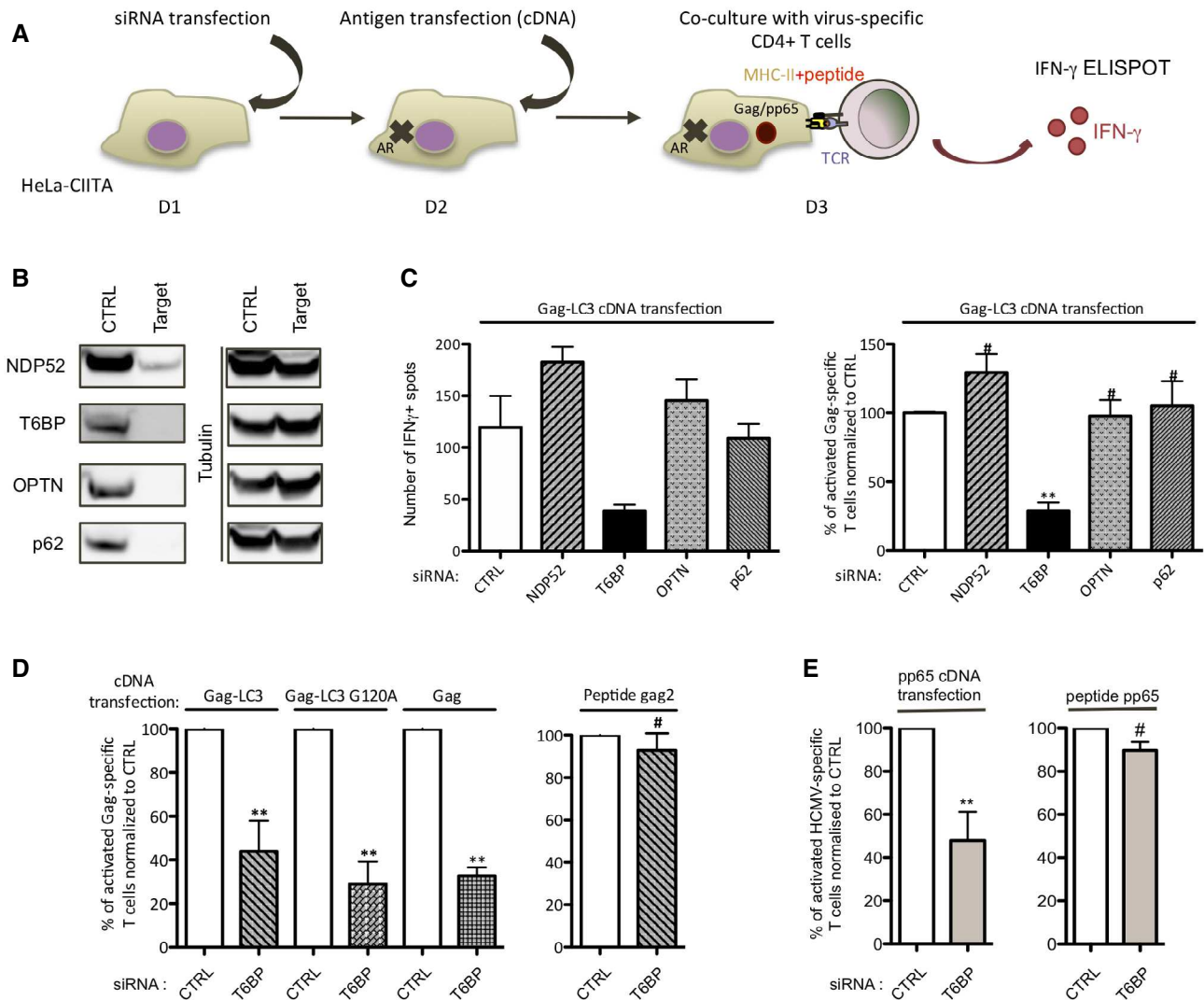


**Figure 1. T6BP silencing decreases endogenous viral Ag presentation and CD4<sup>+</sup> T cell activation.**

- A** Schematic representation of the experiment. HeLa-CIITA cells were transfected with siRNAs targeting ARs and 24 h later with plasmids encoding the antigens: Gag, Gag-LC3, Gag-LC3 G120A, or pp65. 24 h post-DNA transfection, the HeLa-CIITA cells were co-cultured with antigen-specific CD4<sup>+</sup> T cells and T cell activation was assessed using IFN $\gamma$ -ELISPOT. AR: Autophagy Receptor; D: day; TCR: T cell receptor.
- B** 48 h post-transfection of HeLa-CIITA cells with siRNAs targeting NDP52, T6BP, OPTN, and p62, AR expression was analyzed using Western Blot. Tubulin was used as control. The results are representative of at least 3 independent experiments and correspond to AR expression levels of the experiment in (C), left panel.
- C** Monitoring of Gag-specific CD4<sup>+</sup> T cell activation. HeLa-CIITA cells were treated as indicated above and transfected with a plasmid encoding Gag-LC3. Left panel, a representative experiment is shown ( $\pm$  SD of three technical replicates). Right panel, three biological replicates are combined and presented as mean percentage ( $\pm$  SD). The y-axis represents the relative percentage of IFN $\gamma$  spots reported to the secretion of IFN $\gamma$  by the CD4<sup>+</sup> T cell clones incubated with the siCTRL-treated HeLa-CIITA and set to 100%. The mean T cell activation levels of the three experiments using siCTRL or siT6BP were (100, 195, 119) and (35, 53, 38) IFN $\gamma$ <sup>+</sup> spots, respectively. 5,000 T cell clones were seeded per well in technical triplicates.
- D** Left panel, as in (C) right panel, but using DNA encoding Gag-LC3, Gag-LC3<sub>G120A</sub>, or Gag. With Gag-LC3, Gag-LC3 G120A or Gag antigens, the mean T cell activation levels using siCTRL or siT6BP were (199, 435, 384), (91, 141, 119) and (343, 415, 385) or (98, 273, 171), (27, 50, 19) and (97, 148, 131) IFN $\gamma$ <sup>+</sup> spots, respectively. 5,000 T cell clones were seeded per well in technical triplicates. Three biological replicates are combined and presented as mean percentage ( $\pm$  SD). Right panel, influence of T6BP silencing on peptide presentation by HeLa-CIITA cells. The cognate peptide was added exogenously (gag2, 0.1  $\mu$ g/mL) on siRNA-treated cells (2 h, 37°C), washed and T cell activation monitored using IFN $\gamma$ -ELISPOT. The mean T cell activation levels using siCTRL or siT6BP were (100, 45, 42) and (71, 45, 33) IFN $\gamma$ <sup>+</sup> spots, respectively. 1,000 T cell clones were seeded per well in technical triplicates. Three biological replicates are combined and presented as mean percentage ( $\pm$  SD).
- E** As in (D) but using cDNA encoding HCMV pp65 antigen (left panel) or pp65 peptide (0.5  $\mu$ g/mL; right panel) and a pp65-specific CD4<sup>+</sup> T cell line. Results of three independent experiments are represented. The mean T cell activation levels using siCTRL or siT6BP and pp65 DNA were (66, 106, 99) and (39, 50, 33) IFN $\gamma$ <sup>+</sup> spots, respectively. For the peptide: siCTRL or siT6BP: (185, 317, 415) and (163, 292, 381) IFN $\gamma$ <sup>+</sup> spots, respectively. 1,000 or 2000 T cell clones were seeded per well in technical triplicates.

Data information: For all ELISPOT experiments, the background secretions of IFN $\gamma$  by CD4<sup>+</sup> T cells co-cultured with mock-treated HeLa-CIITA cells were used as negative controls and subtracted. CTRL—control. Wilcoxon's test; the symbols correspond to \*\* $P$  < 0.01 and # $P$  > 0.05 comparing each experimental conditions solely with its internal control (siCTRL).

Source data are available online for this figure.

strong reduction in CD4<sup>+</sup> T cell activation (Fig 1E, left panel). As previously, the capacity of HeLa-CIITA cells to present the cognate pp65-derived peptide, added exogenously, was not affected (Fig 1E, right panel). These results demonstrate that regardless of the antigen tested, T6BP silencing dramatically influences the capacity of APCs to activate antigen-specific CD4<sup>+</sup> T cells. The effect of T6BP silencing is broader than we initially anticipated as it impacts both autophagy-dependent and -independent endogenous viral antigen processing and presentation by MHC-II molecules.

### **T6BP silencing lowers the stability of newly formed MHC–peptide complexes but does not significantly influence MHC-II molecule cell-surface expression and internalization**

Although T6BP silencing does not significantly alter the capacity of cells loaded with exogenous peptides to activate antigen-specific CD4<sup>+</sup> T cells (Fig 1D and E right panels), we asked whether T6BP might influence the internalization of MHC-II molecules. Using flow cytometry, we first monitored on T6BP-silenced HeLa-CIITA cells, the expression levels of HLA-DR molecules using the L243 and TÛ36 antibodies that recognize mature HLA  $\alpha\beta$  and immature HLA  $\alpha\beta$  heterodimers associated with the invariant chain (Ii), respectively (Fig 2A, left panel: L243 and right panel: TÛ36). Using both antibodies, we noticed a slight increase in HLA-DR cell-surface expression levels on cells silenced for T6BP expression (Fig 2A). We next analyzed the effect of T6BP silencing on the internalization kinetics of MHC-II molecules. HeLa-CIITA cells treated with siCTRL or siT6BP were coated at 4°C for 30 min with the L243 antibody that has been shown to act as an agonist of MHC-II molecules leading to their cellular internalization (De Gassart *et al*, 2008). The cells were then incubated at 37°C to follow internalization of MHC-II molecules (Fig 2B) or maintained at 4°C to monitor the antibody drop-off (Fig 2C). The cells were collected at the indicated time points and stained at 4°C with a labeled secondary antibody to detect the remaining L243 antibody conjugated with MHC-II molecules at the cell surface (Fig 2B and C). At 4°C, the mean fluorescent intensity (MFI) of HLA-DR molecules remained stable (Fig 2C). By contrast, at 37°C, the MFI dropped reaching a plateau after 40 min in both experimental conditions (Fig 2B, left panel), thus suggesting that the L243 antibody induced the internalization of HLA-DR molecules in the presence or absence of T6BP expression. As previously, compared with control condition, the silencing of T6BP slightly increased the expression levels (MFI) of HLA-DR molecules on the cell surface. However, it did not influence the kinetics of internalization of HLA-DR (Fig 2B, right panel).

We then asked whether the silencing of T6BP might affect the stability of peptide-loaded HLA  $\alpha\beta$  heterodimers. A fraction of peptide-loaded MHC-II  $\alpha\beta$  heterodimers adopts a stable conformation resistant to dissociation by SDS at room temperature but not at 95°C (Germain & Hendrix, 1991). 48 h post-transfection, we thus analyzed the influence of siT6BP on the formation of SDS-stable HLA-DR  $\alpha\beta$  heterodimers (Fig 2D). To this end, cells were pulsed with S<sup>35</sup> labeled methionine and cysteine, and then chased for 4 h, lysed and submitted to immunoprecipitation using TÛ36 that recognizes HLA  $\alpha\beta$  heterodimers and HLA  $\alpha\beta$ Ii complexes but not free  $\alpha$ -,  $\beta$ -chains and Ii (Benaroch *et al*, 1995). Prior to loading onto the SDS–PAGE gel, samples were either boiled (B) or incubated at room temperature (not boiled, NB) for 30 min in SDS-sample buffer

(Fig 2D). Immediately after the pulse, boiling of the samples revealed the  $\alpha$ ,  $\beta$  and the fragment lip33/lip35 of the invariant chain (Fig 2D, B, chase 0 h). As expected from previous work, less  $\alpha$ ,  $\beta$ , and Ii were detectable after 4 h of chase (Fig 2D, NB, chase 4 h) (Benaroch *et al*, 1995). The nonboiled samples revealed the existence of SDS-resistant stable peptide-loaded HLA-DR  $\alpha\beta$  heterodimers but only after 4 h of chase (Fig 2D, NB). Remarkably, in cells silenced for T6BP expression the band corresponding to SDS-resistant MHC  $\alpha\beta$  heterodimers was greatly reduced as compared to cells transfected with siCTRL (Fig 2D, NB, chase 4 h), strongly suggesting that T6BP expression facilitates the formation of stable peptide-loaded HLA molecules. Overall, these results show that T6BP silencing does not influence MHC-II internalization and cellular expression levels, in a significant manner. However, it has a strong impact on the stability of peptide-loaded MHC-II  $\alpha\beta$  heterodimers.

### **T6BP silencing dramatically alters the immunopeptidome of MHC-II molecules**

Various parameters affect the quality of peptide-loaded MHC complexes, including the nature of the peptide itself (Roche & Furuta, 2015). We thus decided to analyze the global peptide repertoire (immunopeptidome) presented by MHC-II molecules. In addition, analyzing the immunopeptidome might also reveal whether T6BP silencing affects a broader range of potential antigens. To study the immunopeptidome, HeLa-CIITA cells were either mock-treated or transfected with CTRL or T6BP-silencing siRNA and MHC-II molecules were immunoprecipitated by using the TÛ39 antibody (specific to mature HLA-DP, DQ, and DR). Finally, the peptide ligands were identified using mass spectrometry (LC–MS/MS). To assess the intrinsic variability of the MHC-II ligandome in HeLa-CIITA cells, we analyzed simultaneously the ligandome of two samples from mock-treated HeLa-CIITA cells that were split 48 h prior to lysis and MHC-II immunoprecipitations (IP). In these settings, 57% of identified peptides were shared by both samples of mock-treated cells (Fig 3A, left panel). Two biological replicates of siRNA-treated cells were analyzed, one is presented in Fig 3. We observed that 1,349 peptides (representing 25% of the peptides) were presented by MHC-II molecules exclusively in HeLa-CIITA cells expressing T6BP (Fig 3A, right panel, siCTRL). Remarkably, in the absence of T6BP expression, 2,198 new MHC-II ligands (40% of the peptides) were identified (Fig 3A, right panel, siT6BP) and only 35% of the peptides (1914 peptides) were shared between control and the T6BP-silenced conditions (Fig 3A, right panel). Overall, siT6BP-treated cells shared significantly less MHC-II peptide ligands with the three other experimental conditions (Mock1, Mock2, or siCTRL) (Fig EV1A). Together these results show that, although there is an intrinsic variability of the MHC-II ligandome in cells, the absence of T6BP has a pronounced and dramatic influence on the repertoire of peptides presented by MHC-II molecules.

We then asked whether T6BP expression might affect the source of peptides, i.e., the set of proteins supplying peptides for MHC-II loading. To this end, we submitted the LC–MS/MS data to cell component enrichment analysis using Funrich software (Pathan *et al*, 2015). As expected from previous work (Dengjel *et al*, 2005; Marcu *et al*, 2021), according to Funrich annotation and as compared with the human proteome, in both siCTRL- and siT6BP-

treated cells, the MHC-II-ligand source proteins were enriched in cellular fractions belonging to membranes, secretory pathways (e.g., exosomes and vesicles) but also to the cytosolic compartment of the cell (Fig EV1B). In siCTRL-treated cells MHC-II source proteins were also augmented in nuclear fractions, which was not the case for siT6BP-transfected cells. By contrast, MHC-II-ligand source proteins

belonging to the cytoplasm were enriched in siT6BP-treated cells (Fig EV1B). Overall, this analysis shows that the bulk of MHC-II-ligand source proteins is provided by the same cellular fractions mainly membranes, secretory pathways, and the cytosol. However, the presence of T6BP might also favor the presentation of peptides derived from the nucleus.

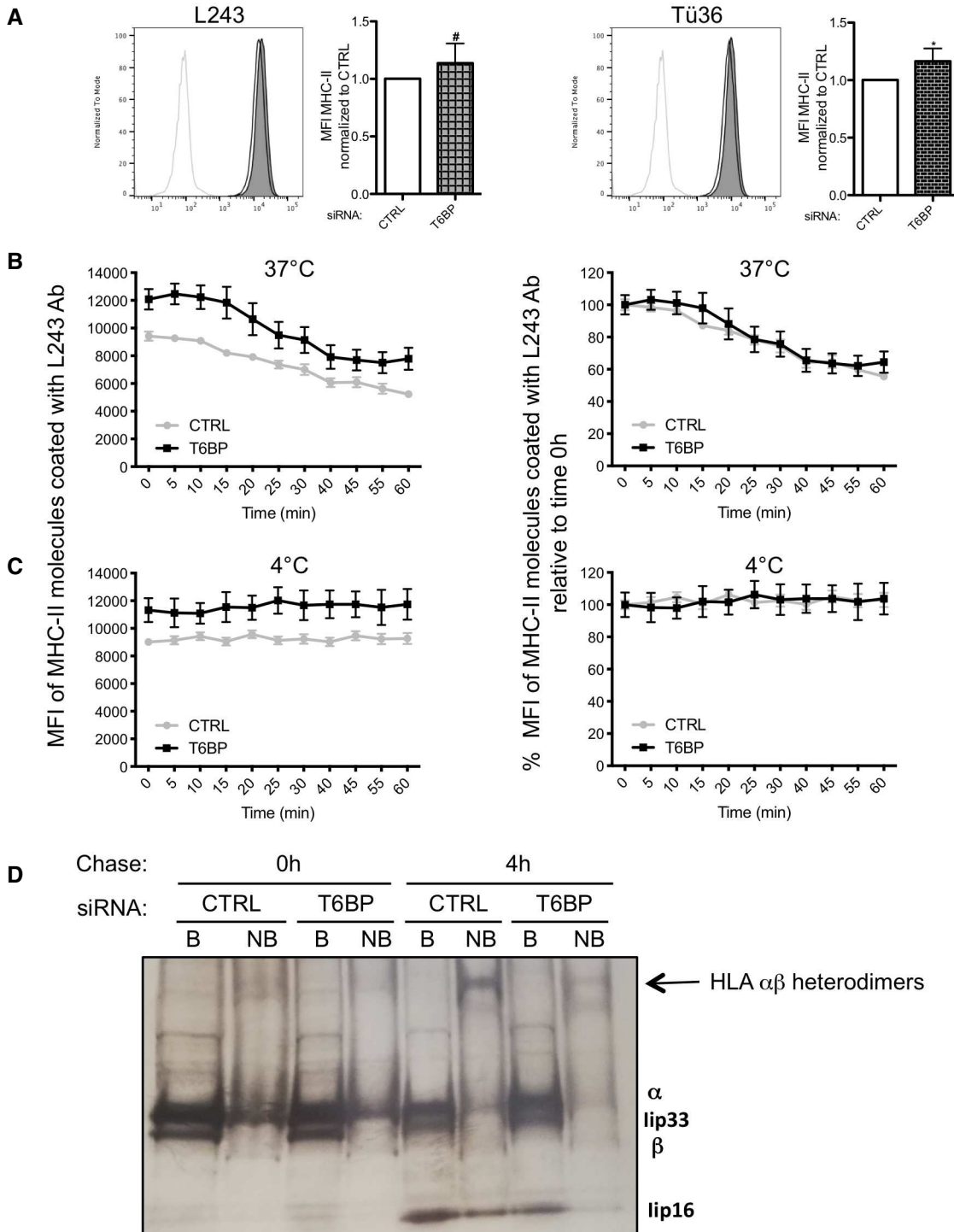


Figure 2.

**Figure 2. T6BP silencing influences the stability of HLA  $\alpha\beta$  dimers, mildly their cell-surface expression levels but has no impact on their internalization kinetics.**

- A** Cell-surface expression of MHC-II molecules was assessed using flow cytometry. HeLa-CIITA cells were transfected with siCTRL and siT6BP. 48 h post-treatment, HLA-DR molecules were detected using L243 (left panels) and T $\dot{U}$ 36 antibodies (right panels) that recognize mature (HLA  $\alpha\beta$  heterodimers) and both mature and immature (HLA  $\alpha\beta$  and  $\alpha\beta$ II complexes), respectively. Left, MFI of one representative experiment is presented as histogram. Light gray lines: isotype negative controls; black lines and filled gray lines: anti-MHC-II staining of siCTRL- and siT6BP-treated cells, respectively. Right, five biological replicates were combined and presented as the means ( $\pm$  SD) of mean fluorescent intensity (MFI) standardized to the control conditions. CTRL: control. Mann–Whitney's test; \* $P < 0.05$ ; # $P > 0.05$ .
- B, C** Internalization kinetics of cell-surface HLA-DR molecules. HeLa-CIITA cells were transfected as above. 48 h post-treatment, mature HLA-DR molecules were stained at 4°C using L243 antibody. Cells were then incubated at 37°C (B) or at 4°C (C). At indicated time points, cells were stained with a fluorescent secondary antibody at 4°C. Results are represented as MFI of MHC-II molecules stained with the L243 antibody remaining at the cell surface (B and C, left panels), or as percentage (%) of MFI relative to time 0 h (100%) (B and C, right panels). Results are presented ( $\pm$  SD) of technical replicates and representative of three independent experiments.
- D** T6BP silencing affects the formation of stable MHC-II-peptide complexes. HeLa-CIITA cells were transfected as above and pulse-labeled with  $^{35}\text{S}$ -Met/Cys for 30 min, washed, and chased for 4 h at 37°C. MHC-II molecules were then immunoprecipitated using T $\dot{U}$ 36 antibody and analyzed on SDS–PAGE after incubation of the immunoprecipitated protein complexes with SDS at 95°C (B: boiled) or room temperature (NB: nonboiled) to visualize  $\alpha$ ,  $\beta$ , and II chains and SDS-resistant  $\alpha\beta$  dimers, respectively. The bands corresponding to  $\alpha$ ,  $\beta$ , and II chains are indicated. The arrow indicates the SDS-resistant stable HLA  $\alpha\beta$  heterodimers. This gel is representative of two independent experiments.

We then sought to analyze the influence of T6BP on the relative abundance and the quality, i.e., the affinity to MHC-II molecules, of peptides presented. However, peptides eluted from MHC-II molecules are variable in length and one core epitope required for MHC-II binding, usually 13 amino acid long, can be found in multiple peptides with N- and C-terminal extensions (Rammensee *et al*, 1999). To circumvent this limitation, we adapted a protocol, published by Alvaro-Benito *et al*, to identify the core epitopes within our datasets using the Peptide Landscape Antigenic Epitope Alignment Utility (PLAtEAU) algorithm (Alvaro-Benito *et al*, 2018). A total of 864 and 1,245 unique core epitopes were identified in the groups Mock1/Mock2 and siCTRL/siT6BP, respectively. PLAtEAU also allows calculating the relative abundance of the core epitopes based on the LC–MS/MS intensities of peptides containing the same core epitope. Between the two mock-treated samples, around 5% of the core epitopes showed a significant difference in their relative abundances (Fig 3B, left panel). Remarkably, between the siCTRL and siT6BP conditions, 55% of the core epitopes displayed a relative abundance that was significantly different between siCTRL and siT6BP conditions, with 436 and 246 epitopes more abundant in the siT6BP or siCTRL-treated cells, respectively, among 1,245 peptides (Fig 3B, right panel). Therefore, T6BP silencing influences both the peptide repertoire (Fig 3A) and the relative abundance of a majority of the core epitopes presented by MHC-II molecules (Fig 3B).

Having identified the core epitopes, using NetMHCIIpan4.0 algorithm (Reynisson *et al*, 2020), we next analyzed the relative binding affinities of exclusive peptides, identified in siCTRL and siT6BP conditions, to the HLA-DR $\beta$ 1\*0102 allele that is expressed by HeLa-CIITA cells. Strikingly, when T6BP is expressed (siCTRL), more than 90% of the epitopes were predicted to be HLA-DR $\beta$ 1\*0102 binders (26% and 65%, strong and weak binders, respectively). By contrast, in T6BP-silenced cells, below 50% of peptides were predicted to bind HLA-DR $\beta$ 1\*0102 (16% and 33%, strong and weak binders, respectively) (Fig 3C). Together, these results suggest that in the absence of T6BP, the peptides presented by HLA-DR $\beta$ 1\*0102 molecules have a predicted weaker relative affinity.

Note that we also analyzed on the same samples whether T6BP might influence the immunopeptidome of MHC-I molecules. Cells transfected with siCTRL or siT6BP and the two mock-treated samples were submitted to IP but using the pan anti-MHC-I antibody, W632, and the peptide ligands sequenced using LC–MS/MS. We did not observe a significant influence of T6BP on the percentage of shared or exclusive peptides comparing siCTRL/siT6BP conditions

(Fig EV2A). We further analyzed the relative affinities of the exclusive peptides bound to siCTRL- and siT6BP-treated cells. In contrast to MHC-II ligands, MHC-I molecules present short 9-mer peptides that correspond to the core epitope (Rammensee *et al*, 1999). We thus directly analyzed the relative affinities using the NetMHCpan 4.0 algorithm (Jurtz *et al*, 2017). The percentages of strong, weak, and nonbinder peptides were similar in control and T6BP-silenced cells (Fig EV2B). Therefore, the action of T6BP seems to be limited to the MHC-II-restricted antigen presentation pathway. T6BP expression has a strong influence on the peptide repertoire, the relative abundance, and the relative affinity of epitopes presented by MHC-II molecules.

### T6BP silencing affects the cellular localization of the MIIC

We then asked whether T6BP might play a role in the intracellular trafficking of MHC-II molecules before mature peptide-loaded MHC-II molecules reach the plasma membrane. To this end, using confocal microscopy analysis, we evaluated in HeLa-CIITA cells the effect of T6BP silencing on endo-lysosomal compartments. We first confirmed previous results (Petkova *et al*, 2017) showing that T6BP silencing leads to the accumulation of LC3-positive puncta corresponding to autophagosomes (Fig EV3A and B). Note that at a steady state in HeLa-CIITA-cells, T6BP did not co-localize with LC3 $^{+}$  puncta (Fig EV3B). We extended this observation using electron microscopy of the morphology of siRNA-treated cells and confirmed that large (around 1  $\mu\text{m}$  in length) vesicles with a double membrane (with 20 to 30 nm interspace) accumulated in about 80% of the cells silenced for T6BP expression (Fig EV3E). These structures were not observed in the siCTRL-treated cells. Two independent experiments were performed and at least 40 cells for each treatment were analyzed. We then analyzed, by confocal microscopy, the sub-cellular localization of MHC-II molecules together with markers of autophagosomes, late endosomes and lysosomes. In HeLa-CIITA cells (Bania *et al*, 2003), MHC-II molecules, stained with an antibody to mature HLA-DR molecules (L243), localized in patches corresponding to intracellular vesicles that did not include T6BP (Fig 4A). Whatever the siRNA treatment, MHC-II molecules did not co-localize with LC3-positive puncta (Fig EV3C and D). However, when compared to the control condition, MHC-II molecules seemed to localize closer to the nucleus upon T6BP silencing (Fig 4A). We determined the average distance to the nucleus and the number of vesicles in more than 150 cells representing over 20,000 MHC $^{+}$

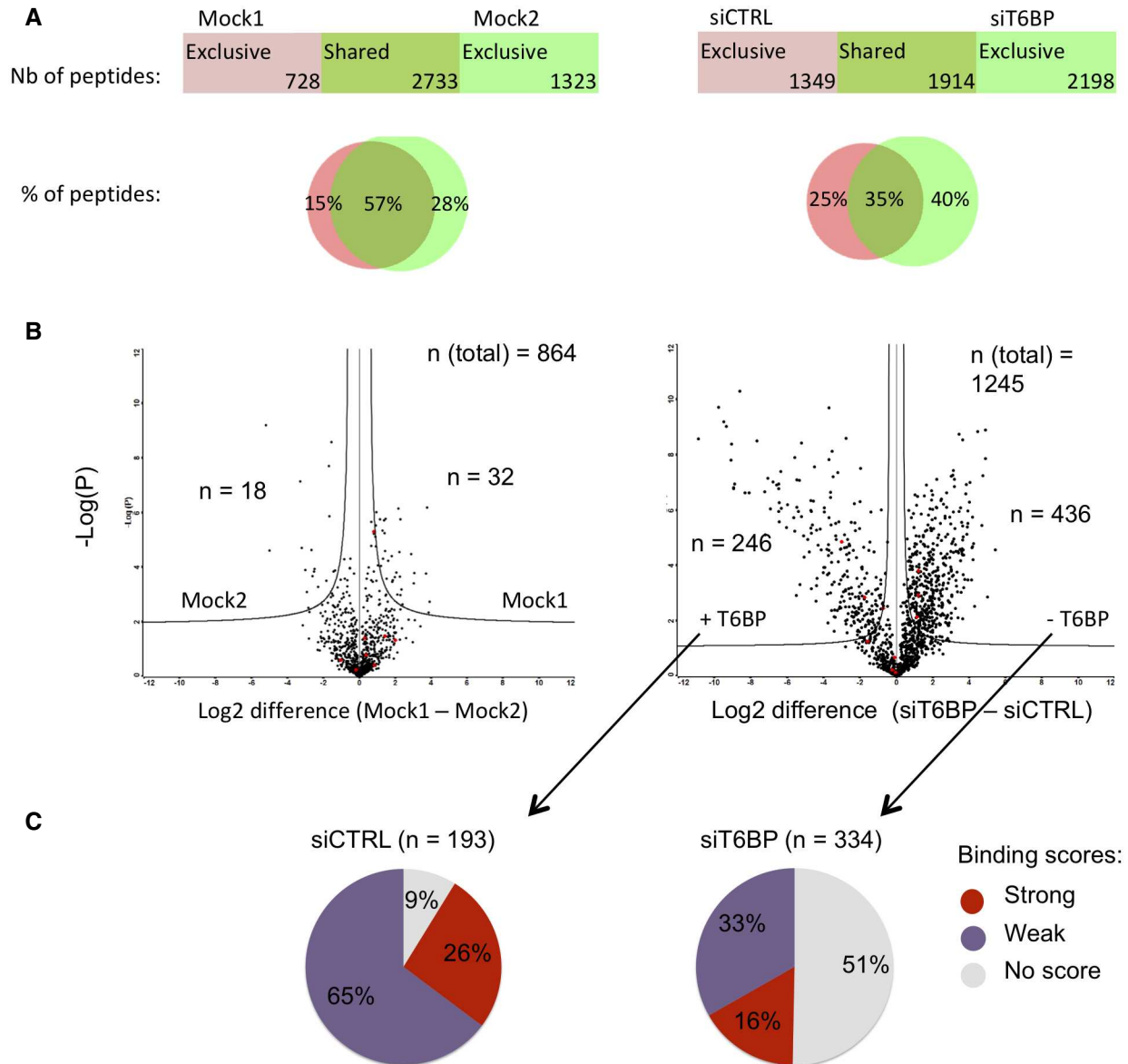


**Figure 3. T6BP silencing alters the immunopeptidome of MHC-II molecules.**

**A** Left panel, mock-treated HeLa-CIITA cells were split and cultured for 48 h (giving rise to Mock1 and Mock2), then cells were lysed, MHC-II molecules were immunoprecipitated using TÛ39 antibody and the peptide ligands sequenced using mass spectrometry (LC-MS/MS). Right panel, HeLa-CIITA cells were transfected with siCTRL and siT6BP siRNA and were treated as in the left panel. The number and the percentage among sequenced peptides (Venn diagrams) of exclusive or shared peptides for each condition are presented.

**B, C** Quantitative (B) and qualitative (C) assessment of T6BP influence on the immunopeptidome. Data from (A) were submitted to PLATEAU algorithm to allow identification and label-free quantification of shared consensus core epitopes. (B) Volcano plots showing the  $\log_2$  fold change of core epitope intensity between siCTRL and siT6BP-treated cells (right panel) and Mock1 and Mock2 (left panel). For peptides exclusive to one or the other conditions, a background score was imputed to allow  $\log_2$  fold-change presentation. An FDR of 0.01 and an SO of 0.2 as a correction factor for differences in the means were used. The resulting interval of confidence is highlighted by solid lines shown in each graph. The total number ( $n$ ) of core epitopes and the number of epitopes with significant fold change are indicated. (C) Relative binding affinities, presented as pie charts, of exclusive core epitopes identified by PLATEAU in siCTRL (left) and siT6BP (right) conditions (number of epitopes are indicated in brackets). NetMHCIIpan was used to predict the relative affinities to HLA-DR $\beta$ 1\*0102 expressed by HeLa-CIITA cells. The results are presented as stated from NetMHCIIpan analysis as strong (for strong binders), weak (for weak binders), and no score (for epitopes for which no binding score could be determined).

Data information: One representative experiment is shown out of two biological replicates. For each experiment, 5 technical replicates per sample were analyzed. Nb—number; %—percentage.

puncta (Fig 4B). We noticed a slight but significant decrease of MHC-II-positive vesicle distance to the nucleus upon T6BP silencing (Fig 4B). The numbers of MHC-II<sup>+</sup> spots per cell were not

significantly different (Fig 4B). Using an anti-LAMP1 antibody, we then analyzed the effect of T6BP expression on late endo-lysosomal compartments. As compared to control cells, we observed a



significant relocalization of LAMP-1-positive vesicles at the proximity of the nucleus in T6BP-silenced cells (Fig 4C and D). The number of LAMP-1-positive vesicles was globally unchanged (Fig 4C and D).

We next asked whether the MIIC itself might be affected by T6BP silencing in HeLa-CIITA cells. The MIIC is a labile ill-defined acidified compartment that has been shown to be positive for multiple markers that do not always overlap (Roche & Furuta, 2015). We used LysoTracker that stains acidified compartments, CD63, a tetraspanin molecule anchored to the membrane of the intraluminal vesicles of the MIIC (Roche & Furuta, 2015), HLA-DM, the chaperone involved in MHC-II peptide loading, and MHC-II molecule staining to identify the MIIC. In the absence of T6BP, we observed a pronounced, statistically significant, relocalization of LysoTracker-positive vesicles close to the nuclei but the number of LysoTracker-positive vesicles was unchanged (Fig 4E and F). Remarkably, in siT6BP-treated cells, LysoTracker-positive vesicles showed increased co-localization with MHC-II molecules (Fig 4E and F). Upon T6BP silencing, CD63-positive vesicles were also strongly relocalized around the nucleus and showed an increased co-localization with MHC-II-positive puncta (Fig 4G and H). The number of CD63-positive vesicles was strongly reduced in T6BP-silenced cells (Fig 4H). Finally, we analyzed the influence of T6BP silencing on the cellular localization of HLA-DM. As for CD63, in T6BP-silenced cells, HLA-DM<sup>+</sup> vesicles were strongly relocalized around the nucleus and their number was reduced as compared to mock-treated cells (Fig EV3F and G). In summary, in T6BP-silenced cells, LAMP-1<sup>+</sup>, HLA-DM<sup>+</sup>, CD63<sup>+</sup>, LysoTracker<sup>+</sup> and MHC-II<sup>+</sup> vesicles showed a repositioning at the proximity of the nucleus (Fig 4).

siT6BP silencing also induced a slight accumulation of EEA1<sup>+</sup> early endosomes in the perinuclear region (Appendix Fig S2A and B). Whatever the treatment, no colocalisation between EEA1 and MHC-II was observed (Appendix Fig S2A and B). Also note that overall, T6BP-silencing did not significantly reduce the expression levels of the various markers analyzed using flow cytometry (Fig 2), WB (Fig 5), and IF (Appendix Fig S2C–H). Taken together these results show that T6BP expression influences the positioning of the MIIC, which is relocalized closer to the nucleus in the absence of T6BP. This repositioning of the MIIC could at least partially account for the defect of MHC-II maturation and could sustain the dramatic changes in the global MHC-II peptide repertoire, observed in the absence of T6BP.

### T6BP silencing leads to exacerbated CD74 degradation in HeLa-CIITA cells

CD74 (Ii) is essential for the traffic and the maturation of MHC-II molecules within the cell (Bakke & Dobberstein, 1990; Lotteau et al, 1990; Neefjes et al, 1990; Roche et al, 1991). In the MIIC, CD74 degradation is also strictly regulated to ensure appropriate loading of MHC-II molecules with high-affinity peptides (Riese et al, 1996; Nakagawa et al, 1998; Shi et al, 2000; Manoury et al, 2003). We thus assessed the effect of T6BP silencing on CD74 expression. Note that in humans, among the four CD74 isoforms (Iip33, Iip35, Iip41, and Iip43) Iip33 is the most abundant (Thibodeau et al, 2019). As previously, HeLa-CIITA cells were transfected with siRNAs, and CD74 expression was assessed by WB. In control cells, Iip33 was readily detected together with its cleavage

product Iip16 (Fig 5A). By contrast, upon T6BP silencing, Iip33 and Iip16 detection was strongly decreased (Fig 5A). Normalized to the housekeeping gene (actin), the decrease in Iip33 expression reached up to 50% (Fig 5A, right panel). As a control, using WB, we also assessed the expression level of HLA-DR molecules. As expected from our flow cytometry and microscopy results (Figs 2 and 4, respectively), the global expression of HLA-DR molecules was similar in siCTRL- and siT6BP-treated cells (Fig 5B). In addition, we asked whether T6BP silencing might also affect the expression of HLA-DM, the chaperone involved in quality control of peptide loading on MHC-II molecules. As for HLA-DR, the expression levels of HLA-DM were not affected by the extinction of T6BP expression (Fig 5C). Using confocal microscopy, we confirmed that T6BP-silenced cells exhibit about 50% lower expression levels of CD74 than control cells (Fig EV4A and B). Note that, in control cells, the T6BP staining did not co-localize with CD74 (Fig EV4A and C).

We then asked at which level CD74 expression was affected, i.e., at the RNA or protein levels. To this end, we first used RT-qPCR to monitor CD74 and T6BP mRNA relative quantities in control and T6BP-silenced HeLa-CIITA cells. As anticipated T6BP mRNA levels were strongly reduced in siT6BP-treated cells (Fig EV4D). By contrast, mRNA levels of CD74 were not influenced by T6BP silencing (Fig EV4E). We next analyzed whether CD74 expression could be reversed, in siT6BP-silenced cells, upon treatment with drugs inhibiting lysosomal or proteasomal degradation, using chloroquine or epoxomicin, respectively. As expected, since the proteolytic cleavages of CD74, required for MHC-II peptide loading are dependent on cathepsin activities (Riese et al, 1996; Nakagawa et al, 1998; Shi et al, 2000; Manoury et al, 2003), the treatment of control cells with chloroquine allowed the detection of the intermediate degradation fragment Iip22 (Fig 5D). Remarkably, when compared to control untreated cells, chloroquine treatment allowed a strong recovery of both Iip33 and Iip16 expression in siT6BP-treated cells (Fig 5D). By contrast, although proteasomal inhibition induced, as expected, the accumulation of polyubiquitinated proteins (Appendix Fig S3), epoxomicin treatment did not affect the expression levels of CD74 (Fig 5D).

These results prompted us to analyze the kinetics of degradation of CD74 complexes. To address CD74 proteolysis in control and T6BP silenced HeLa-CIITA cells, 48 h post-transfection cells were pulsed with S35 Met/Cys for 30 min and chased for different times. HLA-CD74 complexes were isolated by immunoprecipitation with TÛ36 antibody and in a second set of experiments CD74 was first immunoprecipitated, together with HLA molecules, using TÛ36 antibody and then reimmunoprecipitated using VICY1 antibody, which binds the cytosolic tail of CD74. As shown in Fig 5E, in control cells, CD74 isoforms (Iip41 and Iip33) and their fragments (Iip16) appeared in the pulse and during the chase. By contrast, when HeLa-CIITA was silenced for T6BP much less Iip41, Iip33 and Iip16 were detected. In fact, in the control conditions, the invariant chain degradation product, Iip16, was detected mostly after 1 h of chase (Fig 5E). By contrast, Iip16 was immediately detected after the pulse (time 0 h) in the T6BP-silenced cells (Fig 5E) suggesting a rapid CD74 degradation (see quantification on the right panel). Furthermore, when HLA/CD74 complexes were first immunoprecipitated with TÛ36 antibody and reimmunoprecipitated with VICY1 antibody, much less CD74 (Iip33) was detected in T6BP silenced cells (Fig 5F). Altogether these results suggest a much faster degradation

of CD74, either free or associated with MHC-II molecules, in the absence of T6BP.

Interestingly, the expression of CD74 has been shown to influence both the cellular trafficking and the immunopeptidome of MHC-II molecules (Muntasell *et al*, 2004). It has also been suggested that in cells lacking MHC-II expression, CD74 might regulate endosomal maturation (Schröder, 2016).

### T6BP interactome reveals novel binding partners

To decipher the mechanism by which T6BP influences MHC-II-restricted endogenous antigen presentation, we decided to define the interactome of T6BP in HeLa-CIITA cells. To this end, HeLa-CIITA cells were transfected with a plasmid encoding GFP-T6BP, a construct that was previously functionally characterized

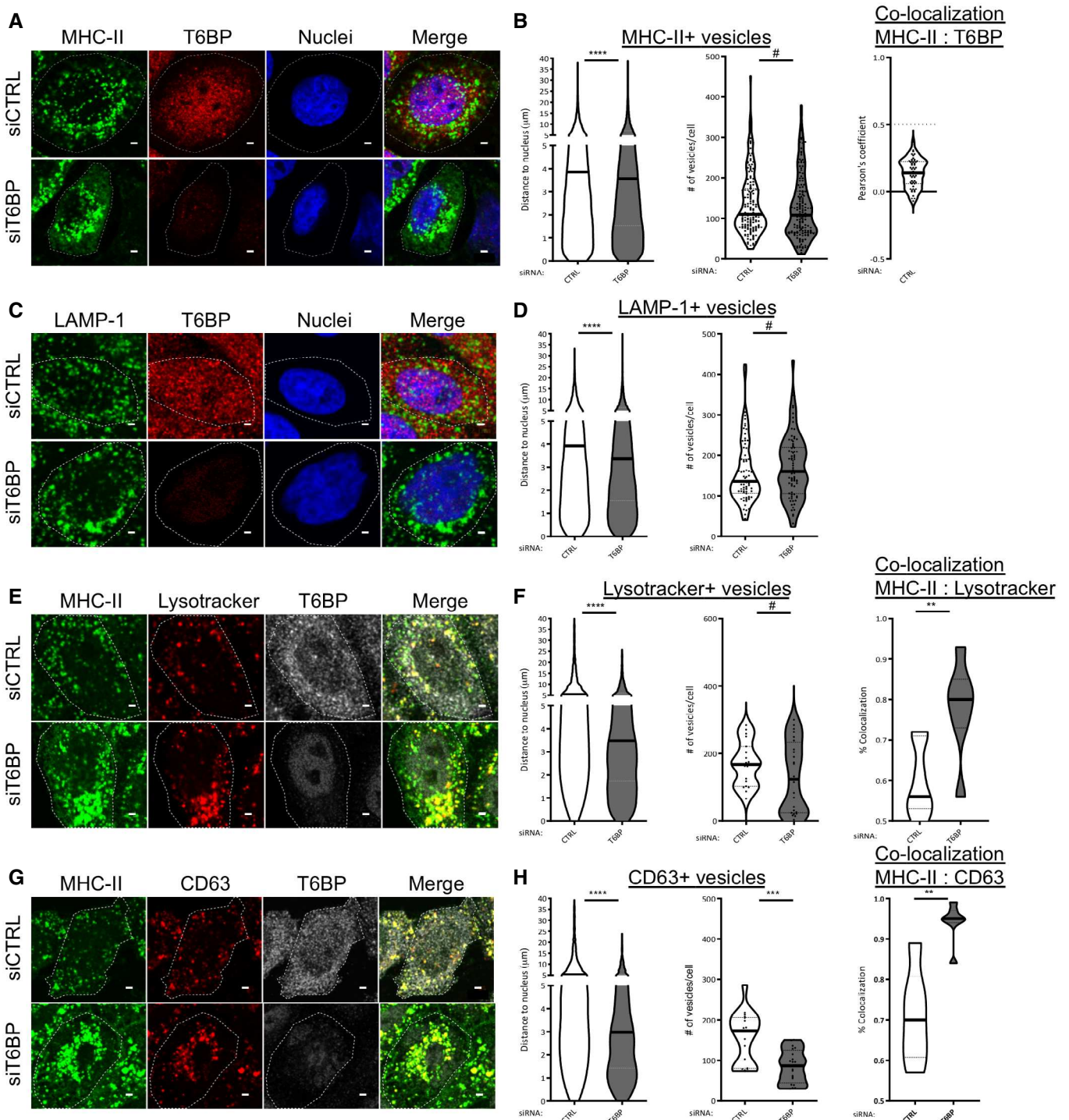


Figure 4.

**Figure 4. T6BP silencing leads to perinuclear relocalization of the MHC.**

- A MHC-II and T6BP expressions were assessed using confocal microscopy. HeLa-CIITA cells were transfected with control and T6BP-silencing siRNAs. 48 h post-treatment, MHC-II and T6BP were detected using L243 and anti-T6BP antibodies, respectively, and revealed with species-specific secondary antibodies. Nuclei were stained using DAPI.
- B Quantitative analysis using in-house ImageJ script displaying distance of each MHC-II<sup>+</sup> vesicles to the nucleus and number of vesicles per cell. At least 20,000 vesicles from 160 cells corresponding to five biological replicates were analyzed. Right panel, quantification in the siCTRL cells of the co-localization between MHC-II<sup>+</sup> and T6BP<sup>+</sup> dots using Pearson's coefficient where the dotted lines (at 0.5) indicate the limit under which no significant co-localization is measured (number of cells = 54).
- C As in A, T6BP and LAMP-1 expressions were analyzed.
- D The localization of LAMP-1<sup>+</sup> vesicles and the number of vesicles per cell were quantified as in B. At least 2000 vesicles from 20 cells corresponding to two biological replicates were analyzed.
- E As in A, adding LysoTracker staining.
- F As in B, quantitative analysis of LysoTracker<sup>+</sup> vesicles: localization to the nucleus and number of vesicles per cell. Co-localization of LysoTracker<sup>+</sup> vesicles with MHC-II<sup>+</sup> puncta was analyzed using JACoP plugin (scales start at 0.5 above which the % of co-localization is considered significant); a number of vesicles >2000 from at least three biological replicates were analyzed corresponding to 20 cells.
- G As in E, CD63 and MHC-II expressions were assessed.
- H Quantitative analysis as represented in F. At least 2000 vesicles from 20 cells corresponding to two biological replicates were analyzed.

Data information: In graphs representing the number of vesicles per cell, each dot displayed corresponds to a single cell. Within the violin plots, continuous and dotted lines correspond to medians and quartiles, respectively. Scale bars: 2  $\mu$ m. CTRL—control. Mann–Whitney's test; \* $P < 0.05$ ; \*\* $P < 0.002$ ; \*\*\* $P < 0.0003$ ; \*\*\*\* $P < 0.0001$ ; # $P > 0.05$ .

(Morriswood *et al*, 2007), and as negative control the same plasmid encoding GFP (Appendix Fig S4A). We then performed a large-scale immunoprecipitation (IP) using GFP as a tag. Three biological replicates were performed. As a quality control, the lysates and the various fractions of the immunoprecipitation procedure were analyzed using Coomassie blue staining and anti-GFP staining in WB (Appendix Fig S4B). The immunoprecipitation products of the three replicates (presented in Appendix Fig S4C) were then submitted to mass spectrometry (LC–MS/MS) analysis to identify the proteins interacting with GFP-T6BP. The Uniprot *Homo sapiens* database was used to assign a protein name to the peptides sequenced by MS. The results were compared against the 3 IP replicates of GFP-transfected cells and a bank of 8 control experiments, also performed with GFP-Trap agarose magnetic beads, using the online contaminants database CRAPome.org (Mellacheruvu *et al*, 2013). Using a fold-change (FC) threshold of  $\geq 10$  and a Significance Analysis of INteractome (SAINT) probability threshold of  $\geq 0.8$  (Choi *et al*, 2011), we identified 116 high-confidence T6BP proximal proteins (Fig 6 and Dataset EV1). These included previously known T6BP-interactants such as the E3 ligase ITCH (Shembade *et al*, 2008), the kinase TBK1 (Richter *et al*, 2016), and TRAF2, all involved in NF- $\kappa$ B signaling pathways (Shembade *et al*, 2010). This screen also confirmed that T6BP interacts with the autophagy receptor p62 (SQSTM1) (Mildenberger *et al*, 2017). It revealed novel potential partners that might bind directly or as part of larger T6BP-associated protein complexes. These candidates could be grouped in 6 major functional cellular pathways based on Ingenuity (Fig 6). As expected, from the known T6BP functions, some candidate partners were enriched in the ubiquitin/proteasome ( $P$ -value = 3,16E-18) and NF- $\kappa$ B signaling ( $P$ -value = 1,15E-02) pathways but also in the unfolded protein response (UPR)/protein folding ( $P$ -value = 2,69E-04), endocytosis ( $P$ -value = 6,03E-05), and antigen presentation ( $P$ -value = 2,34E-06) pathways (Fig 6). The antigen presentation group includes HLA-A, -C, -DQ $\alpha$ 1, -DR $\beta$ 1 molecules (Fig 6). In the UPR/protein folding group, the ER-resident chaperone protein Calnexin (CANX) is 22 times enriched in T6BP-GFP IP as compared to GFP only IP (Fig 6 and Appendix Table S1). CANX drew our attention because: (i) it has been shown to interact with CD74 (Anderson & Cresswell, 1994) and (ii) the inhibition of CANX/CD74 interaction

induces CD74 degradation without influencing the formation of MHC-II complexes (Romagnoli & Germain, 1995).

#### T6BP and Calnexin interaction is observed in professional APC and relies on Calnexin cytosolic tail expression

To verify that CANX interacts with T6BP, as previously, we immunoprecipitated GFP-T6BP and GFP from HeLa-CIITA transfected cells and analyzed, using WB, the presence of Calnexin in the immunoprecipitated fractions. The IP of the GFP-transfected cells leads to the immunoprecipitation of a larger GFP-positive fraction than the IP of the T6BP-GFP-transfected cells (Appendix Fig S4D, anti-GFP Ab). Nonetheless, we observed a 3-fold enrichment of CANX in cells transfected with GFP-T6BP as compared to GFP-transfected cells (Appendix Fig S4D). In HeLa-CIITA cells, we further confirmed the specific interaction between T6BP and CANX using two different techniques: (i) by immunoprecipitation of endogenous T6BP and endogenous CANX, we revealed that the IP fractions of anti-T6BP and anti-CANX IPs contained CANX and T6BP, respectively (Fig 7A and B); (ii) by proximity ligation assay (PLA) on control cells and siT6BP-transfected cells a specific T6BP/CANX interaction was detected only in cells expressing T6BP (Fig 7C). To demonstrate that T6BP/CANX interaction is not restricted to HeLa-CIITA cells, we then immunoprecipitated endogenous T6BP and CANX from two professional APCs, namely B cells and DC. As in HeLa-CIITA, we revealed in the anti-T6BP and anti-CANX IP fractions, of both B cells and DC, the presence of CANX and T6BP, respectively (Fig 7A and B). Altogether, these results strongly support that CANX interacts with T6BP directly or as part of a larger protein complex.

In order to characterize the molecular interactions between CANX and T6BP, we then engineered a construct containing solely the transmembrane domain and the cytosolic tail of CANX fused to a GST tag. Since T6BP expression is mainly cytosolic, we reasoned that T6BP and CANX might interact through the cytosolic tail of CANX. The GST-TM-cytosolic Tail construct was transfected in HeLa-CIITA cells and immunoprecipitated using anti-GST antibodies. Western blotting revealed that T6BP is co-immunoprecipitated with anti-GST in cells transfected with GST-TM-cytoTail-CANX and not in cells transfected with the control vector (Fig 7D). Taken together, we demonstrate here that T6BP interacts with CANX through its

cytosolic tail. We propose that, through the binding to the cytosolic tail of CANX, T6BP promotes the interaction of CANX with CD74 leading to CD74 stabilization.

**Calnexin silencing induces CD74 degradation and reduces MHC-II-restricted antigen presentation to CD4<sup>+</sup> T cells**

Finally, we investigated the direct role of CANX in MHC-II-restricted antigen presentation. To this end, we screened several siRNA targeting

Calnexin and identified an siRNA whose transfection led to a strong decrease in CANX expression (siCANX) (Appendix Fig S4E). Using WB, we first analyzed the influence of CANX-silencing on CD74 expression. In siCANX-treated cells, we observed a strong reduction in CD74 expression levels (Fig 7E) reminiscent of what we observed in cells silenced for T6BP expression (Figs 5A and D, and 7E). Note that neither siT6BP nor siCANX transfections lead to an increased expression of CANX or T6BP, respectively (Fig 7E and Appendix Fig S4E). To monitor the influence of Calnexin on antigen presentation, HeLa-

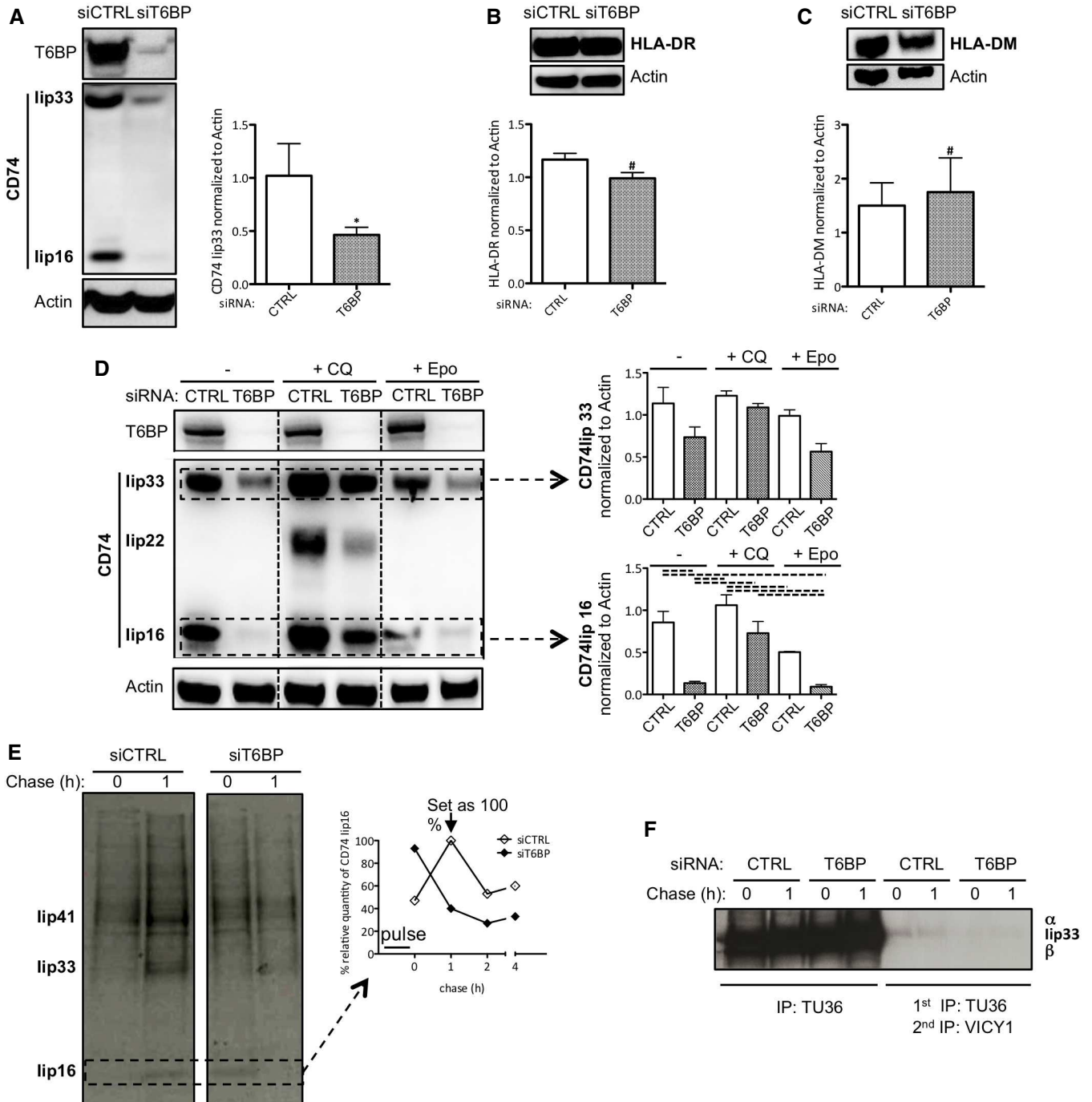


Figure 5.

**Figure 5. T6BP silencing leads to exacerbated CD74 (li) degradation.**

- A CD74 expression was assessed using Western Blot. HeLa-CIITA cells were transfected with siCTRL and siT6BP. 48 h post-treatment, the lip33 CD74 isoform, a degradation product (lip16), T6BP, and actin were detected using indicated antibodies. Left panel, a representative Western Blot experiment is shown. Right panel, expression levels of five biological replicates were quantified using ImageJ and are presented as mean ratios ( $\pm$  SD) of CD74 to actin used as control housekeeping gene expression.
- B As in (A) assessing HLA-DR and actin expression levels. Top panel, a representative Western Blot experiment is shown. Bottom panel, in three biological replicates, HLA-DR expression was quantified using ImageJ and is presented as mean ratios to actin ( $\pm$  SD).
- C As in (B) assessing HLA-DM and actin expression levels. Bottom panel, HLA-DM expression was quantified in three biological replicates and presented as mean ratios to actin ( $\pm$  SD).
- D CD74 expression is partially recovered by blocking lysosomal acidification. As in (A), following siRNA transfection of HeLa-CIITA cells, CD74 expression was assessed. The last 16 h prior to harvesting, cells were treated with chloroquine (CQ) or epoxomicin (Epo). Left panel a representative experiment is shown, membranes were blotted using anti-T6BP, -CD74, and -actin antibodies. The different degradation fragments of CD74 are indicated (lip33, lip22, and lip16). Right panel, expression levels of lip33 (top) and lip16 (bottom) were quantified in three biological replicates using ImageJ and are presented as mean ratios of each fragment to actin ( $\pm$  SD).
- E, F Analysis of CD74 proteolysis. HeLa-CIITA cells were transfected with siCTRL and siT6BP. 48 h post-treatment, cells were pulsed for 30 min with  $^{35}\text{S}$ -Met/Cys, washed, and chased for 1, 2, and 4 h. HLA-DR/CD74 complexes were first immunoprecipitated using Tü36 antibody (E) and then reimmunoprecipitated with VICY1 antibody (F). Samples were boiled and analyzed using SDS-PAGE. The bands corresponding to CD74 isoforms (lip41 and lip33) and the cleavage products (lip16) are indicated. (E right panel) lip16 expression was quantified using ImageJ and presented as a percentage of lip16 normalized to the highest quantity of lip16 detected after 1 h of chase in the control condition. Results are representative of two biological replicates. li: invariant chain (CD74); CTRL: control.

Data information: (A-C) Wilcoxon's test; \* $P < 0.05$ ; # $P > 0.05$ . (D) One-way ANOVA statistical test combined with the Bonferroni's multiple comparison test was applied. Dotted lines indicate statistically significant differences between conditions. Source data are available online for this figure.

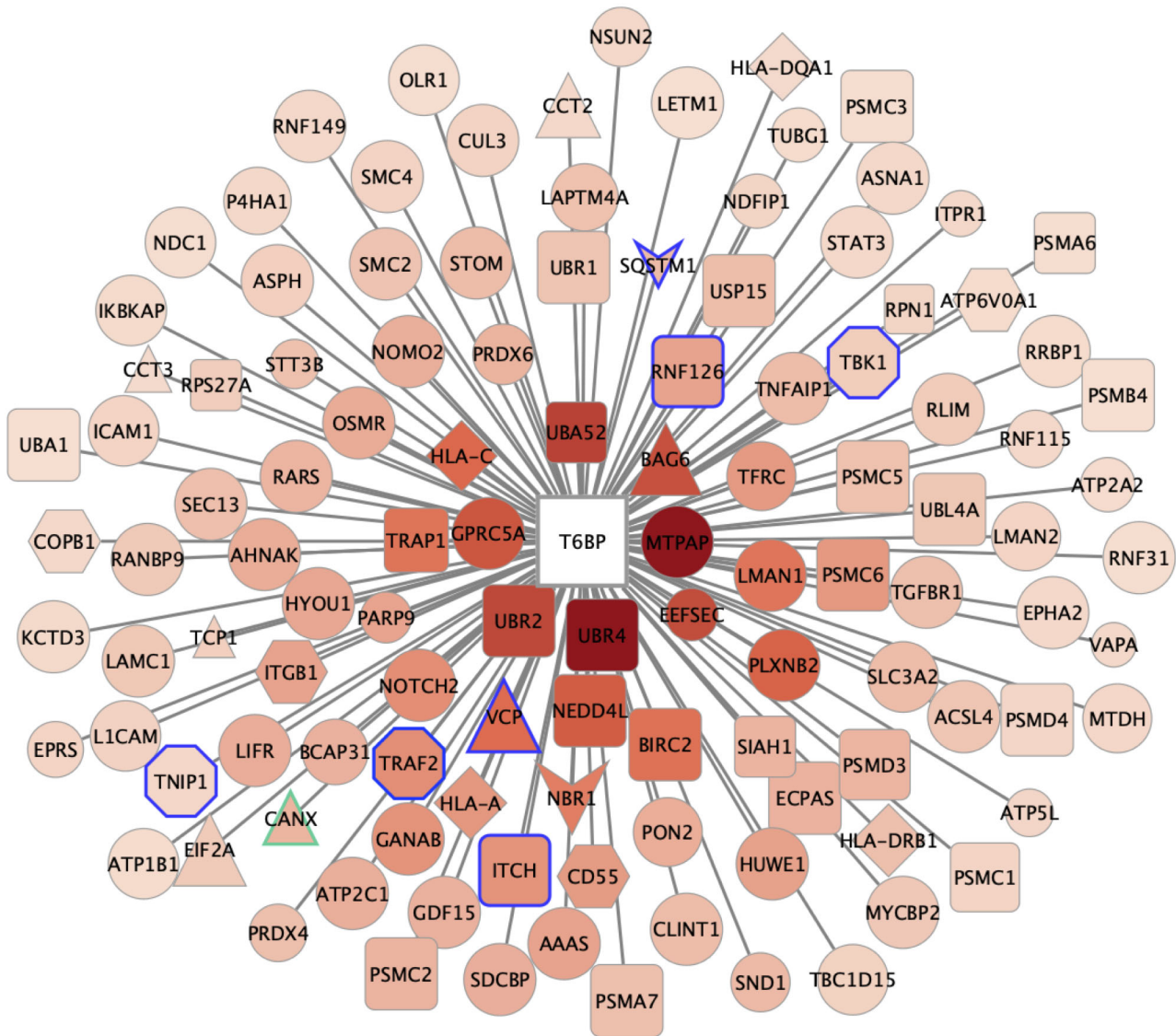
CIITA cells were transfected with siCANX side by side with siCTRL or siT6BP used as negative and positive controls, respectively. As in Fig 1E, the cells were then transfected with the plasmid encoding the HCMV pp65 antigen and co-cultured with the anti-pp65 CD4<sup>+</sup> T cell line. CANX-silencing induced a marked inhibition of CD4<sup>+</sup> T cell activation by pp65-transfected cells (Fig 7F, left and middle panels). By contrast, the inhibition of CANX expression did not influence the capacity of peptide-loaded cells to activate pp65-specific CD4<sup>+</sup> T cells (Fig 7F right panel), confirming that CANX inhibition influences neither HLA-DR expression nor the viability of the cells. We show here that T6BP silencing affects CANX functions resulting in CD74 degradation and aberrant MHC-II peptide loading and antigen presentation to CD4<sup>+</sup> T cells.

## Discussion

We demonstrate here that T6BP regulates the loading and presentation of endogenous viral antigens by MHC-II molecules. This function of T6BP in antigen presentation has a direct implication in the activation of virus-specific CD4<sup>+</sup> T cells. The action of T6BP is broader than what we initially anticipated as it affects the presentation of various antigens whose processing is dependent or independent on autophagy degradation. We further show that T6BP shapes the immunopeptidome of MHC-II molecules. We provide evidence that T6BP controls MHC-II molecule peptide loading in particular through its interaction with the cytosolic tail of CANX that stabilizes the invariant chain. However, this is probably not the only way by which T6BP affects MHC-II-restricted antigen presentation as it also participates in the regulation of the trafficking of MHC-II-loading compartments and more globally of acidified vesicular compartments.

We previously reported that HIV-infected cells present MHC-II-restricted HIV Gag- or Env-derived antigens to HIV-specific CD4<sup>+</sup> T cells (Coulon et al, 2016). The processing of these native antigens does not rely on the autophagy pathway. However, when targeted

to autophagosomes, using LC3, HIV Gag processing is dependent on autophagosomal degradation. In fact, using DC and HeLa-CIITA cells we showed that as compared to native HIV Gag protein, the targeting of HIV Gag to autophagosomes leads to more robust activation of Gag-specific T cells (Coulon et al, 2016). We concluded that depending on the cellular localisation, the same antigens may be degraded by various endogenous routes leading to MHC-II loading. We reveal here that T6BP modulates Gag antigen presentation independently of its cytosolic or autophagosomal cellular localisation. Likewise, T6BP affects the presentation of an HCMV pp65-derived peptide. Our analysis of the immunopeptidome of HeLa-CIITA cells uncovers that T6BP has a broad influence on the repertoire and relative abundance of the peptides presented by MHC-II molecules. Without excluding the possibility, these observations do not indicate whether T6BP also affects the exogenous pathway of antigen presentation by MHC-II molecules. Indeed, others and we (Fig EV1) have demonstrated that the landscape of peptides naturally presented by MHC-II molecules contains a large fraction of peptides derived from intracellular proteins (Rudensky et al, 1991; Rammensee et al, 1999; Muntasell et al, 2002). In our model system, HeLa-CIITA cells, we could not ask whether the silencing of T6BP affects the exogenous pathway because these cells lack the ability to present exogenous viral antigens to CD4<sup>+</sup> T cells (Coulon et al, 2016). This is a weakness but also a strength of this model system since it allowed focusing our work on the endogenous pathway. Nevertheless, we intended to ask whether T6BP might affect antigen presentation by primary APCs. We used several means to silence T6BP in MDDCs including siRNA and shRNA. Unfortunately, whatever the protocol and independently of T6BP expression, the tools used to transfect or to transduce MDDC induced maturation of the cells and affected the traffic of MHC-II molecules, which prohibited drawing any conclusion on the potential role of T6BP in MDDCs. Nonetheless, our results strongly suggest that at least in epithelial cells that can turn into APCs upon inflammation (Wijdeven et al, 2018), T6BP expression shapes the peptide repertoire, the relative abundance, and the relative affinity of epitopes presented



**Main pathways**

- ◇ Antigen presentation
- ▽ Autophagy
- ⬡ Endocytosis
- ⬢ NFkB signaling
- Ub/proteasome
- △ UPR/protein folding
- Other
- ⬢ Known T6BP partners

**Selecting criteria**

- } FC ≥ 10; CRAPome OK; SAINT ≥ 0.8
- } FC ≥ 10; CRAPome OK; SAINT ≥ 0.8
- △ CANX: Calnexin

**Figure 6. T6BP interactome reveals novel binding partners.**

Diagram of the T6BP protein interaction network identified by immunoprecipitation followed by LC-MS/MS and represented using Cytoscape. T6BP (white) coupled to GFP was immunoprecipitated using anti-GFP camel antibodies (GFP-Trap Chromotek). GFP alone was used as control. Proteins were considered as relevant partners based on the following criteria: at least 2 peptides were identified by LC-MS/MS, the fold change (FC) to the GFP control condition ≥10, SAINT probability threshold ≥0.8. For data analysis, the Resource for Evaluation of Protein Interaction Networks (REPRINT) and its contaminant repository (CRAPome V2.0) were used. The edge's length is inversely proportional to the FC score (short edge = high FC) and the node's color intensity is directly proportional to the FC score (the more intense the higher the FC). The size of the node is directly proportional to the SAINT score (lower confidence = smaller node). Blue border indicates previously described partners of T6BP. The shape of the node highlights the functional pathway in which the candidate protein is enriched based on Ingenuity. Green border indicates Calnexin = CANX.

by MHC-II molecules. Indeed, our immunopeptidomic data suggest that the expression of T6BP favors the loading of peptides with a higher binding capacity to HLA-II molecules. As expected, based on

previous work with cell lines (Alvaro-Benito *et al*, 2018) or analyzing tissue samples (Marcu *et al*, 2021), we observed a natural variation of the MHC-II immunopeptidome between two mock-treated

samples with about 60% of shared peptides. However, in these mock samples, we did not notice a significant difference in terms of the relative quantity of core epitopes. This is in sharp contrast to the comparison of wild-type and T6BP-silenced cells where half of the MHC-II binding core epitopes were differentially presented. Remarkably, we also observed a natural variation of the immunopeptidome of MHC-I molecules, with about 50% of shared peptides. Notably, T6BP silencing did not have a strong influence on the repertoire of peptides presented by MHC-I molecules, as the percentage of shared

peptides with the control siRNA-treated cells was also around 50%. In addition, the affinity of MHC-I ligands was comparable in wild-type cells and cells silenced for T6BP expression. Our results strongly suggest that the action of T6BP is restricted to the MHC-II antigen presentation pathway and affects both the abundance and the affinity of core epitopes to HLA molecules.

The chaperones HLA-DM and the invariant chain (Ii) CD74 tightly regulate the loading of peptides on MHC-II molecules. Previous studies have shown that the levels of expression of both HLA-

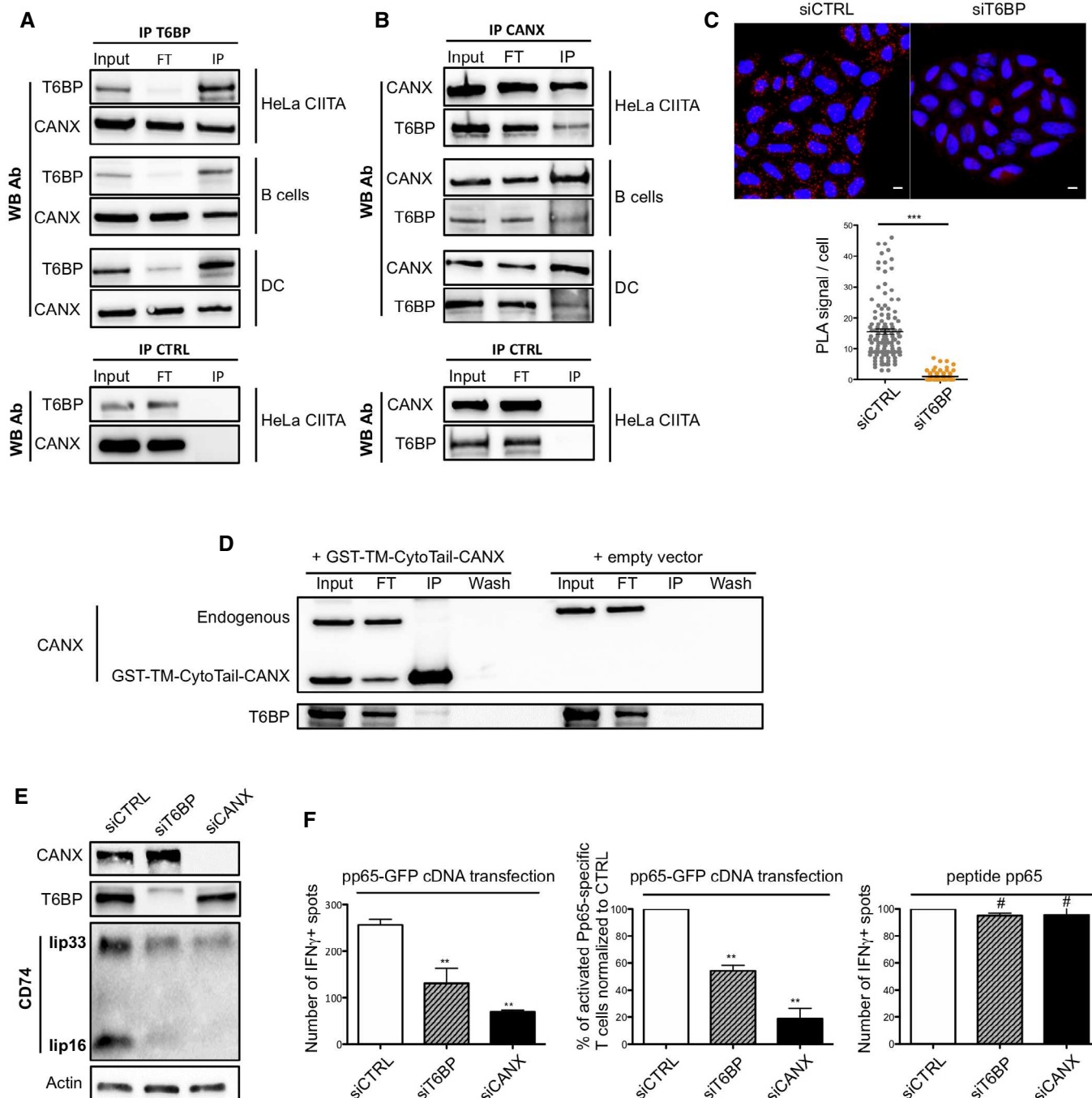


Figure 7.

**Figure 7. Calnexin (CANX) interacts with T6BP through its cytosolic tail and stabilizes CD74 thus favoring MHC-II-restricted antigen presentation to CD4<sup>+</sup> T cells.**

- A, B CANX co-immunoprecipitates with T6BP in model and professional APCs. Endogenous T6BP was immunoprecipitated from HeLa-CIITA, B (DC-75), and dendritic-like (KG-1, DC) cells. The input, the flow-through (FT), and the immunoprecipitation (IP) fractions were analyzed by Western blot using the indicated antibodies. Bottom panels, control IPs using the beads without antibody (IP CTRL) are presented for each IP. (B) As in (A) but using anti-CANX Ab for the IP. For A and B, one representative experiment out of three biological replicates is shown.
- C CANX interacts with T6BP using proximity ligation assay (PLA). 48 h post-transfection with the indicated siRNAs, HeLa-CIITA cells were fixed, stained with anti-T6BP and anti-CANX antibodies and proximity revealed using PLA (Duolink). Nuclei were stained using DAPI. Top panel, two representative fields are shown. Bottom panel, quantitative analysis using ImageJ displaying the number of PLA per cell. The continuous line indicates the mean ( $\pm$  SEM). PLA was quantified in at least 130 cells corresponding to three biological replicates. Scale bars: 10  $\mu$ m. CTRL: control; Mann–Whitney's test; \*\*\* $P$  < 0.0003.
- D Calnexin interacts with T6BP through its cytosolic tail. HeLa-CIITA cells were transfected with a plasmid encoding the GST-tagged transmembrane (TM) and cytosolic (CytoTail) domains of CANX (GST-TM-CytoTail-CANX) or the vector not encoding TM-CytoTail-CANX as control and immunoprecipitated with anti-GST antibodies. The input, FT, the wash, and the IP fractions were analyzed by Western blot and revealed using the indicated antibodies. One representative experiment out of three biological replicates is shown.
- E Silencing of T6BP does not influence CANX expression levels while silencing of CANX reduces the level of CD74 expression. HeLa-CIITA cells transfected with the indicated siRNAs and samples analyzed, 48 h post-transfection, by Western blot with the indicated antibodies. These western blot results are representative of at least three biological replicates.
- F CANX-silencing dampens MHC-II-restricted antigen presentation to CD4<sup>+</sup> T cells. HeLa-CIITA cells were treated with the indicated siRNAs and transfected with a plasmid encoding pp65 HCMV antigen fused to GFP. HeLa-CIITA cells were then co-cultured with pp65-specific T cells. Left panel, a representative experiment is shown. The mean of three technical replicates ( $\pm$  SD) is shown. Middle, three biological replicates are combined and presented as the mean percentage ( $\pm$  SD) of activated cells producing IFN $\gamma$  normalized to CTRL conditions. Right panel, influence of T6BP silencing on peptide presentation by HeLa-CIITA cells. The cognate peptide was added exogenously (pp65, 0.5  $\mu$ g/mL) on siRNA-treated cells (2 h, 37°C), washed and T cell activation monitored using IFN $\gamma$ -ELISPOT. Three biological replicates are combined and presented as the mean percentage ( $\pm$  SD) of activated cells producing IFN $\gamma$  normalized to CTRL conditions. Data information: The background secretions of IFN $\gamma$  by CD4<sup>+</sup> T cells co-cultured with mock-treated HeLa-CIITA cells were used as negative controls and subtracted. CTRL—control. Wilcoxon's test; \*\* $P$  < 0.01; # $P$  > 0.05.

Source data are available online for this figure.

DM and CD74 affect the repertoire and the affinity of the peptides presented by various HLA-DR and HLA-DQ alleles (Ramachandra *et al*, 1996; Muntasell *et al*, 2004; Alvaro-Benito *et al*, 2018). Remarkably, in the absence of T6BP, we noticed a reduced expression level of CD74 whereas HLA-DM and HLA-DR expression levels remained unchanged. Overall, we did not observe a significant influence of T6BP silencing on the expression levels of other intracellular markers/proteins than CD74. Our analysis of the expression kinetics of MHC-II complexes, using pulse/chase experiments, further showed that the lack of T6BP induces a rapid and exacerbated degradation of CD74. The expression levels of CD74 could be rescued by inhibiting lysosomal acidification but not proteasomal functions suggesting that CD74 is aberrantly degraded in endolysosomes in T6BP-depleted cells. These observations probably explain the modifications of the immunopeptidome and the instability of peptide-loaded MHC-II  $\alpha\beta$  heterodimers, observed in the absence of T6BP expression. However, the diversity of the immunopeptidome could also be due to variations in the origin of the peptides presented by MHC-II molecules (Muntasell *et al*, 2004), in particular, since we observed a global modification of the cellular distribution of acidified vesicular compartments in the absence of T6BP. Although we observed, using functional enrichment analysis (Funrich, Fig EV1), a slight influence of T6BP silencing on the cellular distribution of the source protein of MHC-II ligands, this cannot by itself explain the effects of T6BP on the peptide repertoire. In particular since, T6BP expression also dictates the relative affinity of peptides presented by MHC-II molecules. Overall, our observations suggest that T6BP expression influences the degradation kinetics of CD74 with a direct influence on the diversity and affinity of the immunopeptidome of MHC-II molecules.

The ER chaperone CANX that participates in the quality control of protein folding in the ER has been shown to play an important role in the assembly of the nonameric MHC $\alpha\beta$ -CD74 complexes (Arunachalam & Cresswell, 1995). CANX retains and stabilizes

CD74 in the ER until it assembles with the MHC  $\alpha$ - and  $\beta$ -chains (Romagnoli & Germain, 1995). It also binds newly synthesized  $\alpha$ - and  $\beta$ -chains of HLA molecules until it forms, with CD74, a complete nonamer (Anderson & Cresswell, 1994). Interestingly, it has been shown that the treatment with Tunicamycin or the expression of CD74 mutants, lacking N-linked glycosylation, both impeding the interactions with CANX, can induce CD74 degradation (Romagnoli & Germain, 1995). We corroborate here that CANX influences CD74 expression. Using siRNA silencing, we provide a direct demonstration that the lack of CANX expression induces CD74 degradation. Furthermore, we show that the silencing of CANX in APC diminishes their capacity to activate antigen-specific CD4<sup>+</sup> T cells. Remarkably, using co-immunoprecipitation followed by mass spectrometry, we identified CANX as a binding partner of T6BP, among 116 high-confidence T6BP proximal proteins. T6BP and CANX interaction was confirmed in HeLa-CIITA as well as in B cells and DC, strongly suggesting that our observations are not limited to our model APCs.

It has been proposed that the ER distribution of CANX might determine its functions as a chaperone involved in protein quality control or in the regulation of Ca<sup>2+</sup> transfer to mitochondria (Lynes *et al*, 2013). Several post-translational modifications influence both the cellular distribution and the functions of calnexin: phosphorylation of the cytosolic tail of CANX leads to a redistribution from peripheral ER tubules to a juxtannuclear ER (Myhill *et al*, 2008) while palmitoylation of the tail seems to assign specific tasks to calnexin within the ER, in particular, a role in protein folding (Lynes *et al*, 2013) and a localization at the proximity of the ribosome complexes (Lakkaraju *et al*, 2012). We show here that T6BP binds to the cytosolic tail of CANX. To our knowledge, there is no published evidence that CANX is ubiquitinated on its cytosolic tail, but we believe this possibility should be investigated further as T6BP might use its Ub-binding domain to bind to CANX, providing a molecular link between T6BP and CANX functions in the formation of MHC-II



loading complexes and thus antigen presentation. Note that CANX has also been shown to contribute to the assembly of MHC-I molecules by protecting free MHC-I molecules from degradation (Vassilakos *et al*, 1996) and by binding to the TAP-tapasin complex (Diedrich *et al*, 2001). However, CANX action on MHC-I molecule assembly and transport to the cell surface seem dispensable (Scott & Dawson, 1995; Prasad *et al*, 1998), which would explain the lack of influence of CANX on the MHC-I immunopeptidome, in the absence of T6BP.

We suggest here that CANX is a key factor involved in T6BP-mediated regulation of MHC-II loading that strongly influences the repertoire and affinity of presented peptides. However, we do not exclude that other cellular factors or pathways also participate in T6BP action on MHC-II molecules. Jongsma *et al* showed that the ER ubiquitin ligase RNF26 interacts with p62 (SQSTM1) and that it employs a ubiquitin-based communication with Tollip, T6BP, or EPS15 to cluster recycling, early and late endosomes in so-called perinuclear clouds. In the model, deubiquitination of p62 by the DUB UPS15 leads to the release of the vesicles for maturation (Jongsma *et al*, 2016). The authors showed that the silencing of RNF26 leads to the dispersion of EEA1<sup>+</sup> and CD63<sup>+</sup> vesicles, in the cytoplasm of the cells. They also show that the silencing of T6BP has a broad influence on the shape of cells and leads to the dispersion of the cloud of CD63<sup>+</sup> vesicles. Our observations also highlight that T6BP-silencing influences CD63<sup>+</sup> vesicles; however, our results indicate that CD63<sup>+</sup> vesicles are maintained in the perinuclear region. We confirmed these observations using lysotracker and LAMP-1 markers of acidified and late endosomes, respectively. The different behavior of CD63<sup>+</sup> vesicles in siT6BP-treated cells might be due to the expression of the HLA locus driven by CIITA, in our model of APCs. Nonetheless, our work confirms the involvement of T6BP in the traffic of endosomes. In addition, we found, in the interactome study of T6BP, the DUB UPS15. Interestingly, although T6BP affects EEA1<sup>+</sup> early endosomes perinuclear localization, we excluded the possibility that the effect of T6BP on MHC-II-restricted antigen presentation relies on early endosomal defect since EEA1<sup>+</sup> vesicles do not contain MHC-II molecules in our APCs. Overall, we show that T6BP impacts the trafficking of MHC-II-rich compartments that bear hallmarks of the MIIC, namely HLA-DM, CD63<sup>+</sup>, and LAMP-1. More globally T6BP-silencing seems to affect the cellular localization of acidified vesicular compartments corresponding to late endosomes, lysosomes, and as already demonstrated autophagosomes (Petkova *et al*, 2017), without significantly reducing the expression levels of the various markers. Accumulating evidence suggests that the positioning of intracellular vesicles controls their functions (Neeffjes *et al*, 2017) and intravesicular pH in particular (Johnson *et al*, 2016). The repositioning of the MIIC mediated by T6BP could influence the activation of intravesicular pH-dependent proteases that participate in the cleavage of CD74 and antigen processing. In this regard, it is interesting to note that we identified in the interactome of T6BP, ATP6V0A1 a subunit of the vATPase that plays a critical role in mediating vesicular acidification (Forgac, 2007). On the other hand, CD74 has been shown to play, by itself, a role in endosomal membrane trafficking (Romagnoli *et al*, 1993; Margiotta *et al*, 2020) and perhaps in proteolysis of antigens (Schröder, 2016). It was recently reported that the CD74 p41 isoform interacts with cathepsins and regulates their activity in endosomes (Bruchez *et al*, 2020). These studies and others suggest

that CD74 might exert various functions not limited to its canonical role in antigen presentation and as a chaperone (Schröder, 2016). Thereafter, the modifications in late endosomes/lysosomes positioning and of the MHC-II immunopeptidome in T6BP-silenced cells could be an indirect consequence of CD74 degradation.

Our interactome also revealed as candidate partners for T6BP, the HLA-A, -C, -DQ $\alpha$ 1, and -DR $\beta$ 1 molecules. Interestingly, the cellular distribution of both HLA class I and II molecules is regulated by the addition of ubiquitin (Ub) moieties (De Angelis Rigotti *et al*, 2017; Shin *et al*, 2006; Walseng *et al*, 2010). In the case of HLA-DR, ubiquitination of the lysine residue (K235) of HLA-DR $\beta$ 1 plays a major role in regulating the cellular localisation of mature HLA-DR molecules (Lapaque *et al*, 2009). Although T6BP has the capacity to bind ubiquitinated proteins, we favor the hypothesis that T6BP and HLA molecules might be part of larger molecular complexes or lipid compartments in particular since we observed neither a co-localization of T6BP with HLA-DR molecules nor a significant difference in the kinetics of HLA-DR endocytosis in HeLa-CIITA cells silenced for T6BP expression.

The autophagy receptor T6BP as well as OPTN, NDP52, p62, and NBR1 harbor Ub- and LC3-binding motifs, whose functions are well characterized in selective autophagy (Kirkin & Rogov, 2019). In addition, T6BP and NDP52 share a N-terminal SKIP carboxyl homology (SKICH) domain target of TANK-binding kinase-1 (TBK1) phosphorylation that acts as an upstream regulator of mitophagy (Fu *et al*, 2018). Beyond selective autophagy, ARs also modulate the traffic and maturation of autophagosomes and endosomes. The Ub-binding domains of T6BP, OPTN, and p62 have been implicated in regulating the NF- $\kappa$ B pathway where together with A20 they down-modulate the activation of this pathway during inflammation (Weil *et al*, 2018). T6BP, NDP52, and OPTN also bind to myosin-VI, which recruits Tom-1-expressing endosomes and lysosomes, facilitating autophagosome maturation in lytic vesicles (Sahlender *et al*, 2005; Morriswood *et al*, 2007; Tumbarello *et al*, 2012). Recent work suggested that Ub and myosin-VI compete for the binding to T6BP (Hu *et al*, 2018). In T6BP's interactome, we identified known protein partners of T6BP involved for instance in NF- $\kappa$ B signaling pathways (e.g., TBK1, TRAF2, ITCH, SQSTM1/p62). However, other described T6BP partners such as myosin-VI were not identified, likely reflecting that T6BP interactions occur in a cell type-specific manner (O'Loughlin *et al*, 2018). Nonetheless, we revealed novel potential partners of T6BP involved in the ubiquitin/proteasome (e.g., E3 Ub-ligases UBR1, 2 and 4), the UPR/protein folding (e.g., BAG6, EIF2a, calnexin), endocytosis (e.g., COPB1), and antigen presentation pathways (e.g., HLA molecules). We also found that T6BP interacts with NBR1 that has been found together with p62 in larger protein complexes and ubiquitinated protein aggregates (Weil *et al*, 2018). Much remains to be learned on the molecular mechanisms and motifs involved in the variety of T6BP molecular interactions and functions, in particular in MHC-II antigen presentation that we unravel here. Side-by-side comparison of AR functional domains will most likely bring new insights.

Our work reveals that T6BP regulates the cellular positioning of the MHC-II loading compartment and the stability of CD74, through an interaction with CANX, and exerts a direct influence on MHC-II-restricted antigen presentation. This novel role of T6BP in the activation of adaptive antiviral immunity further highlights the diverse nonredundant functions exerted by autophagy receptors.

## Materials and Methods

### Cells

The HeLa-CIITA cells (homozygotes for HLA-DR $\beta$ 1\*0102 allele), the B (DG-75), and the dendritic-like cell lines (KG-1) were kindly provided by Philippe Benaroch (Institut Curie, Paris, France), Hugo Mouquet (Institut Pasteur, France) and Peter Cresswell (Yale University School of Medicine, USA), respectively. Cells were cultured with RPMI GlutaMax 1640 (Gibco) complemented with 10% FBS (Dutscher), 1% penicillin/streptomycin, and 50  $\mu$ g/mL Hygromycin B (Thermo Fisher) only for HeLa-CIITA cells.

### HIV-1- & HCMV-specific CD4<sup>+</sup> T cell clones

Gag-specific CD4<sup>+</sup> T cell clones (F12) are specific for HIV Gag-p24 (gag2: aa 271–290) and restricted by HLA-DR $\beta$ 1\*01 as previously described (Moris *et al*, 2006; Coulon *et al*, 2016). HCMV-specific CD4<sup>+</sup> T cell clones are specific for HCMV pp65 antigen (pp65: aa 108–127) and restricted by HLA-DR $\beta$ 1\*01. Pp65-specific clones were isolated from PBMCs of healthy donors after several rounds of *in vitro* stimulation with synthetic peptide corresponding to immunodominant epitopes from the pp65 protein. Pp65-specific cells were isolated using the IFN $\gamma$  secreting assay from Miltenyi Biotec and cloned by limiting dilution. F12 and pp65 clones were restimulated and expanded, as previously described (Moris *et al*, 2006), using irradiated feeders and autologous or HLA-matched lymphoblastoid cell lines loaded with cognate peptides in T cell cloning medium: RPMI 1640 containing 5% human AB serum (Institut Jacques Boy), recombinant human IL-2 (100 IU/ml, Miltenyi Biotec), PHA (0,25  $\mu$ g/ml, Remel), nonessential amino acids, and sodium pyruvate (both from Life Technologies). At least 1 h before co-culture with HeLa-CIITA cells, T cell clones were thawed and allowed to rest at 37°C in RPMI containing DNase (5  $\mu$ g/mL, New England Biolabs).

### Viral antigens and plasmids

The pTRIP-CMV-Gag (a kind of gift from Nicolas Manel, Institut Curie, Paris, France), pGag-LC3, and Gag-LC3<sub>G120A</sub> plasmids were already described (Coulon *et al*, 2016). The pp65 encoding cDNA (a kind gift from Xavier Saulquin, Université de Nantes, Nantes) was cloned in the lentiviral vector cppT-EF1 $\alpha$ -IRES-GFP. The GFP-T6BP encoding plasmid is a kind gift from Folma Buss (University of Cambridge, UK) (Tumbarello *et al*, 2015).

### Cell transfections

HeLa-CIITA cells were incubated in 6-well plates using 2–4.10<sup>5</sup> cells/well using OPTIMEM (Gibco) complemented with 10% FBS and 1% penicillin/streptomycin. Twenty-four hours later, cells were transfected with 40 pmol of siRNA targeting NDP52 (L-010637-00-0005), OPTN (L-016269-00-0005), p62 (L-010230-00-0005), T6BP (L-016892-00-0020 Dharmacon or SI02781296, Qiagen), CANX (SI02663367 and SI02757300, Qiagen) or a scrambled siRNA as control (D-001810-10-20, Dharmacon), using Lipofectamine RNAiMax (13778–150, Thermo Fisher) as transfection reagent. After 24 h of transfection, cells were transfected with the cDNA encoding the

viral antigens (1  $\mu$ g per well of a 6-well plate) using Viromer RED (Lipocalyx) and following manufacturer instructions. Twenty-four hours later, Gag and pp65 expressions were assessed using anti-Gag antibody (KC57-RD1, Beckman-Coulter) and anti-pp65 antibody (mouse, Argene) combined with goat anti-mouse antibody (AF488, Thermo Fisher), respectively.

### Flow cytometry

Cell viability was evaluated using LIVE/DEAD (Thermo Fisher) or Zombie (Biolegend) and the following antibodies were used: HLA-DR-specific L243 and T $\bar{U}$ 36 (both in-house and kindly provided by Philippe Benaroch, Institut Curie, Paris) and goat anti-mouse (AF488, Thermo Fisher). Forty-eight hours after siRNA transfection, cell-surface staining assays were performed using standard procedures (30 min, 4°C). HIV-Gag and HCMVpp65 production was detected using intracellular staining. Briefly, cells were fixed with 4% PFA (10 min, RT), washed, and permeabilized with PBS containing 0.5% BSA and 0.05% Saponin, prior to antibody staining. Samples were processed on Fortessa cytometer using FACSDiva software (BD Biosciences) and further analyzed using FlowJo2 software (Tree Star).

### IFN $\gamma$ ELISPOT assay

ELISPOT plates (MSIPN4550, Millipore) were prewet and washed with PBS, and coated overnight at 4°C with anti-IFN $\gamma$  antibody (1-DIK, Mabtech). Plates were washed using PBS and then saturated with RPMI complemented with 10% FBS. Plates were washed and HeLa-CIITA cells (10<sup>5</sup> cells/well) were co-cultured with T cell clones (5.10<sup>3</sup> and 1.10<sup>3</sup> cells/well) overnight at 37°C. Cells were removed and plates were then washed with PBS-0,05% Tween-20 prior to incubation with biotinylated anti-IFN $\gamma$  antibody (7-B6-1, Mabtech) (2 h, RT). Spots were revealed using alkaline-phosphatase coupled to streptavidin (0,5 U/ml, Roche Diagnostics) (1 h, RT) and BCIP/NBT substrate (B1911, Sigma-Aldrich) (30 min, RT). Reactions were stopped using water. A number of spots were counted using AID reader (Autoimmun Diagnostika GmbH). For each experimental condition, ELISPOTs were performed mostly in triplicates or at least in duplicates.

### Western Blotting

Forty-eight hours after siRNA transfection, 10<sup>6</sup> HeLa-CIITA cells were washed in cold PBS and lysed in 100–300  $\mu$ l of lysis buffer (30 min, 4°C), mixing every 10 min. When stated, cells were pretreated with chloroquine (50  $\mu$ M, 16 h) or epoxomicin (50 nM, 16 h). Depending on the experiments, three different lysis buffers were used: 1- PBS containing 1% Nonidet P-40; 2–50 mM Tris-HCl pH 7.5 containing 100 mM NaCl, 1% Triton X-100, 0.5 mM EGTA, 5 mM MgCl<sub>2</sub>, 2 mM ATP; 3–50 mM Tris-HCl pH 7.5 containing 150 mM NaCl, 1% IGEPAL, 0.5 mM EDTA, 5 mM MgCl<sub>2</sub>, all three supplemented with 1x protease inhibitor (Roche). Cell lysates were then centrifuged at 20,000 g (10 min, 4°C), supernatants harvested and mixed with Sample Buffer (NuPAGE, Invitrogen) and Sample Reducing Agent (NuPAGE, Invitrogen) and denatured (5 min, 95°C). Denatured samples were analyzed by SDS gel electrophoresis using 4–12% Bis-Tris gels (NuPAGE, Invitrogen), transferred to a nitrocellulose membrane

(NuPAGE, Invitrogen), and immunoblotted. Anti-T6BP (HPA024432, Sigma-Aldrich), anti-NDP52 (HPA023195, Sigma-Aldrich), anti-CANX (PA5-34754, Thermo Fisher), anti-OPTN (ab23666, Abcam), anti-p62 (sc-28,359, Santa Cruz Biotechnology), anti-HLA-DR (TAL1B5, Invitrogen), anti-LC3 (M152, MBL International), anti-actin (3700S, Cell Signaling Technology), anti-tubulin (2148S, Cell Signaling Technology), anti-CD74 (ab22603, Abcam or VIC-Y1, 14-0747-82, Thermo Fisher), anti-GFP (11,814,460,001, Roche), anti-ubiquitin (eBioP4D1, Thermo Fisher), goat anti-mouse (Sigma-Aldrich) and goat anti-rabbit both coupled to HRP (Abcam) antibodies were used according to manufacturer instructions. Blots were revealed using Pierce ECL Plus Substrate (Invitrogen) and chemiluminescence analyzed using ImageQuant LAS 4000.

### Confocal microscopy

Forty-eight hours after siRNA transfections, HeLa-CIITA cells were plated on glass coverslips and then fixed with 4% PFA (10 min, RT). Cells were washed 3 times with PBS, saturated with goat or donkey serum, and permeabilized with PBS containing 0,5% BSA and 0,05% Saponin (1 h, RT). Cells were washed with PBS and incubated (OVN, 4°C) with primary antibodies: L243 or TÛ36 (both in-house and kindly provided by P. Benaroch, Institut Curie, Paris), rabbit anti-HLA-DR (a kind gift from Jacques Neefjes, Leiden University, the Netherlands), anti-LAMP-1 (H4A3, DSHB), anti-CD63 (MA-18149), anti-CD74 (14-0747-82) all from Thermo Fisher, anti-EEA1 (C45B10, Cell signaling), anti-T6BP (HPA024432, Sigma-Aldrich), anti-HLA-DM (sc-32,248, Santa Cruz) and Lysotracker (Deep Red, L12492). Cells were incubated with species-specific antibodies: goat anti-mouse coupled to Alexa Fluor 488 or Alexa Fluor 405 (Thermo Fisher), donkey anti-rabbit coupled to Alexa 546 (A10040, Invitrogen) in PBS containing 0,5% BSA and 0,05% Saponin (1 h, RT). When required sequential stainings were performed. Nuclei were stained with DAPI (17,507, AAT Bioquest). After washing with PBS, samples were mounted on glass slides with Dako fluorescence mounting medium. Samples were imaged using a laser scanning confocal microscope with 63X, NA 1.3 oil immersion objective. The number of vesicles, the intensity, and the distances of each vesicle to nucleus were quantified using an in-house ImageJ Python script (developed by Aziz Fouché, ENS Paris-Saclay, Paris). Potential co-localizations were determined using the object-based co-localization method JACoP (Just Another Co-localization Plugin) and coloc2 (Pearson's coefficient) of the ImageJ software, for punctuated/vesicular and cytosolic/diffuse staining, respectively. For the Proximity ligation assay (PLA), 48 h after siRNA transfections, HeLa-CIITA cells, cultured overnight on coverslips, were fixed with 4% PFA (10 min, RT), washed 3x with PBS, and treated with 50 mM NH<sub>4</sub>Cl (15 min, RT) prior incubation with anti-T6BP (Rabbit, 1:200, HPA024432) and anti-CANX (Mouse, 1:500, MA3-027, Thermo Fisher scientific) in PBS containing 1%, BSA and 0.1% Saponin (1 h, RT). PLA secondary probes (DUO92002, DUO92004) were then used according to the manufacturer's instructions (Sigma-Aldrich). Briefly, 40 µl (1:5 dilution) of the PLA was added (37 °C, 60 min) and washed with buffer A (DUO82049, Sigma-Aldrich). 40 µl of the ligation mix (DUO92014, Sigma-Aldrich) was then applied to each of the coverslips to complete the ligation process (30 min, 37 °C). Coverslips were then incubated with 40 µl polymerization mix (100 min, 37 °C) and washed. Coverslips were

mounted on slides with Fluoromount G (Thermo Fisher). Images were acquired using an SP8 confocal microscope and dots were counted using the find maxima plugin in Fiji software.

### Reverse transcription-quantitative polymerase chain reaction (RT-qPCR)

Total cellular RNA was isolated using RNeasy kit (Qiagen, Valencia, CA). RNA concentrations were determined by spectrophotometry at 260 nm. The relative level of CD74 and T6BP mRNAs was determined using the comparative Cq method. Actin was used as endogenous control. The primers and probes used for quantitation of CD74, T6BP, and actin were designed by Olfert Landt and purchased from TIB MolBiol. Sequences are listed in Appendix Table S1. The RT-qPCRs were performed in a Light Cycler 1.5 instrument in capillaries using a final volume of 20 µl. The reactions were performed using 300 nM specific sense primer, 300 nM specific antisense primer, 200 nM specific TaqMan probe (TM), and the LightCycler® Multiplex RNAVirus Master mix (ROCHE). The programs were: reverse transcription at 55°C for 10 min, initial denaturation at 95°C for 5 min followed by 45 cycles of amplification. For CD74 and T6BP cycles were: 95°C for 5 s, 60°C for 15 s + fluorescence measurement, and 72°C for 5 s. For actin cycles were: 95°C for 20s, 67°C for 30s + fluorescence measurement, and 72°C for 5 s.

### Pulse-Chase experiment

48 h post-siRNA transfection HeLa-CIITA cells were preincubated in Met/Cys-free RPMI 1640 medium containing 1% penicillin/streptomycin, 1% glutamine, and 10% dialyzed FCS for 1 h. Cells (five million) were then pulsed for 30 min with 0.5 mCi of <sup>35</sup>S-Met/Cys (ICN) and chased in an unlabelled medium supplemented with 5 mM cold methionine. Cells were collected at the indicated time points and then lysed in a buffer containing 20 mM Tris-HCl (pH 7.5), 150 mM NaCl, 2 mM MgCl<sub>2</sub>, 1% Triton X-100, and an inhibitor cocktail (Roche). Each sample was normalized for the protein concentration. Lysates were precleared with mouse serum, and MHC class II/Ii complexes were immunoprecipitated with the TÛ36 antibody and/or reimmunoprecipitated with VICY1 antibody (14-0747-82, Thermo Fisher). Samples were boiled (95°C) or unboiled (room temperature) in SDS loading buffer and separated on 12% SDS-PAGE (Novex). Quantification of the results was made using a phosphoimager (Fuji).

### Electron Microscopy

HeLa-CIITA cells (2.10<sup>5</sup> cells/well) were cultured on glass coverslips in 6-well plates. 24 h later, cells were transfected as described with siRNA control or targeting T6BP, cells were cultured for 48 h and fixed with 2.5% glutaraldehyde, 1% PFA for 1 h at room temperature. The coverslips were washed 3 times with 0.2 M phosphate buffer pH 7.4, followed by a 1-h incubation in 1% osmium, and 1.5% ferrocyanide of potassium. After 3 washes in water, the coverslips were successively treated with 50%, 70%, 90%, 100%, and 100% Ethanol for 10 min each. The coverslips were then incubated for 2 h on 50% epoxy in ethanol, followed by 2 h in pure epoxy, and finally in pure epoxy overnight for polymerization at 60°C. Ultrathin (70 nm) sections were cut using a diamond knife (45°

angle) on a Leica UC6 ultramicrotome. Sections were collected on Formvar™ carbon-coated copper grids. Some sections were stained with uranyl acetate at 2% (Merk) for 15 min and lead Citrate (Agar) and washed three times with milliQ water and dried at room temperature. Observations were performed with a JEOL JEM-1400 transmission electron microscope operating at 120 kV. Images were acquired using a postcolumn high-resolution ( $9 \times 10^6$  pixels) camera (Rio9; Gatan) and processed with Digital Micrograph (Gatan) and ImageJ.

## Immunoepitidome

### Isolation of HLA ligands

HLA class I and II molecules of HeLa-CIITA cells were isolated using standard immunoaffinity purification (Falk *et al.*, 1991; Nelde *et al.*, 2019). Snap-frozen samples were lysed in 10 mM CHAPS/PBS (AppliChem, Gibco) with 1x protease inhibitor (Roche). HLA class I- and II-associated peptides were isolated using the pan-HLA class I-specific mAb W6/32 and the pan-HLA class II-specific mAb TŪ39 (both in-house mouse monoclonal) covalently linked to CNBr-activated Sepharose (GE Healthcare). HLA-peptide complexes were eluted by repeated addition of 0.2% TFA (trifluoroacetic acid, Merck). Eluted HLA ligands were purified by ultrafiltration using centrifugal filter units (Millipore). Peptides were desalted using ZipTip C18 pipette tips (Millipore), eluted in 35  $\mu$ l 80% acetonitrile (Merck)/0.2% TFA, vacuum-centrifuged and resuspended in 25  $\mu$ l of 1% acetonitrile/0.05% TFA and samples stored at  $-20^\circ\text{C}$  until LC-MS/MS analysis.

### Analysis of HLA ligands by LC-MS/MS

Isolated peptides were separated by reversed-phase liquid chromatography (nano-UHPLC, UltiMate 3,000 RSLCnano; ThermoFisher) and analyzed in an online-coupled Orbitrap Fusion Lumos mass spectrometer (Thermo Fisher). Samples were analyzed in five technical replicates, and sample shares of 20% were trapped on a 75  $\mu\text{m} \times 2$  cm trapping column (Acclaim PepMap RSLC; Thermo Fisher) at 4  $\mu\text{l}/\text{min}$  for 5.75 min. Peptide separation was performed at  $50^\circ\text{C}$  and a flow rate of 175 nl/min on a 50  $\mu\text{m} \times 25$  cm separation column (Acclaim PepMap RSLC; Thermo Fisher) applying a gradient ranging from 2.4 to 32.0% of acetonitrile over the course of 90 min. Samples were analyzed on the Orbitrap Fusion Lumos implementing a top-speed CID method with survey scans at 120 k resolution and fragment detection in the Orbitrap (OTMS2) at 60 k resolution. The mass range was limited to 400–650 m/z with precursors of charge states 2+ and 3+ eligible for fragmentation.

### Database search and spectral annotation

LC-MS/MS results were processed using Proteome Discoverer (v.1.3; Thermo Fisher) to perform a database search using the Sequest search engine (Thermo Fisher) and the human proteome as reference database annotated by the UniProtKB/Swiss-Prot. The search-combined data of five technical replicates was not restricted by enzymatic specificity, and oxidation of methionine residues was allowed as a dynamic modification. Precursor mass tolerance was set to 5 ppm, and fragment mass tolerance to 0.02 Da. The false discovery rate (FDR) was estimated using the Percolator node (Käll *et al.*, 2007) and was limited to 5%. For HLA class I ligands, peptide lengths were limited to 8–12 amino acids. For HLA class II, peptides

were limited to 12–25 amino acids in length. HLA class I annotation was performed using NetMHCpan 4.0 (Jurtz *et al.*, 2017) annotating peptides with percentile rank below 2% as previously described (Ghosh *et al.*, 2019).

For HLA class II peptides, the Peptide Landscape Antigenic Epitope Alignment Utility (PLATEAU) algorithm (Alvaro-Benito *et al.*, 2018) was used to identify and to estimate the relative abundance of the core epitopes based on the LC-MS/MS intensities. The results are presented as Volcano plots using Perseus software (Tyanova *et al.*, 2016). The relative affinities of the core epitope to HLA-DR $\beta$ 1\*0102, expressed by HeLa-CIITA cells, were estimated using NetMHCIIpan 4.0 (Reynisson *et al.*, 2020).

## Interactome

### Co-immunoprecipitation

HeLa-CIITA cells were harvested 24 h after cDNA transfection with either plasmid encoding GFP-T6BP (kind gift from F.Buss, Cambridge, UK) or encoding GFP.  $2.10^7$  cells were washed in cold PBS and lysed in 300  $\mu$ l of lysis buffer (50 mM Tris-HCl pH 7.5, 100 mM NaCl, 1% Triton X-100, 0.5 mM EGTA, 5 mM MgCl<sub>2</sub>, 2 mM ATP, and 1x protease inhibitor; Roche; 30 min, ice), mixing every 10 min and centrifuged at 20,000 g (20 min,  $4^\circ\text{C}$ ). Lysates were recovered, 300  $\mu$ l of wash buffer (50 mM Tris-HCl pH 7.5, 150 mM NaCl, 0.5 mM EDTA) was added and the pellets were discarded. GFP-Trap agarose magnetic beads (Chromotek) were vortexed, and 25  $\mu$ l of bead slurry was washed 3 times with cold wash buffer. Each diluted lysate was added to 25  $\mu$ l of equilibrated beads and tumbled end-over-end (1 h,  $4^\circ\text{C}$ ). Beads were collected using a magnetic support and washed 3 times. For Western Blot analysis, SDS-sample buffer was added to aliquots and the samples were boiled (5 min,  $99^\circ\text{C}$ ).

### On-bead digestion for mass spectrometry

Following immunoprecipitation with GFP-Trap (Chromotek), digestions were performed using manufacturer instructions on the P3S proteomic core facility of Sorbonne Université. For each sample, beads were resuspended in 25  $\mu$ l of elution buffer I (50 mM Tris-HCl pH 7.5, 2 M urea, 5  $\mu\text{g}/\text{ml}$  sequencing grade Trypsine, 1 mM DTT) and incubated in a thermomixer at 400 rpm (30 min,  $30^\circ\text{C}$ ). Beads were collected using a magnetic support and the supernatants were recovered. For elution, beads were then washed with 50  $\mu$ l of elution buffer II (50 mM Tris-HCl pH 7.5, 2 M urea, 5 mM iodoacetamide) and collected with a magnetic support. Supernatants were harvested and mixed with the previous ones. This elution was repeated once. Combined supernatants were incubated in a thermomixer at 400 rpm (overnight,  $32^\circ\text{C}$ ). Reactions were stopped by adding 1  $\mu$ l trifluoroacetic acid and digests were desalted using homemade StageTips. StageTips were first rehydrated with 100  $\mu$ l of methanol and then equilibrated with 100  $\mu$ l of 50% acetonitrile and 0.5% acetic acid. After peptide loading, StageTips were washed with 200  $\mu$ l of 0.5% acetic acid, and peptides were eluted with 60  $\mu$ l of 80% acetonitrile 0.5% acetic acid. Eluted peptides were totally dried using a SpeedVac vacuum concentrator (Thermo), solubilized in 20  $\mu$ l of 2% acetonitrile 0.1% formic acid before LC-MS/MS analysis.

### LC-MS/MS

Peptide mixtures were analyzed with a nanoElute UHPLC (Bruker) coupled to a timsTOF Pro mass spectrometer (Bruker). Peptides

were separated on an Aurora RP-C18 analytical column (25 cm, 75  $\mu\text{m}$  i.d., 120  $\text{\AA}$ , 1,6  $\mu\text{m}$  IonOpticks) at a flow rate of 300 nL/min, at 40°C, with mobile phase A (ACN 2% / FA 0.1%) and B (ACN 99.9% / FA 0.1%). A 30 min elution gradient was run from 0% to 3% B in 1 min, 3% to 15% B in 17 min then 15% to 23% B in 7 min and 23% to 32% B in 5 min. MS acquisition was run in DDA mode with PASEF. Accumulation time was set to 100 msec in the TIMS tunnel. The capillary voltage was set to 1,6 kV, mass range from 100 to 1700 m/z in MS and MS/MS. Dynamic exclusion was activated for ions within 0.015 m/z and 0.015 V.s/cm<sup>2</sup> and released after 0,4 min. The exclusion was reconsidered if precursor ion intensity was 4 times superior. Low abundance precursors below the target value of 20,000 a.u and intensity of 2,500 a.u. were selected several times for PASEF-MS/MS until the target value was reached. Parent ion selection was achieved by using a two-dimensional m/z and 1/k0 selection area filter allowing the exclusion of singly charged ions. Total cycle time was 1,29 s with 10 PASEF cycles.

### Data Analysis

Raw data were processed with MaxQuant version 1.6.5.0, with no normalization, no matching between runs, and a minimum of 2 peptide ratios for protein quantification. The output protein file was filtered with ProStar 1.14 to keep only proteins detected in 2 samples or more in at least 1 of the 2 conditions. Missing values were imputed using SLSA (Structured Least Square Adaptive) algorithm for partially missing values in each condition and DetQuantile algorithm for missing values in an entire condition. In order to select relevant binding partners, data were statistically processed using the limma test and filtered to retain only differentially expressed preys (FDR 1%) with a fold change  $\geq 10$  between T6BP-GFP and GFP conditions. Selected preys were uploaded to the CRAPome v2 (Contaminant Repository for Affinity Purification) online analysis tool to identify potential contaminants. For each binding partners, a Significance Analysis of INteractome (SAINT) probability threshold was assessed by the Resource for Evaluation of Protein Interaction Networks (REPRINT) using the default settings. Selected preys were then uploaded in Ingenuity Pathway Analysis software version 49,932,394 (QIAGEN Inc.) to perform annotation and over-representation analysis. Finally, network visualization was designed using Cytoscape software (v. 3.7.1).

### Co-immunoprecipitation: CANX / T6BP / GST-TM-cytoTail

HeLa-CIITA cells were harvested, counted, and lysed in two different buffers depending on the experiments: 1- m-RIPA buffer (1% NP40, 1% sodium deoxycholate, 150 mM NaCl, 50 mM Tris-pH 7.5; 2- NP-40 lysis buffer, 50 mM Tris-HCl pH 7.5 containing 150 mM NaCl, 1% IGEPAL, 0.5 mM EDTA, 5 mM MgCl), both supplemented with complete protease inhibitors (Roche, Basel, Switzerland). CANX and T6BP were immunoprecipitated using anti-CANX antibody PA5-34754 (Invitrogen) coupled to protein A Sepharose magnetic beads (Ademtech 0423) and anti-TAX1BP1 antibody HPA024432 (Sigma-Aldrich) together with protein A Sepharose (GE Healthcare), respectively. The GST-TM-cytoTail nucleotide sequence was synthesized and cloned into pLV-EF1a-IRES-Puro by GeneCust. pLV-EF1a-IRES-Puro was a gift from Tobias

Meyer (Addgene plasmid # 85132; <http://n2t.net/addgene:85132>; RRID:Addgene\_85132) (Hayer et al, 2016). GST-TM-cytoTail sequence contains the following sequence: CANX leader, GST, a short fragment of the ER luminal domain of CANX, CANX TM, CANX cytosolic tail; and is: ATGGAAGGGAAGTGGTTGCTGTG-TATGTTACTGGTGCTTGGAACTGCTATTGTTGAGGCTTCCCCTATA CTAGGTTATTGGAAAATTAAGGGCCTTGTGCAACCCACTCGACTTC TTTTGGAAATATCTTGAAGAAAAATGAAGAGCATTGTATGAGC GCGATGAAGGTGATAAATGGCGAAACAAAAAGTTTGAATTGGGTT TGGAGTTTCCCAATCTTCCTTATTATATTGATGGTGATGTTAAATT AACACAGTCTATGGCCATCATACGTTATATAGCTGACAAGCACAAAC ATGTTGGGTGGTTGTCCAAAAGAGCGTGCAGAGATTTCAATGCTTG AAGGAGCGGTTTTGGATATTAGATACGGTGTTCGAGAATTGCATA TAGTAAAGACTTTGAAACTCTCAAAGTTGATTTTCTTAGCAAGCTA CCTGAAATGCTGAAAATGTTGCAAGATCGTTTATGTCATAAAACAT ATTTAAATGGTGATCATGTAACCCATCCTGACTTCATGTTGTATGA CGCTCTTGATGTTGTTTTATACATGGACCCAATGTGCCTGGATGCGT TCCAAAATAGTTTGTGTTTTAAAAAACGTAATTGAAGCTATCCCACA AATTGATAAGTACTTGAATCCAGCAAGTATATAGCATGGCCTTTG CAGGGCTGGCAAGCCACGTTTGGTGGTGGCGACCATCTCCAAAAA AGAAAGTGTGATGGGGCTGCTGAGCCAGGCGTTGTGGGGCAGA TGATCGAGGCGAGTGAAGAGCGCCGGAAGAAAGCTGCTGATGGGG CTGCTGAGCCAGGCGTTGTTGGGGCAGATGATCGAGGCGACTGAAG AGCGCCCGTGGCTGTGGGTAGTCTATATTCTAACTGTAGCCCTTCC TGTGTTCTGTTTATCTCTTCTGCTGTTCTGGAAAGAAACAGACC AGTGGTATGGAGTATAAGAAAAGTATGACCTCAACCCGGATGTGA AGGAAGAGGAAGAAGAGAAGGAAGAGGAAAAGGACAAGGGAGAT GAGGAGGAGGAAGGAGAAGAAAAGTGAAGAGAAAACAGAAAAG TGATGCTGAAGAAGATGGTGGCACTGTCACTCAAGAGGAGGAAGA CAGAAAACCTAAAGCAGAGGAGATGAAATTTTGAACAGATCACCA AGAAACAGAAAGCCACGAAGAGAGTGA. HeLa-CIITA cells were transfected with GST-TM-cytoTail construct or the vector not encoding TM-cytoTail. 24 h post-transfection, cells were harvested and lysed using NP40 lysis buffer (10 mM Tris-HCl pH 7.5, 150 mM NaCl, 0,5 mM EDTA, 0,5% IGEPAL). The GST-immunoprecipitation was performed using GST-Trap Agarose from Chromotek. The immunoprecipitation (IP) fractions were extensively washed (at least 3 times) in NP40 lysis buffer. The input, the flow-through, and the IP fractions were analyzed by SDS-PAGE and the proteins revealed using Western blot.

### Statistical analysis

Statistical significances (*P*-values) were calculated using Prism Software (GraphPad).

### Data availability

The mass spectrometry proteomics data have been deposited to the ProteomeXchange Consortium (<http://proteomecentral.proteomexchange.org>) via the PRIDE (Perez-Riverol et al, 2019) partner repository with the dataset identifier PXD024330 and PXD024417 for the T6BP-interactome and HeLa-CIITA immunoprecipitation, respectively: <http://www.ebi.ac.uk/pride/archive/projects/PXD024330>; <http://www.ebi.ac.uk/pride/archive/projects/PXD024417>

**Expanded View** for this article is available [online](#).

## Acknowledgements

This work was granted by the ANR project AutoVirim (ANR-14-CE14-0022). We thank the “P3S” core facility of Sorbonne University for its expertise. The present work has benefited from the Imagerie facility of Imagerie-Gif, (<http://www.i2bc.paris-saclay.fr>), member of IBISA (<http://www.ibisa.net>), supported by l'Agence Nationale de la Recherche (ANR-11-EQPX-0029/Morphoscope), “France-Biolmaging” (ANR-10-INSB-04-01) and the Labex “Saclay Plant Science” (ANR-11-IDEX-0003-02). C.R. and M.P. were supported by AutoVirim. We thank the Dormeur Foundation, Vaduz, for providing the AID ELISPOT Reader. We also thank the Agence Nationale de Recherche sur le SIDA et les hépatites virales (ANRS) and Sidaction for funding. M.P. and L.B. were supported by Sidaction. A.K. and R.J.-M. were ANRS fellows.

## Author contributions

**Gabriela Sarango:** Formal analysis; investigation; methodology; writing—review and editing. **Clémence Richetta:** Formal analysis; validation; investigation; methodology; writing—original draft; writing—review and editing. **Mathias Pereira:** Formal analysis; investigation; methodology; writing—original draft; writing—review and editing. **Anita Kumari:** Formal analysis; investigation; methodology; writing—review and editing. **Michael Ghosh:** Data curation; formal analysis; investigation; methodology. **Lisa Bertrand:** Investigation; methodology. **Cédric Pionneau:** Data curation; formal analysis; investigation; methodology; writing—review and editing. **Morgane Le Gall:** Data curation; software; formal analysis. **Sylvie Grégoire:** Investigation; methodology. **Raphaël Jeger-Madiot:** Investigation; methodology. **Elina Rosoy:** Investigation; methodology. **Frédéric Subra:** Supervision; validation; investigation; methodology. **Olivier Delelis:** Formal analysis; supervision; validation; investigation; methodology. **Mathias Faure:** Resources; funding acquisition. **Audrey Esclatine:** Resources; funding acquisition. **Stéphanie Graff-Dubois:** Supervision; investigation; methodology. **Stefan Stevanović:** Data curation; formal analysis; validation; investigation; methodology. **Bénédicte Manoury:** Conceptualization; formal analysis; supervision; validation; investigation; methodology; writing—review and editing. **Bertha Cecilia Ramirez:** Formal analysis; supervision; validation; investigation; methodology; writing—review and editing. **Arnaud Moris:** Conceptualization; resources; formal analysis; supervision; funding acquisition; validation; investigation; visualization; methodology; writing—original draft; project administration; writing—review and editing.

## Disclosure and competing interests statement

The authors declare that they have no conflict of interest.

## References

- Aichinger M, Wu C, Nedjic J, Klein L (2013) Macroautophagy substrates are loaded onto MHC class II of medullary thymic epithelial cells for central tolerance. *J Exp Med* 210: 287–300
- Alvaro-Benito M, Morrison E, Abualrous ET, Kuroпка B, Freund C (2018) Quantification of HLA-DM-dependent major histocompatibility complex of class II immunopeptidomes by the peptide landscape antigenic epitope alignment utility. *Front Immunol* 9: 872
- Anderson KS, Cresswell P (1994) A role for calnexin (IP90) in the assembly of class II MHC molecules. *EMBO J* 13: 675–682
- Arunachalam B, Cresswell P (1995) Molecular requirements for the interaction of class II major histocompatibility complex molecules and invariant chain with calnexin. *J Biol Chem* 270: 2784–2790
- Bakke O, Dobberstein B (1990) MHC class II-associated invariant chain contains a sorting signal for endosomal compartments. *Cell* 63: 707–716
- Bania J, Gatti E, Lelouard H, David A, Cappello F, Weber E, Camosseto V, Pierre P (2003) Human cathepsin S, but not cathepsin L, degrades efficiently MHC class II-associated invariant chain in nonprofessional APCs. *Proc Natl Acad Sci U S A* 100: 6664–6669
- Benaroch P, Yilla M, Raposo G, Ito K, Miwa K, Geuze HJ, Ploegh HL (1995) How MHC class II molecules reach the endocytic pathway. *EMBO J* 14: 37–49
- Bijlmakers MJ, Benaroch P, Ploegh HL (1994) Assembly of HLA DR1 molecules translated in vitro: binding of peptide in the endoplasmic reticulum precludes association with invariant chain. *EMBO J* 13: 2699–2707
- Bikoff E, Birshtein BK (1986) T cell clones specific for IgG2a of the a allotype: direct evidence for presentation of endogenous antigen. *J Immunol* 137: 28–34
- Blanchet FP, Moris A, Nikolic DS, Lehmann M, Cardinaud S, Stalder R, Garcia E, Dinkins C, Leuba F, Wu L et al (2010) Human immunodeficiency virus-1 inhibition of immunoamphisomes in dendritic cells impairs early innate and adaptive immune responses. *Immunity* 32: 654–669
- Bruchez A, Sha K, Johnson J, Chen L, Stefani C, McConnell H, Gaucherand L, Prins R, Matreyek KA, Hume AJ et al (2020) MHC class II transactivator CIITA induces cell resistance to Ebola virus and SARS-like coronaviruses. *Science* 370: 241–247
- Busch R, Cloutier I, Sekaly RP, Hammerling GJ (1996) Invariant chain protects class II histocompatibility antigens from binding intact polypeptides in the endoplasmic reticulum. *EMBO J* 15: 418–428
- Choi H, Larsen B, Lin ZY, Breikreutz A, Mellacheruvu D, Fermin D, Qin ZS, Tyers M, Gingras AC, Nesvizhskii AI (2011) SAINT: probabilistic scoring of affinity purification-mass spectrometry data. *Nat Methods* 8: 70–73
- Coulon PG, Richetta C, Rouers A, Blanchet FP, Urrutia A, Guerbois M, Piguet V, Theodorou I, Bet A, Schwartz O et al (2016) HIV-infected dendritic cells present endogenous MHC class II-restricted antigens to HIV-specific CD4<sup>+</sup> T cells. *J Immunol* 197: 517–532
- Crotzer VL, Blum JS (2008) Cytosol to lysosome transport of intracellular antigens during immune surveillance. *Traffic* 9: 10–16
- Dani A, Chaudhry A, Mukherjee P, Rajagopal D, Bhatia S, George A, Bal V, Rath S, Mayor S (2004) The pathway for MHCII-mediated presentation of endogenous proteins involves peptide transport to the endo-lysosomal compartment. *J Cell Sci* 117: 4219–4230
- De Angelis Rigotti F, De Gassart A, Pffor C, Cano F, N'Guessan P, Combes A, Camosseto V, Lehner PJ, Pierre P, Gatti E (2017) MARCH9-mediated ubiquitination regulates MHC I export from the TGN. *Immunol Cell Biol* 95: 753–764
- De Gassart A, Camosseto V, Thibodeau J, Ceppi M, Catalan N, Pierre P, Gatti E (2008) MHC class II stabilization at the surface of human dendritic cells is the result of maturation-dependent MARCH I down-regulation. *Proc Natl Acad Sci U S A* 105: 3491–3496
- Dengjel J, Schoor O, Fischer R, Reich M, Kraus M, Muller M, Kreymborg K, Altenberend F, Brandenburg J, Kalbacher H et al (2005) Autophagy promotes MHC class II presentation of peptides from intracellular source proteins. *Proc Natl Acad Sci U S A* 102: 7922–7927
- Denzin LK, Cresswell P (1995) HLA-DM induces CLIP dissociation from MHC class II alpha beta dimers and facilitates peptide loading. *Cell* 82: 155–165
- Diedrich G, Bangia N, Pan M, Cresswell P (2001) A role for calnexin in the assembly of the MHC class I loading complex in the endoplasmic reticulum. *J Immunol* 166: 1703–1709
- Dorfel D, Appel S, Grunebach F, Weck MM, Muller MR, Heine A, Brossart P (2005) Processing and presentation of HLA class I and II epitopes by dendritic cells after transfection with in vitro-transcribed MUC1 RNA. *Blood* 105: 3199–3205

- Eisenlohr LC, Hackett CJ (1989) Class II major histocompatibility complex-restricted T cells specific for a virion structural protein that do not recognize exogenous influenza virus. Evidence that presentation of labile T cell determinants is favored by endogenous antigen synthesis. *J Exp Med* 169: 921–931
- Falk K, Rotzschke O, Stevanovic S, Jung G, Rammensee HG (1991) Allele-specific motifs revealed by sequencing of self-peptides eluted from MHC molecules. *Nature* 351: 290–296
- Fletcher K, Ulferts R, Jacquin E, Veith T, Gammoh N, Arasteh JM, Mayer U, Carding SR, Wileman T, Beale R et al (2018) The WD40 domain of ATG16L1 is required for its non-canonical role in lipidation of LC3 at single membranes. *EMBO J* 37: e97840
- Fonteneau JF, Brilot F, Munz C, Gannage M (2016) The tumor antigen NY-ESO-1 mediates direct recognition of melanoma cells by CD4<sup>+</sup> T cells after intercellular antigen transfer. *J Immunol* 196: 64–71
- Forgac M (2007) Vacuolar ATPases: rotary proton pumps in physiology and pathophysiology. *Nat Rev Mol Cell Biol* 8: 917–929
- Fu T, Liu J, Wang Y, Xie X, Hu S, Pan L (2018) Mechanistic insights into the interactions of NAP1 with the SKICH domains of NDP52 and TAX1BP1. *Proc Natl Acad Sci U S A* 115: e11651–e11660
- Germain RN, Hendrix LR (1991) MHC class II structure, occupancy and surface expression determined by post-endoplasmic reticulum antigen binding. *Nature* 353: 134–139
- Ghosh M, Di Marco M, Stevanovic S (2019) Identification of MHC ligands and establishing MHC class I peptide motifs. *Methods Mol Biol* 1988: 137–147
- Hayer A, Shao L, Chung M, Joubert LM, Yang HW, Tsai FC, Bisaria A, Betzig E, Meyer T (2016) Engulfed cadherin fingers are polarized junctional structures between collectively migrating endothelial cells. *Nat Cell Biol* 18: 1311–1323
- Hu S, Wang Y, Gong Y, Liu J, Li Y, Pan L (2018) Mechanistic insights into recognitions of ubiquitin and myosin VI by autophagy receptor TAX1BP1. *J Mol Biol* 430: 3283–3296
- Jacobson S, Sekaly RP, Bellini WJ, Johnson CL, McFarland HF, Long EO (1988) Recognition of intracellular measles virus antigens by HLA class II restricted measles virus-specific cytotoxic T lymphocytes. *Ann N Y Acad Sci* 540: 352–353
- Jagannath C, Lindsey DR, Dhandayuthapani S, Xu Y, Hunter RL Jr, Eissa NT (2009) Autophagy enhances the efficacy of BCG vaccine by increasing peptide presentation in mouse dendritic cells. *Nat Med* 15: 267–276
- Jaraquemada D, Marti M, Long EO (1990) An endogenous processing pathway in vaccinia virus-infected cells for presentation of cytoplasmic antigens to class II-restricted T cells. *J Exp Med* 172: 947–954
- Jin Y, Sun C, Feng L, Li P, Xiao L, Ren Y, Wang D, Li C, Chen L (2014) Regulation of SIV antigen-specific CD4<sup>+</sup> T cellular immunity via autophagosome-mediated MHC II molecule-targeting antigen presentation in mice. *PLoS One* 9: e93143
- Johnson DE, Ostrowski P, Jaumouillé V, Grinstein S (2016) The position of lysosomes within the cell determines their luminal pH. *J Cell Biol* 212: 677–692
- Jongsma ML, Berlin I, Wijdeven RH, Janssen L, Janssen GM, Garstka MA, Janssen H, Mensink M, van Veelen PA, Spaapen RM et al (2016) An ER-associated pathway defines endosomal architecture for controlled cargo transport. *Cell* 166: 152–166
- Jurtz V, Paul S, Andreatta M, Marcatili P, Peters B, Nielsen M (2017) NetMHCpan-4.0: improved peptide-MHC class I interaction predictions integrating eluted ligand and peptide binding affinity data. *J Immunol* 199: 3360–3368
- Käll L, Canterbury JD, Weston J, Noble WS, MacCoss MJ (2007) Semi-supervised learning for peptide identification from shotgun proteomics datasets. *Nat Methods* 4: 923–925
- Kirkin V (2020) History of the selective autophagy research: how did it begin and where does it stand today? *J Mol Biol* 432: 3–27
- Kirkin V, Rogov VV (2019) A diversity of selective autophagy receptors determines the specificity of the autophagy pathway. *Mol Cell* 76: 268–285
- Lakkaraju AK, Abrami L, Lemmin T, Blaskovic S, Kunz B, Kihara A, Dal Peraro M, van der Goot FG (2012) Palmitoylated calnexin is a key component of the ribosome-translocon complex. *EMBO J* 31: 1823–1835
- Lapaque N, Jahnke M, Trowsdale J, Kelly AP (2009) The HLA-DRalpha chain is modified by polyubiquitination. *J Biol Chem* 284: 7007–7016
- Lee HK, Mattei LM, Steinberg BE, Alberts P, Lee YH, Chervovsky A, Mizushima N, Grinstein S, Iwasaki A (2010) *In vivo* requirement for Atg5 in antigen presentation by dendritic cells. *Immunity* 32: 227–239
- Leung CS (2015) Endogenous antigen presentation of MHC class II epitopes through non-autophagic pathways. *Front Immunol* 6: 464
- Lich JD, Elliott JF, Blum JS (2000) Cytoplasmic processing is a prerequisite for presentation of an endogenous antigen by major histocompatibility complex class II proteins. *J Exp Med* 191: 1513–1524
- Lin CY, Nozawa T, Minowa-Nozawa A, Toh H, Aikawa C, Nakagawa I (2019) LAMTOR2/LAMTOR1 complex is required for TAX1BP1-mediated xenophagy. *Cell Microbiol* 21: e12981
- Lotteau V, Teyton L, Peleraux A, Nilsson T, Karlsson L, Schmid SL, Quaranta V, Peterson PA (1990) Intracellular transport of class II MHC molecules directed by invariant chain. *Nature* 348: 600–605
- Lynes EM, Raturi A, Shenkman M, Ortiz Sandoval C, Yap MC, Wu J, Janowicz A, Myhill N, Benson MD, Campbell RE et al (2013) Palmitoylation is the switch that assigns calnexin to quality control or ER Ca<sup>2+</sup> signaling. *J Cell Sci* 126: 3893–3903
- Malnati MS, Marti M, LaVaute T, Jaraquemada D, Biddison W, DeMars R, Long EO (1992) Processing pathways for presentation of cytosolic antigen to MHC class II-restricted T cells. *Nature* 357: 702–704
- Manoury B, Mazzeo D, Li DN, Billson J, Loak K, Benaroch P, Watts C (2003) Asparagine endopeptidase can initiate the removal of the MHC class II invariant chain chaperone. *Immunity* 18: 489–498
- Marcu A, Bichmann L, Kuchenbecker L, Kowalewski DJ, Freudenmann LK, Backert L, Mühlenbruch L, Szolek A, Lübke M, Wagner P et al (2021) HLA Ligand Atlas: a benign reference of HLA-presented peptides to improve T-cell-based cancer immunotherapy. *J Immunother Cancer* 9: e002071
- Margiotta A, Frei DM, Sendstad IH, Janssen L, Neefjes J, Bakke O (2020) Invariant chain regulates endosomal fusion and maturation through an interaction with the SNARE Vti1b. *J Cell Sci* 133: jcs244624
- Mellacheruvu D, Wright Z, Couzens AL, Lambert JP, St-Denis NA, Li T, Miteva YV, Hauri S, Sardi ME, Low TY et al (2013) The CRAPome: a contaminant repository for affinity purification-mass spectrometry data. *Nat Methods* 10: 730–736
- Mildenberger J, Johansson I, Sergin I, Kjobli E, Damas JK, Razani B, Flo TH, Bjorkoy G (2017) N-3 PUFAs induce inflammatory tolerance by formation of KEAP1-containing SQSTM1/p62-bodies and activation of NFE2L2. *Autophagy* 13: 1664–1678
- Miller MA, Ganesan AP, Luckashenak N, Mendonca M, Eisenlohr LC (2015) Endogenous antigen processing drives the primary CD4<sup>+</sup> T cell response to influenza. *Nat Med* 21: 1216–1222
- Moris A, Pajot A, Blanchet F, Guivel-Benhassine F, Salcedo M, Schwartz O (2006) Dendritic cells and HIV-specific CD4<sup>+</sup> T cells: HIV antigen presentation, T-cell activation, and viral transfer. *Blood* 108: 1643–1651

- Morris P, Shaman J, Attaya M, Amaya M, Goodman S, Bergman C, Monaco JJ, Mellins E (1994) An essential role for HLA-DM in antigen presentation by class II major histocompatibility molecules. *Nature* 368: 551–554
- Morriswood B, Ryzhakov G, Puri C, Arden SD, Roberts R, Dendrou C, Kendrick-Jones J, Buss F (2007) T6BP and NDP52 are myosin VI binding partners with potential roles in cytokine signalling and cell adhesion. *J Cell Sci* 120: 2574–2585
- Mukherjee P, Dani A, Bhatia S, Singh N, Rudensky AY, George A, Bal V, Mayor S, Rath S (2001) Efficient presentation of both cytosolic and endogenous transmembrane protein antigens on MHC class II is dependent on cytoplasmic proteolysis. *J Immunol* 167: 2632–2641
- Muntasell A, Carrascal M, Alvarez I, Serradell L, van Veelen P, Verreck FA, Koning F, Abian J, Jaraquemada D (2004) Dissection of the HLA-DR4 peptide repertoire in endocrine epithelial cells: strong influence of invariant chain and HLA-DM expression on the nature of ligands. *J Immunol* 173: 1085–1093
- Muntasell A, Carrascal M, Serradell L, Veelen Pv P, Verreck F, Koning F, Raposo G, Abián J, Jaraquemada D (2002) HLA-DR4 molecules in neuroendocrine epithelial cells associate to a heterogeneous repertoire of cytoplasmic and surface self peptides. *J Immunol* 169: 5052–5060
- Myhill N, Lynes EM, Nanji JA, Blagoveshchenskaya AD, Fei H, Carmine Simmen K, Cooper TJ, Thomas G, Simmen T (2008) The subcellular distribution of calnexin is mediated by PACS-2. *Mol Biol Cell* 19: 2777–2788
- Nakagawa T, Roth W, Wong P, Nelson A, Farr A, Deussing J, Villadangos JA, Ploegh H, Peters C, Rudensky AY (1998) Cathepsin L: critical role in li degradation and CD4 T cell selection in the thymus. *Science* 280: 450–453
- Neeffjes J, Jongsma MML, Berlin I (2017) Stop or Go? Endosome positioning in the establishment of compartment architecture, dynamics, and function. *Trends Cell Biol* 27: 580–594
- Neeffjes JJ, Stollorz V, Peters PJ, Geuze HJ, Ploegh HL (1990) The biosynthetic pathway of MHC class II but not class I molecules intersects the endocytic route. *Cell* 61: 171–183
- Nelde A, Kowalewski DJ, Stevanovic S (2019) Purification and identification of naturally presented MHC class I and II ligands. *Methods Mol Biol* 1988: 123–136
- Nuchtern JG, Biddison WE, Klausner RD (1990) Class II MHC molecules can use the endogenous pathway of antigen presentation. *Nature* 343: 74–76
- O'Loughlin T, Masters TA, Buss F (2018) The MYO6 interactome reveals adaptor complexes coordinating early endosome and cytoskeletal dynamics. *EMBO Rep* 19: e44884
- Paludan C, Schmid D, Landthaler M, Vockerodt M, Kube D, Tuschl T, Munz C (2005) Endogenous MHC class II processing of a viral nuclear antigen after autophagy. *Science* 307: 593–596
- Pathan M, Keerthikumar S, Ang CS, Gangoda L, Quek CY, Williamson NA, Mouradov D, Sieber OM, Simpson RJ, Salim A et al (2015) FunRich: An open access standalone functional enrichment and interaction network analysis tool. *Proteomics* 15: 2597–2601
- Perez-Riverol Y, Csordas A, Bai J, Bernal-Llinares M, Hewapathirana S, Kundu DJ, Inuganti A, Griss J, Mayer G, Eisenacher M et al (2019) The PRIDE database and related tools and resources in 2019: improving support for quantification data. *Nucleic Acids Res* 47: D442–D450
- Petkova DS, Verlhac P, Rozieres A, Bague J, Claviere M, Kretz-Remy C, Mahieux R, Viret C, Faure M (2017) Distinct contributions of autophagy receptors in measles virus replication. *Viruses* 9: 123
- Pinet V, Vergelli M, Martin R, Bakke O, Long EO (1995) Antigen presentation mediated by recycling of surface HLA-DR molecules. *Nature* 375: 603–606
- Prasad SA, Yewdell JW, Porgador A, Sadasivan B, Cresswell P, Bennink JR (1998) Calnexin expression does not enhance the generation of MHC class I-peptide complexes. *Eur J Immunol* 28: 907–913
- Ramachandra L, Kovats S, Eastman S, Rudensky AY (1996) Variation in HLA-DM expression influences conversion of MHC class II alpha beta: class II-associated invariant chain peptide complexes to mature peptide-bound class II alpha beta dimers in a normal B cell line. *J Immunol* 156: 2196–2204
- Rammensee H, Bachmann J, Emmerich NP, Bachor OA, Stevanovic S (1999) SYFPEITHI: database for MHC ligands and peptide motifs. *Immunogenetics* 50: 213–219
- Randow F, Youle RJ (2014) Self and nonself: how autophagy targets mitochondria and bacteria. *Cell Host Microbe* 15: 403–411
- Reith W, LeibundGut-Landmann S, Waldburger JM (2005) Regulation of MHC class II gene expression by the class II transactivator. *Nat Rev Immunol* 5: 793–806
- Reynisson B, Barra C, Kaabinejadian S, Hildebrand WH, Peters B, Nielsen M (2020) Improved prediction of MHC II antigen presentation through integration and motif deconvolution of mass spectrometry MHC eluted ligand data. *J Proteome Res* 19: 2304–2315
- Richter B, Sliker DA, Herhaus L, Stolz A, Wang C, Beli P, Zaffagnini G, Wild P, Martens S, Wagner SA et al (2016) Phosphorylation of OPTN by TBK1 enhances its binding to Ub chains and promotes selective autophagy of damaged mitochondria. *Proc Natl Acad Sci U S A* 113: 4039–4044
- Riese RJ, Wolf PR, Bromme D, Natkin LR, Villadangos JA, Ploegh HL, Chapman HA (1996) Essential role for cathepsin S in MHC class II-associated invariant chain processing and peptide loading. *Immunity* 4: 357–366
- Roche PA, Cresswell P (1991) Proteolysis of the class II-associated invariant chain generates a peptide binding site in intracellular HLA-DR molecules. *Proc Natl Acad Sci U S A* 88: 3150–3154
- Roche PA, Furuta K (2015) The ins and outs of MHC class II-mediated antigen processing and presentation. *Nat Rev Immunol* 15: 203–216
- Roche PA, Marks MS, Cresswell P (1991) Formation of a nine-subunit complex by HLA class II glycoproteins and the invariant chain. *Nature* 354: 392–394
- Romagnoli P, Germain RN (1995) Inhibition of invariant chain (II)-calnexin interaction results in enhanced degradation of li but does not prevent the assembly of alpha beta II complexes. *J Exp Med* 182: 2027–2036
- Romagnoli P, Layet C, Yewdell J, Bakke O, Germain RN (1993) Relationship between invariant chain expression and major histocompatibility complex class II transport into early and late endocytic compartments. *J Exp Med* 177: 583–596
- Rudensky A, Preston-Hurlburt P, Hong SC, Barlow A, Janeway CA Jr (1991) Sequence analysis of peptides bound to MHC class II molecules. *Nature* 353: 622–627
- Rudensky AY, Yurin VL (1989) Immunoglobulin-specific T-B cell interaction. I. Presentation of self immunoglobulin determinants by B lymphocytes. *Eur J Immunol* 19: 1677–1683
- Sahlender DA, Roberts RC, Arden SD, Spudich G, Taylor MJ, Luzio JP, Kendrick-Jones J, Buss F (2005) Optineurin links myosin VI to the Golgi complex and is involved in Golgi organization and exocytosis. *J Cell Biol* 169: 285–295
- Sanderson F, Kleijmeer MJ, Kelly A, Verwoerd D, Tulp A, Neeffjes JJ, Geuze HJ, Trowsdale J (1994) Accumulation of HLA-DM, a regulator of antigen presentation, in MHC class II compartments. *Science* 266: 1566–1569
- Schmid D, Pypaert M, Munz C (2007) Antigen-loading compartments for major histocompatibility complex class II molecules continuously receive input from autophagosomes. *Immunity* 26: 79–92



- Schröder B (2016) The multifaceted roles of the invariant chain CD74—more than just a chaperone. *Biochim Biophys Acta* 1863: 1269–1281
- Schuster C, Gerold KD, Schober K, Probst L, Boerner K, Kim MJ, Ruckdeschel A, Serwold T, Kissler S (2015) The autoimmunity-associated gene CLEC16A modulates thymic epithelial cell autophagy and alters T cell selection. *Immunity* 42: 942–952
- Scott JE, Dawson JR (1995) MHC class I expression and transport in a calnexin-deficient cell line. *J Immunol* 155: 143–148
- Sekaly RP, Jacobson S, Richert JR, Tonnelle C, McFarland HF, Long EO (1988) Antigen presentation to HLA class II-restricted measles virus-specific T-cell clones can occur in the absence of the invariant chain. *Proc Natl Acad Sci U S A* 85: 1209–1212
- Shembade N, Harhaj NS, Parvatiyar K, Copeland NG, Jenkins NA, Matesic LE, Harhaj EW (2008) The E3 ligase Itch negatively regulates inflammatory signaling pathways by controlling the function of the ubiquitin-editing enzyme A20. *Nat Immunol* 9: 254–262
- Shembade N, Ma A, Harhaj EW (2010) Inhibition of NF-kappaB signaling by A20 through disruption of ubiquitin enzyme complexes. *Science* 327: 1135–1139
- Shi GP, Bryant RA, Riese R, Verhelst S, Driessen C, Li Z, Bromme D, Ploegh HL, Chapman HA (2000) Role for cathepsin F in invariant chain processing and major histocompatibility complex class II peptide loading by macrophages. *J Exp Med* 191: 1177–1186
- Shin JS, Ebersold M, Pypaert M, Delamarre L, Hartley A, Mellman I (2006) Surface expression of MHC class II in dendritic cells is controlled by regulated ubiquitination. *Nature* 444: 115–118
- Sinnathamby G, Eisenlohr LC (2003) Presentation by recycling MHC class II molecules of an influenza hemagglutinin-derived epitope that is revealed in the early endosome by acidification. *J Immunol* 170: 3504–3513
- Tewari MK, Sinnathamby G, Rajagopal D, Eisenlohr LC (2005) A cytosolic pathway for MHC class II-restricted antigen processing that is proteasome and TAP dependent. *Nat Immunol* 6: 287–294
- Thibodeau J, Moulefera MA, Balthazard R (2019) On the structure-function of MHC class II molecules and how single amino acid polymorphisms could alter intracellular trafficking. *Hum Immunol* 80: 15–31
- Thiele F, Tao S, Zhang Y, Muschaweckh A, Zollmann T, Protzer U, Abele R, Drexler I (2015) Modified vaccinia virus Ankara-infected dendritic cells present CD4<sup>+</sup> T-cell epitopes by endogenous major histocompatibility complex class II presentation pathways. *J Virol* 89: 2698–2709
- Thurston TL, Ryzhakov G, Bloor S, von Muhlinen N, Randow F (2009) The TBK1 adaptor and autophagy receptor NDP52 restricts the proliferation of ubiquitin-coated bacteria. *Nat Immunol* 10: 1215–1221
- Tsuji T, Matsuzaki J, Caballero OL, Jungbluth AA, Ritter G, Odunsi K, Old LJ, Gnjjatic S (2012) Heat shock protein 90-mediated peptide-selective presentation of cytosolic tumor antigen for direct recognition of tumors by CD4(+) T cells. *J Immunol* 188: 3851–3858
- Tumbarello DA, Manna PT, Allen M, Bycroft M, Arden SD, Kendrick-Jones J, Buss F (2015) The autophagy receptor TAX1BP1 and the molecular motor myosin VI are required for clearance of salmonella typhimurium by autophagy. *PLoS Pathog* 11: e1005174
- Tumbarello DA, Waxse BJ, Arden SD, Bright NA, Kendrick-Jones J, Buss F (2012) Autophagy receptors link myosin VI to autophagosomes to mediate Tom1-dependent autophagosome maturation and fusion with the lysosome. *Nat Cell Biol* 14: 1024–1035
- Tyanova S, Temu T, Sinitcyn P, Carlson A, Hein MY, Geiger T, Mann M, Cox J (2016) The Perseus computational platform for comprehensive analysis of (prote)omics data. *Nat Methods* 13: 731–740
- Unanue ER, Turk V, Neeffjes J (2016) Variations in MHC class II antigen processing and presentation in health and disease. *Annu Rev Immunol* 34: 265–297
- Vassilakos A, Cohen-Doyle MF, Peterson PA, Jackson MR, Williams DB (1996) The molecular chaperone calnexin facilitates folding and assembly of class I histocompatibility molecules. *EMBO J* 15: 1495–1506
- Veerappan Ganesan AP, Eisenlohr LC (2017) The elucidation of non-classical MHC class II antigen processing through the study of viral antigens. *Curr Opin Virol* 22: 71–76
- Verlhac P, Gregoire IP, Azocar O, Petkova DS, Baguet J, Viret C, Faure M (2015) Autophagy receptor NDP52 regulates pathogen-containing autophagosome maturation. *Cell Host Microbe* 17: 515–525
- Walseng E, Furuta K, Bosch B, Weih KA, Matsuki Y, Bakke O, Ishido S, Roche PA (2010) Ubiquitination regulates MHC class II-peptide complex retention and degradation in dendritic cells. *Proc Natl Acad Sci U S A* 107: 20465–20470
- Watts C (2004) The exogenous pathway for antigen presentation on major histocompatibility complex class II and CD1 molecules. *Nat Immunol* 5: 685–692
- Weil R, Laplantine E, Curic S, Génin P (2018) Role of optineurin in the mitochondrial dysfunction: potential implications in neurodegenerative diseases and cancer. *Front Immunol* 9: 1243
- Weiss S, Bogen B (1989) B-lymphoma cells process and present their endogenous immunoglobulin to major histocompatibility complex-restricted T cells. *Proc Natl Acad Sci U S A* 86: 282–286
- Wijdeven RH, van Luijn MM, Wierenga-Wolf AF, Akkermans JJ, van den Elsen PJ, Hintzen RQ, Neeffjes J (2018) Chemical and genetic control of IFN-gamma-induced MHCII expression. *EMBO Rep* 19: e45553
- Wild P, Farhan H, McEwan DG, Wagner S, Rogov VV, Brady NR, Richter B, Korac J, Waidmann O, Choudhary C et al (2011) Phosphorylation of the autophagy receptor optineurin restricts Salmonella growth. *Science* 333: 228–233
- Zhou D, Li P, Lin Y, Lott JM, Hislop AD, Canaday DH, Brutkiewicz RR, Blum JS (2005) Lamp-2a facilitates MHC class II presentation of cytoplasmic antigens. *Immunity* 22: 571–581



**License:** This is an open access article under the terms of the [Creative Commons Attribution](https://creativecommons.org/licenses/by/4.0/) License, which permits use, distribution and reproduction in any medium, provided the original work is properly cited.

## Expanded View Figures

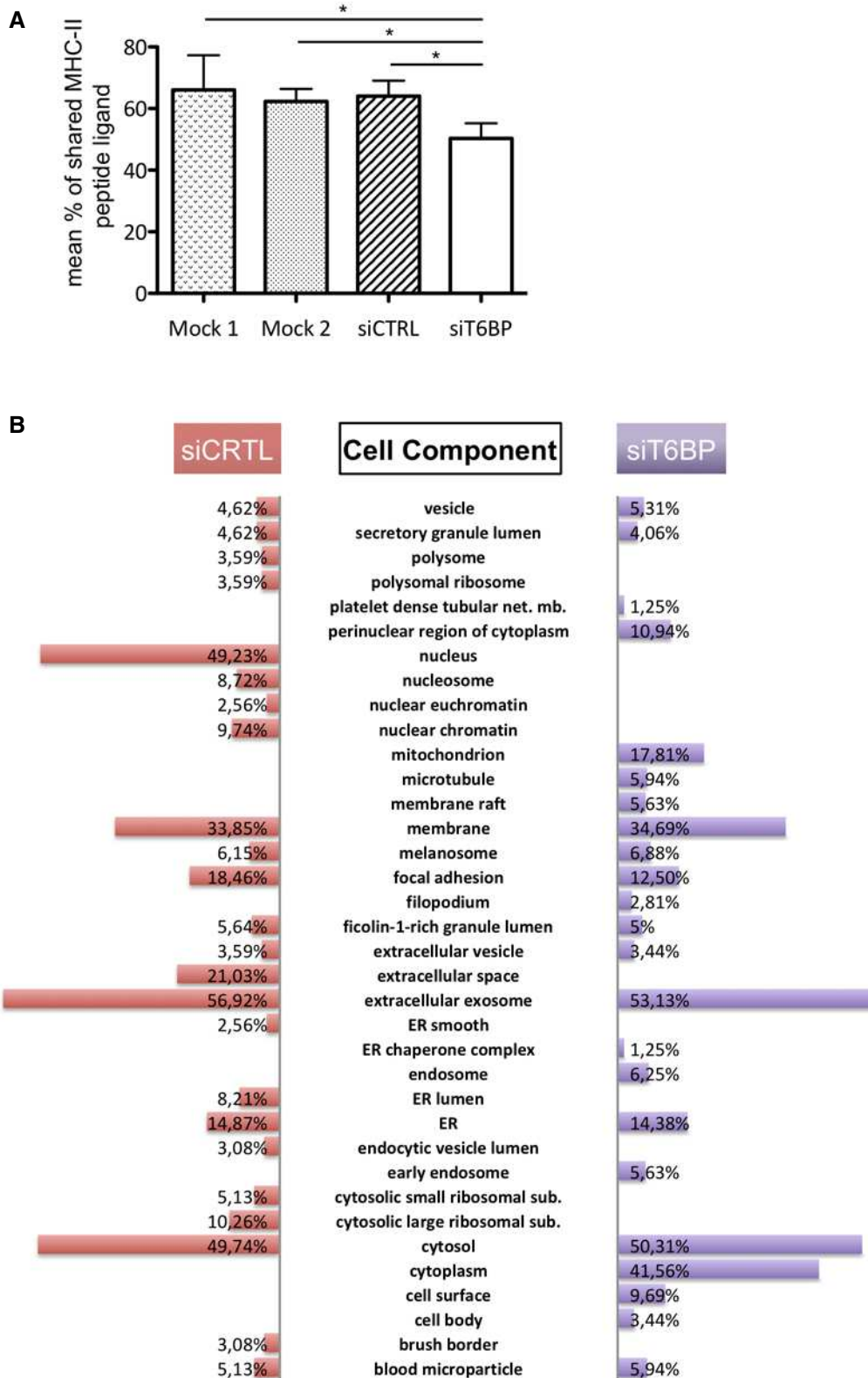
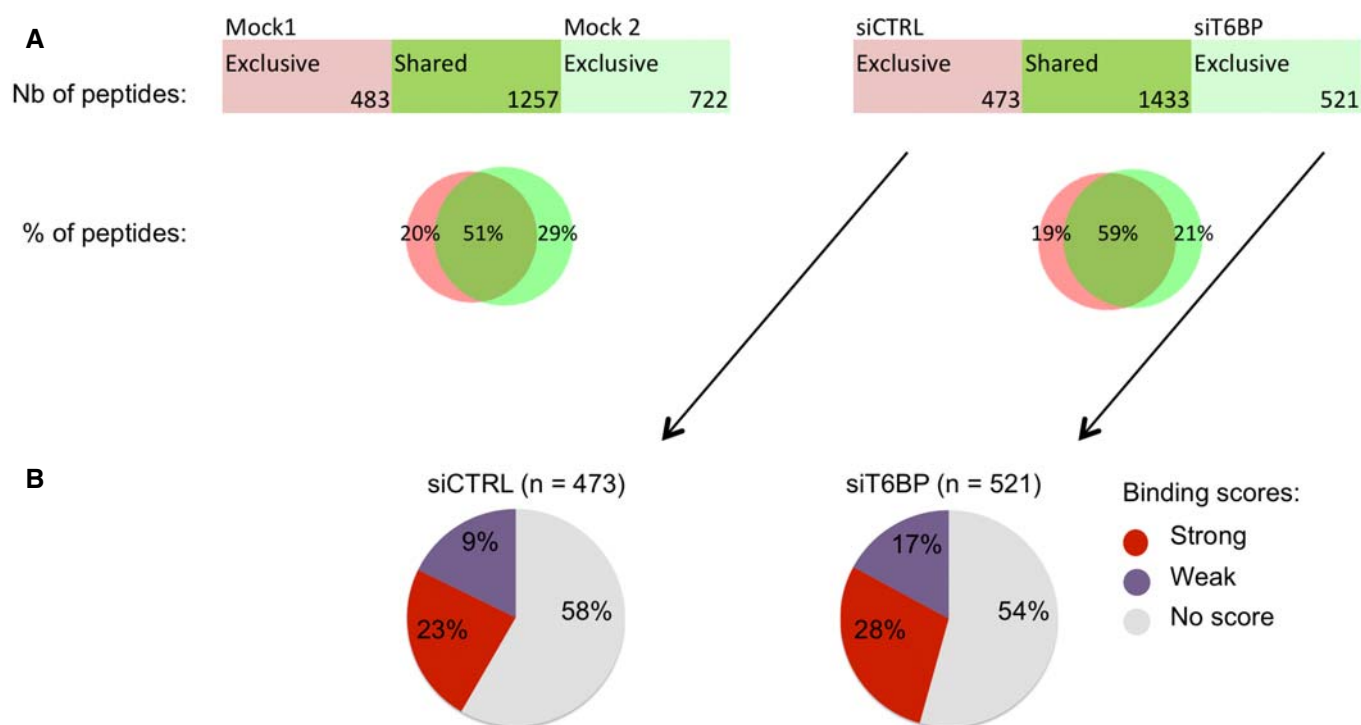


Figure EV1.

**Figure EV1. (Related to Fig 3): T6BP silencing affects the repertoire of peptides presented by MHC-II molecules and has a modest influence on the source of MHC-II ligands.**

- A For each sample the % of MHC-II peptide ligand shared with the 3 other experimental conditions was determined and the mean % of shared MHC-II peptide ligand calculated and plotted ( $\pm$  SD). Comparing the mean % of shared peptides between mock treated cells (Mock1 or Mock2) and the cells transfected with the control (siCTRL) siRNA, no significant differences were observed. By contrast, the mean % of shared MHC-II peptide ligand was significantly different between siT6BP-treated cells and Mock1-, Mock2-, and siCTRL-treated cells. The statistical significance was calculated using a Kruskal–Wallis test followed by a Dunn's test ( $*P < 0.05$ ).
- B Cell component enrichment analysis of peptide sources. As in Fig 3, HeLa-CIITA cells were transfected with siCTRL and siT6BP siRNA, lysed, submitted to MHC-II immunoprecipitation using TÛ39 antibody, and the peptide ligands sequenced using mass spectrometry (LC–MS/MS). The diversity of protein sources was analyzed according to cell component enrichment using Funrich software. Only canonical pathways statistically enriched ( $P < 0.05$ ) for each condition (siCTRL and siT6BP) are shown. The  $P$ -value for pathway enrichment was obtained using the right-tailed Fisher's exact test.



**Figure EV2. (Related to Fig 3): T6BP silencing does not influence the immunopeptidome of MHC-I molecules.**

- A Left panel, mock-treated HeLa-CIITA cells were split and cultured for 48 h (giving rise to Mock1 and Mock2), then cells were lysed, MHC-I molecules were immunoprecipitated using W632 antibody and the peptide ligands sequenced using mass spectrometry (LC–MS/MS). Right panel, HeLa-CIITA cells were transfected with siCTRL and siT6BP siRNA and were treated as in the left panel. The number and the percentage among sequenced peptides (Venn diagrams) of exclusive or shared peptides for each condition are presented.
- B Relative binding affinities, presented as pie charts, of exclusive peptides identified in siCTRL (left) and siT6BP (right) condition (number of peptides are indicated in brackets). NetMHCpan 4.0 algorithm was used to predict the relative affinities to HLA-A\*6802 and -B\*15093 molecules expressed by HeLa-CIITA cells. The relative affinities to the HLA-C\*1203 molecule also expressed by HeLa-CIITA cells were not combined in this figure because many peptides binding to HLA-C\*1203 also bind to HLA-A\*6802. The results are presented as stated from NetMHCpan 4.0 analysis as Strong (for strong binders), Weak (for weak binders), and No score (for epitopes with which a binding score cannot be determined).

Data information: One representative experiment is shown out of two biological replicates. For each experiment, 5 technical replicates per sample were run on the LC–MS/MS. Nb—number; %—percentage.

**Figure EV3. (Related to Fig 4). T6BP silencing leads to autophagosome accumulation.**

- A LC3 and T6BP expressions were assessed using confocal microscopy. HeLa-CIITA cells were transfected with siCTRL or siT6BP. 48 h post-treatment, LC3 and T6BP were detected using anti-LC3 and anti-T6BP antibodies, respectively. Scale bars: 2  $\mu\text{m}$ .
- B Quantitative analysis using in-house ImageJ script displaying the number of LC3<sup>+</sup> vesicles per cell and co-localization using Pearson's coefficient of T6BP and LC3 staining (right panel). 30 cells from two biological replicates were analyzed.
- C, D As in A and B with MHC-II molecule and LC3 staining. A number of cells >40 from two biological replicates were analyzed. Scale bars: 2  $\mu\text{m}$ .
- E siRNA-treated cells were also analyzed using electron microscopy. Top panels and bottom panels, images from siCTRL- and siT6BP-treated cells, respectively, from 6 representative cells. Two biological replicates were performed and at least 40 cells for each treatment were analyzed. The white arrows indicate the autophagosomes. Scale bars: 1  $\mu\text{m}$ .
- F As in (A) with HLA-DM and T6BP staining. Scale bars: 4  $\mu\text{m}$ .
- G The localization of HLA-DM<sup>+</sup> vesicles and the number of vesicles/cells were quantified as in Fig 4. At least 10,000 vesicles in at least 40 cells were analyzed.

Data information: In graphs representing the number of vesicles/cell, each dot corresponds to a single cell. Within the violin plots, continuous and dotted lines correspond to medians and quartiles, respectively. CTRL: control; nb: number. Mann-Whitney's test; \* $P < 0.05$ ; \*\*\* $P < 0.0001$ ; ns >0.05. For Pearson's coefficient, the dotted lines (at 0.5) indicate the limit under which no significant co-localization is measured.

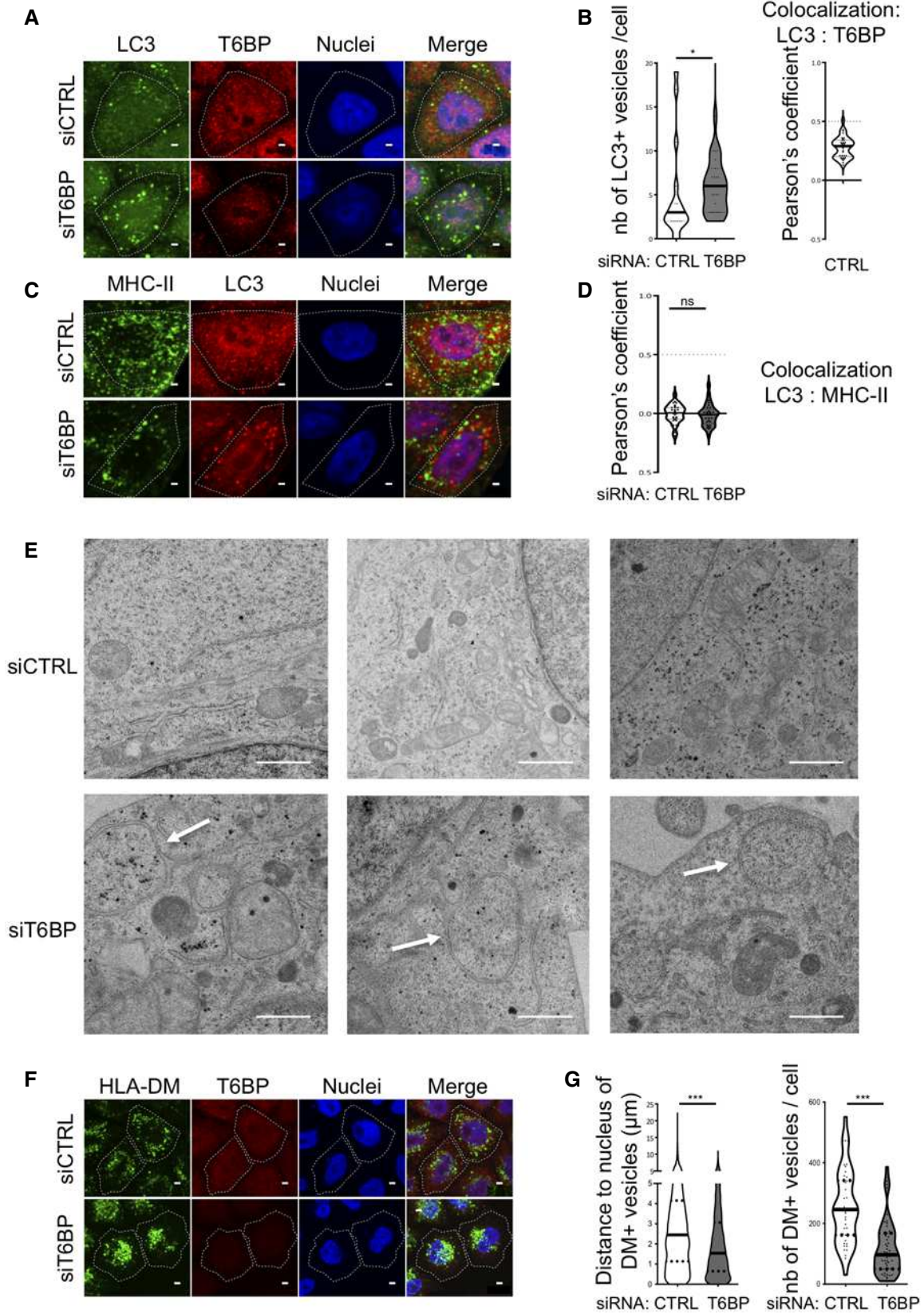
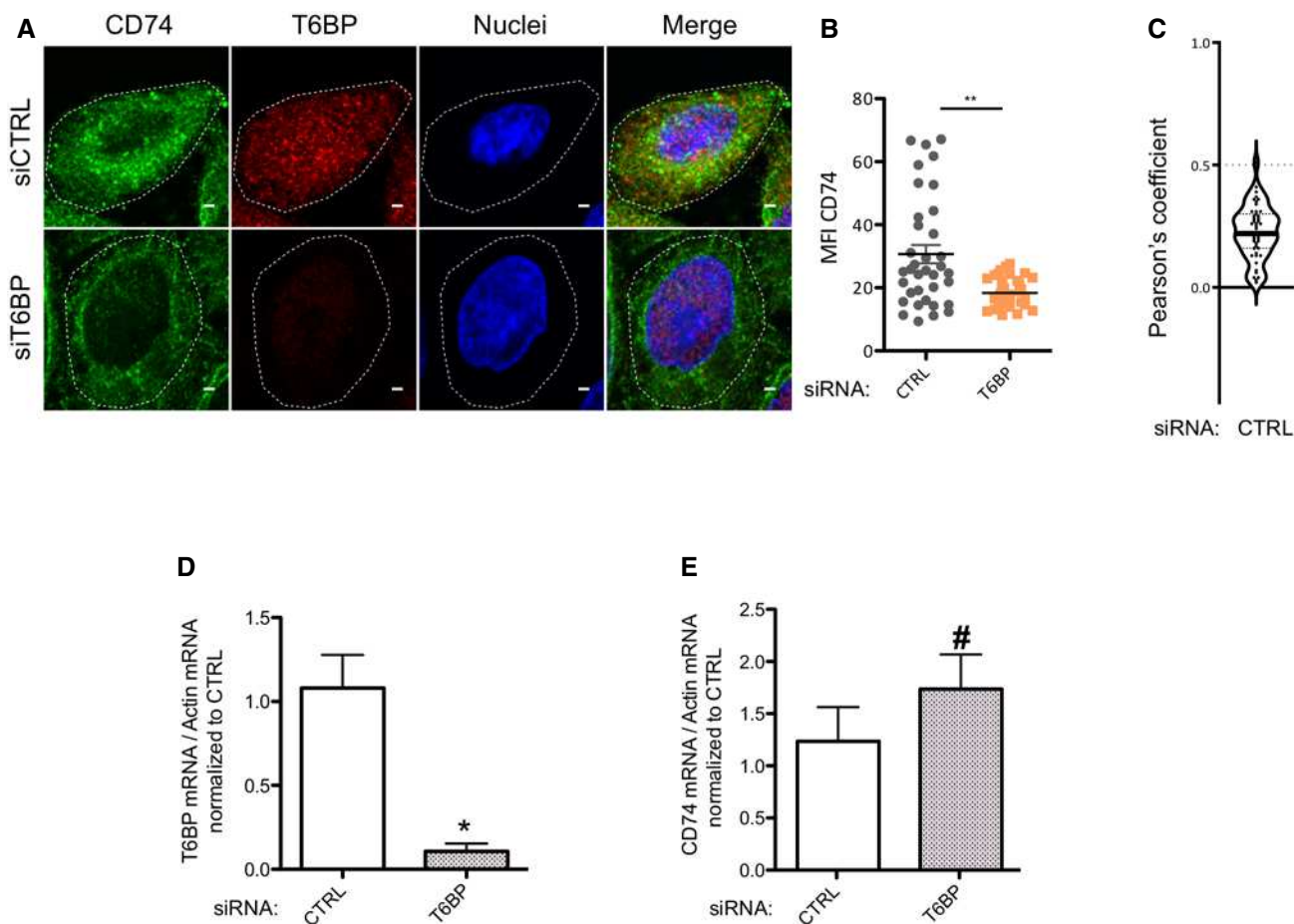


Figure EV3.



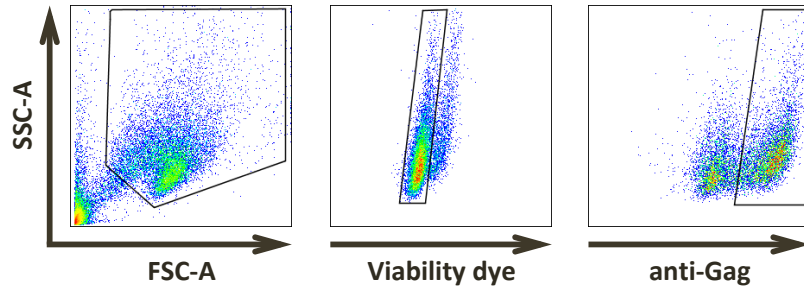
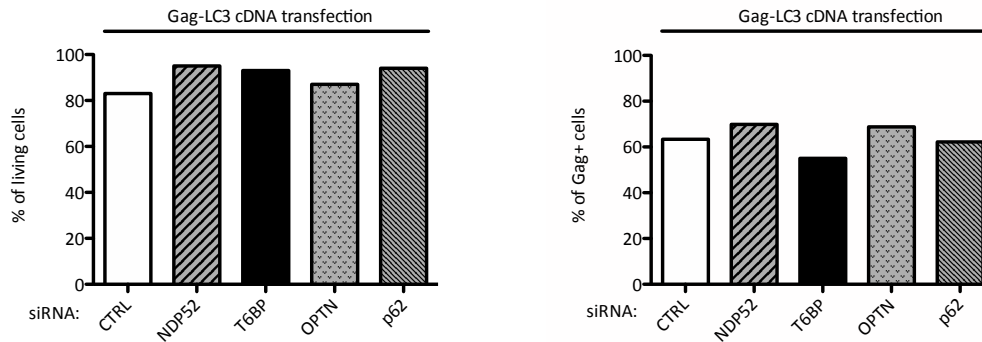
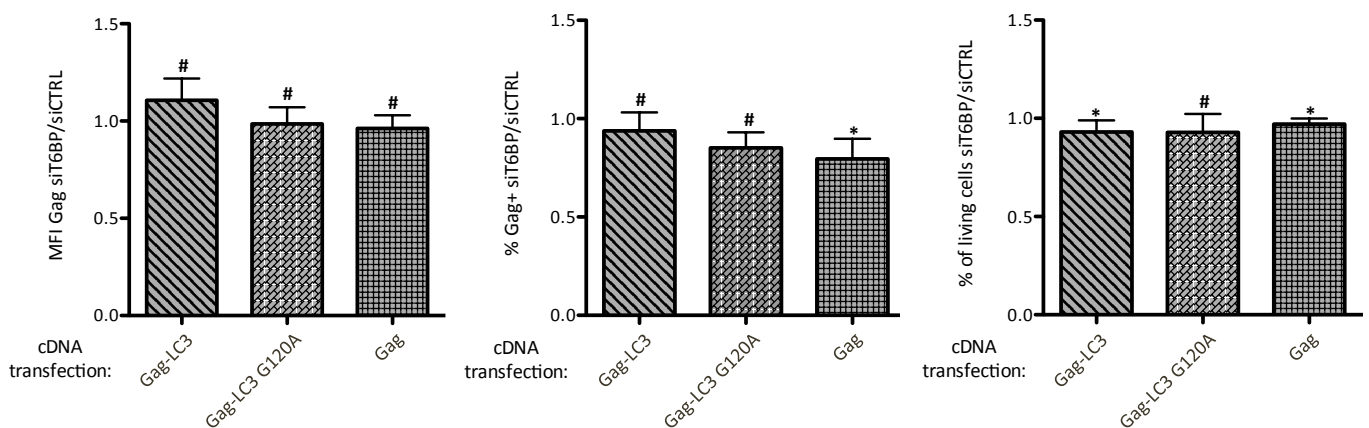
**Figure EV4. (Related to Fig 5): T6BP silencing affects CD74 expression levels as assessed by confocal microscopy but does not affect CD74 mRNA levels.**

- A** CD74 expression assessed using confocal microscopy in HeLa-CIITA cells, 48 h post-treatment with the indicated siRNA. Top panels siCTRL and bottom panels siT6BP. Scale bars: 2  $\mu$ m.
- B** Quantitative analysis using ImageJ of CD74 mean fluorescent intensity (MFI). The data are representative of at least 3 biological replicates. Each dot displayed corresponds to a single cell. At least 75 cells were analyzed. The continuous lines represent the means ( $\pm$  SD). Mann-Whitney's test; \*\* $P < 0.002$ .
- C** Co-localization of CD74 and T6BP assessed, in the control condition, using Pearson's coefficient. Number of cells = 47. Within the violin plots, continuous and dotted lines correspond to medians and quartiles, respectively. The dotted lines at 0.5 indicate the limit under which no significant co-localization is measured.
- D, E** (D) T6BP and (E) CD74 mRNA levels were assessed using RT-qPCR. HeLa-CIITA cells were transfected with siCTRL and siT6BP. 48 h post-treatment, relative T6BP (D) and CD74 (E) mRNA expression levels were analyzed by RT-qPCR using actin as reference gene. Results are presented as the mean ratios of T6BP (D) and CD74 mRNA (E) levels to actin mRNA levels ( $\pm$  SD) from four biological replicates. CTRL—control. Mann-Whitney's test: \* $P < 0.05$ ; # $P > 0.05$ .

## Appendix

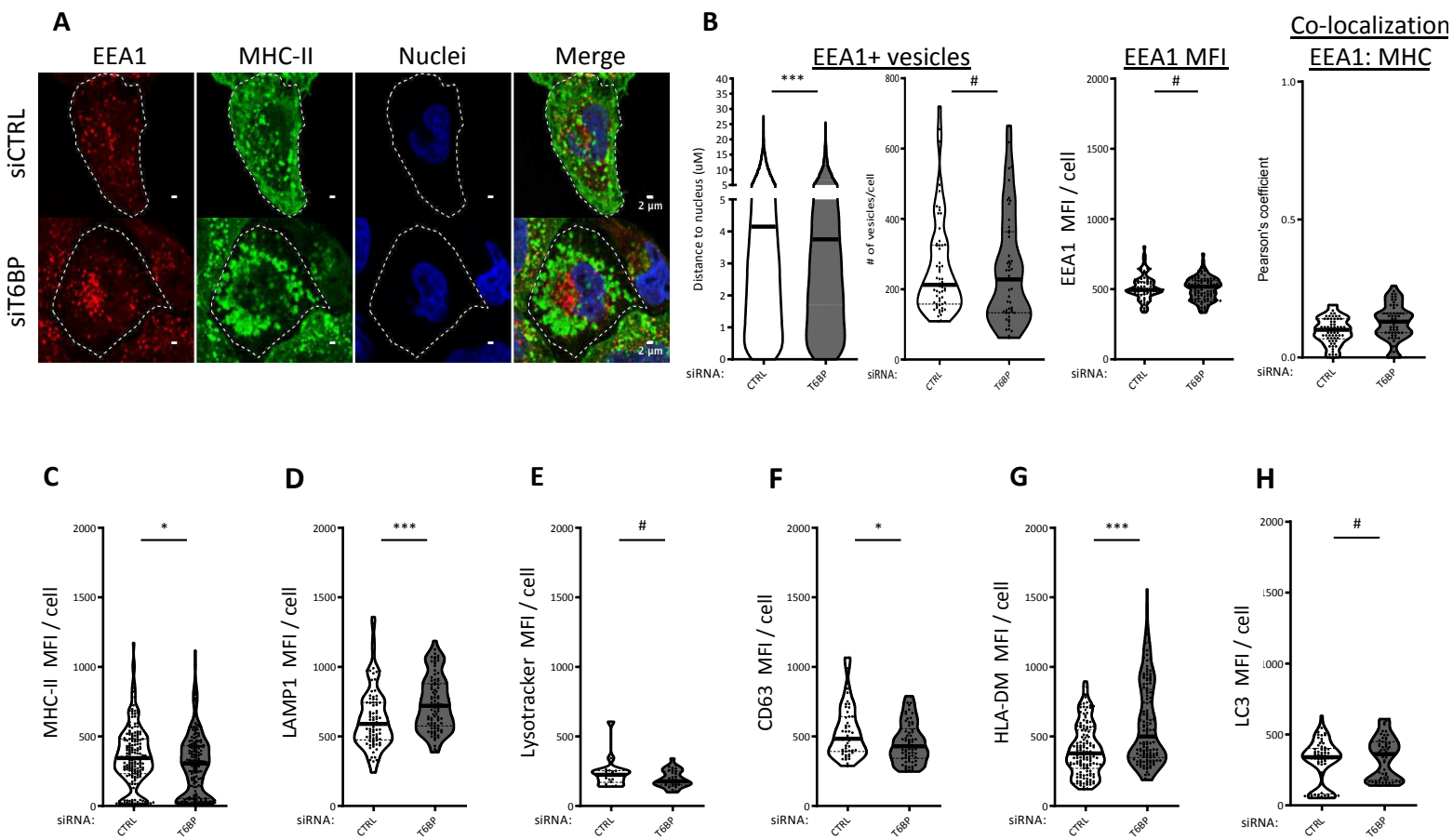
### Table of content:

Appendix Figure-S1 (related to Figure-1)	page-2
Appendix Figure-S2 (related to Figure-4)	page-3
Appendix Figure-S3 (related to Figure-5)	page-4
Appendix Figure-S4 (related to Figure-6)	page-5
Appendix Table S1 (related to EV4)	page-6

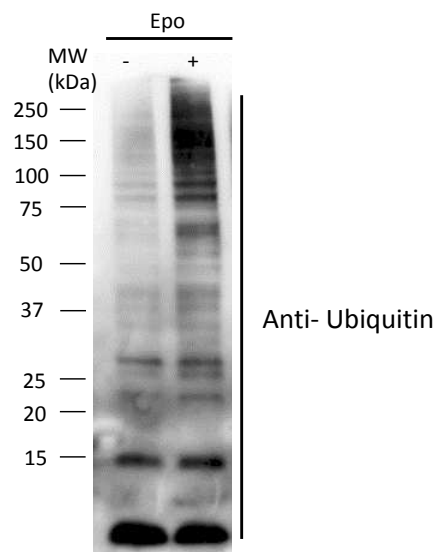
**A****B****C**

**Appendix Figure-S1 (related to Figure-1): The transfection of siRNA targeting autophagy receptors influenced neither the cell viability nor the antigen transfection efficiencies. (A) and (B)** Analysis of cell viability and transfection efficiency using flow cytometry. Results of one representative experiment out of three are shown. **(A)** Gating strategy: left panel: FSC-A: forward-scatter; SSC-A: side-scatter; middle panel: staining of living cells using a viability dye; right panel: staining of Gag<sup>+</sup> cells using anti-Gag antibody intracellular staining. **(B)** Percentage of living and Gag<sup>+</sup> cells in the different siRNA transfection conditions, left and right panel respectively, analyzed 48h post-treatment, prior co-culture with Gag-specific T cells. **(C)** Results of at least three independent experiments are normalized to control conditions and presented as mean (+/- SD). Left panel, ratio of mean fluorescent intensities (MFI) of Gag stainings in Gag<sup>+</sup> cells. Middle panel, ratio of the mean percentage of Gag<sup>+</sup> cells. Right panel, ratio of the mean percentage of living cells. CTRL: control. Mann-Whitney's tests; \*p<0.05; #p>0.05.

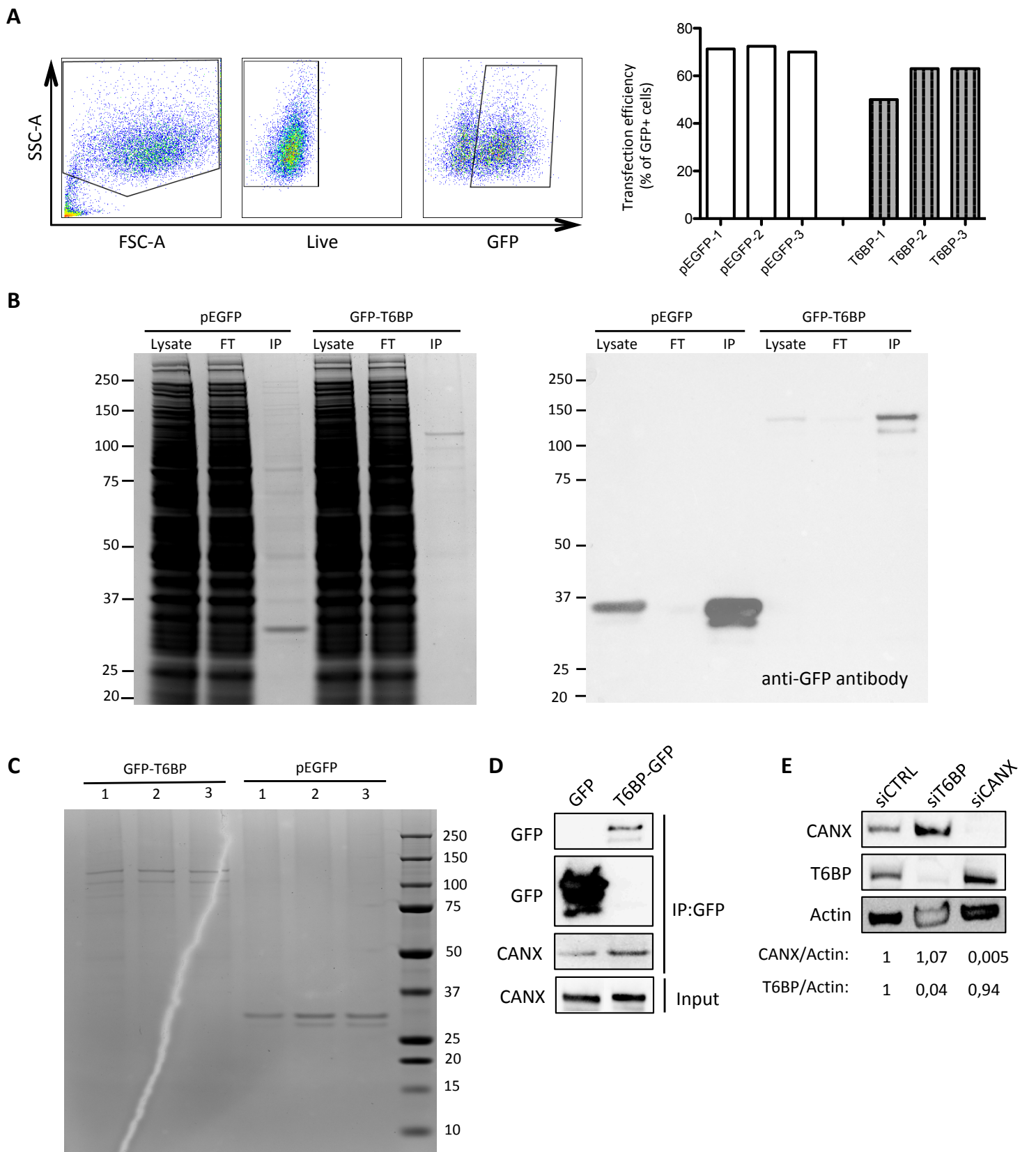




**Appendix Figure S2 (related to Figure-4): T6BP silencing slightly influences EEA1+ vesicle cellular localization (A)** EEA1 expression was assessed using confocal microscopy. HeLa-CIITA cells were transfected with siCTRL and siT6BP. 48h post-treatment, EEA1 were detected using specific antibody and a fluorescent secondary antibody. Nuclei were stained using DAPI. **(B)** Quantitative analysis using in-house ImageJ script displaying distance of each EEA1<sup>+</sup> vesicles to the nucleus, number of EEA1<sup>+</sup> vesicles per cell and EEA1 total MFI per cell. At least 16 000 vesicles from 90 cells corresponding to 3 independent experiments were analyzed. **(B, Right panel) EEA1 and MHC-II stainings do not colocalize.** Quantification of the potential colocalization between MHC-II<sup>+</sup> and EEA1<sup>+</sup> dots using Pearson's coefficient where the dotted lines (at 0.5) indicate the limit under which no significant co-localization is measured. **(C-H) Effect of siT6BP silencing on the expression levels of the various vesicular markers.** As in A, HeLa-CIITA cells were transfected with siCTRL and siT6BP. 48h post-treatment, cells were fixed and labeled and the MFI of the indicated markers were analyzed. **(C)** MHC-II, at least 170 cells corresponding to 5 independent experiments were analyzed. **(D)** LAMP-1, at least 85 cells corresponding to 3 independent experiments were analyzed. **(E)** Lysotracker, at least 30 cells corresponding to 2 independent experiments were analyzed. **(F)** CD63, at least 60 cells corresponding to 2 independent experiments were analyzed. **(G)** HLA-DM, at least 140 cells corresponding to 3 independent experiments were analyzed. **(H)** LC3, at least 60 cells corresponding to 2 independent experiments were analyzed. In graphs representing the number of vesicles or the MFI per cell, each dot displayed corresponds to a single cell. Scale bars, 2 $\mu$ m. CTRL: control. Mann-Whitney's tests; \*: p<0.05; \*\*: p<0.002; \*\*\*: p<0.0003; #: p>0.05.



**Appendix Figure-S3 (related to Figure-5D): Quality control of the proteasome inhibitor Epoxomicin (Epo) treatment.** HeLa-CIITA cells were treated with Epoxomicin (+) or mock treated (-) for 16h and total ubiquitin levels assessed using Western Blot. The membrane was blotted using an anti-ubiquitin antibody. MW: molecular weight markers.



**Appendix Fig S4 (related to Figure-6): Quality controls of T6BP interactome definition. (A)** Left panels, gating strategy for the analysis of GFP<sup>+</sup> cells after transfection of cDNA encoding wild-type T6BP fused to GFP using flow cytometry. FSC: forward-scatter; SSC: side-scatter. Right panels, side to side comparison of the percentage of GFP<sup>+</sup> HeLa-CIITA cells transfected with plasmid encoding GFP-T6BP or GFP-only (pEGFP) in the three biological replicates. **(B)** Coomassie blue staining (left panel) and Western Blot analysis (right panel) of the indicated fraction of protein samples from GFP-T6BP and GFP expressing cells. Results from one of the three biological replicates are shown. Briefly, cells were lysed and submitted to IP using anti-GFP camel antibodies (GFP-Trap from Chromotek). Right panel, GFP and GFP-T6BP were revealed using anti-GFP antibody. FT = Flow through. IP = Immunoprecipitation. **(C)** Coomassie blue staining of immunoprecipitated proteins (1/10 of the sample volume) used for LC-MS/MS analysis (9/10 of the sample volume) of the three biological replicates for both GFP-T6BP and GFP. Due to a mishandling, a crack was unfortunately introduced to the gel when scanning **(D)** GFP nanobody immunoprecipitates from HeLa-CIITA cells transfected with GFP and T6BP-GFP. 48h post-transfection, IP (IP:GFP) and the total lysate (input) samples were analyzed by Western blot with the indicated antibodies. Input and FT of GFP or T6BP-GFP IP are presented in panel B. **(E)** Silencing of T6BP expression does not influence calnexin (CANX) expression levels. HeLa-CIITA cells transfected with the indicated siRNAs and samples analyzed, 48h post transfection, by Western blot with the indicated antibodies. The ratio of CANX or T6BP expression to actin was quantified using Image J and set at 1 for the control condition.

**Appendix Table S1 (related to EV4)**

Primers and Probes	Sequence
CD74_S	gAATgCCACCAAgTATggCAA
CD74_R	gggggTCAgCATTCTggA
CD74_P TM	6FAM-CAggTgCATCACATggTCCTCTgT--BBQ
TAX1BP1_L	ggAgTCTTTCCACTggATTAC
TAX1BP1_R	ggCCACATTTTgAAAgATgACA
TAX1BP1_P	6FAM-CCATTgCAgACTTCCAACCTTgCC--BBQ
ACTIN_F	AgCCTCgCCTTTgCCgA
ACTIN_R	CTggTgCCTggggCg
ACTIN_TM	6FAM-CCgCCgCCCgTCCACACCCgCC--BBQ

**Reverse transcription quantitative Polymerase Chain Reaction (RT-qPCR) primers:** The primers and probes used for quantitation of CD74, T6BP and actin were designed by Olfert Landt and purchased from TIB MolBiol. Sequences are listed in the table below. The RT-qPCRs were performed in a Light Cycler 1.5 instrument in capillaries using a final volume of 20 µl. The reactions were performed using 300 nM specific sense primer, 300 nM specific antisense primer, 200 nM specific TaqMan probe (TM) and the LightCycler® Multiplex RNAVirus Master mix (ROCHE). The programs were: reverse-transcription 55°C for 10min, initial denaturation 95°C for 5min followed by 45 cycles of amplification. For CD74 and T6BP cycles were: 95°C for 5s, 60°C for 15s + fluorescence measurement and 72°C for 5s. For actin cycles were: 95°C for 20s, 67°C for 30s + fluorescence measurement and 72°C for 5s.

## Project 2: unpublished article

In the second part of my thesis, the aim was to assess whether viruses could target SARs to escape MHC-II antigen presentation and antiviral immunity.

I used HTLV-1 Tax oncoprotein, known to recruit TAX1BP1, OPTN and p62 to a cytosolic Signalosome to sustain NF- $\kappa$ B activation<sup>482,489</sup> as a tool to study the recruitment and relocalization of SARs. After confirmation of SAR recruitment by Tax in our model HeLa-CIITA cells, I assessed the influence of Tax on MHC-II-restricted viral antigen presentation. Remarkably, Tax expression induces a decrease in MHC-II viral antigen presentation and CD4<sup>+</sup>T cell activation. I then evaluated MHC-II expression levels and found no significant effect of Tax expression on immature MHC-II molecules and a slight increase in mature MHC-II molecules, respectively. To extend the observation made with a single viral antigen, we then analyzed the influence of Tax expression on the global MHC-II immunopeptidome. We showed that Tax expression influences the peptide repertoire and the relative abundance of one out of five epitopes. In contrast, Tax expression did not influence the affinity of core epitopes to MHC-II molecules. We then asked whether Tax might affect intracellular trafficking of MHC-II molecules and the MIIC before MHC-II-peptide complexes reach the plasma membrane. Using confocal microscopy analysis, we evaluated, in HeLa-CIITA cells, the effect of Tax expression on different MIIC and endo-lysosomal markers, including HLA-DM, Lamp-1 and CD63. Strikingly, we observed that Tax expression induces a relocalization of the different markers towards the nuclei of the cells and seems to induce a more important co-localization of MHC-II positive vesicles with acidified Lamp-1 positive vesicles. These results suggest that Tax influences the trafficking of acidified compartments and might affect the maturation of the MIIC.

We then decided to study the functional consequences of the effect of Tax expression on the MIIC. HLA-DM is essential for CLIP removal and ensures quality control of peptide loading on MHC-molecules<sup>257</sup>. We observed no effect on HLA-DM expression levels upon Tax expression. In addition, Tax expression did not influence li expression levels. Remarkably, by monitoring cathepsin activity with a fluorescent probe, we observed higher activities for cathepsins B, L and S, involved in li and antigen processing, in cells expressing Tax. These results suggest that Tax influences the pH of the MIIC and other acidified vesicles.

Finally, to assess whether the recruitment of SARs by Tax influenced Tax inhibition of MHC-II-restricted antigen presentation, I performed a siRNA screen targeting the expressions of TAX1BP1, OPTN and p62. I analyzed the effect of SAR silencing coupled to Tax expression on MHC-II viral antigen presentation and CD4<sup>+</sup>T cell activation. Remarkably, silencing OPTN abrogated Tax inhibition of MHC-II viral antigen presentation whereas TAX1BP1 and p62 silencing induced a more pronounced inhibition of MHC-II viral antigen presentation. These results suggested that Tax-mediated inhibition of CD4<sup>+</sup>T cell activation is independent of TAX1BP1 and p62 expression but relies on OPTN expression. To characterize further the potential interactions of Tax with OPTN and their effect on inhibiting antigen presentation, I made use of well-characterized mutants of Tax. Tax contains 10 lysine (K) residues (K1 to K10) of which K4 through K10 are the main targets of both monoubiquitination and polyubiquitination. Polyubiquitin mediates the interaction of Tax with different actors of the NF-κB pathway, including SARs TAX1BP1, p62 and OPTN. I used three ubiquitin mutants of Tax: Tax<sub>K10R</sub>, Tax<sub>K7-8</sub>, and Tax<sub>K4-8</sub> in which lysines have been replaced by arginines and can no longer bind mono- or polyubiquitin. Of the three mutants, Tax<sub>K7-8</sub> is the only one that is still partially ubiquitinated and can induce the Signalosome and recruit NEMO and OPTN to modulate NF-κB. Remarkably, Tax<sub>K10R</sub> and Tax<sub>K4-8</sub> no longer inhibited CD4<sup>+</sup>T cell activation. In contrast, mutating K7-8 did not abrogate Tax inhibition of CD4<sup>+</sup>T cell activation. Altogether, these results strongly suggest that Tax interacts with OPTN through lysines 4 to 6 and these seem to be required for Tax to act on MHC-II antigen presentation and CD4<sup>+</sup>T cell activation

## Unpublished results

### **HTLV-1 Tax protein inhibits MHC-II-restricted antigen presentation in an Optineurin-dependent mechanism.**

Gabriela Sarango<sup>1</sup>, Clémence Richetta<sup>2,3</sup>, Annika Nelde<sup>4</sup>, Bertha Cecilia Ramirez<sup>1</sup>, Anita Kumari<sup>1</sup>, Hélène Dutartre<sup>5</sup>, Hans-Georg Rammensee<sup>4</sup>, Juliane Walz<sup>4</sup>, Bénédicte Manoury<sup>6</sup>, Chloé Journo<sup>5</sup> and Arnaud Moris<sup>1,2</sup>.

<sup>1</sup>Institute for Integrative Biology of the Cell (I2BC), Université Paris-Saclay, CEA, CNRS, Gif-sur-Yvette, France.

<sup>2</sup>Sorbonne Université, INSERM, CNRS, Center for Immunology and Microbial Infections (CIMI-Paris), Paris, France.

<sup>3</sup>LBPA, ENS-Paris Saclay, CNRS UMR8113, Université Paris Saclay, Gif-sur-Yvette, France.

<sup>4</sup>Department of Immunology, Institute for Cell Biology, University of Tübingen, Tübingen, Germany.

<sup>5</sup>Centre International de Recherche en Infectiologie, équipe d'Oncogenèse Rétrovirale, INSERM U1111 - Université Claude Bernard Lyon 1, CNRS, UMR5308, Ecole Normale Supérieure de Lyon, Université Lyon, Lyon, France.

<sup>6</sup>Institut Necker Enfants Malades, INSERM U1151-CNRS UMR 8253, Faculté de médecine Necker, Université de Paris, Paris, France.

## **Abstract**

Human T cell leukemia virus type 1 (HTLV-1) retroviral oncoprotein Tax, an etiological factor causing adult T cell leukemia and various neurological pathologies, plays a crucial role in inducing T lymphocyte transformation by modulating the NF- $\kappa$ B signaling pathway. Tax recruits selective autophagy receptors (SARs) TAX1BP1, OPTN and p62 in a ubiquitin-dependent manner to induce a sustained activation of NF- $\kappa$ B. Here, we show a novel role of the highjacking of SAR function by Tax in CD4<sup>+</sup>T cell activation. These cells play a major role in the establishment and maintenance of immunity. We show that Tax induces a decrease of MHC-II endogenous antigen presentation and CD4<sup>+</sup>T cell activation. By studying the immunopeptidome of MHC-II molecules, we show that Tax affects both the quantity and quality of peptides presented. Tax also seems to induce a mislocalization of the MIIC and other lysosomal vesicles, which seems to lead to a heightened cathepsin activity. In addition, we show that Tax-mediated inhibition of CD4<sup>+</sup>T cell activation relies on the interaction of Tax with OPTN and this interaction depends on the ability of Tax to be polyubiquitinated.

**Key Words:** HTLV-1/Tax-1/MHC-II/ CD4<sup>+</sup>T cell activation/Selective Autophagy Receptors/NF- $\kappa$ B/Immunopeptidome/ Virus



## Introduction

Human T cell leukemia virus type 1 (HTLV-1) is the etiological agent of several neurological disorders such as tropical spastic paraparesis (TSP)/HTLV-1-associated myelopathy (HAM)<sup>1</sup>. HTLV-1 is also associated with Adult T cell Leukemia (ATL), a fatal hematopoietic disease due to the transformation of CD4<sup>+</sup>T lymphocytes and inflammatory diseases including associated uveitis, myositis, alveolitis and infective dermatitis<sup>2-5</sup>. Five to ten million people worldwide are estimated to be infected by HTLV-1; endemic regions include southern Japan, the Caribbean, some countries of South America, Sub-Saharan Africa and part of Eastern-Europe<sup>6,7</sup>. Of the estimated infected individuals, 90% are believed to be asymptomatic carriers<sup>8</sup>. Primary infection occurs vertically from mother to child through breastfeeding and horizontally via contaminated blood products or during intimate mucosal contact<sup>9</sup>.

HTLV-1 establishes a chronic infection, suggesting a manipulation of immune responses normally elicited upon primo-infection. The unbalance between viral replication and HTLV-1-specific T cell responses determines disease progression<sup>10</sup>. Strong HTLV-1-specific CD8<sup>+</sup> cytotoxic T cell (CTL) and CD4<sup>+</sup> helper T cell responses are observed in the blood of infected individuals and Tax-specific CTL from patients have been shown to kill Tax-expressing autologous cells *ex vivo*<sup>11-15</sup>. Strikingly, there is no clear correlation between the magnitude of T cell responses and the proviral load<sup>16</sup>, which reflects viral replication; instead the quality of HTLV-1-specific T cell responses seems to be determinant for chronicity and disease outcome. In fact, efficient control of HTLV-1 replication and clinical evolution have been shown to be dependent on the quality of CTL responses<sup>17-19</sup>. In turn, CTL activity in HTLV-1-infected individuals is regulated by a population of CD4<sup>+</sup>FoxP3<sup>+</sup>Tregs, suggesting that the quality of CD4<sup>+</sup>T cell responses might be determinant for HTLV-1-specific CTL responses<sup>20</sup>. CD4<sup>+</sup>T cells are activated by antigen presenting cells (APCs), such as DCs, which dictate the quality of T cell responses via antigen presentation and through co-stimulatory or co-inhibitory signals. Interestingly, productive HTLV-1 infection of myeloid DCs and of monocytes-derived DCs (MDDCs) has been shown *in vitro* and proviral DNA has been reported in blood DCs from infected individuals<sup>21-24</sup>. Therefore, it is believed that DCs might be the first targeted cells upon primo-infection, prior to viral amplification and dissemination to T cells<sup>24,25</sup>, but little is known about the capacity of HTLV-1-infected DCs to prime efficient T cell responses. Several studies have shown that infected DCs and DCs from healthy individuals exposed to HTLV-1 *in vitro* abnormally influence CD4<sup>+</sup>T cell activation. In addition, MDDC in ATL patients show phenotypic and functional alterations with a lower expression of maturation markers<sup>22,26</sup>. Both DC exposure to HTLV-1 and DC infection seem to influence their capacity to stimulate T cells<sup>22,23</sup>. The antigen presentation pathways leading to the activation of HTLV-1-specific T cells have not been studied exhaustively<sup>10</sup>.

CD4<sup>+</sup>T cells recognize antigenic peptides presented by the major histocompatibility complex class II (MHC-II) molecules. The MHC-II is expressed at the surface of professional APCs, which include DCs, B cells, macrophages, thymic epithelial cells (TEC); and nonprofessional APCs in inflammatory conditions<sup>27,28</sup>. MHC-II molecules present peptides derived from extra- and intracellular sources of antigens, so-called exogenous and endogenous presentation, respectively<sup>29,30</sup>. Extracellular antigens are captured and internalized into APCs by various

means including macropinocytosis, phagocytosis, or receptor-mediated endocytosis<sup>27</sup>. The endogenous pathway relies on protein antigen synthesis by virus-infected<sup>31–36</sup> or tumor cells<sup>37</sup>. The MHC-II transactivator, CIITA, governs the transcription of the MHC-II locus that includes genes encoding for the MHC-II  $\alpha$  and  $\beta$  chains, the invariant chain li and chaperones HLA-DM/HLA-DO<sup>38</sup>. The transmembrane  $\alpha$  and  $\beta$  chains assemble in the endoplasmic reticulum (ER), where they associate with li leading to the formation of nonameric MHC $\alpha\beta$ -li complexes that traffic into late endo-lysosomal compartments named MIIC<sup>39–42</sup>. In the MIIC, li is progressively cleaved by vesicular cathepsins<sup>43–46</sup>, leaving a residual MHC-II-associated li peptide (CLIP) that occupies the peptide binding groove<sup>47–49</sup>. HLA-DM then facilitates the exchange of CLIP fragments with high affinity peptides, ranging from 12 to 25 amino acids<sup>50,51</sup>, generated from pathogen- or tumor-derived antigens<sup>52–54</sup>. MHC-II molecules are then transported to the plasma membrane to expose antigenic peptides to CD4<sup>+</sup>T cells<sup>55</sup>.

The pX region located in the 3' portion of the genome of HTLV-1 encodes regulatory and accessory proteins involved in viral replication and proliferation including the viral transactivator Tax. Tax plays a crucial role in triggering T lymphocyte transformation through different mechanisms including activation of both canonical and non-canonical NF- $\kappa$ B signaling pathways<sup>56–58</sup>. In non-infected cells, inhibitory I $\kappa$ B proteins tightly regulate NF- $\kappa$ B signaling pathway. Transient activation of the NF- $\kappa$ B signaling pathway is highly regulated to prevent inflammation-induced damage or malignancy associated with persistent NF- $\kappa$ B activation. Different stimuli (bacterial lipopolysaccharide (LPS), tumor necrosis factor (TNF)- $\alpha$ , antigen, etc) trigger intracellular signaling cascades that lead to the recruitment of the I $\kappa$ B kinase (IKK) complex by K63-linked and linear M1-linked polyubiquitin on signaling intermediates, such as TRAF6, RIP1 or MALT1<sup>59</sup>. The IKK complex contains two homologous catalytic subunits (IKK $\alpha$  and IKK $\beta$ ) and a regulatory subunit, NF- $\kappa$ B Essential Modulator (NEMO/IKK $\gamma$ ). The interaction of NEMO with K63-linked polyubiquitin is required for NF- $\kappa$ B activation<sup>60–62</sup>. IKK activation promotes the I $\kappa$ B $\alpha$  inhibitor phosphorylation and its subsequent ubiquitination and proteasomal degradation, allowing NF- $\kappa$ B nuclear translocation and target gene transactivation.

Tax has 10 lysine (K) residues (K1 to K10) of which K4 through K10 are the main targets of both monoubiquitination and polyubiquitination<sup>63</sup>. Ubiquitinated Tax localizes in the cytoplasm and in the nucleus. Tax recruits IKK $\gamma$ <sup>64–66</sup> through a direct interaction strengthened by Tax-conjugated K63-polyubiquitin chains<sup>67</sup> which leads to I $\kappa$ B $\alpha$  degradation and NF- $\kappa$ B activation<sup>68</sup>. Tax also induces the synthesis of polyubiquitin chains by different E3 Ubiquitin ligases thus generating a macromolecular cytoplasmic IKK Signalosome based on ubiquitin-dependent interactions. This Signalosome, assembling mainly on lipid rafts<sup>69</sup>, is a cytoplasmic complex associated with the centrosome and the Golgi<sup>70</sup>. Tax-1-binding protein (TAX1BP1), originally discovered in a yeast –two-hybrid experiment<sup>71,72</sup>, is recruited by Tax to the Signalosome and participates in the enhancement of Tax K63-polyubiquitination by Optineurin (OPTN) and in Tax-induced NF- $\kappa$ B activation<sup>73</sup>. In addition, TAX1BP1 recruitment by Tax impairs the assembly of the inhibitory TAX1BP1/A20 complex, necessary for the negative regulation of the NF- $\kappa$ B signaling pathway<sup>74–78</sup>. More recently, Schwob *et al.* demonstrated that p62/SQTM1 (hereafter called p62) is also recruited to the Tax-induced Signalosome through the binding of ubiquitin chains and potentiates NF- $\kappa$ B activation<sup>79</sup>. In DCs, the canonical NF- $\kappa$ B signaling

pathway controls the expression of maturation markers (such as CD80, CD86 and CD83) upon danger sensing through PRR and other immune receptor signaling<sup>80,81</sup>. In agreement with the properties of Tax in T cells, recombinant Tax disturbs the expression of activation maturation markers, the secretion of pro-inflammatory cytokines and the induction of Ag-independent T-cell proliferation in MDDCs in an NF- $\kappa$ B-dependent manner<sup>82,83</sup>. However, the signaling properties of Tax in DCs remain to be elucidated.

OPTN, TAX1BP1 and p62 belong to the selective autophagy receptor (SAR) family and participate in pathways such as mitophagy and xenophagy<sup>84</sup>. Our team recently demonstrated that TAX1BP1 plays a major role in regulating the loading and presentation of endogenous viral antigens by MHC-II molecules with a direct implication in the activation of virus-specific CD4<sup>+</sup>T cells. In model APCs, we showed a broad role of TAX1BP1 in shaping the immunopeptidome of MHC-II molecules, affecting the presentation of various antigens whose processing is dependent or independent of autophagy degradation. Via its interaction with ER chaperone Calnexin (CANX), TAX1BP1 stabilizes the invariant chain Ii and controls peptide loading on MHC-II molecules. This, however, is probably not the only way by which TAX1BP1 affects MHC-II-restricted antigen presentation as it also participates in the regulation of the trafficking of MHC-II-loading compartments and more globally of acidified vesicular compartments<sup>85</sup>. Other viruses, such as human cytomegalovirus (HCMV), target MHC-II molecules for degradation<sup>86</sup> or, like HSV-1, disturb the function of Ii<sup>87</sup>. Viruses also target SARs to degradation to avoid their own clearance<sup>88</sup> or hijack SARs to promote their own replication<sup>89</sup>. Given the effect of Tax on the altered function of DCs<sup>82,83</sup>, we hypothesize that HTLV-1 Tax protein might also target SARs as a means to modulate MHC-II-restricted antigen presentation in APCs and escape CD4<sup>+</sup>T cell antiviral immunity.

First, we asked whether Tax expression might induce the relocalization of SARs in our model APCs. We dispose of HeLa cells stably expressing CIITA (HeLa-CIITA) as model APCs for endogenous antigen presentation. We show in HeLa-CIITA that Tax expression induces the recruitment of TAX1BP1, OPTN and p62. We then asked whether Tax affects MHC-II-restricted presentation of a viral antigen. We show that ectopic expression of Tax significantly affects the presentation of a viral antigen to antigen-specific CD4<sup>+</sup>T cells. The effect of Tax does not seem to be limited to a viral antigen since the global repertoire of peptides presented by MHC-II molecules (immunopeptidome) is changed upon Tax expression without altering HLA-DR expression levels. Remarkably, Tax expression induces a significant relocalization of the MIIC towards the nucleus. We then aimed at deciphering the mechanism underlying the effect of Tax on the MHC-II immunopeptidome. We show that Tax expression does not affect HLA-DM and Ii expression levels but increases global cathepsin activity and overall affects the nature of the MIIC. To assess if SARs recruited by Tax mediate the effect of Tax on MHC-II antigen presentation, we silenced individually TAX1BP1, OPTN and p62 with siRNAs and analyzed the capacity of the cells to present a viral antigen to virus-specific CD4<sup>+</sup>T cells. Strikingly, we show that the effect of Tax on MHC-II antigen presentation and CD4<sup>+</sup>T cell activation is dependent on OPTN expression. Finally, to confirm whether the effect of Tax is dependent on the interaction of Tax with OPTN through the ubiquitin scaffolding role of OPTN, we assessed the capacity of different Tax ubiquitin mutants to activate virus-specific CD4<sup>+</sup>T cells. We show that

OPTN interaction with ubiquitinated Tax is necessary for Tax-mediated MHC-II antigen presentation inhibition.

## Results

### **Tax expression inhibits endogenous viral antigen presentation and CD4<sup>+</sup> T cell activation.**

The HTLV-1 oncoprotein Tax, produced upon infection, induces the transformation of CD4<sup>+</sup>T cells through the sustained activation of the NF- $\kappa$ B pathway via the macromolecular cytosolic complex called Signalosome<sup>67</sup>. The recruitment of OPTN, TAX1BP1 and p62 by Tax to the Signalosome relies on their ubiquitin-binding domains and is necessary for NF- $\kappa$ B activation<sup>73,79,90</sup>. In DCs, Tax influences their capacity to stimulate T cells and impacts maturation marker expression, which is dependent on the NF- $\kappa$ B pathway. Our team recently described TAX1BP1 as a novel player in MHC-II endogenous antigen presentation and CD4<sup>+</sup>T cell activation. We hypothesize that Tax might recruit SARs to modulate immune signaling in APCs and ask whether Tax expression in APCs might influence MHC-II-restricted antigen presentation and subsequent CD4<sup>+</sup>T cell activation.

We first evaluated the effect of Tax expression on TAX1BP1, OPTN and p62 in our model APCs. HeLa-CIITA were transfected with a control plasmid or a plasmid encoding HTLV-1-Tax protein fused to a His tag. Using confocal microscopy analysis, 24h post DNA transfection, we analyzed the localization of Tax and the SARs in the cells. In control cells, TAX1BP1, OPTN and p62 all localize evenly in the cytosol. Upon Tax expression, we observed an important relocalization of the three markers to perinuclear spots (Fig1A). These perinuclear spots co-localize with Tax. We confirmed previous results showing that Tax expression leads to the recruitment of TAX1BP1, OPTN and p62 to perinuclear Tax positive spots<sup>72,73,79</sup>. The capacity to recruit SARs proves that Tax is functional in our cell model.

To assess if Tax expression has an effect on endogenous viral antigen presentation by MHC-II molecules and their capacity to activate CD4<sup>+</sup>T cell clones, HeLa-CIITA were co-transfected with a plasmid encoding HIV-Gag protein and a plasmid encoding Tax-His or a control plasmid. 24h post DNA transfection, we analyzed by flow cytometry the percentages of living and of Gag-positive (Gag<sup>+</sup>) cells, using a viability dye and Gag intracellular staining, respectively. In the control condition and Tax-His condition, levels of Gag<sup>+</sup> cells were similar and Tax transfection did not significantly influence cell viability (Fig S1). HeLa-CIITA cells were then co-cultured with Gag-specific CD4<sup>+</sup>T cells that we previously isolated and characterized<sup>91</sup>. These Gag-specific CD4<sup>+</sup>T cell clones recognize cells infected with HIV or expressing the HIV-Gag protein<sup>85,91,92</sup>. We monitored CD4<sup>+</sup>T cell activation using IFN- $\gamma$ -ELISPOT (Fig 1B). As compared to cells transfected with the control plasmid and Gag, Tax expression significantly decreased the activation of Gag-specific T cells (Fig 1C). We next analyzed the effect of different doses of Tax on endogenous viral antigen processing by MHC-II molecules. HeLa-CIITA cells were co-transfected with four different doses of control plasmid or Tax-encoding plasmid and a steady amount of Gag-encoding plasmid, and co-cultured with the Gag-specific CD4<sup>+</sup>T cells (Fig 1D). 24h-post transfection and prior co-culture with the CD4<sup>+</sup>T cells, the percentage of Gag<sup>+</sup> cells and Gag<sup>+</sup>/Tax<sup>+</sup> cells and the cell viability were analyzed in all tested conditions. As previously,

Tax expression induced, in a dose-dependent manner, a strong decrease in CD4<sup>+</sup>T cell activation (Fig 1D left panel). Importantly, Tax expression did not interfere with the ability of HeLa-CIITA cells to present the cognate peptide recognized by Gag-specific T cells when added exogenously (Fig 1C and 1D, right panels). These results suggest that Tax expression influences the generation of Gag-derived endogenous epitopes and their subsequent presentation by MHC-II molecules to Gag-specific CD4<sup>+</sup>T cells but does not affect the ability of APCs to present exogenous peptides by MHC-II molecules.

### **Tax expression alters the immunopeptidome of MHC-II molecules but does not influence MHC-II molecule expression levels.**

Although Tax expression does not significantly alter the capacity of MHC-II molecules to present exogenous peptides to activate CD4<sup>+</sup>T cells, we asked whether Tax might influence MHC-II expression levels. As previously, HeLa-CIITA cells were transfected with a plasmid encoding HTLV-1-Tax protein fused to a His tag. Using WB, we assessed HLA-DR expression levels and found no difference upon Tax expression in two independent experiments (Fig 2A). Using flow cytometry, we monitored, on control and Tax-expressing HeLa-CIITA cells (Fig 2B, left panel) the intracellular expression levels of HLA-DR molecules using the L243 and TU36 antibodies that recognize mature and both mature and immature HLA  $\alpha\beta$  heterodimers associated with the invariant chain (Ii), respectively (Fig 2B, top right panels). Using both antibodies, we noticed a slight increase of MHC-II molecule expression levels in cells expressing Tax.

To extend the observation made with a single viral antigen, we then analyzed the influence of Tax expression on the global peptide repertoire (immunopeptidome) presented by MHC-II molecules. To this end, HeLa-CIITA cells were transfected with control or Tax-encoding plasmids and, 24h post-transfection, MHC-II molecules were immunoprecipitated with the TÛ39 antibody (specific for mature HLA-DR, DP and DQ molecules). The peptide ligands were then eluted and identified using mass spectrometry (LC-MS/MS). To take into account the variability of immunopeptidomes, we used three biological replicates for each condition. Following a classical procedure, each biological replicate was run five times on the LC-MS/MS, thus corresponding to five technical replicates. A peptide was considered as an MHC ligand when detected in at least three out of five technical replicates and in at least two out of three biological replicates. A total 8276 and 8847 peptide ligands were identified in the control and Tax-expressing cells, respectively. 6832 peptides (66% of the peptides) were shared between control and Tax-expressing cells (Fig 2C, Shared). Remarkably, 1444 (14% of peptides) and 2015 MHC-II peptide ligands (20% of the peptides) were presented by MHC-II molecules exclusively in control or Tax-expressing HeLa-CIITA cells, respectively (Fig 2C, Ctrl and Tax). Together, these results show that Tax expression influences the peptide repertoire presented by MHC-II molecules.

We then sought to analyze the influence of Tax expression on the relative peptide abundance and their affinity to MHC-II molecules. Nevertheless, peptides eluted from MHC-II molecules are variable in length and the same core epitope inserted in the MHC-II peptide-binding groove can be found in multiple peptides with N- or C-terminal extensions. To circumvent this limitation, we adapted a protocol, published by Alvaro-Benito *et al.* to identify the core epitopes within our dataset using the Peptide Landscape Antigenic Epitope Alignment Utility (PLAtEAU) algorithm<sup>93</sup>. A total 1347 unique core epitopes were identified in the group Ctrl/Tax (Fig 2D). PLAtEAU also allows calculating the relative abundance of the core epitopes based on the LC-MS/MS intensities of peptides containing the same core epitope. Two abundant Tax-derived epitopes could be identified in Tax-expressing cells (Fig 2D). Remarkably, between the Ctrl and Tax-expressing cells, 18% of the core epitopes displayed a relative abundance that was significantly different between conditions, with 177 and 69 core epitopes more abundant in the Tax-expressing or Control cells, respectively (p value 0,05 and fold change 2) (Fig 2D). Therefore, Tax expression influences both the peptide repertoire (Fig 2B) and the relative abundance of one core epitope out of five presented by MHC-II molecules (Fig 2D).

After identification of the core epitopes, using the NetMHCIIpan4.0 algorithm<sup>94</sup>, we next analyzed the relative binding affinities of exclusive peptides, identified in Ctrl and Tax-expressing conditions, to the HLA-DR $\beta$ 1\*0102 and HLA-DQ $\alpha$ \*10102-DQ $\beta$ \*10501 alleles expressed by HeLa-CIITA cells. Interestingly, in Ctrl cells, only 33% of the core epitopes were predicted to be HLA-DQ $\alpha$ \*10102-DQ $\beta$ \*10501 binders (12% and 20%, strong and weak binders, respectively). The binding scores do not significantly vary upon Tax expression in our data set (13% and 21%, strong and weak binders, respectively). We predicted slightly less strong HLA-DR $\beta$ 1\*0102 binders in Tax-expressing cells (50% in Ctrl cells versus 44% in Tax-expressing cells) and less weak binders (26% in Ctrl cells versus 15% in Tax-expressing cells). We found more core epitopes non-predicted to bind to HLA-DR $\beta$ 1\*0102 in Tax-expressing cells compared to control cells (41% in Tax-expressing cells versus 24% in Ctrl cells) (Fig 2E).

We concluded that Tax expression has an important influence on the peptide repertoire and the relative abundance of core epitopes. In contrast, we observe a weak, if any, effect of Tax expression on the predicted relative affinity of core epitopes to MHC-II molecules in our cell system.

### **Tax expression affects the cellular localization and maturation of the MIIC.**

We then asked whether Tax expression might play a role in the intracellular trafficking of MHC-II molecules and the MIIC before MHC-II-peptide complexes reach the plasma membrane. The MIIC is a late endosome-like/lysosomal compartment that assembles MHC-II molecules and contains lysosomal proteases<sup>95</sup>. Conventional markers of this compartment are MHC-II and HLA-DM<sup>52-54</sup> as well as late-endosome and tetraspanin markers Lamp-1 and CD63. Using confocal microscopy analysis, we evaluated, in HeLa-CIITA cells, the effect of Tax expression on these different endo-lysosomal markers.

We first analyzed the subcellular localization of MHC-II molecules stained with L243, recognizing mature HLA  $\alpha\beta$  heterodimers. When compared to the control condition, MHC-II molecules seemed to localize closer to the nucleus and further away from the cell membrane (Fig 3A). In order to surpass a possible change in cell shape upon Tax expression, we determined the ratio between the distance to the nucleus and the sum of the distance to the nucleus and the distance to the membrane. The lowest the ratio, the closest a vesicle clusters toward the nucleus. We noticed a significant decrease in the calculated ratio for MHC-II-positive vesicles upon Tax expression (Fig 3B).

Using an anti-HLA-DM antibody, we then analyzed the effect of Tax expression as another way to describe the MIIC. As compared to control cells, we noticed an important relocalization of this marker in cells expressing Tax (Fig 3C). The distance ratio for HLA-DM-positive vesicles was also significantly lower in cells expressing Tax (Fig 3D).

In addition, we sought to analyze the composition of the MIIC in Tax-expressing cells by combining markers specific to various compartments including Lamp-1, a marker of late lysosomal compartments. We observed that, as for MHC-II and HLA-DM, Lamp-1 positive vesicles seem to cluster around the nucleus of Tax-expressing cells (Fig 3E). We co-stained with anti-Lamp1 and anti-HLA-DM antibodies and noticed a slight increase of the Pearson's coefficient, which could suggest that Lamp1 and HLA-DM might co-localize more upon Tax expression (Fig 4C, right panel). In addition, we observed that Tax expression also induced a slight accumulation of EEA1+ and CD63+ vesicles around the nucleus (Fig S2). Taken together, these results show that Tax expression influences the positioning of the MIIC by re-localizing it towards the nucleus. Moreover, the increase of co-localization between Lamp-1+ and HLA-DM+ vesicles suggests a modification of the pH, which could affect MIIC maturation and at least partially account for the changes in the global MHC-II peptide repertoire, observed upon Tax expression.

### **Tax expression modifies cathepsin activity but does not alter HLA-DM and li expression levels.**

We then decided to study the functional consequences of the effect of Tax expression on the localization and maturation of the MIIC.

HLA-DM is essential for CLIP removal and ensures quality control of peptide loading on MHC-II molecules<sup>50,51</sup>. Given the effect of Tax expression on HLA-DM+ vesicles, we first asked whether Tax might alter HLA-DM expression levels. As previously, Hela-CIITA cells were transfected with a Ctrl or a Tax-encoding plasmid. 24h post DNA transfection, HLA-DM $\beta$  expression was assessed by WB. The global expression of HLA-DM molecules was similar in Ctrl and Tax-expressing cells (Fig 4A).

We next asked if Tax expression might influence li degradation. The invariant chain li is essential for trafficking and maturation of MHC-II molecules<sup>39-42</sup>. Its degradation is regulated in the MIIC



to ensure proper loading of MHC-II molecules with high-affinity peptides<sup>43–46</sup>. In addition, li has also been shown to influence the immunopeptidome of MHC-II molecules<sup>96</sup>. As before, 24h post DNA transfection, we assessed li expression by WB. In control and Tax-expression cells, lip33 was readily detected together with its cleavage product lip16 (Fig 4B, left panel). Normalized to the housekeeping gene (actin), the global expressions of lip33 and lip16 were similar in Ctrl and Tax-expressing cells (Fig 4B, right panels).

Given that Tax expression alters the peptide repertoire presented by MHC-II molecules, we then asked if Tax expression could affect cathepsin activity and the generation of MHC-II peptides in acidified vesicles. To this end, HeLa-CIITA cells were transfected with Ctrl or Tax-encoding plasmids and, 24h post-transfection, lysed in cold acid citrate buffer. This buffer allows the extraction of cathepsins active at low pH. We then incubated the whole cell lysates with substrates specific for cathepsins B or L and cathepsin S at 37°C. Substrate degradation was monitored by following the accumulation of a fluorescent cleavage product over time, which translates cathepsin activity of transforming the substrate into the fluorescent product. We observed in control HeLa-CIITA cells that the cathepsins B/L and S reached a plateau of activity after 380 and 300 min, respectively (Fig 4C). In Tax-expressing cells, these plateaus of catalytic activities were reached already after 300 and 200 min, respectively (Fig 4C). We then calculated the initial substrate degradation rates (Fig 4D). In Tax-expressing cells, substrate degradation by both cathepsins B/L and S on average 1.6 times faster than in control cells. (Fig 4D). Therefore, Tax expression affects the cathepsin activities, probably explaining the generation of a slightly different set of MHC-II peptide ligands.

### **Tax interaction with Optineurin is required for Tax inhibition of CD4<sup>+</sup>T cell activation**

We recently demonstrated that TAX1BP1 regulates the loading and presentation of endogenous viral antigens by MHC-II molecules with a direct implication in the activation of virus-specific CD4<sup>+</sup>T cells. TAX1BP1 shapes the MHC-II immunopeptidome and participates in the regulation of the trafficking of MHC-II-loading compartments and more globally of acidified vesicular compartments<sup>85</sup>. Of note, Tax induces the recruitment of TAX1BP1, OPTN and p62 to a macromolecular cytosolic Signalosome where they play a role in sustaining NF- $\kappa$ B activation in CD4<sup>+</sup>T cells. We asked if these SARs might be involved in the effect of Tax on MHC-II-restricted viral antigen presentation to virus-specific CD4<sup>+</sup>T cells.

To assess whether SARs play a role in Tax-mediated inhibition of MHC-II antigen presentation, the expression of TAX1BP1, OPTN and p62 in HeLa-CIITA cells was silenced using siRNAs. As previously, 24 h post-siRNA transfection, the cells were co-transfected with plasmids encoding HIV Gag protein and Tax protein or a control plasmid. 48 h post-siRNA treatment (24 h post-DNA transfection), we analyzed by flow cytometry the percentages of living and of Gag-positive (Gag<sup>+</sup>) and Gag<sup>+</sup>/Tax<sup>+</sup> cells, using a viability dye and Gag and Tax intracellular staining, respectively. In all tested conditions, the levels of Gag<sup>+</sup> and Gag<sup>+</sup>/Tax<sup>+</sup> cells were similar and the sequential transfections (siRNA and cDNA) had no significant influence on cell viability (Fig

S3). The silencing of AR expression was also analyzed by Western Blot (WB) (Fig 5A). As compared to the control siRNA (CTRL), all siRNAs led to a marked decrease of SAR expression (Fig 5A). As previously, HeLa-CIITA cells were then co-cultured with Gag-specific CD4<sup>+</sup>T cells and T cell activation was monitored. As expected, silencing TAX1BP1 induced a significant decrease of CD4<sup>+</sup>T cell activation (Fig 5B, left panel, comparing white columns). Silencing of p62 and OPTN expression induced a slight, but not significant, and no decrease of CD4<sup>+</sup>T cell activation, respectively (Fig 5B, middle and right panels, comparing white columns). As previously, Tax expression induced a reduction of CD4<sup>+</sup>T cell activation (Fig 5B, left grey columns of each panel). Remarkably, silencing TAX1BP1 or p62 in Tax-expressing cells seems to induce a more potent inhibition of CD4<sup>+</sup>T cell activation (Fig 5B, left and middle panels, grey columns). In sharp contrast, silencing of OPTN abrogated the Tax-mediated inhibition of T cell activation (Fig 5B, right panel, comparing grey columns). Overall, these results suggest that Tax-mediated inhibition of CD4<sup>+</sup>T cell activation acts independently of TAX1BP1 and p62 expression but is dependent on OPTN expression.

To further characterize potential interactions of Tax with OPTN in inhibiting antigen presentation, we made use of well-characterized mutants of Tax<sup>63</sup>. Tax contains 10 lysine (K) residues (K1 to K10) of which K4 through K10 are the main targets of both monoubiquitination and polyubiquitination. Polyubiquitin mediates the interaction of Tax with different actors of the NF- $\kappa$ B pathway, including SARs TAX1BP1, p62 and OPTN<sup>73,79</sup>. We used three ubiquitin mutants of Tax: Tax<sub>K10R</sub>, Tax<sub>K7-8</sub>, and Tax<sub>K4-8</sub> in which lysines have been replaced by arginines and can no longer bind mono- or polyubiquitin. Of the three mutants, Tax<sub>K7-8</sub> is the only one that is still partially ubiquitinated and can induce the Signalosome and recruit NEMO and OPTN to modulate NF- $\kappa$ B to an extent<sup>97,98</sup>. As previously, HeLa-CIITA cells were transfected with Tax and Tax mutant-expressing plasmids together with the Gag encoding vector and then co-cultured with Gag-specific CD4<sup>+</sup>T cells and CD4<sup>+</sup>T cell activation was monitored. We further confirmed that Tax expression induces a decrease in CD4<sup>+</sup>T cell activation (Fig 5C). Remarkably, the mutants Tax<sub>K10R</sub> and Tax<sub>K4-8</sub> no longer inhibited CD4<sup>+</sup>T cell activation. In contrast, mutating K7-8 did not abrogate Tax inhibition of CD4<sup>+</sup>T cell activation (Fig 5C). Altogether, these results strongly suggest that Tax interacts with OPTN through lysines 4 to 6 and these seem to be required for Tax to act on MHC-II antigen presentation and CD4<sup>+</sup>T cell activation.

## Discussion

We demonstrate here that HTLV-1 Tax protein interferes with endogenous antigen presentation by MHC-II molecules and subsequent activation of virus-specific CD4<sup>+</sup>T cells. Tax expression affects the trafficking of acidified vesicles and the MIIC as well as its "maturation". We also suggest that Tax affects lysosomal cathepsin activities, which could explain the modification of the immunopeptidome of MHC-II molecules. By silencing different SARs, known to be manipulated by Tax for viral profit, we showed that OPTN is required for Tax

inhibition of CD4<sup>+</sup>T cell activation. In addition, we showed that specific Tax ubiquitination is required for its interaction with OPTN.

Although we did not see a difference in HLA-DR expression levels upon Tax expression, we cannot exclude at this stage that MHC-II molecule synthesis, internalization and maturation kinetics could be affected by Tax expression. Monitoring MHC-II surface expression as well as MHC-II internalization kinetics are necessary to rule out a possible effect of Tax on MHC-II trafficking, especially considering that our confocal microscopy results suggest that MHC-II – positive vesicles relocate upon Tax expression. HLA-DM is a chaperone that regulates peptide loading on MHC-II molecules and its expression levels are known to affect the peptide repertoire presented on several MHC-II molecules, as well as their affinity<sup>96,99</sup>. Upon Tax expression, we did not observe a modification in HLA-DM levels but HLA-DM-positive vesicles seem to cluster closer to the cell nuclei. In addition, our experiments suggest that HLA-DM-positive vesicles might co-localize more with Lamp1-positive vesicles in Tax-expressing cells compared to control cells. Recent studies suggest that the localization of intracellular vesicles controls their functions<sup>100</sup> and particularly their intravesicular pH<sup>101</sup>. Indeed, in relation to our results, we could suggest that we might have an alteration in intravesicular pH given the increase on cathepsin activity in cells expressing Tax and its effect on the immunopeptidome. Although we have no direct evidence of the effect of Tax on the processing of gag, it has been previously shown that modulating cathepsin activity can alter antigen processing and presentation<sup>102</sup> and cathepsins B and S are optimally active at low pH and participate in generating HIV-derived MHC-II restricted epitopes<sup>103</sup>. Nevertheless, altered intravesicular pH and cathepsin activities could directly affect li processing, MHC-II antigen loading and presentation. This is not the case in our model of Hela-CIITA cells expressing Tax since we do not detect any changes in li expression levels and processing at a steady state. Still, we should consider performing pulse chase experiments to evaluate the degradation kinetics of li upon Tax expression. It is therefore necessary to better characterize the MIIC when Tax is expressed in our system, specially the evolution of MHC-II+/HLA-DM+ vesicles. It has been previously demonstrated that MHC-II-peptide complexes are transported to the plasma membrane via the actin-myosin cytoskeleton by the ARL14/ARF7EP complex and Myosins 1E and II or by the dynein-kinesin cytoskeleton and Rab7<sup>104</sup>. In our system, we observed no impact of Tax expression on the actin cytoskeleton (not shown). Therefore, it would be interesting to look at other markers such as Rab7, myosins or pericentrin, to confirm the impact of Tax expression on lysosomal trafficking.

We identified in our study a novel role for the SAR OPTN in mediating Tax-induced inhibition of MHC-II antigen presentation and CD4<sup>+</sup>T cell activation. This role seems to depend on the ubiquitinated status of Tax. Interestingly, Tax recruits different SARs and the IKK complex to a Golgi-associated cytosolic macromolecular complex called Signalosome. The Signalosome formation is polyubiquitin-dependent and is the platform from which Tax drives NF-κB modulation. Since SAR recruitment by Tax is necessary for NF-κB sustained activation, we could hypothesize that NF-κB could play a role in MHC-II antigen presentation. Previous studies have

shown, in inflammatory conditions, a role for NF- $\kappa$ B in the modulation of MHC-II molecule expression dependently and independently of the Jak/STAT pathway (which can regulate CIITA expression) in different APCs<sup>105-107</sup>. In our model, Tax expression could be a driver of an inflammatory context. It is important to assess NF- $\kappa$ B activation alone in our system to evaluate its role on MHC-II antigen presentation. This is particularly relevant considering that CIITA has been previously shown to inhibit Tax-induced sustained NF- $\kappa$ B activation<sup>108</sup>. In addition, we dispose of previously characterized Tax mutants that are positively and negatively dominant for NF- $\kappa$ B sustained activation (M22 and M47) that can be used to further characterize the impact of Tax on MHC-II antigen presentation and CD4<sup>+</sup>T cell activation. However, it is interesting to note that silencing of TAX1BP1, OPTN or p62 expression, individually, significantly abrogates NF- $\kappa$ B activation in Tax-expressing cells<sup>73,79</sup>. Remarkably, we observed CD4<sup>+</sup>T cell activation was further decreased in cells silenced for TAX1BP1 or p62 in presence of Tax. Thus, we could be looking here at a novel role of OPTN in Tax-mediated MHC-II antigen presentation. In addition to assessing the effect of NF- $\kappa$ B activation alone on MHC-II antigen presentation, it would be interesting to target other elements of the Signalosome such as IKK $\gamma$  or to target ubiquitin ligases. Moreover, a role of OPTN in the Tax-driven alteration of vesicular trafficking and MHC-II immunopeptidome remains to be elucidated.

Several groups have documented the productive in vitro infection of myeloid DCs and of monocyte-derived DCs (MDDCs). DCs dictate the quality of T cell responses but very little is known about the capacity of HTLV-1-infected DCs to prime efficient T cell responses. Several studies have shown that blood DCs from HTLV-1-infected patients and DCs from uninfected individuals, exposed in vitro to HTLV-1, induce an abnormal proliferation of CD4<sup>+</sup>T cells and present an unresponsive status of limited maturation. These observations suggest that both DC exposure to HTLV-1 and DC infection can influence their capacity to stimulate T cells. Since the canonical NF- $\kappa$ B signaling pathway regulates DC maturation, it will be interesting in the future to investigate, in DCs, a potential role of SARs in the modulation of NF- $\kappa$ B and MHC-II antigen presentation. Given that OPTN and TAX1BP1 also regulate the IRF3 pathway, it would be interesting to analyze the effect of Tax on IRF3 and the induction of IFN I in DCs expressing Tax or exposed to HTLV-1. IFN I acts in a paracrine way on the Jak/STAT signaling pathway<sup>109</sup>, which can regulate MHC-II molecule expression in certain cell types. In addition, other HTLV-1 protein such as p12 can also reduce CTL-mediated killing through the induction of MHC-I molecule degradation<sup>110</sup>. This feature could be studied in relation to MHC-II molecules in model APCs and DCs. Overall; we suggest in this work that HTLV-1 targets OPTN as a means to escape antiviral adaptive immunity.

## **Materials and Methods**

### **Cells**

HeLa-CIITA cells (homozygotes for HLA-DR $\beta$ 1\*0102 allele) were kindly provided by Philippe Benaroch (Institut Curie, Paris, France). Cells were cultured with RPMI GlutaMax 1640 (Gibco) complemented with 10% FBS (Dutscher), 1% Penicillin/Streptomycin and 50 $\mu$ g/mL Hygromycin B (Thermo Fisher).

### **HIV-specific CD4<sup>+</sup> T cell clones**

Gag-specific CD4<sup>+</sup>T cell clones (F12) are specific for HIV Gag-p24 (gag2: aa 271-290) and restricted by HLA-DR $\beta$ 1\*01 as previously described (Moris et al., 2006; Coulon et al., 2016). F12 clones were restimulated and expanded, as previously described (Moris et al., 2006), using irradiated feeders and autologous or HLA-matched lymphoblastoid cell lines loaded with cognate peptides in T cell cloning medium: RPMI 1640 containing 5% human AB serum (Institut Jacques Boy), recombinant human IL-2 (100 IU/ml, Miltenyi Biotec), PHA (0,25  $\mu$ g/ml, Remel), non-essential amino acids, and sodium pyruvate (both from Life Technologies). At least 1h before co-culture with HeLa-CIITA cells, T cell clones were thawed and allowed to rest at 37°C in RPMI containing DNase (5 $\mu$ g/mL, New England Biolabs).

### **Viral antigens and plasmids**

The pTRIP-CMV-Gag (a kind a gift from Nicolas Manel (Institut Curie, Paris, France) plasmid was already described (Coulon et al., 2016). pSG5M-Tax1(control) and Tax1-6His (Tax-encoding) plasmids were previously described (Meertens et al., 2004; Kfoury et al., 2008). Tax mutants harboring substitutions of all (K1–10R) or some (K7–8R) lysines into arginines were described elsewhere and were kindly provided by C. Journo (Chiari et al., 2004).

### **Cell transfections**

HeLa-CIITA cells were incubated in 6-well plates using 2-4.10<sup>5</sup> cells/well using OPTIMEM (Gibco) complemented with 10% FBS, 1% Penicillin/Streptomycin. Twenty-four hours later, cells were transfected with the viral antigen encoding (1 $\mu$ g per well of a 6-well plate) plasmid and the Tax-expressing or control plasmid (1 $\mu$ g per well of a 6-well plate) using Eugene HD (Promega), following manufacturer instructions. Twenty-four hours later, Gag expression was assessed using anti-Gag-PE antibody (KC57-RD1, Beckman-Coulter). For siRNA transfections, twenty-four hours after cell seeding, cells were transfected with 100 pmol of siRNA targeting OPTN (L-016269-00-0005), p62 (L-010230-00-0005), TAX1BP1 (L-016892-00-0020 Dharmacon), or a scrambled siRNA as control (D-001810-10-20, Dharmacon), using Lipofectamine RNAiMax (13778-150, Thermo Fisher) as transfection reagent. 24h after siRNA transfection, cells were transfected with cDNA as mentioned above.

## **Flow cytometry**

Cell viability was evaluated using LIVE/DEAD (Thermo Fisher) and the following antibodies were used: HLA-DR specific L243 and TÜ36 (both in house and kindly provided by Philippe Benaroch, Institut Curie, Paris) and goat anti-mouse (AF488, Thermo Fisher). Twenty-four hours after cDNA transfection, staining assays were performed using standard procedures (30min, 4°C). HIVGag production was detected using intracellular staining. Briefly, cells were fixed with 4% PFA (10min, RT), washed, and permeabilized with PBS containing 1% BSA and 0,05% Saponin, prior to antibody staining. Samples were processed on CytoFLEX cytometer using CytExpert software (BD Biosciences) and further analysed using FlowJo10 software (Tree Star).

## **IFN- $\gamma$ ELISPOT assay**

ELISPOT plates (MSIPN4550, Millipore) were pre-wet and washed with PBS, and coated overnight at 4°C with anti-IFN- $\gamma$  antibody (1-DIK, Mabtech). Plates were washed using PBS and then saturated with RPMI complemented with 10% FBS. Plates were washed and HeLa-CIITA cells (105 cells/well) were co-cultured with T cell clones (5.103 and 1.103 cells/well) overnight at 37°C. Cells were removed and plates were then washed with PBS-0,05% Tween-20 prior incubation with biotinylated anti-IFN- $\gamma$  antibody (7-B6-1, Mabtech) (2h, RT). Spots were revealed using alkaline-phosphatase coupled to streptavidin (0,5U/ml, Roche Diagnostics) (1h, RT) and BCIP/NBT substrate (B1911, Sigma-Aldrich) (30min, RT). Reactions were stopped using water. Number of spots were counted using AID reader (Autoimmun Diagnostika GmbH). For each experimental condition, ELISPOTs were performed in triplicates.

## **Western Blotting**

Twenty-four hours after cDNA transfection, 106 HeLa-CIITA cells were washed in cold PBS and lysed in 100 $\mu$ l of lysis buffer (30min, 4°C), mixing every 10 min. The lysis buffer used contained 50 mM Tris-HCl pH 7.5, 150 mM NaCl, 1% IGEPAL, 0.5 mM EDTA, 5 mM MgCl, supplemented with 1X protease inhibitor (Roche). Cell lysates were then centrifuged at 12,000 g (10 min, 4°C), supernatants harvested and mixed with Sample Buffer (NuPAGE, Invitrogen) and Sample Reducing Agent (NuPAGE, Invitrogen) and denatured (5 min, 95°C). Denatured samples were analysed by SDS gel electrophoresis using 4-12% Bis-Tris gels (NuPAGE, Invitrogen), transferred to a nitrocellulose membrane (NuPAGE, Invitrogen) and immunoblotted. Anti-TAX1BP1 (HPA024432, Sigma-Aldrich), anti-OPTN (sc-166576, Santa Cruz Biotechnology), anti-p62 (610832, BD Biosciences), anti-HLA-DR (TAL1B5, Invitrogen), anti-actin (3700S, Cell Signaling Technology), anti-li (CD74) (14-0747-82, eBioscience), goat anti-mouse (Jackson ImmunoResearch) and goat anti-rabbit both coupled to HRP (Jackson ImmunoResearch) antibodies were used according to manufacturer instructions. Blots were revealed using Immobilon Western Chemiluminiscent HRP substrate and chemiluminescence analyzed using ChemiDoc MP (Biorad).

## Confocal microscopy

Twenty-four hours after , HeLa-CIITA cells were plated on glass coverslips and then fixed with 4% PFA (10min, RT). Cells were washed 3 times with PBS, saturated with goat or donkey serum and permeabilized with PBS containing 0,5% BSA and 0,05% Saponin (1h, RT). Cells were washed with PBS and incubated (OVN, 4°C) with primary antibodies: L243 or TÜ36 (both in house and kindly provided by P. Benaroch, Institut Curie, Paris), rabbit anti-HLA-DR (a kind gift from Jack Neefjes), LAMP-1 (H4A3, DSHB), CD63 (MA-18149), anti-CD74 (14-0747-82) all from ThermoFisher, anti-EEA1 (C45B10, Cell signalling), T6BP (HPA024432, Sigma-Aldrich) and Lysotracker (Deep Red, L12492). Cells were incubated with species specific antibodies: goat anti-mouse coupled to Alexa Fluor 488 or Alexa Fluor 405 (ThermoFischer), donkey anti-rabbit coupled to Alexa 546 (A10040, Invitrogen) in PBS containing 0,5% BSA and 0,05% Saponin (1h, RT). When required sequential stainings were performed. Nuclei were stained with DAPI (17507, AAT Bioquest). After washing with PBS, samples were mounted on glass slides with Dako fluorescence mounting medium. Samples were imaged using a laser scanning confocal microscope with 63X, NA 1.3 oil immersion objective. The number of vesicles, the intensity and the distances of each vesicle to nucleus were quantified using an in-house ImageJ Python script (developed by Aziz Fouché, ENS Paris-Saclay, Paris). Potential co-localizations were determined using the object based co-localization method JACoP (Just Another Co-localization Plugin) and coloc2 (Pearson's coefficient) of the ImageJ software, for punctuated/vesicular and cytosolic/diffuse staining, respectively. For the Proximity ligation assay (PLA), 48h after siRNA transfections, HeLa-CIITA cells, cultured overnight on coverslips, were fixed with 4% PFA (10min, RT), washed 3x with PBS and treated with 50mM NH<sub>4</sub>Cl (15min, RT) prior incubation with anti-T6BP (Rabbit, 1:200, HPA024432) and anti-CANX (Mouse, 1:500, MA3-027, Thermo fisher scientific) in PBS containing 1%, BSA and 0.1% Saponin (1h, RT). PLA secondary probes (DUO92002, DUO92004) were then used according to the manufacturer's instructions (Sigma-Aldrich). Briefly, 40 µl (1:5 dilution) of the PLA were added (37 °C, 60 min), washed with buffer A (DUO82049, Sigma-Aldrich). 40 µl of the ligation mix (DUO92014, Sigma-Aldrich) was then applied to each of the coverslips to complete the ligation process (30min, 37 °C). Coverslips were then incubated with 40µl polymerisation mix (100min, 37 °C) and washed. Coverslips were mounted on slides with Fluoromount G (Thermo fisher). Images were acquired using SP8 confocal microscope and dots were counted using find maxima plugin in Fiji software.

## Immuno-peptidome

### *Isolation of HLA ligands*

HLA class-I and -II molecules of HeLa-CIITA cells were isolated using standard immunoaffinity purification (Falk et al, 1991; Nelde et al, 2019). Snap-frozen samples were lysed in 10 mM CHAPS/PBS (AppliChem, Gibco) with 1x protease inhibitor (Roche). HLA class-I and -II-associated peptides were isolated using the pan-HLA class I-specific mAb W6/32 and the pan-HLA class II-specific mAb TÜ39 (both in house mouse monoclonal) covalently linked to CNBr-activated Sepharose (GE Healthcare). HLA-peptide complexes were eluted by repeated addition of 0.2% TFA (trifluoroacetic acid, Merck). Eluted HLA ligands were purified by

ultrafiltration using centrifugal filter units (Millipore). Peptides were desalted using ZipTip C18 pipette tips (Millipore), eluted in 35  $\mu$ l 80% acetonitrile (Merck)/0.2% TFA, vacuum-centrifuged and resuspended in 25  $\mu$ l of 1% acetonitrile/0.05% TFA and samples stored at -20 °C until LC-MS/MS analysis.

#### *Analysis of HLA ligands by LC-MS/MS*

Isolated peptides were separated by reversed-phase liquid chromatography (nano-UHPLC, UltiMate 3000 RSLCnano; ThermoFisher) and analysed in an online-coupled Orbitrap Fusion Lumos mass spectrometer (Thermo Fisher). Samples were analysed in five technical replicates and sample shares of 20% trapped on a 75  $\mu$ m  $\times$  2 cm trapping column (Acclaim PepMap RSLC; Thermo Fisher) at 4  $\mu$ l/min for 5.75 min. Peptide separation was performed at 50 °C and a flow rate of 175 nl/min on a 50  $\mu$ m  $\times$  25 cm separation column (Acclaim PepMap RSLC; Thermo Fisher) applying a gradient ranging from 2.4 to 32.0% of acetonitrile over the course of 90 min. Samples were analysed on the Orbitrap Fusion Lumos implementing a top-speed CID method with survey scans at 120k resolution and fragment detection in the Orbitrap (OTMS2) at 60k resolution. The mass range was limited to 400–650 m/z with precursors of charge states 2+ and 3+ eligible for fragmentation.

#### *Database search and spectral annotation*

LC-MS/MS results were processed using Proteome Discoverer (v.1.3; Thermo Fisher) to perform database search using the Sequest search engine (Thermo Fisher) and the human proteome as reference database annotated by the UniProtKB/Swiss-Prot. The search-combined data of five technical replicates was not restricted by enzymatic specificity, and oxidation of methionine residues was allowed as dynamic modification. Precursor mass tolerance was set to 5 ppm, and fragment mass tolerance to 0.02 Da. False discovery rate (FDR) was estimated using the Percolator node (Käll et al, 2007) and was limited to 5%. For HLA class-I ligands, peptide lengths were limited to 8–12 amino acids. For HLA class-II, peptides were limited to 12–25 amino acids of length. HLA class-I annotation was performed using NetMHCpan 4.0 (Jurtz et al., 2017) annotating peptides with percentile rank below 2% as previously described (Ghosh et al, 2019).

For HLA class-II peptides, the Peptide Landscape Antigenic Epitope Alignment Utility (PLAtEAU) algorithm (Alvaro-Benito et al., 2018) was used to identify and to estimate the relative abundance of the core epitopes based on the LC-MS/MS intensities. The results are presented as Volcano plots using Perseus software (Tyanova et al, 2016). The relative affinities of the core epitope to HLA-DR\*1\*0102, expressed by HeLa-CIITA cells, was estimated using NetMHCIIpan 4.0 (Reynisson et al., 2020).



## References

1. Gessain, A. *et al.* HTLV ANTIBODIES IN PATIENTS WITH NON-HODGKIN LYMPHOMAS IN MARTINIQUE. *The Lancet* **323**, 1183–1184 (1984).
2. Sugimoto, M. *et al.* T-lymphocyte alveolitis in HTLV-I-associated myelopathy. *Lancet* **2**, 1220 (1987).
3. Morgan, O. S., Rodgers-Johnson, P., Mora, C. & Char, G. HTLV-1 and polymyositis in Jamaica. *Lancet* **2**, 1184–1187 (1989).
4. Hanchard, B. *et al.* Childhood infective dermatitis evolving into adult T-cell leukaemia after 17 years. *The Lancet* **338**, 1593–1594 (1991).
5. Nakao, K., Matsumoto, M. & Ohba, N. Seroprevalence of antibodies to HTLV-I in patients with ocular disorders. *British Journal of Ophthalmology* **75**, 76–78 (1991).
6. Gessain, A. & Mahieux, R. Tropical spastic paraparesis and HTLV-1 associated myelopathy: Clinical, epidemiological, virological and therapeutic aspects. *Revue Neurologique* **168**, 257–269 (2012).
7. Willems, L. *et al.* Reducing the global burden of HTLV-1 infection: An agenda for research and action. *Antiviral Research* **137**, 41–48 (2017).
8. Gonçalves, D. U. *et al.* Epidemiology, Treatment, and Prevention of Human T-Cell Leukemia Virus Type 1-Associated Diseases. *Clin Microbiol Rev* **23**, 577–589 (2010).
9. Shimauchi, T. & Pigué, V. DC-T cell virological synapses and the skin: novel perspectives in dermatology. *Exp Dermatol* **24**, 1–4 (2015).
10. Bangham, C. R. M. CTL quality and the control of human retroviral infections: Highlight. *Eur. J. Immunol.* **39**, 1700–1712 (2009).
11. Kitze, B. *et al.* Human CD4+ T lymphocytes recognize a highly conserved epitope of human T lymphotropic virus type 1 (HTLV-1) env gp21 restricted by HLA DRB1\*0101. *Clinical and Experimental Immunology* **111**, 278–285 (2001).
12. Goon, P. K. C. *et al.* High frequencies of Th1-type CD4+ T cells specific to HTLV-1 Env and Tax proteins in patients with HTLV-1-associated myelopathy/tropical spastic paraparesis. *Blood* **99**, 3335–3341 (2002).
13. Vine, A. M. *et al.* The Role of CTLs in Persistent Viral Infection: Cytolytic Gene Expression in CD8+ Lymphocytes Distinguishes between Individuals with a High or Low Proviral Load of Human T Cell Lymphotropic Virus Type 1. *The Journal of Immunology* **173**, 5121–5129 (2004).
14. Goon, P. K. C. *et al.* Human T Cell Lymphotropic Virus (HTLV) Type-1-Specific CD8 + T Cells: Frequency and Immunodominance Hierarchy. *J INFECT DIS* **189**, 2294–2298 (2004).
15. Goon, P. K. C. *et al.* Human T Cell Lymphotropic Virus Type I (HTLV-I)-Specific CD4+ T Cells: Immunodominance Hierarchy and Preferential Infection with HTLV-I. *The Journal of Immunology* **172**, 1735–1743 (2004).
16. Bangham, C. R. M. Human T Cell Leukemia Virus Type 1: Persistence and Pathogenesis. *Annu Rev Immunol* **36**, 43–71 (2018).
17. Sabouri, A. H. *et al.* Impaired function of human T-lymphotropic virus type 1 (HTLV-1)-specific CD8+ T cells in HTLV-1-associated neurologic disease. *Blood* **112**, 2411–2420 (2008).
18. Kattan, T. *et al.* The Avidity and Lytic Efficiency of the CTL Response to HTLV-1. *The Journal of Immunology* **182**, 5723–5729 (2009).
19. Masaki, A. *et al.* Human T-cell lymphotropic/leukemia virus type 1 (HTLV-1) Tax-specific T-cell exhaustion in HTLV-1-infected individuals. *Cancer Sci* **109**, 2383–2390 (2018).
20. Toulza, F. *et al.* FoxP3+ regulatory T cells are distinct from leukemia cells in HTLV-1-associated adult T-cell leukemia. *Int J Cancer* **125**, 2375–2382 (2009).
21. Macatonia, S. E., Cruickshank, J. K., Rudge, P. & Knight, S. C. Dendritic Cells from Patients with Tropical Spastic Paraparesis Are Infected with HTLV-1 and Stimulate Autologous Lymphocyte Proliferation. *AIDS Research and Human Retroviruses* **8**, 1699–1706 (1992).
22. Makino, M., Shimokubo, S., Wakamatsu, S. I., Izumo, S. & Baba, M. The role of human T-lymphotropic virus type 1 (HTLV-1)-infected dendritic cells in the development of HTLV-1-associated myelopathy/tropical spastic paraparesis. *J Virol* **73**, 4575–4581 (1999).
23. Makino, M., Wakamatsu, S., Shimokubo, S., Arima, N. & Baba, M. Production of Functionally Deficient Dendritic Cells from HTLV-I-Infected Monocytes: Implications for the Dendritic Cell Defect in Adult T Cell Leukemia. *Virology* **274**, 140–148 (2000).
24. Rizkallah, G. *et al.* Dendritic cell maturation, but not type I interferon exposure, restricts infection by HTLV-1, and viral transmission to T-cells. *PLoS Pathog* **13**, e1006353 (2017).
25. Pique, C. & Jones, K. S. Pathways of cell-cell transmission of HTLV-1. *Front. Microbio.* **3**, (2012).
26. Nascimento, C. R. *et al.* Monocytes from HTLV-1-infected patients are unable to fully mature into dendritic cells. *Blood* **117**, 489–499 (2011).

27. Roche, P. A. & Furuta, K. The ins and outs of MHC class II-mediated antigen processing and presentation. *Nat Rev Immunol* **15**, 203–216 (2015).
28. Wijdeven, R. H. *et al.* Chemical and genetic control of IFN $\gamma$ -induced MHCII expression. *EMBO Rep* **19**, e45553 (2018).
29. Watts, C. The exogenous pathway for antigen presentation on major histocompatibility complex class II and CD1 molecules. *Nat Immunol* **5**, 685–692 (2004).
30. Veerappan Ganesan, A. P. & Eisenlohr, L. C. The elucidation of non-classical MHC class II antigen processing through the study of viral antigens. *Current Opinion in Virology* **22**, 71–76 (2017).
31. Jacobson, S. *et al.* Recognition of Intracellular Measles Virus Antigens by HLA Class II Restricted Measles Virus-Specific Cytotoxic T Lymphocytes. *Ann NY Acad Sci* **540**, 352–353 (1988).
32. Sekaly, R. P. *et al.* Antigen presentation to HLA class II-restricted measles virus-specific T-cell clones can occur in the absence of the invariant chain. *Proc. Natl. Acad. Sci. U.S.A.* **85**, 1209–1212 (1988).
33. Eisenlohr, L. C. & Hackett, C. J. Class II major histocompatibility complex-restricted T cells specific for a virion structural protein that do not recognize exogenous influenza virus. Evidence that presentation of labile T cell determinants is favored by endogenous antigen synthesis. *Journal of Experimental Medicine* **169**, 921–931 (1989).
34. Jaraquemada, D., Marti, M. & Long, E. O. An endogenous processing pathway in vaccinia virus-infected cells for presentation of cytoplasmic antigens to class II-restricted T cells. *Journal of Experimental Medicine* **172**, 947–954 (1990).
35. Nuchtern, J. G., Biddison, W. E. & Klausner, R. D. Class II MHC molecules can use the endogenous pathway of antigen presentation. *Nature* **343**, 74–76 (1990).
36. Thiele, F. *et al.* Modified Vaccinia Virus Ankara-Infected Dendritic Cells Present CD4 + T-Cell Epitopes by Endogenous Major Histocompatibility Complex Class II Presentation Pathways. *J Virol* **89**, 2698–2709 (2015).
37. Tsuji, T. *et al.* Heat shock protein 90-mediated peptide-selective presentation of cytosolic tumor antigen for direct recognition of tumors by CD4(+) T cells. *J Immunol* **188**, 3851–3858 (2012).
38. Reith, W., LeibundGut-Landmann, S. & Waldburger, J.-M. Regulation of MHC class II gene expression by the class II transactivator. *Nat Rev Immunol* **5**, 793–806 (2005).
39. Bakke, O. & Dobberstein, B. MHC class II-associated invariant chain contains a sorting signal for endosomal compartments. *Cell* **63**, 707–716 (1990).
40. Lotteau, V. *et al.* Intracellular transport of class II MHC molecules directed by invariant chain. *Nature* **348**, 600–605 (1990).
41. Neefjes, J. J., Stollorz, V., Peters, P. J., Geuze, H. J. & Ploegh, H. L. The biosynthetic pathway of MHC class II but not class I molecules intersects the endocytic route. *Cell* **61**, 171–183 (1990).
42. Roche, P. A., Marks, M. S. & Cresswell, P. Formation of a nine-subunit complex by HLA class II glycoproteins and the invariant chain. *Nature* **354**, 392–394 (1991).
43. Riese, R. J. *et al.* Essential role for cathepsin S in MHC class II-associated invariant chain processing and peptide loading. *Immunity* **4**, 357–366 (1996).
44. Nakagawa, T. *et al.* Cathepsin L: critical role in Ii degradation and CD4 T cell selection in the thymus. *Science* **280**, 450–453 (1998).
45. Shi, G. P. *et al.* Role for cathepsin F in invariant chain processing and major histocompatibility complex class II peptide loading by macrophages. *J Exp Med* **191**, 1177–1186 (2000).
46. Manoury, B. *et al.* Asparagine endopeptidase can initiate the removal of the MHC class II invariant chain chaperone. *Immunity* **18**, 489–498 (2003).
47. Roche, P. A. & Cresswell, P. Proteolysis of the class II-associated invariant chain generates a peptide binding site in intracellular HLA-DR molecules. *Proc Natl Acad Sci U S A* **88**, 3150–3154 (1991).
48. Bijlmakers, M. J., Benaroch, P. & Ploegh, H. L. Assembly of HLA DR1 molecules translated in vitro: binding of peptide in the endoplasmic reticulum precludes association with invariant chain. *The EMBO Journal* **13**, 2699–2707 (1994).
49. Busch, R., Cloutier, I., Sékaly, R. P. & Hämmerling, G. J. Invariant chain protects class II histocompatibility antigens from binding intact polypeptides in the endoplasmic reticulum. *EMBO J* **15**, 418–428 (1996).
50. Rudensky, A., Preston-Hurlburt, P., Hong, S. C., Barlow, A. & Janeway, C. A. Sequence analysis of peptides bound to MHC class II molecules. *Nature* **353**, 622–627 (1991).
51. Unanue, E. R., Turk, V. & Neefjes, J. Variations in MHC Class II Antigen Processing and Presentation in Health and Disease. *Annu. Rev. Immunol.* **34**, 265–297 (2016).
52. Morris, P. *et al.* An essential role for HLA-DM in antigen presentation by class II major histocompatibility molecules. *Nature* **368**, 551–554 (1994).
53. Sanderson, F. *et al.* Accumulation of HLA-DM, a regulator of antigen presentation, in MHC class II compartments. *Science* **266**, 1566–1569 (1994).

54. Denzin, L. K. & Cresswell, P. HLA-DM induces CLIP dissociation from MHC class II alpha beta dimers and facilitates peptide loading. *Cell* **82**, 155–165 (1995).
55. Thibodeau, J., Moulefera, M. A. & Balthazard, R. On the structure-function of MHC class II molecules and how single amino acid polymorphisms could alter intracellular trafficking. *Hum Immunol* **80**, 15–31 (2019).
56. Akagi, T., Ono, H. & Shimotohno, K. Characterization of T cells immortalized by Tax1 of human T-cell leukemia virus type 1. *Blood* **86**, 4243–4249 (1995).
57. Sun, S.-C. & Yamaoka, S. Activation of NF- $\kappa$ B by HTLV-I and implications for cell transformation. *Oncogene* **24**, 5952–5964 (2005).
58. Kfoury, Y. *et al.* The Multifaceted Oncoprotein Tax. in *Advances in Cancer Research* vol. 113 85–120 (Elsevier, 2012).
59. Chen, J. & Chen, Z. J. Regulation of NF- $\kappa$ B by ubiquitination. *Current Opinion in Immunology* **25**, 4–12 (2013).
60. Kovalenko, A. & Wallach, D. If the Prophet Does Not Come to the Mountain: Dynamics of Signaling Complexes in NF- $\kappa$ B Activation. *Molecular Cell* **22**, 433–436 (2006).
61. Wu, C.-J. & Ashwell, J. D. NEMO recognition of ubiquitinated Bcl10 is required for T cell receptor-mediated NF- $\kappa$ B activation. *Proc. Natl. Acad. Sci. U.S.A.* **105**, 3023–3028 (2008).
62. Ordureau, A. *et al.* The IRAK-catalysed activation of the E3 ligase function of Pellino isoforms induces the Lys63-linked polyubiquitination of IRAK1. *Biochemical Journal* **409**, 43–52 (2008).
63. Lavorgna, A. & Harhaj, E. W. Regulation of HTLV-1 tax stability, cellular trafficking and NF- $\kappa$ B activation by the ubiquitin-proteasome pathway. *Viruses* **6**, 3925–3943 (2014).
64. Harhaj, E. W. & Sun, S.-C. IKK $\gamma$  Serves as a Docking Subunit of the I $\kappa$ B Kinase (IKK) and Mediates Interaction of IKK with the Human T-cell Leukemia Virus Tax Protein. *Journal of Biological Chemistry* **274**, 22911–22914 (1999).
65. Chu, Z.-L., Shin, Y.-A., Yang, J.-M., DiDonato, J. A. & Ballard, D. W. IKK $\gamma$  Mediates the Interaction of Cellular I $\kappa$ B Kinases with the Tax Transforming Protein of Human T Cell Leukemia Virus Type 1. *Journal of Biological Chemistry* **274**, 15297–15300 (1999).
66. Jin, D.-Y., Giordano, V., Kibler, K. V., Nakano, H. & Jeang, K.-T. Role of Adapter Function in Oncoprotein-mediated Activation of NF- $\kappa$ B. *Journal of Biological Chemistry* **274**, 17402–17405 (1999).
67. Shembade, N., Harhaj, N. S., Liebl, D. J. & Harhaj, E. W. Essential role for TAX1BP1 in the termination of TNF- $\alpha$ -, IL-1- and LPS-mediated NF- $\kappa$ B and JNK signaling. *EMBO J* **26**, 3910–3922 (2007).
68. Good, L. & Sun, S.-C. Persistent Activation of NF- $\kappa$ B/Rel by Human T-Cell Leukemia Virus Type 1 Tax Involves Degradation of I $\kappa$ B $\beta$ . *VIROL.* **70**, (1996).
69. Huang, J., Ren, T., Guan, H., Jiang, Y. & Cheng, H. HTLV-1 Tax Is a Critical Lipid Raft Modulator That Hijacks I $\kappa$ B Kinases to the Microdomains for Persistent Activation of NF- $\kappa$ B. *Journal of Biological Chemistry* **284**, 6208–6217 (2009).
70. Kfoury, Y. *et al.* Ubiquitylated Tax targets and binds the IKK Signalingosome at the centrosome. *Oncogene* **27**, 1665–1676 (2008).
71. Chun, A. C. *et al.* Coiled-coil motif as a structural basis for the interaction of HTLV type 1 Tax with cellular cofactors. *AIDS Res Hum Retroviruses* **16**, 1689–1694 (2000).
72. Chin, K.-T., Chun, A. C. S., Ching, Y.-P., Jeang, K.-T. & Jin, D.-Y. Human T-cell leukemia virus oncoprotein tax represses nuclear receptor-dependent transcription by targeting coactivator TAX1BP1. *Cancer Res* **67**, 1072–1081 (2007).
73. Journo, C. *et al.* NRP/Optineurin Cooperates with TAX1BP1 to potentiate the activation of NF- $\kappa$ B by human T-lymphotropic virus type 1 tax protein. *PLoS Pathog* **5**, e1000521 (2009).
74. De Valck, D. *et al.* The zinc finger protein A20 interacts with a novel anti-apoptotic protein which is cleaved by specific caspases. *Oncogene* **18**, 4182–4190 (1999).
75. Wertz, I. E. *et al.* De-ubiquitination and ubiquitin ligase domains of A20 downregulate NF- $\kappa$ B signalling. *Nature* **430**, 694–699 (2004).
76. Shembade, N. *et al.* The E3 ligase Itch negatively regulates inflammatory signaling pathways by controlling the function of the ubiquitin-editing enzyme A20. *Nat Immunol* **9**, 254–262 (2008).
77. Shembade, N., Parvatiyar, K., Harhaj, N. S. & Harhaj, E. W. The ubiquitin-editing enzyme A20 requires RNF11 to downregulate NF- $\kappa$ B signalling. *EMBO J* **28**, 513–522 (2009).
78. Shembade, N., Pujari, R., Harhaj, N. S., Abbott, D. W. & Harhaj, E. W. The kinase IKK $\alpha$  inhibits activation of the transcription factor NF- $\kappa$ B by phosphorylating the regulatory molecule TAX1BP1. *Nat Immunol* **12**, 834–843 (2011).
79. Schwob, A. *et al.* SQSTM-1/p62 potentiates HTLV-1 Tax-mediated NF- $\kappa$ B activation through its ubiquitin binding function. *Sci Rep* **9**, 16014 (2019).
80. Hayden, M. S. & Ghosh, S. Shared Principles in NF- $\kappa$ B Signaling. *Cell* **132**, 344–362 (2008).
81. Iwasaki, A. & Medzhitov, R. Control of adaptive immunity by the innate immune system. *Nat Immunol* **16**, 343–353 (2015).

82. Mostoller, K., Norbury, C. C., Jain, P. & Wigdahl, B. Human T-cell leukemia virus type I Tax induces the expression of dendritic cell markers associated with maturation and activation. *J Neurovirol* **10**, 358–371 (2004).
83. Jain, P. *et al.* DC-SIGN Mediates Cell-Free Infection and Transmission of Human T-Cell Lymphotropic Virus Type 1 by Dendritic Cells. *J Virol* **83**, 10908–10921 (2009).
84. Kirkin, V. History of the Selective Autophagy Research: How Did It Begin and Where Does It Stand Today? *J Mol Biol* **432**, 3–27 (2020).
85. Sarango, G. *et al.* The Autophagy Receptor TAX1BP1 ( T6BP ) improves antigen presentation by MHC-II molecules. *EMBO Reports* **23**, (2022).
86. Tomazin, R. *et al.* Cytomegalovirus US2 destroys two components of the MHC class II pathway, preventing recognition by CD4+ T cells. *Nat Med* **5**, 1039–1043 (1999).
87. Neumann, J., Eis-Hübinger, A. M. & Koch, N. Herpes simplex virus type 1 targets the MHC class II processing pathway for immune evasion. *J Immunol* **171**, 3075–3083 (2003).
88. Waisner, H. & Kalamvoki, M. The ICP0 Protein of Herpes Simplex Virus 1 (HSV-1) Downregulates Major Autophagy Adaptor Proteins Sequestosome 1 and Optineurin during the Early Stages of HSV-1 Infection. *J Virol* **93**, e01258-19 (2019).
89. Petkova, D. S. *et al.* Distinct Contributions of Autophagy Receptors in Measles Virus Replication. *Viruses* **9**, 123 (2017).
90. Verstrepen, L., Verhelst, K., Carpentier, I. & Beyaert, R. TAX1BP1, a ubiquitin-binding adaptor protein in innate immunity and beyond. *Trends in Biochemical Sciences* S096800041100048X (2011) doi:10.1016/j.tibs.2011.03.004.
91. Moris, A. *et al.* Dendritic cells and HIV-specific CD4+ T cells: HIV antigen presentation, T-cell activation, and viral transfer. *Blood* **108**, 1643–1651 (2006).
92. Coulon, P.-G. *et al.* HIV-Infected Dendritic Cells Present Endogenous MHC Class II-Restricted Antigens to HIV-Specific CD4+ T Cells. *J Immunol* **197**, 517–532 (2016).
93. Álvaro-Benito, M., Morrison, E., Abualrous, E. T., Kuroпка, B. & Freund, C. Quantification of HLA-DM-Dependent Major Histocompatibility Complex of Class II Immunopeptidomes by the Peptide Landscape Antigenic Epitope Alignment Utility. *Front Immunol* **9**, 872 (2018).
94. Reynisson, B., Alvarez, B., Paul, S., Peters, B. & Nielsen, M. NetMHCpan-4.1 and NetMHCIIpan-4.0: improved predictions of MHC antigen presentation by concurrent motif deconvolution and integration of MS MHC eluted ligand data. *Nucleic Acids Res* **48**, W449–W454 (2020).
95. Chapman, H. A. Endosomal proteases in antigen presentation. *Curr Opin Immunol* **18**, 78–84 (2006).
96. Muntasell, A. *et al.* Dissection of the HLA-DR4 peptide repertoire in endocrine epithelial cells: strong influence of invariant chain and HLA-DM expression on the nature of ligands. *J Immunol* **173**, 1085–1093 (2004).
97. Nasr, R. *et al.* Tax ubiquitylation and sumoylation control critical cytoplasmic and nuclear steps of NF-κB activation. *Blood* **107**, 4021–4029 (2006).
98. Kfoury, Y. *et al.* Tax ubiquitylation and SUMOylation control the dynamic shuttling of Tax and NEMO between Ubc9 nuclear bodies and the centrosome. *Blood* **117**, 190–199 (2011).
99. Ramachandra, L., Kovats, S., Eastman, S. & Rudensky, A. Y. Variation in HLA-DM expression influences conversion of MHC class II alpha beta: class II-associated invariant chain peptide complexes to mature peptide-bound class II alpha beta dimers in a normal B cell line. *J Immunol* **156**, 2196–2204 (1996).
100. Neeffjes, J., Jongsma, M. M. L. & Berlin, I. Stop or Go? Endosome Positioning in the Establishment of Compartment Architecture, Dynamics, and Function. *Trends Cell Biol* **27**, 580–594 (2017).
101. Johnson, D. E., Ostrowski, P., Jaumouillé, V. & Grinstein, S. The position of lysosomes within the cell determines their luminal pH. *Journal of Cell Biology* **212**, 677–692 (2016).
102. Kourjian, G. *et al.* HIV Protease Inhibitor-Induced Cathepsin Modulation Alters Antigen Processing and Cross-Presentation. *The Journal of Immunology* **196**, 3595–3607 (2016).
103. Vaithilingam, A. *et al.* A simple methodology to assess endolysosomal protease activity involved in antigen processing in human primary cells. *BMC Cell Biol* **14**, 35 (2013).
104. Neeffjes, J., Jongsma, M. L. M., Paul, P. & Bakke, O. Towards a systems understanding of MHC class I and MHC class II antigen presentation. *Nat Rev Immunol* **11**, 823–836 (2011).
105. Yoshimura, S., Bondeson, J., Foxwell, B. M. J., Brennan, F. M. & Feldmann, M. Effective antigen presentation by dendritic cells is NF-κB dependent: coordinate regulation of MHC, co-stimulatory molecules and cytokines. *International Immunology* **13**, 675–683 (2001).
106. Lee, K.-W., Lee, Y., Kim, D.-S. & Kwon, H.-J. Direct role of NF-κB activation in Toll-like receptor-triggered HLA-DRA expression. *Eur. J. Immunol.* **36**, 1254–1266 (2006).
107. Hang, D. T. T., Song, J.-Y., Kim, M.-Y., Park, J.-W. & Shin, Y.-K. Involvement of NF-κB in changes of IFN-γ-induced CIITA/MHC-II and iNOS expression by influenza virus in macrophages. *Molecular Immunology* **48**, 1253–1262 (2011).

108. Forlani, G., Abdallah, R., Accolla, R. S. & Tosi, G. The MHC-II transactivator CIITA, a restriction factor against oncogenic HTLV-1 and HTLV-2 retroviruses: similarities and differences in the inhibition of Tax-1 and Tax-2 viral transactivators. *Front Microbiol* **4**, 234 (2013).
109. Mogensen, T. H. IRF and STAT Transcription Factors - From Basic Biology to Roles in Infection, Protective Immunity, and Primary Immunodeficiencies. *Front Immunol* **9**, 3047 (2018).
110. Johnson, J. M. *et al.* Free Major Histocompatibility Complex Class I Heavy Chain Is Preferentially Targeted for Degradation by Human T-Cell Leukemia/Lymphotropic Virus Type 1 p12<sup>1</sup> Protein. *J Virol* **75**, 6086–6094 (2001).

## Figure legends

### Figure 1. Tax expression in APC leads to a decrease in antigen-specific CD4<sup>+</sup> T cell activation.

A TAX1BP1, OPTN, p62 and Tax expressions were assessed using confocal microscopy. HeLa-CIITA cells were transfected with control and Tax-His-encoding plasmids. 24 h post-treatment, TAX1BP1 and Tax-His were detected using anti-TAX1BP1 and anti-His antibodies, respectively, and revealed with species-specific secondary antibodies. Nuclei were stained using DAPI. The results are representative of at least 2 independent experiments.

B Schematic representation of the experiment. HeLa-CIITA cells were co-transfected with a plasmid encoding Gag and with control or Tax-His-encoding plasmids. 24 h post-DNA transfection, HeLa-CIITA cells were co-cultured with antigen-specific CD4<sup>+</sup>T cells and T cell activation was assessed using IFN $\gamma$ -ELISPOT. D: day; TCR: T cell receptor.

C Monitoring of Gag-specific CD4<sup>+</sup>T cell activation. HeLa-CIITA cells were treated as indicated above. Left panel, a representative experiment is shown ( $\pm$ SD of three technical replicates). Middle panel, three biological replicates are combined and presented as mean percentage ( $\pm$ SD). The y-axis represents the relative percentage of IFN $\gamma$  spots reported to the secretion of IFN $\gamma$  by the CD4<sup>+</sup>T cell clones incubated with the CTRL-treated HeLa-CIITA and set to 100%. 5,000 T cell clones were seeded per well in technical triplicates. Right panel, influence of Tax expression on peptide presentation by HeLa-CIITA cells. The cognate peptide was added exogenously (gag2, 1  $\mu$ g/mL) on cDNA-treated cells (2 h, 37°C), washed and T cell activation monitored using IFN $\gamma$ -ELISPOT. 1,000 T cell clones were seeded per well in technical triplicates. Three biological replicates are combined and presented as mean percentage ( $\pm$  SD).

D Left panel, as in Fig 1C, using different doses of Tax and control plasmids. Left panel, a representative experiment is shown ( $\pm$ SD of three technical replicates). The cognate peptide was added exogenously (gag2, 1  $\mu$ g/mL) on cDNA-treated cells (2 h, 37°C), washed and T cell activation monitored using IFN $\gamma$ -ELISPOT. A representative experiment is shown ( $\pm$ SD of three technical replicates).

Data information: : For all ELISPOT experiments, the background secretions of IFN $\gamma$  by CD4<sup>+</sup>T cells co-cultured with mock-treated HeLa-CIITA cells were used as negative controls and subtracted. Scale bars: 10  $\mu$ m. Ctrl-Control.

Mann-Whitney's tests; \*:  $p < 0.05$ ; \*\*:  $p < 0.002$ ; \*\*\*:  $p < 0.0003$ ; #:  $p > 0.05$ .

### Figure 2. Tax expression does not significantly influence MHC-II molecule expression levels but alters the MHC-II immunopeptidome.

A MHC-II expression levels was assessed using Western Blot. HeLa-CIITA cells were transfected with Ctrl or Tax-encoding cDNAs. 24h h post-transfection , HLA-DR and actin were detected using indicated antibodies. Top panel, a representative Western Blot experiment is shown. Lower panel, expression levels of two biological replicates were quantified using ImageJ and are presented as mean ratios ( $\pm$ SD) of HLA-DR to actin used as control housekeeping gene expression.

B Tax influence on expression levels of MHC-II molecules was assessed using flow cytometry. HeLa-CIITA cells were transfected with Ctrl or Tax-encoding cDNAs. 24h h post-transfection, Tax-negative and Tax-positive cells were detected using indicated antibodies (Left panel).Top right panels, HLA-DR molecules were detected using L243 and TU36 antibodies that recognize mature (HLA  $\alpha\beta$  heterodimers) and both mature and immature (HLA  $\alpha\beta$  and  $\alpha\beta$ -li complexes), respectively, in Tax-negative (Ctrl) and Tax-positive (Tax) cells. One representative experiment is presented as histogram (n=1). MFI of one representative experiment is presented as histogram (Lower right panel).

C As previously, HeLa-CIITA cells were transfected with Ctrl and Tax-encoding plasmids. 24h post-treatment, cells were lysed and MHC-II molecules were immunoprecipitated using T $\ddot{U}$ 39 antibody and ligands sequenced using mass spectrometry (LC-MS/MS). The number of sequenced peptides are presented for each condition and the percentage of exclusive or shared peptides among all sequenced peptides is presented in Venn diagrams.

D,E Quantitative (D) and qualitative (E) assessment of Tax influence on the MHC-II immunopeptidome. Data from (C) were submitted to Plateau algorithm to allow identification and label-free quantification of shared consensus core epitopes. (D) Volcano plots showing the log<sub>2</sub> fold change of core epitope distribution between Tax-expressing and control cells. The total number (n) of core epitopes and the number of epitopes with significant fold change are indicated. (E) Relative binding affinities, presented as pie charts, of exclusive core epitopes identified by PLAtEAU in Ctrl and Tax conditions (indicated in brackets). NetMHCIpan was used to predict the relative affinities to DRβ1\*0102 and DQα\*10102-DQβ\*10501 expressed by HeLa-CIITA cells. The results are presented as stated from NetMHCIpan analysis as strong (for strong binders), weak (for weak binders), and no score (epitopes for which no binding score could be determined).

### Figure 3. Tax expression affects the nature of the MIIC.

A MHC-II and Tax expressions were assessed using confocal microscopy. HeLa-CIITA cells were transfected with control and Tax-encoding plasmids. 24 h post treatment, MHC-II and Tax-His were detected using anti-MHC-II and anti-His antibodies, respectively, and revealed with species-specific secondary antibodies. Nuclei were stained using DAPI.

B Quantitative analysis using in-house ImageJ script displaying distance of each MHC-II+ vesicles to the nucleus and the membrane. The ratio between the distance to the nucleus and the sum of distances to the nucleus and membrane are shown. At least 2000 vesicles from 20 cells corresponding to two biological replicates were analyzed.

C As in (A) HLA-DM and Tax expressions were analyzed.

D The localization of HLA-DM+ vesicles was quantified as in B. At least 3000 vesicles from 30 cells corresponding to three biological replicates were analyzed.

E Lamp-1, HLA-DM and Tax expressions were assessed using confocal microscopy. Co-localization of Lamp-1+ vesicles with HLA-DM+ puncta was analyzed using JACoP plugin (scales starts at 0 and above 0.5 the % of co-localization is considered significant); a number of vesicles >2000 from one biological replicate were analyzed corresponding to 20 cells.

Scale bars, 10µm. Ctrl: control. Mann-Whitney's tests; \*: p<0.05; \*\*: p<0.002; \*\*\*: p<0.0003; #: p>0.05.

### Figure 4. Tax expression impacts cathepsin activity without altering li and HLA-DM expression levels.

A Evaluation of HLA-DM expression levels. HLA-DM and actin expression levels were assessed by WB using anti-HLA-DMβ and anti-actin antibodies. Top panel, a representative Western Blot experiment is shown. Lower panel, expression levels of two biological replicates are presented as mean ratios (± SD) to actin used as control housekeeping gene expression.

B Invariant chain li expression was assessed using Western Blot. HeLa-CIITA cells were transfected with control and Tax-encoding plasmids. 24h post-treatment, the lip33 li isoform, a degradation product (lip16) and actin were detected using anti-li and anti-actin antibodies. Left panel, a representative Western Blot experiment is shown. Right panel, expression levels of three biological replicates are presented as mean ratios (± SD) of li to actin used as control housekeeping gene expression.

C Assessment of cathepsin activity. As previously, HeLa-CIITA cells were transfected with control and Tax-encoding plasmids. 24h post-treatment, the activities of cathepsins S, B and L present in total cell lysates were assayed using cathepsin-specific fluorogenic substrates. Fluorescence of two technical replicates (± SD) was measured and plotted over time. A representative experiment is shown.

D Analysis of initial substrate degradation. HeLa-CIITA cells were treated as in (C). Initial slopes of fluorescence over time curve of two biological replicates are presented as mean fluorescence (± SD) normalized to control.

Ctrl: control. Mann-Whitney's tests; \*p<0.05; #p>0.05.

**Figure 5. Interaction with OPTN is required for Tax-mediated inhibition of antigen presentation to CD4<sup>+</sup>T cells.**

A Silencing SARs expression. 48 h post-transfection of HeLa-CIITA cells with siRNAs targeting TAX1BP1, OPTN, and p62; SAR expression was analyzed using Western Blot. Actin was used as control. The results are representative of at least 3 independent experiments and correspond to AR expression levels of the experiment in Fig 5B.

B Monitoring the role of SARs on the effect of Tax on Gag-specific CD4<sup>+</sup>T cell activation. 24h post-transfection with siRNAs, cells were co-transfected with a plasmid encoding Gag and with control or Tax-His-encoding plasmids. 24 h post-DNA transfection, HeLa-CIITA cells were co-cultured with Gag-specific CD4<sup>+</sup>T cells and T cell activation was assessed using IFN $\gamma$ -ELISPOT. Results are combined and presented as mean percentage ( $\pm$ SD). The results are representative of two or three independent experiments and shown as mean percentages of control.

C Assessing the role of Tax interaction with OPTN on Tax-mediated effect on CD4<sup>+</sup>T cell activation. HeLa-CIITA cells were co-transfected with a plasmid encoding Gag and with plasmids encoding different mutants of Tax. 24 h post-DNA transfection, HeLa-CIITA cells were co-cultured with Gag-specific CD4<sup>+</sup>T cells and T cell activation was assessed using IFN $\gamma$ -ELISPOT. The results are representative of three independent experiments and shown as mean percentages of control.

Ctrl: control; siCTRL: control siRNA. Mann-Whitney's tests; \*p<0.05; #p>0.05.



## Supplemental material

### **Figure S1. The transfection of Tax-encoding plasmid influenced neither the cell viability nor antigen transfection efficiency.**

A and B Analysis of cell viability and transfection efficiency using flow cytometry.

A Gating strategy: left panels: FSC-A: forward-scatter; SSC-A: side-scatter; middle panels: staining of living cells using a viability dye; right panels: staining of Gag+ cells and Tax-His+ using anti-Gag and anti-His antibodies intracellular staining.

B and C Percentage of living and Gag+ cells in control and Tax-expressing conditions, left and right panel respectively, analyzed 24h post-treatment, prior co-culture with Gag-specific T cells. Results of three independent experiments are presented as mean ( $\pm$  SD). Ctrl: control. Mann-Whitney's tests; \* $p < 0.05$ ; # $p > 0.05$ .

### **Figure S2. Tax expression influences EEA1+ and CD63+ vesicle cellular localization**

A EEA1 expression was assessed using confocal microscopy. HeLa-CIITA cells were transfected with control and Tax-encoding plasmids. 24h post-treatment, EEA1 and Tax were detected using specific antibodies and fluorescent secondary antibodies. Nuclei were stained using DAPI.

B Quantitative analysis using in-house ImageJ script displaying distance of each EEA1+ vesicles to the nucleus and the membrane. The ratio between the distance to the nucleus and the sum of distances to the nucleus and membrane are shown. At least 2000 vesicles from 20 cells corresponding to one biological replicate were analyzed.

C As in (A) CD63 and Tax expressions were analyzed.

D Quantitative analysis using in-house ImageJ script displaying distance of each CD63+ vesicles to the nucleus and the membrane. The ratio between the distance to the nucleus and the sum of distances to the nucleus and membrane are shown. At least 2000 vesicles from 20 cells corresponding to one biological replicate were analyzed.

E-I Effect of Tax on the expression levels of the various vesicular markers. As in A, HeLa-CIITA cells were transfected with control and Tax-encoding plasmids. 24h post-treatment, cells were fixed and labeled and the MFI of the indicated markers were analyzed. E MHC-II, at least 170 cells corresponding to 5 independent experiments were analyzed. F MHC-II, at least 20 cells corresponding to 2 independent experiments were analyzed. G HLA-DM, at least 30 cells corresponding to 3 independent experiments were analyzed. F Lamp-1, at least 20 cells corresponding to 1 independent experiment were analyzed. H EEA1, at least 20 cells corresponding to 1 independent experiment were analyzed. I CD63, at least 20 cells corresponding to 1 independent experiment were analyzed. Scale bars, 10 $\mu$ m. Ctrl: control. Mann-Whitney's tests; \*:  $p < 0.05$ ; \*\*:  $p < 0.002$ ; \*\*\*:  $p < 0.0003$ ; #:  $p > 0.05$ .

### **Figure S3. The transfection of siRNAs and Tax-encoding plasmid influenced neither the cell viability nor transfection efficiency.**

A Percentage of living cells in control cells and cells silenced for SARs expression and transfected with control or Tax-encoding plasmids, analyzed 24h post-treatment, prior co-culture with Gag-specific T cells.

B Percentage of Gag+, Gag+/Tax+ and Tax+ cells in control cells and cells silenced for SARs expression and transfected with control or Tax-encoding plasmids, analyzed 24h post-treatment, prior co-culture with Gag-specific T cells.

Ctrl: control. Kruskal-Wallis tests; \*:  $p < 0.05$ ; \*\*:  $p < 0.002$ ; \*\*\*:  $p < 0.0003$ ; #:  $p > 0.05$ .

**Figure 1**

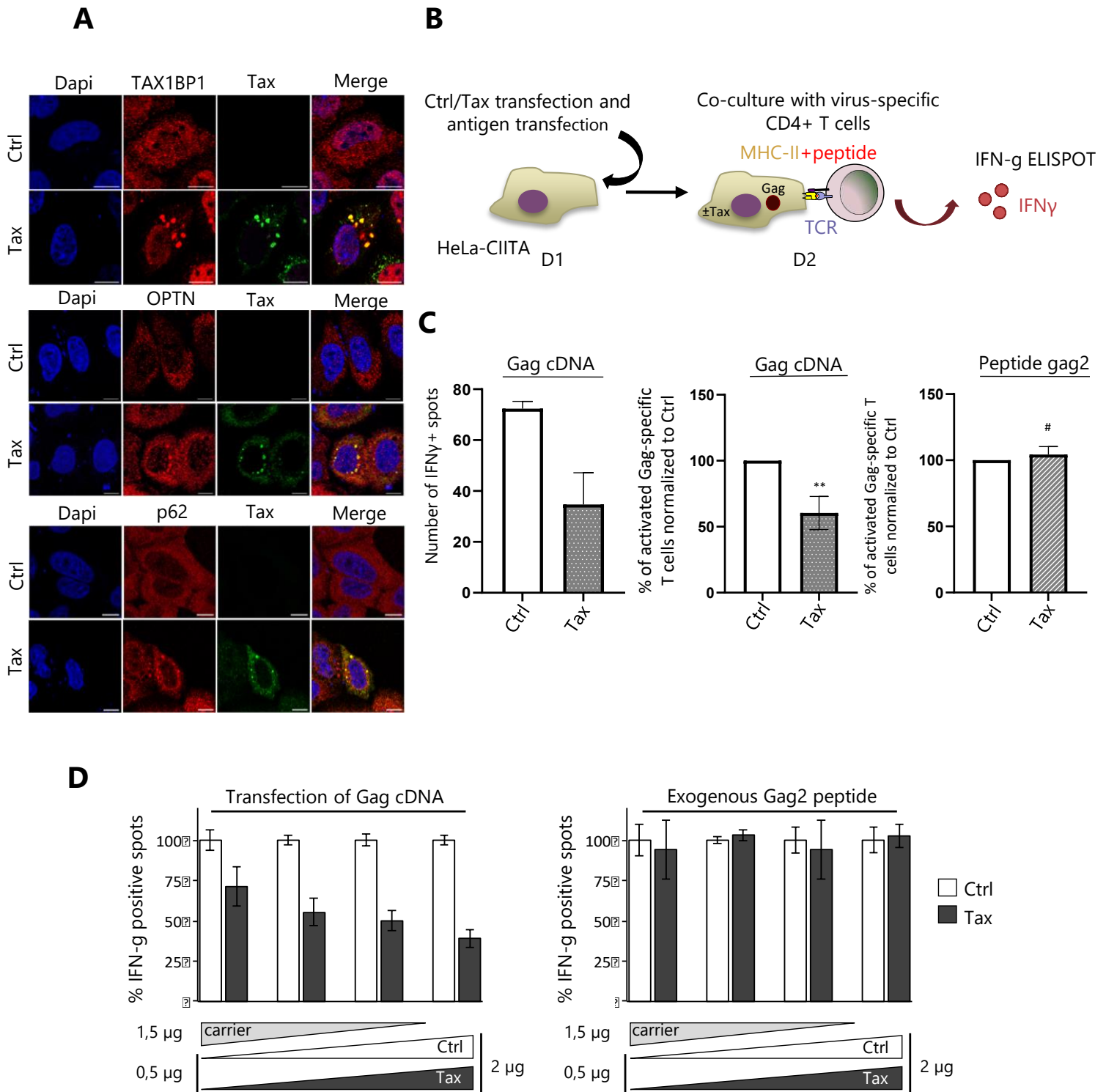


**Figure 2**

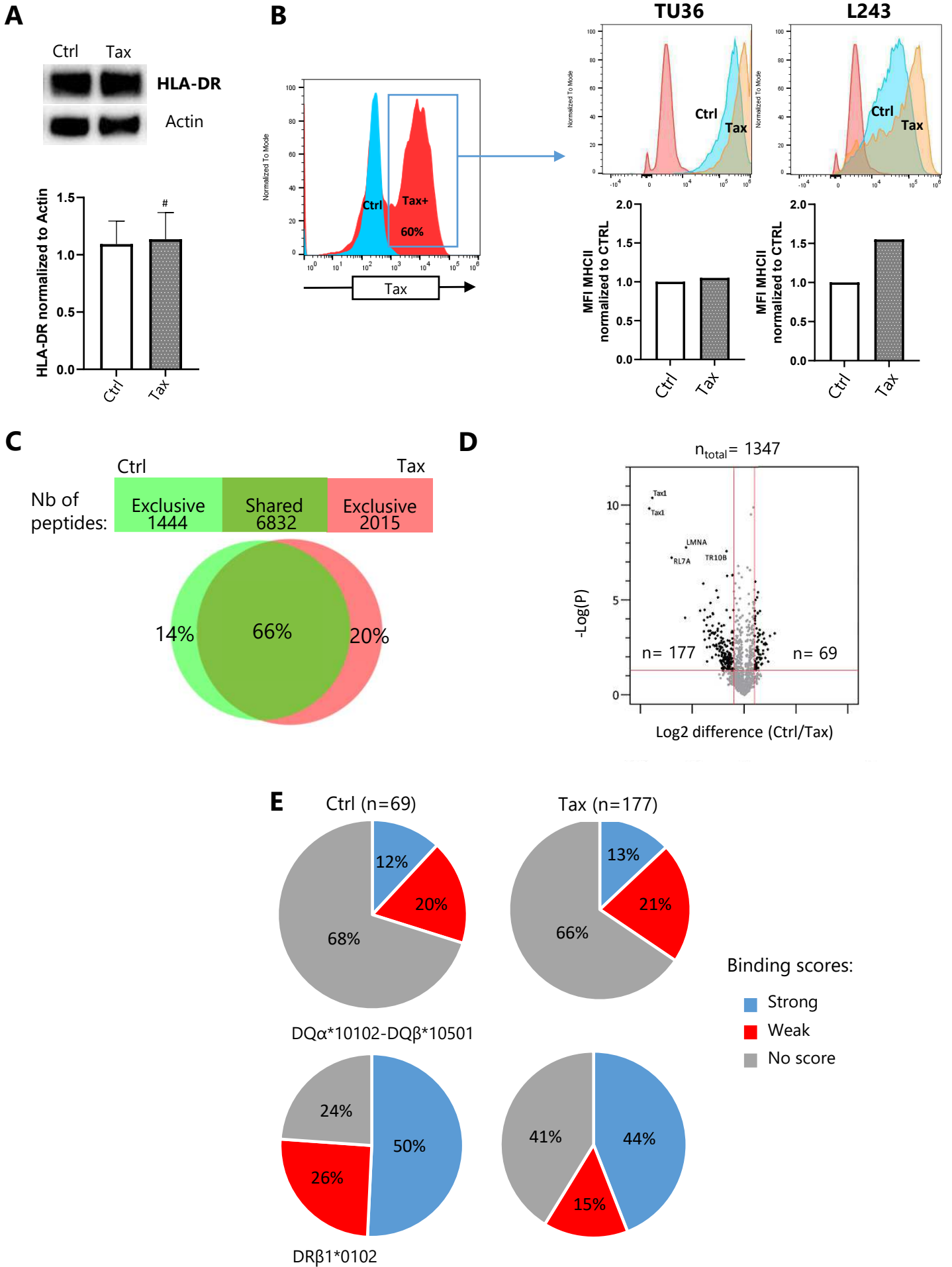


**Figure 3**

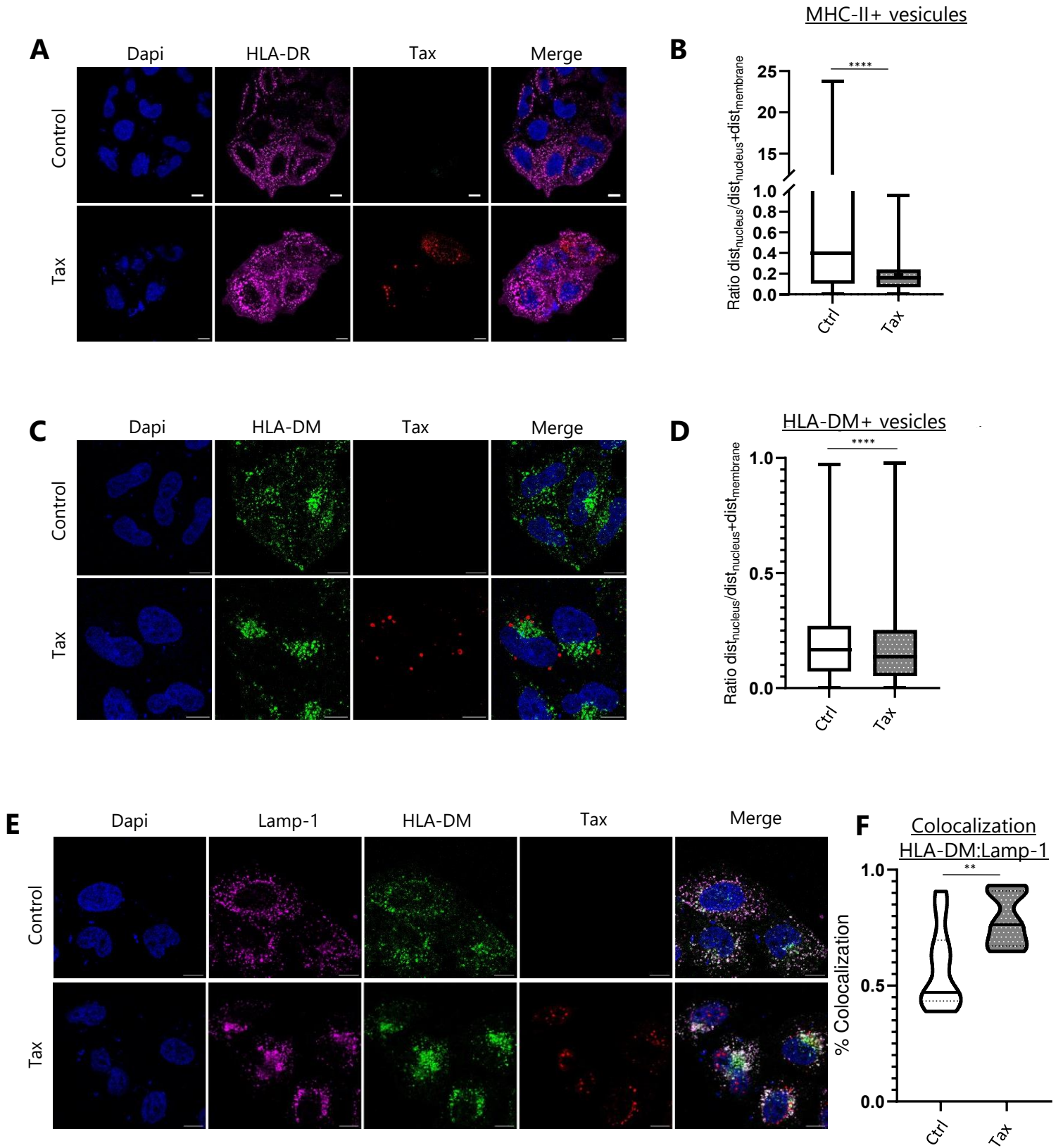


**Figure 4**

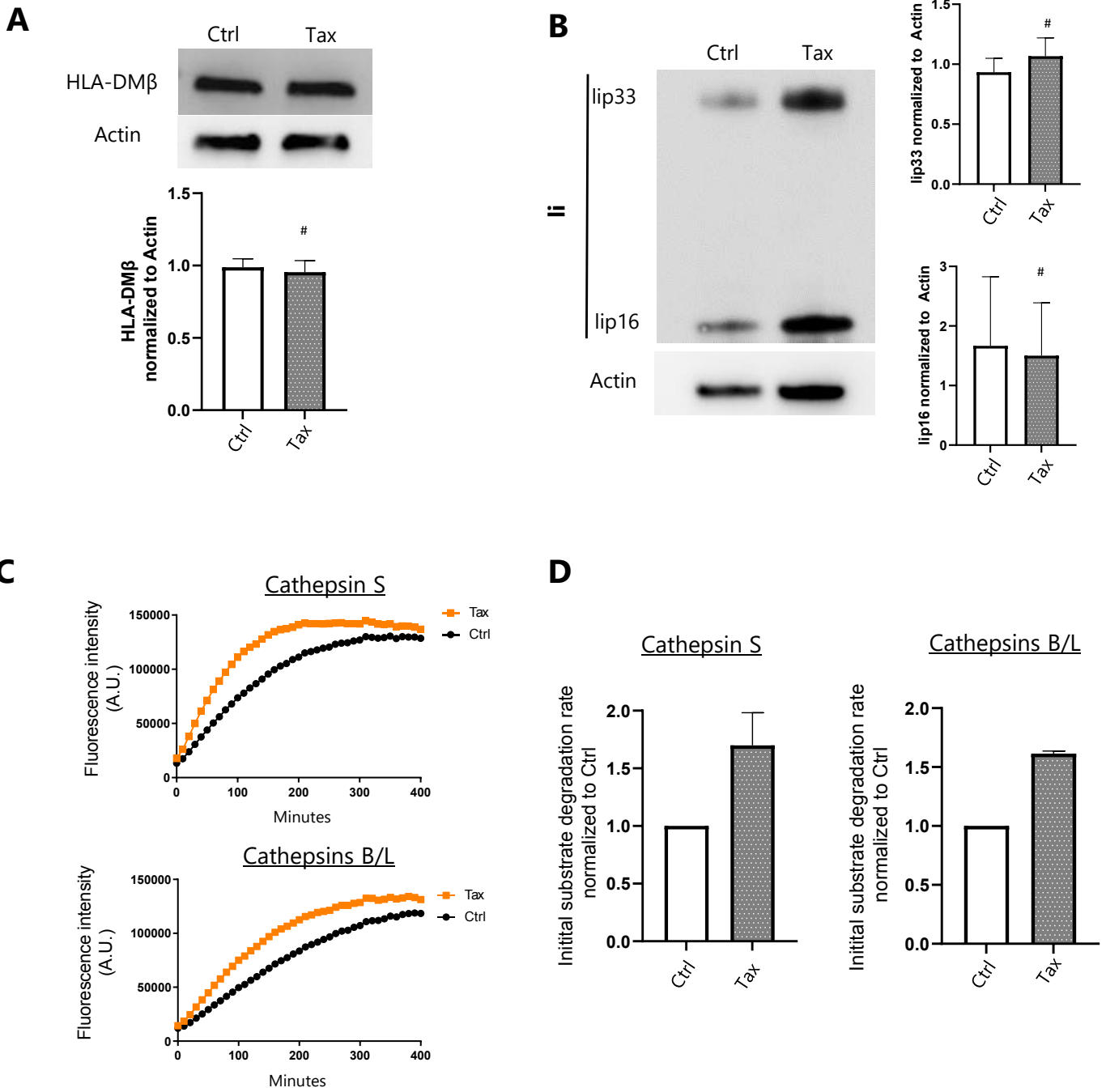
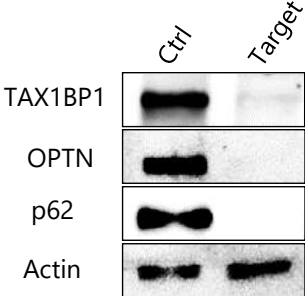
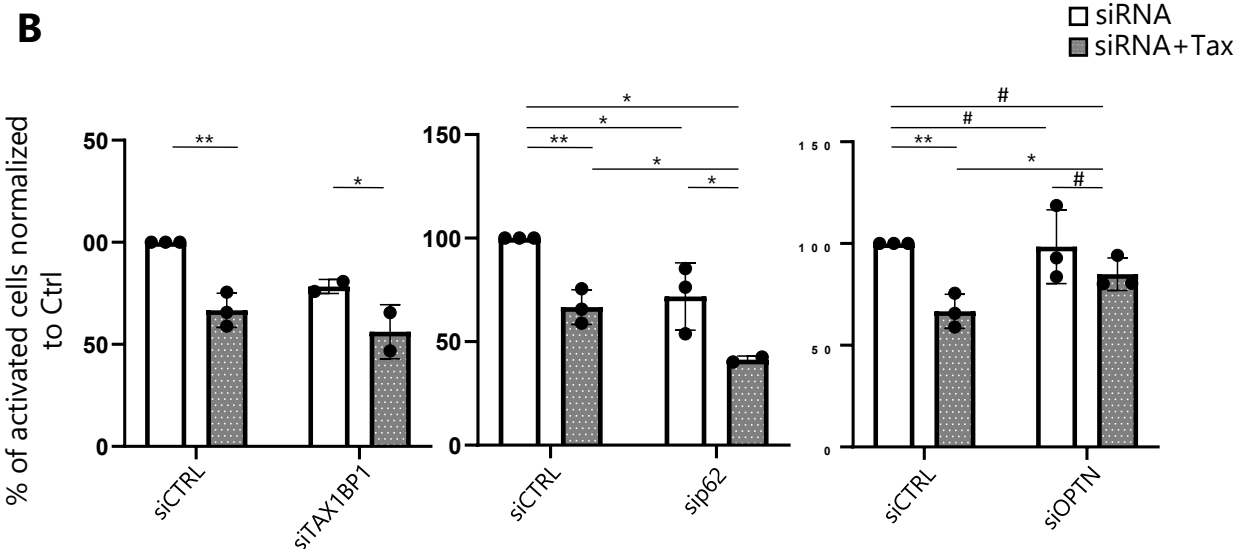


**Figure 5**

**A**



**B**



**C**

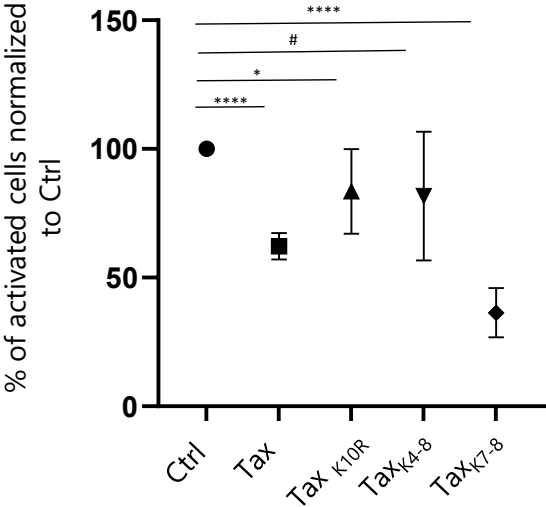
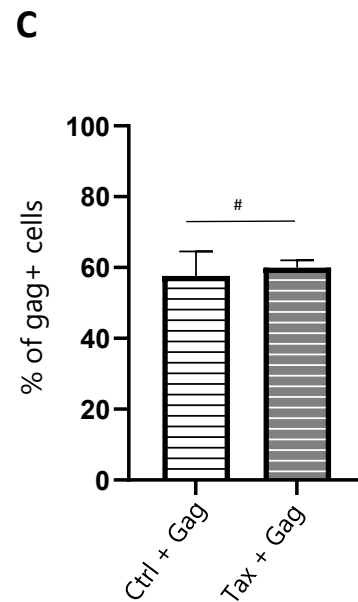
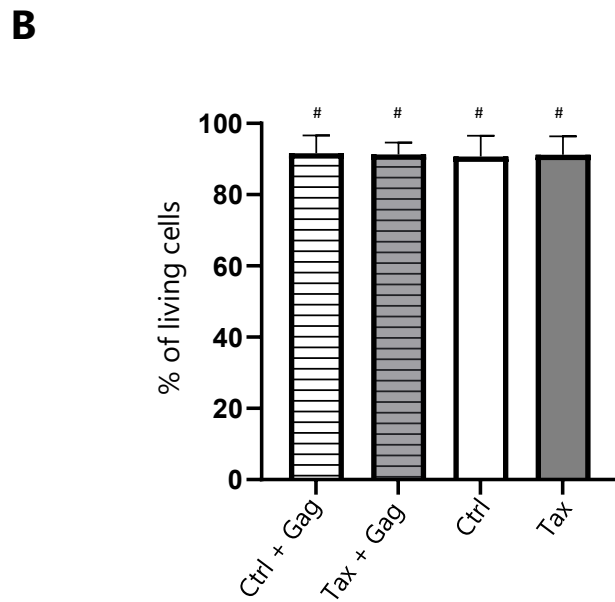
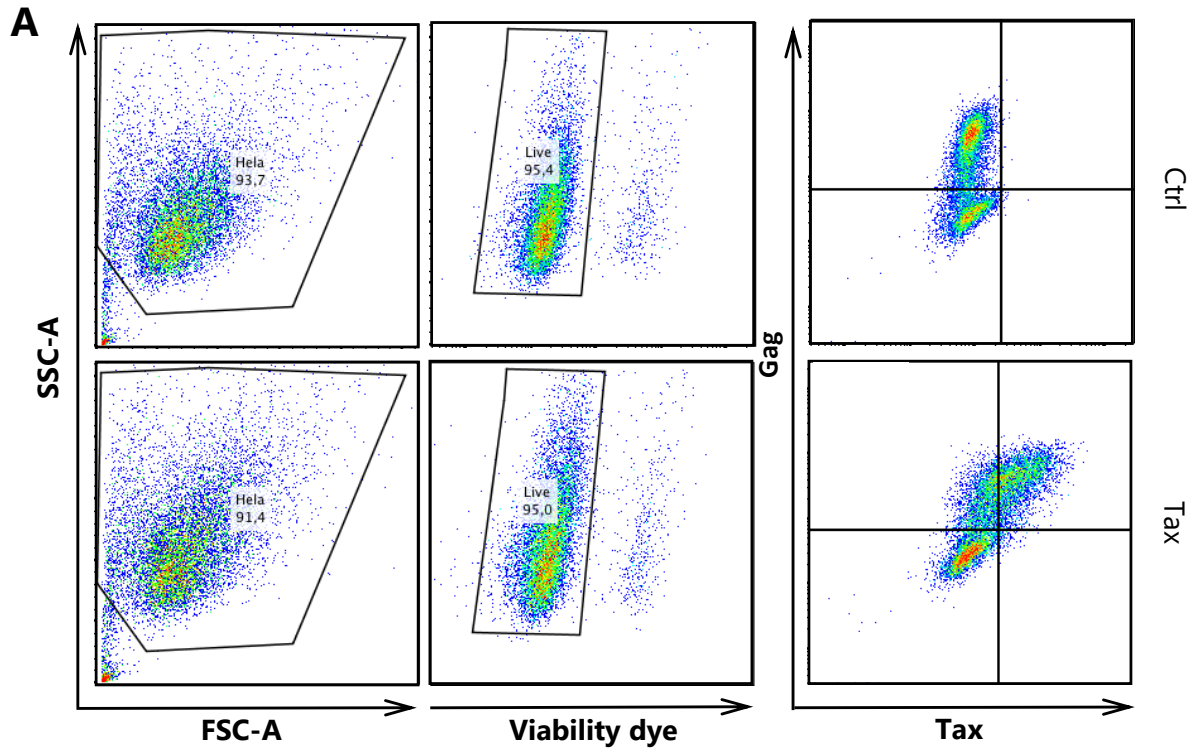


Figure S1



**Figure S2**

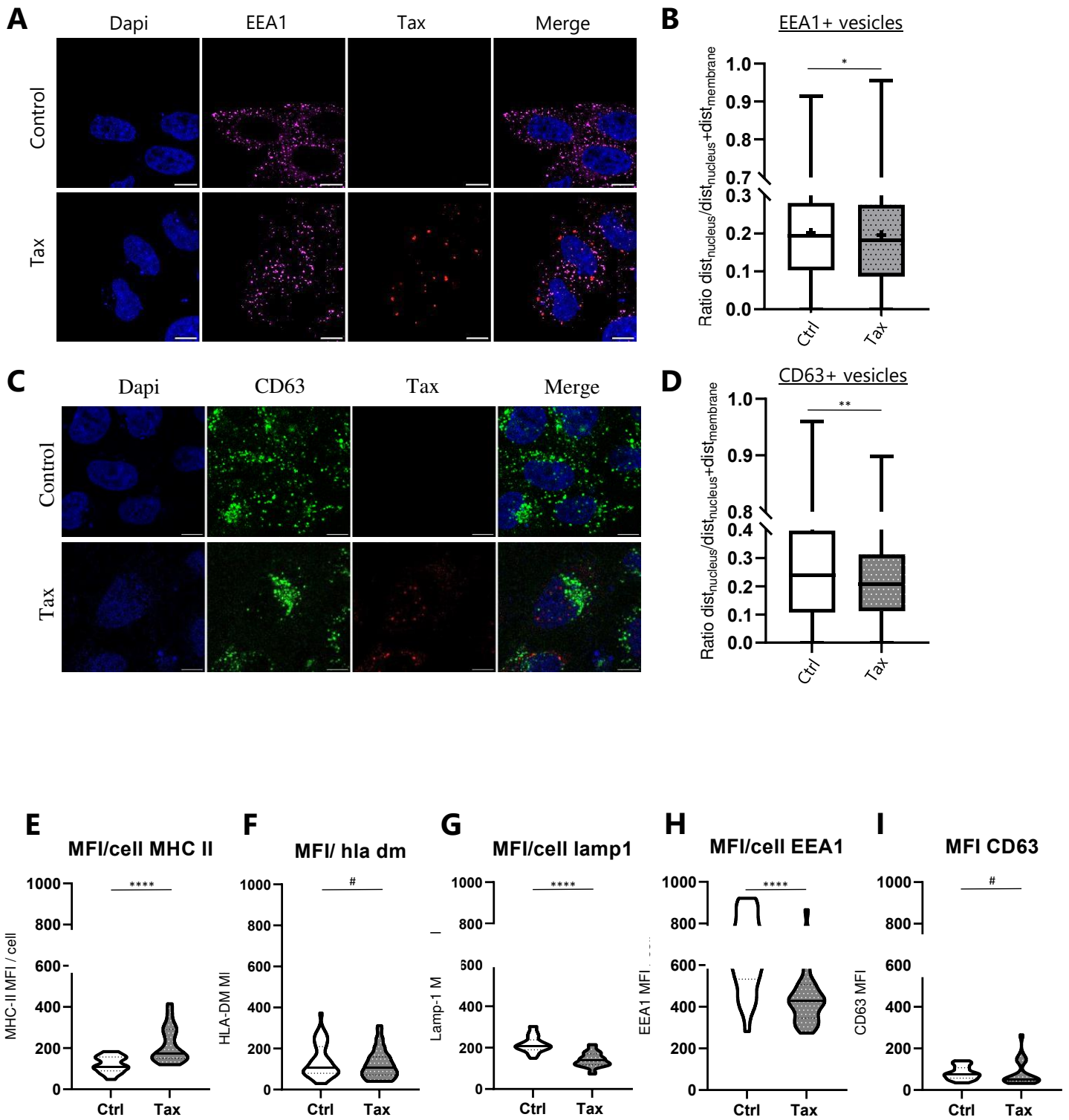
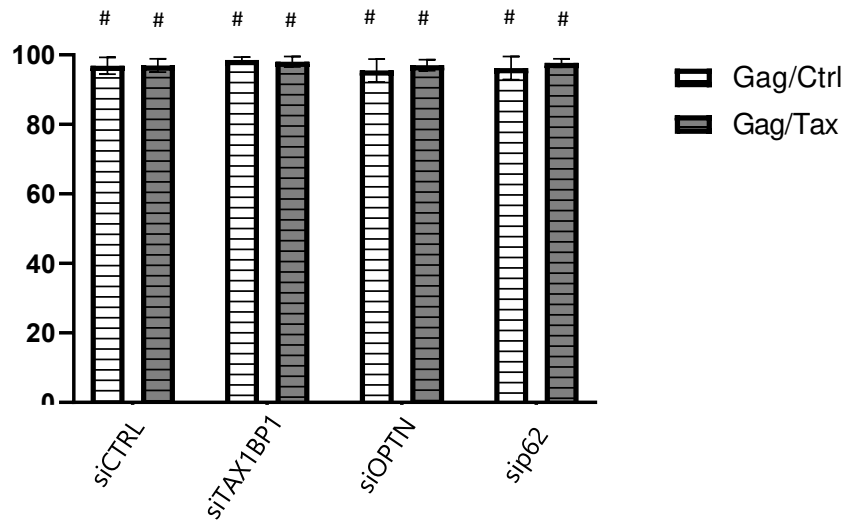


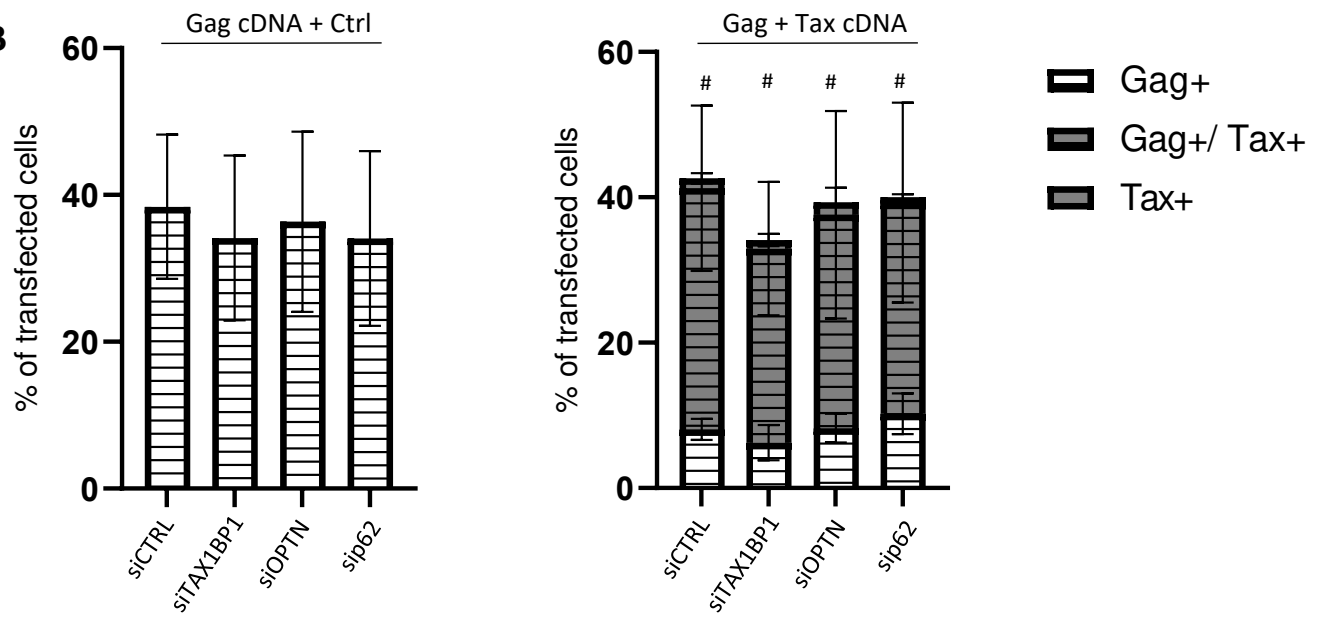


Figure S3

A



B



## Discussion and perspectives

Adaptive immunity has evolved to allow a broad and regulated recognition of both self- and nonself-antigens. It involves a complex interplay between antigen presenting cells and effector immune cells, which drives pathogen-specific response pathways, production of immunological memory and regulation of host immune homeostasis. Antigen-specific CD4<sup>+</sup>T cell responses are key actors in adaptive immunity. CD4<sup>+</sup>T cells, via their differentiation in T<sub>FH</sub> cells, control several stages of B cell activation for the generation of neutralizing antibodies<sup>517</sup>. CD4<sup>+</sup>T cell responses are also associated with improved antiviral CTL responses<sup>518</sup> and have been described as having cytotoxic properties<sup>519</sup>. These diverse roles underline the importance of understanding the mechanisms that govern CD4<sup>+</sup>T cell activation, which depend on the recognition of antigenic peptides presented by MHC-II molecules at the surface of APCs. Therefore, the capacity of APCs to present MHC-II-restricted peptides is essential for efficient adaptive immune responses. It is historically admitted that MHC-II molecules present peptides derived from extracellular sources, such as extracellular pathogens, to CD4<sup>+</sup>T cells leading to their subsequent activation. Nevertheless, as research on this field has progressed overtime and more tools have become available, this paradigm has changed and it is now known that MHC-II molecules can present peptides derived from endogenous sources<sup>333,355,520</sup>. Several cellular degradation pathways, amongst them autophagy, have been identified as contributing to MHC-II antigen presentation<sup>335</sup> but how antigens are transported to MHC-II-enriched compartments and then loaded on MHC-II molecules remains unclear. Several teams have demonstrated that targeting antigens to autophagosomes through their fusion to LC3 increases the capacity of APCs to activate antigen-specific CD4<sup>+</sup>T cells, underlining the importance of autophagy in endogenous antigen presentation. Autophagy is now being regarded as a selective process where autophagosomes target their substrate and exclude the rest of the cytoplasm<sup>521</sup>. Selective autophagy relies on SARs that ensure the targeting of ubiquitinated substrates to autophagosomes. In addition, some of these SARs are involved in autophagosomes maturation (TAX1BP1, NDP52 and OPTN)<sup>45</sup> and early endosome maturation (p62, TAX1BP1 and NDP52)<sup>131</sup>. During my thesis, we first hypothesized that SARs could contribute at various levels to MHC-II-restricted viral antigen presentation, including the fusion of autophagosomes with MHC-II molecules and thus in antigen presentation by MHC-II molecules. I addressed this scientific question in the first part of my work and described TAX1BP1 as a novel

player in MHC-II antigen presentation. SARs, as I showed in the introduction of this manuscript, play multiple roles in the cell such as adaptors in innate immunity signaling pathways in addition to their roles in selective autophagy. The multifunctional role of SARs make them suitable targets for viruses and other pathogens to counteract multiple cell functions. During viral infections, viruses can target SARs to their benefit<sup>362</sup>. HTLV-1 recruits TAX1BP1, OPTN and p62 specifically to promote cell transformation and the establishment of a persistent infection<sup>482,489</sup>. In the second part of my work, I addressed the question if HTLV-1, via its oncoprotein Tax, might target SARs to escape MHC-II antigen presentation. I showed that Tax affects MHC-II antigen presentation and suggest a novel role for OPTN in Tax-mediated MHC-II antigen presentation inhibition.

### **I.-Do SARs play a role in MHC-II endogenous antigen presentation?**

To answer this first scientific question, we dispose in the lab of a cell line model of HeLa cells stably expressing the CIITA transactivator (HeLa-CIITA). These cells express all the MHC-II antigen presentation machinery that I presented in the introduction. A functional screen silencing different SARs showed that silencing TAX1BP1 impairs the presentation of an autophagosome-targeted gag antigen (gag-LC3) by MHC-II molecules to gag-specific CD4<sup>+</sup>T cells, preventing their further activation. Interestingly, we observed similar results using a native gag antigen, not directed to autophagosomes, and an HCMV-specific CD4<sup>+</sup>T cells recognizing a pp65-derived antigen. This suggested that the effect of TAX1BP1 on MHC-II-restricted antigen presentation is not limited to antigens degraded by autophagy. In fact, my team had previously demonstrated that the presentation of peptides derived from HIV-gag is not autophagy-dependent<sup>337</sup>. Remarkably, we found that silencing NDP52 and OPTN, also involved in autophagosome maturation, did not have an effect on MHC-II antigen presentation and CD4<sup>+</sup>T cell activation. These results show a broader role than anticipated for TAX1BP1 in the presentation of antigens presented by MHC-II molecules. We therefore decided to broaden the observations concerning the role of TAX1BP1 on the whole of the MHC-II antigenic peptide repertoire. In collaboration with the Immunology Department of HG Rammensee from the University of Tübingen, we eluted and analyzed by mass spectrometry the peptides associated to HLA-DR, DQ and DP molecules in our cell model to study the impact of TAX1BP1 silencing on the MHC-II immunopeptidome. We found that, as expected, around 60% of shared peptides presented by MHC-II molecules between the mock and siTAX1BP1 treated cells<sup>266</sup>. This rather

low percentage of shared peptides might be due to the intrinsic variability of the peptide repertoire exposed by MHC-II molecules at a given time that is influenced, for example, by the cell cycle, activation status of the cell. Alternatively, this might be due to the variability of the MHC-immunoprecipitation and LC-MS/MS procedures. Remarkably, when silencing TAX1BP1, the amount of shared peptides decreases to 35%. We concluded that the absence of TAX1BP1 drastically affects the peptide repertoire, the relative abundance of core epitopes binding to MHC-II molecules (half of the core epitopes were significantly differentially presented when comparing wild type and TAX1BP1-silenced cells) as well as their relative affinity to MHC-II molecules, predicted by the NetMHCIIpan 4.0 software. This immunopeptidomics data suggests that TAX1BP1 expression favors the loading of peptides with a high binding capacity to MHC-II molecules. We did not find a significant effect of TAX1BP1 silencing on the MHC-I immunopeptidome, which suggests that the action of TAX1BP1 is restricted to the MHC-II antigen presentation pathway.

A decrease in CD4<sup>+</sup>T cell activation could be due to an impairment of APCs in presenting MHC-II-peptide complexes loaded with high affinity peptides at their surface. Chaperones HLA-DM and Ii tightly regulate the loading of high affinity peptides on MHC-II molecules and Ii expression regulates the trafficking of immature MHC-II molecules bound to be expressed at the surface of APCs. Perturbing the expression levels of any of these chaperones can influence the MHC-II immunopeptidome and its peptide affinity<sup>264-266</sup>. Remarkably, we showed that silencing TAX1BP1 induced an important decrease of Ii expression whereas HLA-DM and HLA-DR expression levels remained unperturbed. In collaboration with Bénédicte Manoury's team, I performed pulse/chase experiments in which we confirmed that silencing TAX1BP1 induces a rapid and exacerbated degradation of Ii. The expression levels of Ii were rescued with lysosomal acidification inhibitors but not with proteasome inhibitors, suggesting that Ii is aberrantly degraded in endo-lysosomal compartments in cells depleted for TAX1BP1. These results could explain the dramatic effect of TAX1BP1 silencing on the MHC-II immunopeptidome and the instability of MHC-II-peptide complexes that we observed in the absence of TAX1BP1 in further pulse/chase experiments. However, although TAX1BP1 silencing does not alter HLA-DM expression levels, we cannot exclude that the HLA-DR/HLA-DM interaction could be modified. In fact, the role of HLA-DM is broader than exchanging CLIP with high affinity peptides, HLA-DM also stabilizes empty HLA-DR molecules at lysosomal pH<sup>253,260,522</sup> and its interaction with

HLA-DR controls the quality of the MHC-II immunopeptidome even in the absence of Ii<sup>523</sup>. It would be relevant in our APC model to immunoprecipitate MHC-II molecules in control and cells depleted for TAX1BP1 and assess HLA-DR/HLA-DM interactions. This is all the more relevant considering that we observed a global modification of the cellular distribution of acidified vesicular compartments in the absence of TAX1BP1, including HLA-DM+ vesicles. Assessing HLA-DR/HLA-DM colocalization in TAX1BP1-depleted cells could give us an idea of the localization of these markers compared to cells expressing TAX1BP1. Indeed, we observed that EEA1, LAMP-1 and CD63, like HLA-DM and MHC-II, markers were relocated towards the nucleus in cells depleted for TAX1BP1. These markers, when combined, are used to describe the MIIC. Our observations suggested that, globally, TAX1BP1 regulates vesicular compartment trafficking, including trafficking of the endolysosomal MIIC. Since the localization of intracellular vesicles might control their functions<sup>524</sup> and their intravesicular pH in particular<sup>525</sup>, the aberrant localization induced by TAX1BP1 silencing could explain the effect on the MHC-II immunopeptidome. In fact, a perturbed vesicular trafficking could alter cathepsin delivery to the MIIC and a modified intravesicular pH could alter cathepsin activities, both are in turn essential for antigen degradation and the cleavage of Ii to ensure loading of high affinity peptides on MHC-II molecules. Moreover, HLA-DM-mediated peptide exchange is also dependent on endolysosomal pH<sup>526</sup>. The increased co-localization of MHC-II+ vesicles with Lamp-1+ vesicles we observed in TAX1BP1 depleted cells suggests an altered pH in the MIIC and we could confirm this by analyzing the pH in MHC-II+ and HLA-DM+ vesicles by means of pH-sensitive probe such as LysoSensor. Interestingly, Ii can itself control MHC-II trafficking through the endocytic pathway<sup>203</sup> and endosomal membrane trafficking<sup>209,527</sup>. Moreover, the isoform p41 of Ii can interact with cathepsins and regulate their endosomal activity<sup>244,245,528</sup> and can also interact with cystatins, regulators of cathepsins<sup>299</sup>. Therefore, the impact of TAX1BP1 silencing on endosomes/lysosomes positioning and the MHC-II immunopeptidome could be a bystander effect of Ii degradation. Jongsma et al. described a role for ER ubiquitin ligase RNF26 as an architect of the endosomal system, recruiting p62 as a Ub-binding scaffold protein which in turn attracts Ub-binding domains of TAX1BP1 and Tollip that act as vesicular adaptors. This system allows the clustering of early, recycling and late endosomes in perinuclear clouds. The action of deubiquitinase (DUB) USP15 counteracts vesicle retention and promotes endosome maturation and cargo trafficking<sup>131</sup>. Although our results show a different distribution of CD63+ vesicles upon TAX1BP1 silencing than observed in Jongsam et al,

perhaps due to the expression of CIITA in our cell line, and we confirm that TAX1BP1 plays a role in vesicle trafficking. The absence of TAX1BP1 could perturb the balance between the activities of RNF26 and DUB USP15. It would therefore be interesting to assess the impact of RNF26 and DUB USP15 silencing on MHC-II antigen presentation and CD4<sup>+</sup>T cell activation in our cell system. Given the effect of TAX1BP1 silencing on vesicular trafficking, we wondered whether the vesicles delivering antigens to the MHC-II might be affected, thus potentially modifying the source of peptides to be presented by MHC-II molecules. By using a functional enrichment analysis, we observed a slight influence of TAX1BP1 silencing on the cellular protein sources of MHC-II peptides. This however, is not sufficient to explain the decrease in predicted peptide relative affinity to MHC-II molecules.

To characterize further the mechanism of action of TAX1BP1 involved in MHC-II antigen presentation, we searched for its protein interactants. In collaboration with Cédric Pionneau from the P3S platform, we established the TAX1BP1 interactome via a mass spectrometry approach using HeLa-CIITA cells overexpressing a TAX1BP1-GFP construct. We were able to identify previously described partners of TAX1BP1 such as p62, the E3 ligase Itch<sup>486</sup> or TBK1<sup>50</sup>; confirming the robustness of the technique and further analysis. We identified the ER chaperone CANX as a new interactant of TAX1BP1 and confirmed the interaction by immunoprecipitation of both endogenous proteins in HeLa-CIITA cells and other APCs. CANX is involved in protein folding quality control<sup>529,530</sup> plays an important role in the assembly of nonameric MHC $\alpha\beta$ -li complexes<sup>207</sup>. CANX retains and stabilizes li in the ER<sup>205</sup> and binds neosynthesized  $\alpha$  and  $\beta$  chains prior to their assembly<sup>204</sup>. Using siRNA silencing, we confirmed that silencing CANX induces li degradation. Previously, it was demonstrated that perturbing li-CANX interaction induced li degradation<sup>205</sup>. We showed that silencing CANX in our APC cell model decreases their capacity to activate antigen-specific CD4<sup>+</sup>T cells, showing that silencing CANX recapitulates the effect of silencing TAX1BP1 on li degradation and MHC-II antigen presentation. Different post-translational modifications can regulate both CANX function and cellular distribution, such as phosphorylation or palmitoylation of its cytosolic tail<sup>531,532</sup>. We showed, by means of a construct containing only the transmembrane region and cytosolic tail of CANX, that TAX1BP1 binds to the cytosolic tail of CANX. Although no ubiquitination has been demonstrated on the cytosolic tail of CANX, this possibility should be further investigated as a potential direct link with the Ub-binding domains of TAX1BP1 and thus MHC-II antigen

presentation. To address this question in the future, we obtained from Folma Buss a set of cDNA encoding for TAX1BP1 with mutation in the Ub-binding domains. Performing co-immunoprecipitations of the cytosolic tail construct of CANX with each TAX1BP1 mutant would answer if any of the two Ub-binding domains of TAX1BP1 might be involved in the interaction with the cytoplasmic tail of CANX. Although we did not observe a significant effect of TAX1BP1 silencing on ER cellular distribution and morphology using markers such as CANX, PDI or KDEL in confocal microscopy (not shown), we can hypothesize that TAX1BP1 impacts CANX function which in turn can no longer stabilize li. We also used the TAX1BP1-GFP and the Ub-binding mutants in complementation experiments to assess if we could recover li expression levels and determine if the effect of TAX1BP1 on MHC-II antigen presentation is mediated through its binding of ubiquitin. Unfortunately, it was technically difficult to obtain high expression levels of TAX1BP1-GFP or its mutants post siRNA transfection, which made it difficult to draw a conclusion. To circumvent this issue, we expressed CIITA in HeLa cells invalidated for TAX1BP1 expression using CRISPR-Cas9 (obtained from Richard Youle's laboratory, NIH, USA). We obtained cells invalidated for one SAR expression, TAX1BP1 (TAX1BP1 KO), NDP52 (NDP52 KO), OPTN (OPTN KO) or invalidated for all three SARs (TKO). Remarkably, when used in functional experiments with virus-specific CD4<sup>+</sup>T cells, TAX1BP1 KO cells did not induce a decrease in virus-specific CD4<sup>+</sup>T cell activation when gag or pp65 antigens were used. Youle's Team had described a compensatory effect, exerted by other SARs, on a mitophagy defect in OPTN KO that was highlighted in TKO cells upon transfection of CDNA encoding a single SAR<sup>82</sup>. We could be facing a similar compensatory effect although in our case neither the absence of NDP52 nor OPTN reproduce the effect of TAXBP1 silencing on MHC-II antigen presentation and CD4<sup>+</sup>T cell activation.

Interestingly, we identified NBR1, a SAR that we did not include in our initial functional screen, as a partner of TAX1BP1 in our interactome. In recent preliminary experiments, I have confirmed that NBR1 immunoprecipitates with endogenous TAX1BP1 in HeLa-CIITA. I could also show that silencing NBR1 also induces a decrease of CD4<sup>+</sup>T cell activation (not shown). The effects of NBR1 silencing on the MHC-II immunopeptidome, vesicle trafficking and li expression levels remain to be addressed. To verify if NBR1 might compensate the stable invalidation of TAX1BP1, we plan to use HeLa cells stably invalidated for TAX1BP1, NDP52, OPTN, p62 and

NBR1 (penta KO) (also from the Youles' lab.) and stably expressing CIITA to assess their ability to present viral antigens to virus-specific CD4<sup>+</sup>T cells.

In our study of the TAX1BP1 interactome, we also identified novel potential partners that could be involved in the role of TAX1BP1 in MHC-II antigen presentation and that should be studied further. Among these, we found proteins involved in vesicular acidification such as a vATPase<sup>533</sup>, endocytosis, the ubiquitin/proteasome pathway and antigen presentation (HLA-A, -C, -DQ $\alpha$ 1 and -DR $\beta$ 1 molecules). Ubiquitination plays an important role in the cellular localization and recycling of mature MHC-II molecules<sup>56,283,286,287</sup>. We could assess MHC-II ubiquitination levels upon TAX1BP1 silencing as well as E3 March1 expression levels since this ubiquitin ligase ubiquitinates MHC-II under Tollip regulation<sup>56</sup>. The interaction of TAX1BP1 and MHC-II molecules could be mediated by ubiquitin. Nevertheless, it is unlikely that this interaction is direct since we observed no co-localization between TAX1BP1 and HLA-DR and we did not pulldown HLA-DR in TAX1BP1 immunoprecipitations. In addition, we see no effect of TAX1BP1 silencing on MHC-II internalization or expression levels; therefore, TAX1BP1 does not seem to affect MHC-II recycling. Interestingly, we also identified deubiquitinase (DUB) USP15 a new partner of TAX1BP1. As we mentioned before, this DUB participates in endosome maturation and could therefore link TAX1BP1 to the localization and maturation of the endolysosomal MIIC. Altogether, we showed that TAX1BP1 influences vesicular trafficking and the cellular positioning of the MIIC as well as li stability via an interaction with CANX. TAX1BP1 influences the MHC-II immunopeptidome and thus the loading of MHC-II with high affinity peptides, which affects CD4<sup>+</sup>T cell activation (Fig 21).



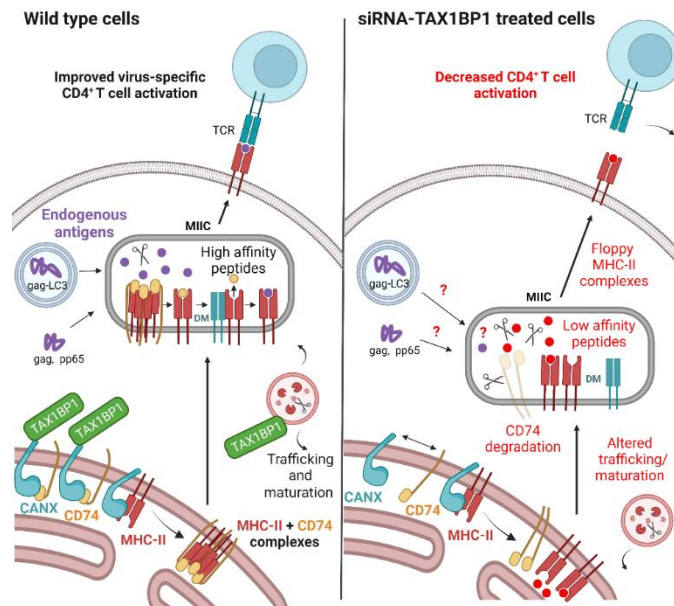


**Figure 32. Model of the impact of TAX1BP1 silencing on MHC-II endogenous antigen presentation.** In wild type cells, TAX1BP1 regulates vesicular trafficking and CANX function, which stabilizes the Ii invariant chain and promotes loading of high affinity peptides on MHC-II molecules. In depleted cells, Ii is degraded and the MIIC and acidified vesicles relocated towards the nucleus. The loading of low affinity peptides decreases activation of CD4<sup>+</sup>T cells.

Our APC model of HeLa cells expressing CIITA constitutes a strong model for endogenous antigen presentation since these cells do not actively uptake antigens through endocytosis or phagocytosis. It would therefore be interesting to assess if TAX1BP1 also plays a role in exogenous antigen presentation, especially given the effect of TAX1BP1 silencing on Ii degradation and vesicular trafficking. To answer this question, another model of APCs could be used, such as B cells or DCs. My team tried to silence TAX1BP1 expression in model DCs. Unfortunately, every transfection reagent used induced cell maturation, which in turn affects MHC-II molecule trafficking and thus made assessing antigen presentation not possible.

Our results add a novel aspect to the role of TAX1BP1 in immunity. In fact, TAX1BP1 has been well characterized in its role in innate immunity as a negative regulator of the NF- $\kappa$ B and IRF3 signaling pathways. We show that TAX1BP1 is also a key player in adaptive immunity with a direct effect on antigen presentation and T cell immune responses. A defect in mounting normal CD4<sup>+</sup>T cell responses can lead to immunodeficiency or induction of autoimmunity. Therefore, our findings could help to better characterize the phenotypes of TAX1BP1 KO mice, which present prevalent treatment-refractory skin inflammation, succumb to sub lethal doses of TNF and IL-1 and die of hypertrophic cardiac valvulitis<sup>534</sup>. In another model, TAX1BP1 KO

induces embryonic lethality due to systemic hemorrhaging and multiple cardiac defects<sup>138</sup>. Given the severity of the phenotypes, the use of a conditional KO might be more relevant to validate our results *in vivo*. Interestingly, TAXBP1 serves different functions in addition to its role as a SAR, these include the negative regulation of apoptosis and cell growth, positive regulation of gene expression and the role we have previously mentioned in innate immunity<sup>139</sup>. Although we have yet to confirm its role as a protein adaptor in our model, the ability of TAX1BP1 to bind ubiquitin seems to drive its major role in immune cells. .

## **II.-Does HTLV-1 Tax protein target SARs to escape antiviral immunity?**

HTLV-1 Tax is necessary for immortalization and transformation of T cells as well as for persistent infection in the host<sup>452</sup>. Tax drives cell immortalization through the constitutive activation of the NF- $\kappa$ B pathway by recruiting IKK $\gamma$  as well as SARs and negative feedback regulators TAX1BP1, OPTN and p62 to a macromolecular Signalosome<sup>138,473,482,489</sup>. Tax has also been shown to affect signaling in DCs<sup>512,513</sup>. Based on the results I obtained in the first part of my thesis, the next question was then whether HTLV-1 might escape antiviral immunity via the recruitment of SARs by Tax.

To address this question, we first asked if Tax expression might influence CD4<sup>+</sup>T cell activation. Our results show that Tax expression interferes with endogenous antigen presentation by MHC-II molecules and subsequent activation of virus-specific CD4<sup>+</sup>T cells without affecting the presentation of exogenous peptides. To extend the observation made with a single viral antigen, we analyzed the effect of Tax expression on the global MHC-II immunopeptidome. From the total eluted peptides, one third was found exclusively in control cells and the cells expressing Tax and the rest of the peptides were shared by both conditions. We then identified the unique core epitopes since peptides eluted from MHC-II molecules are variable in length and the same core epitope inserted in the MHC-II peptide-binding groove can be found in multiple peptides with N- or C-terminal extensions<sup>266</sup>. We analyzed the influence of Tax expression on the relative core peptide abundance and their affinity to MHC-II molecules. A portion of core epitopes is significantly differentially presented when comparing control to Tax-expressing cells. However, Tax expression does not seem to influence peptide relative affinity to HLA-DR and HLA-DQ molecules, predicted by the NetMHCIIpan 4.0 software.

Therefore, Tax does not seem to modulate the relative affinity of MHC-II ligands. This is different from what we observed in cells silenced for TAX1BP1 expression where the relative binding affinity of peptides on HLA-DR was decreased. We hypothesize that the strong influence of TAX1BP1 expression on the quality of peptides might be explained by its important role in the stabilization and degradation of the invariant chain. The absence of Tax influence on li expression levels might explain why Tax does not influence the quality of MHC-II ligands. In order to confirm this hypothesis, pulse chase experiments could be performed to assess the fate of the li and the formation of stable MHC-peptide complexes in cells expressing Tax. We concluded that Tax expression has an important influence on the peptide repertoire and the relative abundance of core epitopes (Tax influences the relative abundance of one out of five core epitopes) but does not influence their relative affinity to MHC-II molecules.

Although we did not observe a significant difference in MHC-II expression levels, we cannot exclude that Tax expression could influence the synthesis, internalization or maturation kinetics of MHC-II molecules. We plan to monitor surface expression of mature and immature MHC-II molecules and assess their internalization kinetics by flow cytometry. This is even more relevant considering that, upon Tax expression, acidified vesicles and the MIIC relocate towards the nucleus, thus suggesting a role for Tax in vesicular trafficking. In addition, although I did not observe a modification in HLA-DM expression levels in cells expressing Tax, we found that HLA-DM-positive vesicles co-localize more with Lamp1-positive vesicles in these cells, thus suggesting an effect of Tax on the trafficking of acidified compartments with potential consequences on the maturation of the MIIC and its intravesicular pH. Of note, HLA-DM is a chaperone involved in quality control of peptide loading on MHC-II molecules. A variation in pH could alter HLA-DM functions with a direct impact on the MHC-II immunopeptidome. Moreover, recent studies suggested that the localization of intracellular vesicles controls their functions<sup>524</sup> and particularly their intravesicular pH<sup>525</sup>. I intended to address this point by analyzing the activity of pH-sensitive cathepsins also involved in antigen processing. I observed an increase of cathepsin activity in cells expressing Tax, as compared to control cells. An altered lysosomal cathepsin activity could explain the effect of Tax on the MHC-II molecule peptide repertoire. It has been previously shown that modulating cathepsin activity can alter antigen processing and presentation<sup>535</sup> and cathepsins B and S are optimally active at low pH and participate in generating HIV-derived MHC-II restricted epitopes<sup>536</sup>. Altered intravesicular pH

and cathepsin activities could also directly affect li processing. However, this does not seem to be the case in our model of HeLa-CIITA cells expressing Tax since we do not detect any changes in li expression levels and processing at steady state. As mentioned, we should consider performing pulse chase experiments to evaluate the degradation kinetics of li upon Tax expression. A more exhaustive characterization of the MIIC in cells expressing Tax is probably necessary. In addition, it would be important to look at other markers, such as the Rab protein family given their role as drivers of vesicle maturation and vesicle trafficking<sup>537,538</sup>. Altogether, Tax expression affects the trafficking of different vesicles including the MIIC as well as vesicular pH, translated by an increase in cathepsin activity.

We then assessed whether Tax-mediated inhibition of MHC-II-restricted antigen presentation might be dependent on SARs recruitment by Tax to the Signalosome. I first confirmed that in our model system, HeLa cells expressing CIITA, Tax expression also induces the recruitment of TAX1BP1, OPTN and p62. I then assessed the influence of SARs expression on the inhibition of antigen presentation by Tax. To this end, Tax was expressed in cells silenced for the expression of TAX1BP1, OPTN or p62. Interestingly, in cells silenced for TAX1BP1 and p62, the decrease of CD4<sup>+</sup>T cell activation was even more pronounced than in Tax-expressing cells treated with irrelevant siRNAs. Remarkably, Tax-mediated inhibition of MHC-II antigen presentation and CD4<sup>+</sup>T cell activation was abrogated in cells silenced for OPTN. The cumulative effect of TAX1BP1 silencing and Tax expression confirms that TAX1BP1 and Tax modulate MHC-II-restricted antigen presentation via different mechanisms. Although we initially did not observe an effect of p62 silencing on MHC-II antigen presentation, this could be due to the nature of the antigen. In fact, in our initial screen we used gag-LC3 and not native gag. More experiments must be performed to confirm the cumulative effect observed for sip62 and Tax expression. We confirmed in this set of experiments that OPTN does not affect MHC-II antigen presentation but is subverted by Tax to inhibit this pathway. Given our results on TAX1BP1 and MHC-II antigen presentation in the first part of my work and that Tax and TAX1BP1 are well known interactants, we initially expected that the recruitment of TAX1BP1 by Tax would recapitulate the effects of TAX1BP1 silencing in HeLa-CIITA cells and were surprised that it was not the case.

To further characterize potential interactions of Tax with OPTN in inhibiting antigen presentation, we made use of well-characterized ubiquitination mutants of Tax. Indeed, it has

been shown that Tax recruits SARs to the Signalosome for sustained NF- $\kappa$ B activation in a ubiquitin-dependent manner<sup>466</sup>. Tax contains 10 lysine (K) residues (K1 to K10) of which K4 through K10 are the main targets of both monoubiquitination and polyubiquitination. We used three ubiquitin mutants of Tax: Tax<sub>K10R</sub>, Tax<sub>K7-8</sub>, and Tax<sub>K4-8</sub> in which lysines have been replaced by arginines and can no longer bind mono- or polyubiquitin. Of the three mutants, Tax<sub>K7-8</sub> is the only one that can still interact with OPTN through polyubiquitin. Remarkably, the mutants Tax<sub>K10R</sub> and Tax<sub>K4-8</sub> no longer inhibited CD4<sup>+</sup>T cell activation, when expressed in our model APC, whereas the mutant Tax<sub>K7-8</sub> still inhibited CD4<sup>+</sup>T cell activation. These results strongly suggest that Tax interaction with OPTN through lysines 4-6 is required for Tax to act on MHC-II antigen presentation and CD4<sup>+</sup>T cell activation.

Since OPTN is required for Tax-mediated sustained NF- $\kappa$ B activation<sup>482,489</sup>, we could hypothesize that NF- $\kappa$ B could play a role in Tax-mediated inhibition of MHC-II antigen presentation. Indeed, previous studies have shown, in inflammatory conditions, a role for NF- $\kappa$ B in the modulation of MHC-II molecule expression dependently and independently of the Jak/STAT pathway (which can regulate CIITA expression) in different APCs<sup>539-541</sup>. In our model, Tax expression could be a driver of an inflammatory context. It is necessary to assess NF- $\kappa$ B activation alone in our system to evaluate its role on MHC-II antigen presentation. This is particularly relevant considering that CIITA has been previously shown to inhibit Tax-induced sustained NF- $\kappa$ B activation in B cells and in HeLa cells transfected with CIITA<sup>542</sup>. In addition, we recently obtained, from Dr. Chloé Journo, well-characterized Tax mutants that positively or negatively regulate NF- $\kappa$ B activation (M22 and M47) (smith green) that will be used to further characterize the impact of Tax-induced NF- $\kappa$ B signaling on MHC-II-restricted antigen presentation and CD4<sup>+</sup>T cell activation. However, it is interesting to note that silencing of TAX1BP1, OPTN or p62 expression, individually, significantly abrogates NF- $\kappa$ B activation in Tax-expressing cells<sup>482,489</sup>. In contrast, we observed that CD4<sup>+</sup>T cell activation was further decreased in cells silenced for TAX1BP1 or p62 in the presence of Tax. Thus, we could be looking here at a novel role of OPTN in Tax-mediated MHC-II antigen presentation. In addition to assessing the effect of NF- $\kappa$ B activation alone on MHC-II antigen presentation, it would be interesting to target other elements of the Signalosome such as IKK $\gamma$  or to target ubiquitin ligases such as Ubc13 or LUBAC. Moreover, a role of OPTN in the Tax-driven alteration of vesicular trafficking and the MHC-II immunopeptidome remains to be elucidated. Of note, Ducasa et al. showed

that Tax recruits the autophagy proteins BECN1, Bif-1 and the PI3KC3 complex through its direct interaction with BECN1. Tax deregulates the autophagy pathway by increasing autophagosomes biogenesis whilst blocking the autophagosome-lysosome fusion. It would be relevant to study the effect of Tax on the autophagy pathway in our cell model to assess if the autophagosome accumulation, also observed in other cell lines<sup>514</sup>, impacts MHC-II antigen presentation and CD4<sup>+</sup>T cell activation. The interaction of Tax with OPTN in this context would need to be evaluated although it is likely that OPTN is also recruited since the whole IKK complex participates in Tax-induced autophagy modulation<sup>469</sup>.

During chronic HTLV-1 infection, the virus manipulates immune responses to counteract antiviral immunity. Several groups have documented the productive in vitro infection of myeloid DCs and of monocytes-derived DCs (MDDCs). DCs dictate the quality of T cell responses but very little is known about the capacity of HTLV-1-infected DCs to prime efficient T cell responses. Several studies have shown that blood DCs from HTLV-1-infected patients and DCs from uninfected individuals, exposed in vitro to HTLV-1 induce an abnormal proliferation of CD4<sup>+</sup>T cells and MDDC exposure induces an unresponsive status of limited maturation. These observations suggest that both DC exposure to HTLV-1 and DC infection can influence their capacity to stimulate T cells. Since the canonical NF- $\kappa$ B signaling pathway regulates DC maturation, it will be interesting in the future to investigate in DCs, a potential role of SARs in the modulation of NF- $\kappa$ B and MHC-II antigen presentation. Given that OPTN and TAX1BP1 also regulate the IRF3 pathway, it would be interesting to analyze the effect of Tax on IRF3 and the induction of IFN I in DCs expressing Tax or exposed to HTLV-1. IFN I acts in a paracrine way on the Jak/STAT signaling pathway<sup>543</sup> which can regulate MHC-II molecule expression. Interestingly, other HTLV-1 protein such as p12 can also reduce CTL-mediated killing through the induction of MHC-I molecule degradation<sup>544</sup>. This feature could be studied in relation to MHC-II molecules in model APCs and DCs.

Overall, my thesis work has allowed to describe novel roles for TAX1BP1 and OPTN in MHC-II antigen presentation. This highlights the importance and diversity of functions exerted by SARs outside of their role in autophagy and justifies that their targeting by viruses has converged during evolution. For both axis of my thesis, it will be important in the future to extend our results to more physiological conditions, such as model DC or B cell lines or primary immune cells. Perhaps using penta KO model DCs can be considered in the future. Using DCs to study

the impact of Tax on MHC-II antigen presentation will also be convenient and even more so in combination with HTLV-1 infected donor cells. In fact, recreating the whole infectious environment allows the interplay of various viral proteins which, as Tax and HBZ exerting opposite roles in the modulation of NF- $\kappa$ B<sup>545</sup>, gives a more realistic view of immune signaling in APCs.

Finally, several viral proteins hijack SARs either to degrade them or to exhort them to accomplish different functions. Besides being targeted by Tax, TAX1BP1 itself is targeted by different proteins including N protein from MEV or N protein from RSV to promote viral replication and escape innate immune signaling. Studying the interactions between viral proteins and SARs can constitute a good tool to dissect the different functions exerted by SARs, including their role in MHC-II-restricted antigen presentation.

## References

1. Mortimore, G. E. & Pösö, A. R. Intracellular protein catabolism and its control during nutrient deprivation and supply. *Annu Rev Nutr* **7**, 539–564 (1987).
2. Meijer, A. J. & Codogno, P. Regulation and role of autophagy in mammalian cells. *Int J Biochem Cell Biol* **36**, 2445–2462 (2004).
3. Klionsky, D. J. *et al.* A unified nomenclature for yeast autophagy-related genes. *Dev Cell* **5**, 539–545 (2003).
4. Harding, T. M., Morano, K. A., Scott, S. V. & Klionsky, D. J. Isolation and characterization of yeast mutants in the cytoplasm to vacuole protein targeting pathway. *J Cell Biol* **131**, 591–602 (1995).
5. Hutchins, M. U., Veenhuis, M. & Klionsky, D. J. Peroxisome degradation in *Saccharomyces cerevisiae* is dependent on machinery of macroautophagy and the Cvt pathway. *J Cell Sci* **112 ( Pt 22)**, 4079–4087 (1999).
6. Kim, I., Rodriguez-Enriquez, S. & Lemasters, J. J. Selective degradation of mitochondria by mitophagy. *Arch Biochem Biophys* **462**, 245–253 (2007).
7. Weidberg, H., Shvets, E. & Elazar, Z. Biogenesis and cargo selectivity of autophagosomes. *Annu Rev Biochem* **80**, 125–156 (2011).
8. Boyle, K. B. & Randow, F. The role of ‘eat-me’ signals and autophagy cargo receptors in innate immunity. *Curr Opin Microbiol* **16**, 339–348 (2013).
9. Johansen, T. & Lamark, T. Selective autophagy mediated by autophagic adapter proteins. *Autophagy* **7**, 279–296 (2011).
10. Randow, F. & Youle, R. J. Self and nonself: how autophagy targets mitochondria and bacteria. *Cell Host Microbe* **15**, 403–411 (2014).
11. Khaminets, A., Behl, C. & Dikic, I. Ubiquitin-Dependent And Independent Signals In Selective Autophagy. *Trends Cell Biol* **26**, 6–16 (2016).
12. Deretic, V. Thematic issue on how autophagosomes find their targets. *Autophagy* **7**, 257–259 (2011).
13. Joung, I., Strominger, J. L. & Shin, J. Molecular cloning of a phosphotyrosine-independent ligand of the p56lck SH2 domain. *Proc Natl Acad Sci U S A* **93**, 5991–5995 (1996).
14. Vadlamudi, R. K., Joung, I., Strominger, J. L. & Shin, J. p62, a phosphotyrosine-independent ligand of the SH2 domain of p56lck, belongs to a new class of ubiquitin-binding proteins. *J Biol Chem* **271**, 20235–20237 (1996).
15. Kuusisto, E., Salminen, A. & Alafuzoff, I. Ubiquitin-binding protein p62 is present in neuronal and glial inclusions in human tauopathies and synucleinopathies. *Neuroreport* **12**, 2085–2090 (2001).
16. Zatloukal, K. *et al.* p62 Is a common component of cytoplasmic inclusions in protein aggregation diseases. *Am J Pathol* **160**, 255–263 (2002).
17. Lamark, T. *et al.* Interaction codes within the family of mammalian Phox and Bem1p domain-containing proteins. *J Biol Chem* **278**, 34568–34581 (2003).
18. Wilson, M. I., Gill, D. J., Perisic, O., Quinn, M. T. & Williams, R. L. PB1 domain-mediated heterodimerization in NADPH oxidase and signaling complexes of atypical protein kinase C with Par6 and p62. *Mol Cell* **12**, 39–50 (2003).
19. Bjørkøy, G. *et al.* p62/SQSTM1 forms protein aggregates degraded by autophagy and has a protective effect on huntingtin-induced cell death. *J Cell Biol* **171**, 603–614 (2005).
20. Pankiv, S. *et al.* p62/SQSTM1 binds directly to Atg8/LC3 to facilitate degradation of ubiquitinated protein aggregates by autophagy. *J Biol Chem* **282**, 24131–24145 (2007).
21. White, J., Suklabaidya, S., Vo, M. T., Choi, Y. B. & Harhaj, E. W. Multifaceted roles of TAX1BP1 in autophagy. *Autophagy* **19**, 44–53 (2023).
22. Kirkin, V. & Rogov, V. V. A Diversity of Selective Autophagy Receptors Determines the Specificity of the Autophagy Pathway. *Mol Cell* **76**, 268–285 (2019).
23. Rogov, V. V. *et al.* Structural basis for phosphorylation-triggered autophagic clearance of Salmonella. *Biochem J* **454**, 459–466 (2013).
24. Wild, P., McEwan, D. G. & Dikic, I. The LC3 interactome at a glance. *J Cell Sci* **127**, 3–9 (2014).
25. Zhu, Y. *et al.* Modulation of serines 17 and 24 in the LC3-interacting region of Bnip3 determines pro-survival mitophagy versus apoptosis. *J Biol Chem* **288**, 1099–1113 (2013).
26. Matsumoto, G., Shimogori, T., Hattori, N. & Nukina, N. TBK1 controls autophagosomal engulfment of polyubiquitinated mitochondria through p62/SQSTM1 phosphorylation. *Hum Mol Genet* **24**, 4429–4442 (2015).
27. Lim, J. *et al.* Proteotoxic stress induces phosphorylation of p62/SQSTM1 by ULK1 to regulate selective autophagic clearance of protein aggregates. *PLoS Genet* **11**, e1004987 (2015).



28. Cavey, J. R. *et al.* Loss of ubiquitin-binding associated with Paget's disease of bone p62 (SQSTM1) mutations. *J Bone Miner Res* **20**, 619–624 (2005).
29. Garner, T. P., Long, J., Layfield, R. & Searle, M. S. Impact of p62/SQSTM1 UBA domain mutations linked to Paget's disease of bone on ubiquitin recognition. *Biochemistry* **50**, 4665–4674 (2011).
30. Kirkin, V. *et al.* A role for NBR1 in autophagosomal degradation of ubiquitinated substrates. *Mol Cell* **33**, 505–516 (2009).
31. Mardakheh, F. K., Auciello, G., Dafforn, T. R., Rappoport, J. Z. & Heath, J. K. Nbr1 is a novel inhibitor of ligand-mediated receptor tyrosine kinase degradation. *Mol Cell Biol* **30**, 5672–5685 (2010).
32. Deosaran, E. *et al.* NBR1 acts as an autophagy receptor for peroxisomes. *J Cell Sci* **126**, 939–952 (2013).
33. Perrin, A. J., Jiang, X., Birmingham, C. L., So, N. S. Y. & Brumell, J. H. Recognition of bacteria in the cytosol of Mammalian cells by the ubiquitin system. *Curr Biol* **14**, 806–811 (2004).
34. Kraft, C., Deplazes, A., Sohrmann, M. & Peter, M. Mature ribosomes are selectively degraded upon starvation by an autophagy pathway requiring the Ubp3p/Bre5p ubiquitin protease. *Nat Cell Biol* **10**, 602–610 (2008).
35. Thurston, T. L. M., Ryzhakov, G., Bloor, S., von Muhlinen, N. & Randow, F. The TBK1 adaptor and autophagy receptor NDP52 restricts the proliferation of ubiquitin-coated bacteria. *Nat Immunol* **10**, 1215–1221 (2009).
36. Newman, A. C. *et al.* TBK1 kinase addiction in lung cancer cells is mediated via autophagy of Tax1bp1/Ndp52 and non-canonical NF- $\kappa$ B signalling. *PLoS One* **7**, e50672 (2012).
37. Tumbarello, D. A. *et al.* The Autophagy Receptor TAX1BP1 and the Molecular Motor Myosin VI Are Required for Clearance of Salmonella Typhimurium by Autophagy. *PLoS Pathog* **11**, e1005174 (2015).
38. Nthiga, T. M. *et al.* CALCOCO1 acts with VAMP-associated proteins to mediate ER-phagy. *EMBO J* **39**, e103649 (2020).
39. Chen, W., Ouyang, X., Chen, L. & Li, L. Multiple functions of CALCOCO family proteins in selective autophagy. *J Cell Physiol* **237**, 3505–3516 (2022).
40. von Muhlinen, N. *et al.* LC3C, bound selectively by a noncanonical LIR motive in NDP52, is required for antibacterial autophagy. *Mol Cell* **48**, 329–342 (2012).
41. Nthiga, T. M. *et al.* Regulation of Golgi turnover by CALCOCO1-mediated selective autophagy. *J Cell Biol* **220**, e202006128 (2021).
42. Xie, X. *et al.* Molecular basis of ubiquitin recognition by the autophagy receptor CALCOCO2. *Autophagy* **11**, 1775–1789 (2015).
43. Hu, S. *et al.* Mechanistic Insights into Recognitions of Ubiquitin and Myosin VI by Autophagy Receptor TAX1BP1. *J Mol Biol* **430**, 3283–3296 (2018).
44. Randow, F., MacMicking, J. D. & James, L. C. Cellular self-defense: how cell-autonomous immunity protects against pathogens. *Science* **340**, 701–706 (2013).
45. Tumbarello, D. A. *et al.* Autophagy receptors link myosin VI to autophagosomes to mediate Tom1-dependent autophagosome maturation and fusion with the lysosome. *Nat Cell Biol* **14**, 1024–1035 (2012).
46. Thurston, T. L. M., Wandel, M. P., von Muhlinen, N., Foeglein, A. & Randow, F. Galectin 8 targets damaged vesicles for autophagy to defend cells against bacterial invasion. *Nature* **482**, 414–418 (2012).
47. Osawa, T. *et al.* Optineurin in neurodegenerative diseases. *Neuropathology* **31**, 569–574 (2011).
48. Korac, J. *et al.* Ubiquitin-independent function of optineurin in autophagic clearance of protein aggregates. *J Cell Sci* **126**, 580–592 (2013).
49. Heo, J.-M., Ordureau, A., Paulo, J. A., Rinehart, J. & Harper, J. W. The PINK1-PARKIN Mitochondrial Ubiquitylation Pathway Drives a Program of OPTN/NDP52 Recruitment and TBK1 Activation to Promote Mitophagy. *Mol Cell* **60**, 7–20 (2015).
50. Richter, B. *et al.* Phosphorylation of OPTN by TBK1 enhances its binding to Ub chains and promotes selective autophagy of damaged mitochondria. *Proc Natl Acad Sci U S A* **113**, 4039–4044 (2016).
51. Prag, G. *et al.* Mechanism of ubiquitin recognition by the CUE domain of Vps9p. *Cell* **113**, 609–620 (2003).
52. Lu, K., Psakhye, I. & Jentsch, S. Autophagic clearance of polyQ proteins mediated by ubiquitin-Atg8 adaptors of the conserved CUET protein family. *Cell* **158**, 549–563 (2014).
53. Biederer, T., Volkwein, C. & Sommer, T. Role of Cue1p in ubiquitination and degradation at the ER surface. *Science* **278**, 1806–1809 (1997).
54. Marshall, R. S., McLoughlin, F. & Vierstra, R. D. Autophagic Turnover of Inactive 26S Proteasomes in Yeast Is Directed by the Ubiquitin Receptor Cue5 and the Hsp42 Chaperone. *Cell Rep* **16**, 1717–1732 (2016).
55. Capelluto, D. G. S. Tollip: a multitasking protein in innate immunity and protein trafficking. *Microbes Infect* **14**, 140–147 (2012).
56. Roche, P. A. & Furuta, K. The ins and outs of MHC class II-mediated antigen processing and presentation. *Nat Rev Immunol* **15**, 203–216 (2015).

57. Mitra, S., Traugher, C. A., Brannon, M. K., Gomez, S. & Capelluto, D. G. S. Ubiquitin interacts with the Tollip C2 and CUE domains and inhibits binding of Tollip to phosphoinositides. *J Biol Chem* **288**, 25780–25791 (2013).
58. Dobson, C. M. Protein folding and misfolding. *Nature* **426**, 884–890 (2003).
59. Lamark, T. & Johansen, T. Aggrephagy: selective disposal of protein aggregates by macroautophagy. *Int J Cell Biol* **2012**, 736905 (2012).
60. Clausen, T. H. *et al.* p62/SQSTM1 and ALFY interact to facilitate the formation of p62 bodies/ALIS and their degradation by autophagy. *Autophagy* **6**, 330–344 (2010).
61. Muscolino, E. *et al.* Herpesviruses induce aggregation and selective autophagy of host signalling proteins NEMO and RIPK1 as an immune-evasion mechanism. *Nat Microbiol* **5**, 331–342 (2020).
62. Seibenhener, M. L. *et al.* Sequestosome 1/p62 is a polyubiquitin chain binding protein involved in ubiquitin proteasome degradation. *Mol Cell Biol* **24**, 8055–8068 (2004).
63. Tan, J. M. M. *et al.* Lysine 63-linked ubiquitination promotes the formation and autophagic clearance of protein inclusions associated with neurodegenerative diseases. *Hum Mol Genet* **17**, 431–439 (2008).
64. Johnston, J. A., Ward, C. L. & Kopito, R. R. Aggresomes: a cellular response to misfolded proteins. *J Cell Biol* **143**, 1883–1898 (1998).
65. Kawaguchi, Y. *et al.* The deacetylase HDAC6 regulates aggresome formation and cell viability in response to misfolded protein stress. *Cell* **115**, 727–738 (2003).
66. Iwata, A., Riley, B. E., Johnston, J. A. & Kopito, R. R. HDAC6 and microtubules are required for autophagic degradation of aggregated huntingtin. *J Biol Chem* **280**, 40282–40292 (2005).
67. Strnad, P., Zatloukal, K., Stumptner, C., Kulaksiz, H. & Denk, H. Mallory-Denk-bodies: lessons from keratin-containing hepatic inclusion bodies. *Biochim Biophys Acta* **1782**, 764–774 (2008).
68. Nagaoka, U. *et al.* Increased expression of p62 in expanded polyglutamine-expressing cells and its association with polyglutamine inclusions. *J Neurochem* **91**, 57–68 (2004).
69. Lelouard, H. *et al.* Transient aggregation of ubiquitinated proteins during dendritic cell maturation. *Nature* **417**, 177–182 (2002).
70. Lelouard, H. *et al.* Dendritic cell aggresome-like induced structures are dedicated areas for ubiquitination and storage of newly synthesized defective proteins. *J Cell Biol* **164**, 667–675 (2004).
71. Pierre, P. Dendritic cells, DRiPs, and DALIS in the control of antigen processing. *Immunol Rev* **207**, 184–190 (2005).
72. Lelouard, H. *et al.* Regulation of translation is required for dendritic cell function and survival during activation. *J Cell Biol* **179**, 1427–1439 (2007).
73. Ketterer, N., Rogon, C., Limmer, A., Schild, H. & Höhfeld, J. The Hsc/Hsp70 co-chaperone network controls antigen aggregation and presentation during maturation of professional antigen presenting cells. *PLoS One* **6**, e16398 (2011).
74. Youle, R. J. & van der Bliek, A. M. Mitochondrial fission, fusion, and stress. *Science* **337**, 1062–1065 (2012).
75. Ding, W.-X. & Yin, X.-M. Mitophagy: mechanisms, pathophysiological roles, and analysis. *Biol Chem* **393**, 547–564 (2012).
76. Narendra, D., Tanaka, A., Suen, D.-F. & Youle, R. J. Parkin is recruited selectively to impaired mitochondria and promotes their autophagy. *J Cell Biol* **183**, 795–803 (2008).
77. Narendra, D. P. *et al.* PINK1 is selectively stabilized on impaired mitochondria to activate Parkin. *PLoS Biol* **8**, e1000298 (2010).
78. Matsuda, N. *et al.* PINK1 stabilized by mitochondrial depolarization recruits Parkin to damaged mitochondria and activates latent Parkin for mitophagy. *J Cell Biol* **189**, 211–221 (2010).
79. Kitada, T. *et al.* Mutations in the parkin gene cause autosomal recessive juvenile parkinsonism. *Nature* **392**, 605–608 (1998).
80. Sarraf, S. A. *et al.* Landscape of the PARKIN-dependent ubiquitylome in response to mitochondrial depolarization. *Nature* **496**, 372–376 (2013).
81. Ordureau, A. *et al.* Dynamics of PARKIN-Dependent Mitochondrial Ubiquitylation in Induced Neurons and Model Systems Revealed by Digital Snapshot Proteomics. *Mol Cell* **70**, 211–227.e8 (2018).
82. Lazarou, M. *et al.* The ubiquitin kinase PINK1 recruits autophagy receptors to induce mitophagy. *Nature* **524**, 309–314 (2015).
83. Wong, Y. C. & Holzbaur, E. L. F. Optineurin is an autophagy receptor for damaged mitochondria in parkin-mediated mitophagy that is disrupted by an ALS-linked mutation. *Proc Natl Acad Sci U S A* **111**, E4439–4448 (2014).
84. Chen, K. *et al.* Optineurin inhibits NLRP3 inflammasome activation by enhancing mitophagy of renal tubular cells in diabetic nephropathy. *FASEB J* **33**, 4571–4585 (2019).
85. Ogawa, M. *et al.* Escape of intracellular Shigella from autophagy. *Science* **307**, 727–731 (2005).

86. Py, B. F., Lipinski, M. M. & Yuan, J. Autophagy limits *Listeria monocytogenes* intracellular growth in the early phase of primary infection. *Autophagy* **3**, 117–125 (2007).
87. Birmingham, C. L., Smith, A. C., Bakowski, M. A., Yoshimori, T. & Brumell, J. H. Autophagy controls *Salmonella* infection in response to damage to the *Salmonella*-containing vacuole. *J Biol Chem* **281**, 11374–11383 (2006).
88. Zheng, Y. T. *et al.* The adaptor protein p62/SQSTM1 targets invading bacteria to the autophagy pathway. *J Immunol* **183**, 5909–5916 (2009).
89. Wild, P. *et al.* Phosphorylation of the autophagy receptor optineurin restricts *Salmonella* growth. *Science* **333**, 228–233 (2011).
90. Lin, C.-Y. *et al.* Autophagy Receptor Tollip Facilitates Bacterial Autophagy by Recruiting Galectin-7 in Response to Group A *Streptococcus* Infection. *Front Cell Infect Microbiol* **10**, 583137 (2020).
91. Jin, J. *et al.* The kinase TBK1 controls IgA class switching by negatively regulating noncanonical NF- $\kappa$ B signaling. *Nat Immunol* **13**, 1101–1109 (2012).
92. Balka, K. R. *et al.* TBK1 and IKK $\epsilon$  Act Redundantly to Mediate STING-Induced NF- $\kappa$ B Responses in Myeloid Cells. *Cell Rep* **31**, 107492 (2020).
93. Cuervo, A. M. & Wong, E. Chaperone-mediated autophagy: roles in disease and aging. *Cell Res* **24**, 92–104 (2014).
94. Zhou, D. *et al.* Lamp-2a Facilitates MHC Class II Presentation of Cytoplasmic Antigens. *Immunity* **22**, 571–581 (2005).
95. Crotzer, V. L. & Blum, J. S. Autophagy and its role in MHC-mediated antigen presentation. *J Immunol* **182**, 3335–3341 (2009).
96. Galluzzi, L. *et al.* Molecular definitions of autophagy and related processes. *EMBO J* **36**, 1811–1836 (2017).
97. Oku, M. & Sakai, Y. Three Distinct Types of Microautophagy Based on Membrane Dynamics and Molecular Machineries. *Bioessays* **40**, e1800008 (2018).
98. Axe, E. L. *et al.* Autophagosome formation from membrane compartments enriched in phosphatidylinositol 3-phosphate and dynamically connected to the endoplasmic reticulum. *J Cell Biol* **182**, 685–701 (2008).
99. Russell, R. C., Yuan, H.-X. & Guan, K.-L. Autophagy regulation by nutrient signaling. *Cell Res* **24**, 42–57 (2014).
100. Hayashi-Nishino, M. *et al.* A subdomain of the endoplasmic reticulum forms a cradle for autophagosome formation. *Nat Cell Biol* **11**, 1433–1437 (2009).
101. Ylä-Anttila, P., Vihinen, H., Jokitalo, E. & Eskelinen, E.-L. 3D tomography reveals connections between the phagophore and endoplasmic reticulum. *Autophagy* **5**, 1180–1185 (2009).
102. Hailey, D. W. *et al.* Mitochondria supply membranes for autophagosome biogenesis during starvation. *Cell* **141**, 656–667 (2010).
103. Ravikumar, B., Moreau, K., Jahreiss, L., Puri, C. & Rubinsztein, D. C. Plasma membrane contributes to the formation of pre-autophagosomal structures. *Nat Cell Biol* **12**, 747–757 (2010).
104. van der Vaart, A., Griffith, J. & Reggiori, F. Exit from the Golgi is required for the expansion of the autophagosomal phagophore in yeast *Saccharomyces cerevisiae*. *Mol Biol Cell* **21**, 2270–2284 (2010).
105. Mizushima, N., Yoshimori, T. & Ohsumi, Y. The role of Atg proteins in autophagosome formation. *Annu Rev Cell Dev Biol* **27**, 107–132 (2011).
106. Trocoli, A. & Djavaheri-Mergny, M. The complex interplay between autophagy and NF- $\kappa$ B signaling pathways in cancer cells. *Am J Cancer Res* **1**, 629–649 (2011).
107. Matsunaga, K. *et al.* Two Beclin 1-binding proteins, Atg14L and Rubicon, reciprocally regulate autophagy at different stages. *Nat Cell Biol* **11**, 385–396 (2009).
108. Sun, T. *et al.* Acetylation of Beclin 1 inhibits autophagosome maturation and promotes tumour growth. *Nat Commun* **6**, 7215 (2015).
109. Jäger, S. *et al.* Role for Rab7 in maturation of late autophagic vacuoles. *J Cell Sci* **117**, 4837–4848 (2004).
110. Eskelinen, E.-L. Maturation of autophagic vacuoles in Mammalian cells. *Autophagy* **1**, 1–10 (2005).
111. Fader, C. M., Sánchez, D., Furlán, M. & Colombo, M. I. Induction of autophagy promotes fusion of multivesicular bodies with autophagic vacuoles in k562 cells. *Traffic* **9**, 230–250 (2008).
112. Zhao, Y. G. & Zhang, H. Autophagosome maturation: An epic journey from the ER to lysosomes. *J Cell Biol* **218**, 757–770 (2019).
113. Lee, J.-A., Beigneux, A., Ahmad, S. T., Young, S. G. & Gao, F.-B. ESCRT-III dysfunction causes autophagosome accumulation and neurodegeneration. *Curr Biol* **17**, 1561–1567 (2007).
114. Kruppa, A. J., Kendrick-Jones, J. & Buss, F. Myosins, Actin and Autophagy. *Traffic* **17**, 878–890 (2016).
115. Sahlender, D. A. *et al.* Optineurin links myosin VI to the Golgi complex and is involved in Golgi organization and exocytosis. *J Cell Biol* **169**, 285–295 (2005).

116. Morriswood, B. *et al.* T6BP and NDP52 are myosin VI binding partners with potential roles in cytokine signalling and cell adhesion. *J Cell Sci* **120**, 2574–2585 (2007).
117. Rogov, V., Dötsch, V., Johansen, T. & Kirkin, V. Interactions between autophagy receptors and ubiquitin-like proteins form the molecular basis for selective autophagy. *Mol Cell* **53**, 167–178 (2014).
118. Fracchiolla, D., Sawa-Makarska, J. & Martens, S. Beyond Atg8 binding: The role of AIM/LIR motives in autophagy. *Autophagy* **13**, 978–979 (2017).
119. Sawa-Makarska, J. *et al.* Cargo binding to Atg19 unmasks additional Atg8 binding sites to mediate membrane-cargo apposition during selective autophagy. *Nat Cell Biol* **16**, 425–433 (2014).
120. Wurzer, B. *et al.* Oligomerization of p62 allows for selection of ubiquitinated cargo and isolation membrane during selective autophagy. *Elife* **4**, e08941 (2015).
121. Johansen, T. & Lamark, T. Selective Autophagy: ATG8 Family Proteins, LIR Motives and Cargo Receptors. *J Mol Biol* **432**, 80–103 (2020).
122. Vargas, J. N. S. *et al.* Spatiotemporal Control of ULK1 Activation by NDP52 and TBK1 during Selective Autophagy. *Mol Cell* **74**, 347–362.e6 (2019).
123. Ravenhill, B. J. *et al.* The Cargo Receptor NDP52 Initiates Selective Autophagy by Recruiting the ULK Complex to Cytosol-Invasive Bacteria. *Mol Cell* **74**, 320–329.e6 (2019).
124. Turco, E. *et al.* FIP200 Claw Domain Binding to p62 Promotes Autophagosome Formation at Ubiquitin Condensates. *Mol Cell* **74**, 330–346.e11 (2019).
125. Alemu, E. A. *et al.* ATG8 family proteins act as scaffolds for assembly of the ULK complex: sequence requirements for LC3-interacting region (LIR) motives. *J Biol Chem* **287**, 39275–39290 (2012).
126. Kraft, C. *et al.* Binding of the Atg1/ULK1 kinase to the ubiquitin-like protein Atg8 regulates autophagy. *EMBO J* **31**, 3691–3703 (2012).
127. Nakatogawa, H. *et al.* The autophagy-related protein kinase Atg1 interacts with the ubiquitin-like protein Atg8 via the Atg8 family interacting motive to facilitate autophagosome formation. *J Biol Chem* **287**, 28503–28507 (2012).
128. Birgisdottir, Á. B. *et al.* Members of the autophagy class III phosphatidylinositol 3-kinase complex I interact with GABARAP and GABARAPL1 via LIR motives. *Autophagy* **15**, 1333–1355 (2019).
129. Park, B. *et al.* Impairment of protein trafficking upon overexpression and mutation of optineurin. *PLoS One* **5**, e11547 (2010).
130. Ying, H. & Yue, B. Y. J. T. Cellular and molecular biology of optineurin. *Int Rev Cell Mol Biol* **294**, 223–258 (2012).
131. Jongsma, M. L. M. *et al.* An ER-Associated Pathway Defines Endosomal Architecture for Controlled Cargo Transport. *Cell* **166**, 152–166 (2016).
132. Pai, S. & Thomas, R. Immune deficiency or hyperactivity-Nf-kappab illuminates autoimmunity. *J Autoimmun* **31**, 245–251 (2008).
133. Hayden, M. S. & Ghosh, S. Shared Principles in NF-κB Signaling. *Cell* **132**, 344–362 (2008).
134. Wertz, I. E. *et al.* De-ubiquitination and ubiquitin ligase domains of A20 downregulate NF-κB signalling. *Nature* **430**, 694–699 (2004).
135. Boone, D. L. *et al.* The ubiquitin-modifying enzyme A20 is required for termination of Toll-like receptor responses. *Nat Immunol* **5**, 1052–1060 (2004).
136. De Valck, D. *et al.* The zinc finger protein A20 interacts with a novel anti-apoptotic protein which is cleaved by specific caspases. *Oncogene* **18**, 4182–4190 (1999).
137. Li, Q. & Verma, I. M. NF-kappaB regulation in the immune system. *Nat Rev Immunol* **2**, 725–734 (2002).
138. Shembade, N., Harhaj, N. S., Liebl, D. J. & Harhaj, E. W. Essential role for TAX1BP1 in the termination of TNF-alpha-, IL-1- and LPS-mediated NF-kappaB and JNK signaling. *EMBO J* **26**, 3910–3922 (2007).
139. Verstrepen, L., Verhelst, K., Carpentier, I. & Beyaert, R. TAX1BP1, a ubiquitin-binding adaptor protein in innate immunity and beyond. *Trends in Biochemical Sciences* S096800041100048X (2011) doi:10.1016/j.tibs.2011.03.004.
140. Shembade, N., Ma, A. & Harhaj, E. W. Inhibition of NF-kappaB signaling by A20 through disruption of ubiquitin enzyme complexes. *Science* **327**, 1135–1139 (2010).
141. Schwamborn, K., Weil, R., Courtois, G., Whiteside, S. T. & Israël, A. Phorbol esters and cytokines regulate the expression of the NEMO-related protein, a molecule involved in a NF-kappa B-independent pathway. *J Biol Chem* **275**, 22780–22789 (2000).
142. Sudhakar, C., Nagabushana, A., Jain, N. & Swarup, G. NF-kappaB mediates tumor necrosis factor alpha-induced expression of optineurin, a negative regulator of NF-kappaB. *PLoS One* **4**, e5114 (2009).
143. Seibenhener, M. L., Geetha, T. & Wooten, M. W. Sequestosome 1/p62--more than just a scaffold. *FEBS Lett* **581**, 175–179 (2007).

144. Miyashita, H. *et al.* Crosstalk Between NDP52 and LUBAC in Innate Immune Responses, Cell Death, and Xenophagy. *Front Immunol* **12**, 635475 (2021).
145. Dausset, J. [Iso-leuko-antibodies]. *Acta Haematol* **20**, 156–166 (1958).
146. Beck, S. & Trowsdale, J. The human major histocompatibility complex: lessons from the DNA sequence. *Annu Rev Genomics Hum Genet* **1**, 117–137 (2000).
147. Brown, J. H. *et al.* Three-dimensional structure of the human class II histocompatibility antigen HLA-DR1. *Nature* **364**, 33–39 (1993).
148. Stern, L. J. *et al.* Crystal structure of the human class II MHC protein HLA-DR1 complexed with an influenza virus peptide. *Nature* **368**, 215–221 (1994).
149. Jardetzky, T. S. *et al.* Three-dimensional structure of a human class II histocompatibility molecule complexed with superantigen. *Nature* **368**, 711–718 (1994).
150. Falk, K., Rötzschke, O., Stevanović, S., Jung, G. & Rammensee, H. G. Pool sequencing of natural HLA-DR, DQ, and DP ligands reveals detailed peptide motives, constraints of processing, and general rules. *Immunogenetics* **39**, 230–242 (1994).
151. Yewdell, J. W., Reits, E. & Neefjes, J. Making sense of mass destruction: quantitating MHC class I antigen presentation. *Nat Rev Immunol* **3**, 952–961 (2003).
152. Glickman, M. H. & Ciechanover, A. The ubiquitin-proteasome proteolytic pathway: destruction for the sake of construction. *Physiol Rev* **82**, 373–428 (2002).
153. Neefjes, J., Jongsmma, M. L. M., Paul, P. & Bakke, O. Towards a systems understanding of MHC class I and MHC class II antigen presentation. *Nat Rev Immunol* **11**, 823–836 (2011).
154. Blum, J. S., Wearsch, P. A. & Cresswell, P. Pathways of antigen processing. *Annu Rev Immunol* **31**, 443–473 (2013).
155. Rammensee, H. G., Friede, T. & Stevanović, S. MHC ligands and peptide motives: first listing. *Immunogenetics* **41**, 178–228 (1995).
156. Rammensee, H., Bachmann, J., Emmerich, N. P., Bachor, O. A. & Stevanović, S. SYFPEITHI: database for MHC ligands and peptide motives. *Immunogenetics* **50**, 213–219 (1999).
157. Ferrington, D. A. & Gregerson, D. S. Immunoproteasomes: structure, function, and antigen presentation. *Prog Mol Biol Transl Sci* **109**, 75–112 (2012).
158. Chen, W., Norbury, C. C., Cho, Y., Yewdell, J. W. & Bennink, J. R. Immunoproteasomes shape immunodominance hierarchies of antiviral CD8(+) T cells at the levels of T cell repertoire and presentation of viral antigens. *J Exp Med* **193**, 1319–1326 (2001).
159. de Verteuil, D. *et al.* Deletion of immunoproteasome subunits imprints on the transcriptome and has a broad impact on peptides presented by major histocompatibility complex I molecules. *Mol Cell Proteomics* **9**, 2034–2047 (2010).
160. Rock, K. L., York, I. A. & Goldberg, A. L. Post-proteasomal antigen processing for major histocompatibility complex class I presentation. *Nat Immunol* **5**, 670–677 (2004).
161. Michalek, M. T., Grant, E. P., Gramm, C., Goldberg, A. L. & Rock, K. L. A role for the ubiquitin-dependent proteolytic pathway in MHC class I-restricted antigen presentation. *Nature* **363**, 552–554 (1993).
162. Qian, S.-B. *et al.* Tight linkage between translation and MHC class I peptide ligand generation implies specialized antigen processing for defective ribosomal products. *J Immunol* **177**, 227–233 (2006).
163. Wherry, E. J. *et al.* Re-evaluating the Generation of a “Proteasome-Independent” MHC Class I-Restricted CD8 T Cell Epitope. *The Journal of Immunology* **176**, 2249–2261 (2006).
164. Yewdell, J. W., Antón, L. C. & Bennink, J. R. Defective ribosomal products (DRiPs): a major source of antigenic peptides for MHC class I molecules? *The Journal of Immunology* **157**, 1823–1826 (1996).
165. Schubert, U. *et al.* Rapid degradation of a large fraction of newly synthesized proteins by proteasomes. *Nature* **404**, 770–774 (2000).
166. Reits, E. A., Vos, J. C., Grommé, M. & Neefjes, J. The major substrates for TAP in vivo are derived from newly synthesized proteins. *Nature* **404**, 774–778 (2000).
167. Yewdell, J. W. & Nicchitta, C. V. The DRiP hypothesis decennial: support, controversy, refinement and extension. *Trends in Immunology* **27**, 368–373 (2006).
168. Antón, L. C. & Yewdell, J. W. Translating DRiPs: MHC class I immunosurveillance of pathogens and tumors. *J Leukoc Biol* **95**, 551–562 (2014).
169. Rock, K. L., Farfán-Arribas, D. J., Colbert, J. D. & Goldberg, A. L. Re-examining class-I presentation and the DRiP hypothesis. *Trends Immunol* **35**, 144–152 (2014).
170. Apcher, S. *et al.* Major source of antigenic peptides for the MHC class I pathway is produced during the pioneer round of mRNA translation. *Proc Natl Acad Sci U S A* **108**, 11572–11577 (2011).
171. Esquivel, F., Yewdell, J. & Bennink, J. RMA/S cells present endogenously synthesized cytosolic proteins to class I-restricted cytotoxic T lymphocytes. *J Exp Med* **175**, 163–168 (1992).

172. Shastri, N., Nguyen, V. & Gonzalez, F. Major histocompatibility class I molecules can present cryptic translation products to T-cells. *J Biol Chem* **270**, 1088–1091 (1995).
173. Fettes, J. V., Roy, N. & Gilboa, E. A frameshift mutation at the NH2 terminus of the nucleoprotein gene does not affect generation of cytotoxic T lymphocyte epitopes. *J Immunol* **147**, 2697–2705 (1991).
174. Bullock, T. N. & Eisenlohr, L. C. Ribosomal scanning past the primary initiation codon as a mechanism for expression of CTL epitopes encoded in alternative reading frames. *J Exp Med* **184**, 1319–1329 (1996).
175. Berglund, P., Finzi, D., Bennink, J. R. & Yewdell, J. W. Viral alteration of cellular translational machinery increases defective ribosomal products. *J Virol* **81**, 7220–7229 (2007).
176. Gout, J.-F., Thomas, W. K., Smith, Z., Okamoto, K. & Lynch, M. Large-scale detection of in vivo transcription errors. *Proc Natl Acad Sci U S A* **110**, 18584–18589 (2013).
177. Saric, T. *et al.* An IFN-gamma-induced aminopeptidase in the ER, ERAP1, trims precursors to MHC class I-presented peptides. *Nat Immunol* **3**, 1169–1176 (2002).
178. Saveanu, L. *et al.* Concerted peptide trimming by human ERAP1 and ERAP2 aminopeptidase complexes in the endoplasmic reticulum. *Nat Immunol* **6**, 689–697 (2005).
179. Chang, S.-C., Momburg, F., Bhutani, N. & Goldberg, A. L. The ER aminopeptidase, ERAP1, trims precursors to lengths of MHC class I peptides by a ‘molecular ruler’ mechanism. *Proc Natl Acad Sci U S A* **102**, 17107–17112 (2005).
180. Hammer, G. E., Gonzalez, F., James, E., Nolla, H. & Shastri, N. In the absence of aminopeptidase ERAAP, MHC class I molecules present many unstable and highly immunogenic peptides. *Nat Immunol* **8**, 101–108 (2007).
181. Paulsson, K. & Wang, P. Chaperones and folding of MHC class I molecules in the endoplasmic reticulum. *Biochim Biophys Acta* **1641**, 1–12 (2003).
182. Wearsch, P. A. & Cresswell, P. Selective loading of high-affinity peptides onto major histocompatibility complex class I molecules by the tapasin-ERp57 heterodimer. *Nat Immunol* **8**, 873–881 (2007).
183. Thomas, C. & Tampé, R. Proofreading of Peptide-MHC Complexes through Dynamic Multivalent Interactions. *Front Immunol* **8**, 65 (2017).
184. Domnick, A. *et al.* Molecular basis of MHC I quality control in the peptide loading complex. *Nat Commun* **13**, 4701 (2022).
185. Joffre, O. P., Segura, E., Savina, A. & Amigorena, S. Cross-presentation by dendritic cells. *Nat Rev Immunol* **12**, 557–569 (2012).
186. Geijtenbeek, T. B. *et al.* DC-SIGN, a dendritic cell-specific HIV-1-binding protein that enhances trans-infection of T cells. *Cell* **100**, 587–597 (2000).
187. Moris, A. *et al.* DC-SIGN promotes exogenous MHC-I-restricted HIV-1 antigen presentation. *Blood* **103**, 2648–2654 (2004).
188. Gros, M. & Amigorena, S. Regulation of Antigen Export to the Cytosol During Cross-Presentation. *Front Immunol* **10**, 41 (2019).
189. Firat, E. *et al.* The role of endoplasmic reticulum-associated aminopeptidase 1 in immunity to infection and in cross-presentation. *J Immunol* **178**, 2241–2248 (2007).
190. Saveanu, L. *et al.* IRAP identifies an endosomal compartment required for MHC class I cross-presentation. *Science* **325**, 213–217 (2009).
191. Shen, L., Sigal, L. J., Boes, M. & Rock, K. L. Important Role of Cathepsin S in Generating Peptides for TAP-Independent MHC Class I Crosspresentation In Vivo. *Immunity* **21**, 155–165 (2004).
192. Ackerman, A. L., Kyritsis, C., Tampé, R. & Cresswell, P. Early phagosomes in dendritic cells form a cellular compartment sufficient for cross presentation of exogenous antigens. *Proc Natl Acad Sci U S A* **100**, 12889–12894 (2003).
193. Lizée, G. *et al.* Control of dendritic cell cross-presentation by the major histocompatibility complex class I cytoplasmic domain. *Nat Immunol* **4**, 1065–1073 (2003).
194. Howe, C. *et al.* Calreticulin-dependent recycling in the early secretory pathway mediates optimal peptide loading of MHC class I molecules. *EMBO J* **28**, 3730–3744 (2009).
195. Steimle, V., Siegrist, C. A., Mottet, A., Lisowska-Grospierre, B. & Mach, B. Regulation of MHC class II expression by interferon-gamma mediated by the transactivator gene CIITA. *Science* **265**, 106–109 (1994).
196. Masternak, K. *et al.* CIITA is a transcriptional coactivator that is recruited to MHC class II promoters by multiple synergistic interactions with an enhanceosome complex. *Genes Dev* **14**, 1156–1166 (2000).
197. van den Elsen, P. J. Expression Regulation of Major Histocompatibility Complex Class I and Class II Encoding Genes. *Front. Immun.* **2**, (2011).
198. Choi, N. M., Majumder, P. & Boss, J. M. Regulation of major histocompatibility complex class II genes. *Curr Opin Immunol* **23**, 81–87 (2011).
199. Chang, C. H., Fontes, J. D., Peterlin, M. & Flavell, R. A. Class II transactivator (CIITA) is sufficient for the inducible expression of major histocompatibility complex class II genes. *J Exp Med* **180**, 1367–1374 (1994).

200. Reith, W., LeibundGut-Landmann, S. & Waldburger, J.-M. Regulation of MHC class II gene expression by the class II transactivator. *Nat Rev Immunol* **5**, 793–806 (2005).
201. Muhlethaler-Mottet, A., Otten, L. A., Steimle, V. & Mach, B. Expression of MHC class II molecules in different cellular and functional compartments is controlled by differential usage of multiple promoters of the transactivator CIITA. *EMBO J* **16**, 2851–2860 (1997).
202. Wijdeven, R. H. *et al.* Chemical and genetic control of IFN $\gamma$ -induced MHCII expression. *EMBO Rep* **19**, e45553 (2018).
203. Roche, P. A., Marks, M. S. & Cresswell, P. Formation of a nine-subunit complex by HLA class II glycoproteins and the invariant chain. *Nature* **354**, 392–394 (1991).
204. Anderson, K. S. & Cresswell, P. A role for calnexin (IP90) in the assembly of class II MHC molecules. *EMBO J* **13**, 675–682 (1994).
205. Romagnoli, P. & Germain, R. N. Inhibition of invariant chain (Ii)-calnexin interaction results in enhanced degradation of Ii but does not prevent the assembly of alpha beta Ii complexes. *J Exp Med* **182**, 2027–2036 (1995).
206. Cresswell, P. Assembly, transport, and function of MHC class II molecules. *Annu Rev Immunol* **12**, 259–293 (1994).
207. Arunachalam, B. & Cresswell, P. Molecular requirements for the interaction of class II major histocompatibility complex molecules and invariant chain with calnexin. *J Biol Chem* **270**, 2784–2790 (1995).
208. Roche, P. A. & Cresswell, P. Proteolysis of the class II-associated invariant chain generates a peptide binding site in intracellular HLA-DR molecules. *Proc Natl Acad Sci U S A* **88**, 3150–3154 (1991).
209. Romagnoli, P. & Germain, R. N. The CLIP region of invariant chain plays a critical role in regulating major histocompatibility complex class II folding, transport, and peptide occupancy. *Journal of Experimental Medicine* **180**, 1107–1113 (1994).
210. Busch, R., Cloutier, I., Sékaly, R. P. & Hämmerling, G. J. Invariant chain protects class II histocompatibility antigens from binding intact polypeptides in the endoplasmic reticulum. *EMBO J* **15**, 418–428 (1996).
211. Sadegh-Nasseri, S., Stern, L. J., Wiley, D. C. & Germain, R. N. MHC class II function preserved by low-affinity peptide interactions preceding stable binding. *Nature* **370**, 647–650 (1994).
212. Bakke, O. & Dobberstein, B. MHC class II-associated invariant chain contains a sorting signal for endosomal compartments. *Cell* **63**, 707–716 (1990).
213. Claesson, L., Larhammar, D., Rask, L. & Peterson, P. A. cDNA clone for the human invariant gamma chain of class II histocompatibility antigens and its implications for the protein structure. *Proc Natl Acad Sci U S A* **80**, 7395–7399 (1983).
214. Strubin, M., Mach, B. & Long, E. O. The complete sequence of the mRNA for the HLA-DR-associated invariant chain reveals a polypeptide with an unusual transmembrane polarity. *EMBO J* **3**, 869–872 (1984).
215. Neefjes, J. J., Stollorz, V., Peters, P. J., Geuze, H. J. & Ploegh, H. L. The biosynthetic pathway of MHC class II but not class I molecules intersects the endocytic route. *Cell* **61**, 171–183 (1990).
216. Roche, P. A., Teletski, C. L., Stang, E., Bakke, O. & Long, E. O. Cell surface HLA-DR-invariant chain complexes are targeted to endosomes by rapid internalization. *Proc Natl Acad Sci U S A* **90**, 8581–8585 (1993).
217. Cloutier, M., Fortin, J.-S. & Thibodeau, J. The transmembrane domain and luminal C-terminal region independently support invariant chain trimerization and assembly with MHCII into nonamers. *BMC Immunol* **22**, 56 (2021).
218. Shachar, I., Elliott, E. A., Chasnoff, B., Grewal, I. S. & Flavell, R. A. Reconstitution of invariant chain function in transgenic mice in vivo by individual p31 and p41 isoforms. *Immunity* **3**, 373–383 (1995).
219. Thibodeau, J., Moulefera, M. A. & Balthazard, R. On the structure-function of MHC class II molecules and how single amino acid polymorphisms could alter intracellular trafficking. *Hum Immunol* **80**, 15–31 (2019).
220. Rodionov, D. G. & Bakke, O. Medium chains of adaptor complexes AP-1 and AP-2 recognize leucine-based sorting signals from the invariant chain. *J Biol Chem* **273**, 6005–6008 (1998).
221. McCormick, P. J., Martina, J. A. & Bonifacio, J. S. Involvement of clathrin and AP-2 in the trafficking of MHC class II molecules to antigen-processing compartments. *Proc Natl Acad Sci U S A* **102**, 7910–7915 (2005).
222. Dugast, M., Toussaint, H., Dousset, C. & Benaroch, P. AP2 clathrin adaptor complex, but not AP1, controls the access of the major histocompatibility complex (MHC) class II to endosomes. *J Biol Chem* **280**, 19656–19664 (2005).
223. Santambrogio, L. Molecular Determinants Regulating the Plasticity of the MHC Class II Immunopeptidome. *Front Immunol* **13**, 878271 (2022).
224. Peters, P. J., Neefjes, J. J., Oorschot, V., Ploegh, H. L. & Geuze, H. J. Segregation of MHC class II molecules from MHC class I molecules in the Golgi complex for transport to lysosomal compartments. *Nature* **349**, 669–676 (1991).

225. Ziegler, H. K. & Unanue, E. R. Decrease in macrophage antigen catabolism caused by ammonia and chloroquine is associated with inhibition of antigen presentation to T cells. *Proc. Natl. Acad. Sci. U.S.A.* **79**, 175–178 (1982).
226. Hartman, I. Z. *et al.* A reductionist cell-free major histocompatibility complex class II antigen processing system identifies immunodominant epitopes. *Nat Med* **16**, 1333–1340 (2010).
227. van den Hoorn, T., Paul, P., Janssen, L., Janssen, H. & Neefjes, J. Dynamics within tetraspanin pairs affect MHC class II expression. *Journal of Cell Science* **125**, 328–339 (2012).
228. Potoличchio, I. *et al.* Conformational Variation of Surface Class II MHC Proteins during Myeloid Dendritic Cell Differentiation Accompanies Structural Changes in Lysosomal MIIC. *The Journal of Immunology* **175**, 4935–4947 (2005).
229. Sanderson, F. *et al.* Accumulation of HLA-DM, a regulator of antigen presentation, in MHC class II compartments. *Science* **266**, 1566–1569 (1994).
230. Hsing, L. C. & Rudensky, A. Y. The lysosomal cysteine proteases in MHC class II antigen presentation. *Immunol Rev* **207**, 229–241 (2005).
231. Blum, J. S. & Cresswell, P. Role for intracellular proteases in the processing and transport of class II HLA antigens. *Proc Natl Acad Sci U S A* **85**, 3975–3979 (1988).
232. Nguyen, Q. V., Knapp, W. & Humphreys, R. E. Inhibition by leupeptin and antipain of the intracellular proteolysis of Ii. *Hum Immunol* **24**, 153–163 (1989).
233. Manoury, B. *et al.* Asparagine endopeptidase can initiate the removal of the MHC class II invariant chain chaperone. *Immunity* **18**, 489–498 (2003).
234. Xu, M., Capraro, G. A., Daibata, M., Reyes, V. E. & Humphreys, R. E. Cathepsin B cleavage and release of invariant chain from MHC class II molecules follow a staged pattern. *Mol Immunol* **31**, 723–731 (1994).
235. Nakagawa, T. *et al.* Cathepsin L: critical role in Ii degradation and CD4 T cell selection in the thymus. *Science* **280**, 450–453 (1998).
236. Nakagawa, T. Y. *et al.* Impaired invariant chain degradation and antigen presentation and diminished collagen-induced arthritis in cathepsin S null mice. *Immunity* **10**, 207–217 (1999).
237. Riese, R. J. *et al.* Cathepsin S activity regulates antigen presentation and immunity. *J Clin Invest* **101**, 2351–2363 (1998).
238. Shi, G. P. *et al.* Cathepsin S required for normal MHC class II peptide loading and germinal center development. *Immunity* **10**, 197–206 (1999).
239. Riese, R. J. *et al.* Essential role for cathepsin S in MHC class II-associated invariant chain processing and peptide loading. *Immunity* **4**, 357–366 (1996).
240. Bania, J. *et al.* Human cathepsin S, but not cathepsin L, degrades efficiently MHC class II-associated invariant chain in nonprofessional APCs. *Proc Natl Acad Sci U S A* **100**, 6664–6669 (2003).
241. Costantino, C. M., Ploegh, H. L. & Hafler, D. A. Cathepsin S regulates class II MHC processing in human CD4+ HLA-DR+ T cells. *J Immunol* **183**, 945–952 (2009).
242. Bevec, T., Stoka, V., Pungercic, G., Dolenc, I. & Turk, V. Major histocompatibility complex class II-associated p41 invariant chain fragment is a strong inhibitor of lysosomal cathepsin L. *Journal of Experimental Medicine* **183**, 1331–1338 (1996).
243. Fineschi, B., Sakaguchi, K., Appella, E. & Miller, J. The proteolytic environment involved in MHC class II-restricted antigen presentation can be modulated by the p41 form of invariant chain. *The Journal of Immunology* **157**, 3211–3215 (1996).
244. Lennon-Dumenil, A.-M. The p41 isoform of invariant chain is a chaperone for cathepsin L. *The EMBO Journal* **20**, 4055–4064 (2001).
245. Mihelič, M., Doberšek, A., Gunčar, G. & Turk, D. Inhibitory Fragment from the p41 Form of Invariant Chain Can Regulate Activity of Cysteine Cathepsins in Antigen Presentation. *Journal of Biological Chemistry* **283**, 14453–14460 (2008).
246. Pierre, P. & Mellman, I. Developmental regulation of invariant chain proteolysis controls MHC class II trafficking in mouse dendritic cells. *Cell* **93**, 1135–1145 (1998).
247. Shi, G. P. *et al.* Role for cathepsin F in invariant chain processing and major histocompatibility complex class II peptide loading by macrophages. *J Exp Med* **191**, 1177–1186 (2000).
248. Sercarz, E. E. & Maverakis, E. Mhc-guided processing: binding of large antigen fragments. *Nat Rev Immunol* **3**, 621–629 (2003).
249. Bijlmakers, M. J., Benaroch, P. & Ploegh, H. L. Assembly of HLA DR1 molecules translated in vitro: binding of peptide in the endoplasmic reticulum precludes association with invariant chain. *The EMBO Journal* **13**, 2699–2707 (1994).



250. Riberdy, J. M., Newcomb, J. R., Surman, M. J., Barbosat, J. A. & Cresswell, P. HLA-DR molecules from an antigen-processing mutant cell line are associated with invariant chain peptides. *Nature* **360**, 474–477 (1992).
251. Kropshofer, H., Vogt, A. B. & Hämmerling, G. J. Structural features of the invariant chain fragment CLIP controlling rapid release from HLA-DR molecules and inhibition of peptide binding. *Proc Natl Acad Sci U S A* **92**, 8313–8317 (1995).
252. Zhong, G., Castellino, F., Romagnoli, P. & Germain, R. N. Evidence that binding site occupancy is necessary and sufficient for effective major histocompatibility complex (MHC) class II transport through the secretory pathway redefines the primary function of class II-associated invariant chain peptides (CLIP). *Journal of Experimental Medicine* **184**, 2061–2066 (1996).
253. Kropshofer, H. *et al.* Editing of the HLA-DR-peptide repertoire by HLA-DM. *EMBO J* **15**, 6144–6154 (1996).
254. Denzin, L. K. & Cresswell, P. HLA-DM induces CLIP dissociation from MHC class II alpha beta dimers and facilitates peptide loading. *Cell* **82**, 155–165 (1995).
255. Schulze, M.-S. E. & Wucherpennig, K. W. The mechanism of HLA-DM induced peptide exchange in the MHC class II antigen presentation pathway. *Current Opinion in Immunology* **24**, 105–111 (2012).
256. Kelly, A. P., Monaco, J. J., Cho, S. G. & Trowsdale, J. A new human HLA class II-related locus, DM. *Nature* **353**, 571–573 (1991).
257. Morris, P. *et al.* An essential role for HLA-DM in antigen presentation by class II major histocompatibility molecules. *Nature* **368**, 551–554 (1994).
258. Fling, S. P., Arp, B. & Pious, D. HLA-DMA and -DMB genes are both required for MHC class II/peptide complex formation in antigen-presenting cells. *Nature* **368**, 554–558 (1994).
259. Denzin, L. K., Robbins, N. F., Carboy-Newcomb, C. & Cresswell, P. Assembly and intracellular transport of HLA-DM and correction of the class II antigen-processing defect in T2 cells. *Immunity* **1**, 595–606 (1994).
260. Denzin, L. K., Hammond, C. & Cresswell, P. HLA-DM Interactions with Intermediates in HLA-DR Maturation and a Role for HLA-DM in Stabilizing Empty HLA-DR Molecules. *Journal of Experimental Medicine* **184**, 2153–2166 (1996).
261. Neumann, J., König, A. & Koch, N. Detection of aberrant association of DM with MHC class II subunits in the absence of invariant chain. *Int Immunol* **19**, 31–39 (2007).
262. Denzin, L. K. & Cresswell, P. Sibling rivalry: competition between MHC class II family members inhibits immunity. *Nat Struct Mol Biol* **20**, 7–10 (2013).
263. Denzin, L. K., Sant'Angelo, D. B., Hammond, C., Surman, M. J. & Cresswell, P. Negative regulation by HLA-DO of MHC class II-restricted antigen processing. *Science* **278**, 106–109 (1997).
264. Ramachandra, L., Kovats, S., Eastman, S. & Rudensky, A. Y. Variation in HLA-DM expression influences conversion of MHC class II alpha beta: class II-associated invariant chain peptide complexes to mature peptide-bound class II alpha beta dimers in a normal B cell line. *J Immunol* **156**, 2196–2204 (1996).
265. Muntasell, A. *et al.* Dissection of the HLA-DR4 peptide repertoire in endocrine epithelial cells: strong influence of invariant chain and HLA-DM expression on the nature of ligands. *J Immunol* **173**, 1085–1093 (2004).
266. Álvaro-Benito, M., Morrison, E., Abualrous, E. T., Kuroпка, B. & Freund, C. Quantification of HLA-DM-Dependent Major Histocompatibility Complex of Class II Immunopeptidomes by the Peptide Landscape Antigenic Epitope Alignment Utility. *Front Immunol* **9**, 872 (2018).
267. Wubbolts, R. *et al.* Direct vesicular transport of MHC class II molecules from lysosomal structures to the cell surface. *Journal of Cell Biology* **135**, 611–622 (1996).
268. Kleijmeer, M. *et al.* Reorganization of multivesicular bodies regulates MHC class II antigen presentation by dendritic cells. *J Cell Biol* **155**, 53–63 (2001).
269. Chow, A., Toomre, D., Garrett, W. & Mellman, I. Dendritic cell maturation triggers retrograde MHC class II transport from lysosomes to the plasma membrane. *Nature* **418**, 988–994 (2002).
270. Vascotto, F. *et al.* The actin-based motor protein myosin II regulates MHC class II trafficking and BCR-driven antigen presentation. *Journal of Cell Biology* **176**, 1007–1019 (2007).
271. Paul, P. *et al.* A Genome-wide multidimensional RNAi screen reveals pathways controlling MHC class II antigen presentation. *Cell* **145**, 268–283 (2011).
272. Buss, F. Myosin VI isoform localized to clathrin-coated vesicles with a role in clathrin-mediated endocytosis. *The EMBO Journal* **20**, 3676–3684 (2001).
273. Buss, F., Spudich, G. & Kendrick-Jones, J. MYOSIN VI: Cellular Functions and Motor Properties. *Annu. Rev. Cell Dev. Biol.* **20**, 649–676 (2004).
274. Wubbolts, R. & Neefjes, J. Intracellular transport and peptide loading of MHC class II molecules: regulation by chaperones and motors. *Immunol Rev* **172**, 189–208 (1999).

275. Rocha, N. & Neefjes, J. MHC class II molecules on the move for successful antigen presentation. *EMBO J* **27**, 1–5 (2008).
276. Germain, R. N. & Hendrix, L. R. MHC class II structure, occupancy and surface expression determined by post-endoplasmic reticulum antigen binding. *Nature* **353**, 134–139 (1991).
277. Sadegh-Nasseri, S. & Germain, R. N. A role for peptide in determining MHC class II structure. *Nature* **353**, 167–170 (1991).
278. Nelson, C. A., Petzold, S. J. & Unanue, E. R. Identification of two distinct properties of class II major histocompatibility complex-associated peptides. *Proc Natl Acad Sci U S A* **90**, 1227–1231 (1993).
279. Bosch, B., Heipertz, E. L., Drake, J. R. & Roche, P. A. Major histocompatibility complex (MHC) class II-peptide complexes arrive at the plasma membrane in cholesterol-rich microclusters. *J Biol Chem* **288**, 13236–13242 (2013).
280. Kropshofer, H. *et al.* Tetraspan microdomains distinct from lipid rafts enrich select peptide-MHC class II complexes. *Nat Immunol* **3**, 61–68 (2002).
281. Eren, E. *et al.* Location of major histocompatibility complex class II molecules in rafts on dendritic cells enhances the efficiency of T-cell activation and proliferation. *Scand J Immunol* **63**, 7–16 (2006).
282. Tewari, M. K., Sinnathamby, G., Rajagopal, D. & Eisenlohr, L. C. A cytosolic pathway for MHC class II-restricted antigen processing that is proteasome and TAP dependent. *Nat Immunol* **6**, 287–294 (2005).
283. Shin, J.-S. *et al.* Surface expression of MHC class II in dendritic cells is controlled by regulated ubiquitination. *Nature* **444**, 115–118 (2006).
284. Matsuki, Y. *et al.* Novel regulation of MHC class II function in B cells. *EMBO J* **26**, 846–854 (2007).
285. De Gassart, A. *et al.* MHC class II stabilization at the surface of human dendritic cells is the result of maturation-dependent MARCH I down-regulation. *Proc Natl Acad Sci U S A* **105**, 3491–3496 (2008).
286. Lapaque, N., Jahnke, M., Trowsdale, J. & Kelly, A. P. The HLA-DRalpha chain is modified by polyubiquitination. *J Biol Chem* **284**, 7007–7016 (2009).
287. Walseng, E. *et al.* Ubiquitination regulates MHC class II-peptide complex retention and degradation in dendritic cells. *Proc. Natl. Acad. Sci. U.S.A.* **107**, 20465–20470 (2010).
288. Cella, M., Engering, A., Pinet, V., Pieters, J. & Lanzavecchia, A. Inflammatory stimuli induce accumulation of MHC class II complexes on dendritic cells. *Nature* **388**, 782–787 (1997).
289. Pierre, P. *et al.* Developmental regulation of MHC class II transport in mouse dendritic cells. *Nature* **388**, 787–792 (1997).
290. Cho, K.-J. & Roche, P. A. Regulation of MHC Class II-Peptide Complex Expression by Ubiquitination. *Front Immunol* **4**, 369 (2013).
291. Tze, L. E. *et al.* CD83 increases MHC II and CD86 on dendritic cells by opposing IL-10-driven MARCH1-mediated ubiquitination and degradation. *J Exp Med* **208**, 149–165 (2011).
292. Thibodeau, J. *et al.* Interleukin-10-induced MARCH1 mediates intracellular sequestration of MHC class II in monocytes. *Eur. J. Immunol.* **38**, 1225–1230 (2008).
293. Ma, J. K., Platt, M. Y., Eastham-Anderson, J., Shin, J.-S. & Mellman, I. MHC class II distribution in dendritic cells and B cells is determined by ubiquitin chain length. *Proc Natl Acad Sci U S A* **109**, 8820–8827 (2012).
294. McGehee, A. M. *et al.* Ubiquitin-dependent control of class II MHC localization is dispensable for antigen presentation and antibody production. *PLoS One* **6**, e18817 (2011).
295. Clague, M. J. & Urbé, S. Integration of cellular ubiquitin and membrane traffic systems: focus on deubiquitylases. *FEBS J* **284**, 1753–1766 (2017).
296. Bourgeois-Daigneault, M.-C. *et al.* Tollip-induced down-regulation of MARCH1. *Results Immunol* **3**, 17–25 (2013).
297. Allen, P. M. & Unanue, E. R. Antigen processing and presentation by macrophages. *Am J Anat* **170**, 483–490 (1984).
298. Neefjes, J. J. & Ploegh, H. L. Intracellular transport of MHC class II molecules. *Immunol Today* **13**, 179–184 (1992).
299. Unanue, E. R., Turk, V. & Neefjes, J. Variations in MHC Class II Antigen Processing and Presentation in Health and Disease. *Annu. Rev. Immunol.* **34**, 265–297 (2016).
300. Rudensky, A., Preston-Hurlburt, P., Hong, S. C., Barlow, A. & Janeway, C. A. Sequence analysis of peptides bound to MHC class II molecules. *Nature* **353**, 622–627 (1991).
301. Arunachalam, B., Phan, U. T., Geuze, H. J. & Cresswell, P. Enzymatic reduction of disulfide bonds in lysosomes: Characterization of a Gamma-interferon-inducible lysosomal thiol reductase (GILT). *Proc. Natl. Acad. Sci. U.S.A.* **97**, 745–750 (2000).
302. Delamarre, L., Pack, M., Chang, H., Mellman, I. & Trombetta, E. S. Differential lysosomal proteolysis in antigen-presenting cells determines antigen fate. *Science* **307**, 1630–1634 (2005).

303. McCurley, N. & Mellman, I. Monocyte-Derived Dendritic Cells Exhibit Increased Levels of Lysosomal Proteolysis as Compared to Other Human Dendritic Cell Populations. *PLoS ONE* **5**, e11949 (2010).
304. Turk, B. *et al.* Acidic pH as a physiological regulator of human cathepsin L activity. *Eur J Biochem* **259**, 926–932 (1999).
305. Trombetta, E. S., Ebersold, M., Garrett, W., Pypaert, M. & Mellman, I. Activation of lysosomal function during dendritic cell maturation. *Science* **299**, 1400–1403 (2003).
306. Delamarre, L., Couture, R., Mellman, I. & Trombetta, E. S. Enhancing immunogenicity by limiting susceptibility to lysosomal proteolysis. *J Exp Med* **203**, 2049–2055 (2006).
307. Zavasnik-Bergant, T. Differentiation- and maturation-dependent content, localization, and secretion of cystatin C in human dendritic cells. *Journal of Leukocyte Biology* **78**, 122–134 (2005).
308. Chapman, H. A. Endosomal proteases in antigen presentation. *Curr Opin Immunol* **18**, 78–84 (2006).
309. Bikoff, E. & Birshtein, B. K. T cell clones specific for IgG2a of the a allotype: direct evidence for presentation of endogenous antigen. *The Journal of Immunology* **137**, 28–34 (1986).
310. Sekaly, R. P. *et al.* Antigen presentation to HLA class II-restricted measles virus-specific T-cell clones can occur in the absence of the invariant chain. *Proc. Natl. Acad. Sci. U.S.A.* **85**, 1209–1212 (1988).
311. Callahan, K. M., Rowell, J. F., Soloski, M. J., Machamer, C. E. & Siliciano, R. F. HIV-1 envelope protein is expressed on the surface of infected cells before its processing and presentation to class II-restricted T lymphocytes. *The Journal of Immunology* **151**, 2928–2942 (1993).
312. Eisenlohr, L. C. & Hackett, C. J. Class II major histocompatibility complex-restricted T cells specific for a virion structural protein that do not recognize exogenous influenza virus. Evidence that presentation of labile T cell determinants is favored by endogenous antigen synthesis. *Journal of Experimental Medicine* **169**, 921–931 (1989).
313. Jaraquemada, D., Marti, M. & Long, E. O. An endogenous processing pathway in vaccinia virus-infected cells for presentation of cytoplasmic antigens to class II-restricted T cells. *J Exp Med* **172**, 947–954 (1990).
314. Lee, S. P. *et al.* MHC class II-restricted presentation of endogenously synthesized antigen: Epstein-Barr virus transformed B cell lines can present the viral glycoprotein gp340 by two distinct pathways. *Int Immunol* **5**, 451–460 (1993).
315. Lorenz, R. G., Blum, J. S. & Allen, P. M. Constitutive competition by self proteins for antigen presentation can be overcome by receptor-enhanced uptake. *The Journal of Immunology* **144**, 1600–1606 (1990).
316. McCoy, K. L., Page, M. S., Merkel, B. J., Inman, J. K. & Stutzman, R. Differences among various lineages of antigen-presenting cells in processing exogenous antigen internalized through transferrin receptors. *The Journal of Immunology* **151**, 6757–6768 (1993).
317. Bonifaz, L. C. *et al.* In Vivo Targeting of Antigens to Maturing Dendritic Cells via the DEC-205 Receptor Improves T Cell Vaccination. *Journal of Experimental Medicine* **199**, 815–824 (2004).
318. Moris, A. *et al.* Dendritic cells and HIV-specific CD4+ T cells: HIV antigen presentation, T-cell activation, and viral transfer. *Blood* **108**, 1643–1651 (2006).
319. Rock, K. L., Benacerraf, B. & Abbas, A. K. Antigen presentation by hapten-specific B lymphocytes. I. Role of surface immunoglobulin receptors. *J Exp Med* **160**, 1102–1113 (1984).
320. Barroso, M., Tucker, H., Drake, L., Nichol, K. & Drake, J. R. Antigen-B Cell Receptor Complexes Associate with Intracellular major histocompatibility complex (MHC) Class II Molecules. *Journal of Biological Chemistry* **290**, 27101–27112 (2015).
321. Leung, C. S. *et al.* Robust T-cell stimulation by Epstein-Barr virus-transformed B cells after antigen targeting to DEC-205. *Blood* **121**, 1584–1594 (2013).
322. Stuart, L. M. & Ezekowitz, R. A. B. Phagocytosis. *Immunity* **22**, 539–550 (2005).
323. Cebrian, I. *et al.* Sec22b Regulates Phagosomal Maturation and Antigen Crosspresentation by Dendritic Cells. *Cell* **147**, 1355–1368 (2011).
324. Blander, J. M. & Medzhitov, R. On regulation of phagosome maturation and antigen presentation. *Nat Immunol* **7**, 1029–1035 (2006).
325. Mercer, J., Schelhaas, M. & Helenius, A. Virus Entry by Endocytosis. *Annu. Rev. Biochem.* **79**, 803–833 (2010).
326. Harding, C. V. & Unanue, E. R. Cellular mechanisms of antigen processing and the function of class I and II major histocompatibility complex molecules. *Cell Regul* **1**, 499–509 (1990).
327. Pinet, V., Vergelli, M., Martini, R., Bakke, O. & Long, E. O. Antigen presentation mediated by recycling of surface HLA-DR molecules. *Nature* **375**, 603–606 (1995).
328. Sinnathamby, G. & Eisenlohr, L. C. Presentation by recycling MHC class II molecules of an influenza hemagglutinin-derived epitope that is revealed in the early endosome by acidification. *J Immunol* **170**, 3504–3513 (2003).
329. Chicz, R. M. *et al.* Specificity and promiscuity among naturally processed peptides bound to HLA-DR alleles. *Journal of Experimental Medicine* **178**, 27–47 (1993).

330. Marrack, P., Ignatowicz, L., Kappler, J. W., Boymel, J. & Freed, J. H. Comparison of peptides bound to spleen and thymus class II. *Journal of Experimental Medicine* **178**, 2173–2183 (1993).
331. Dongre, A. R. *et al.* In vivo MHC class II presentation of cytosolic proteins revealed by rapid automated tandem mass spectrometry and functional analyses. *Eur J Immunol* **31**, 1485–1494 (2001).
332. Dengjel, J. *et al.* Autophagy promotes MHC class II presentation of peptides from intracellular source proteins. *Proc. Natl. Acad. Sci. U.S.A.* **102**, 7922–7927 (2005).
333. Paludan, C. *et al.* Endogenous MHC Class II Processing of a Viral Nuclear Antigen After Autophagy. *Science* **307**, 593–596 (2005).
334. Leung, C. S., Haigh, T. A., Mackay, L. K., Rickinson, A. B. & Taylor, G. S. Nuclear location of an endogenously expressed antigen, EBNA1, restricts access to macroautophagy and the range of CD4 epitope display. *Proc Natl Acad Sci U S A* **107**, 2165–2170 (2010).
335. Schmid, D., Pypaert, M. & Münz, C. Antigen-loading compartments for major histocompatibility complex class II molecules continuously receive input from autophagosomes. *Immunity* **26**, 79–92 (2007).
336. Fonteneau, J. F., Brilot, F., Münz, C. & Gannagé, M. The Tumor Antigen NY-ESO-1 Mediates Direct Recognition of Melanoma Cells by CD4+ T Cells after Intercellular Antigen Transfer. *J Immunol* **196**, 64–71 (2016).
337. Coulon, P.-G. *et al.* HIV-Infected Dendritic Cells Present Endogenous MHC Class II-Restricted Antigens to HIV-Specific CD4+ T Cells. *J Immunol* **197**, 517–532 (2016).
338. Lee, H. K. *et al.* In Vivo Requirement for Atg5 in Antigen Presentation by Dendritic Cells. *Immunity* **32**, 227–239 (2010).
339. Blanchet, F. P. *et al.* Human Immunodeficiency Virus-1 Inhibition of Immunoamphisomes in Dendritic Cells Impairs Early Innate and Adaptive Immune Responses. *Immunity* **32**, 654–669 (2010).
340. Ireland, J., Herzog, J. & Unanue, E. R. Cutting Edge: Unique T Cells That Recognize Citrullinated Peptides Are a Feature of Protein Immunization. *The Journal of Immunology* **177**, 1421–1425 (2006).
341. Ireland, J. M. & Unanue, E. R. Autophagy in antigen-presenting cells results in presentation of citrullinated peptides to CD4 T cells. *Journal of Experimental Medicine* **208**, 2625–2632 (2011).
342. Sanjuan, M. A. *et al.* Toll-like receptor signalling in macrophages links the autophagy pathway to phagocytosis. *Nature* **450**, 1253–1257 (2007).
343. Münz, C. The different autophagic roads by which phagosomes travel to lysosomes. *EMBO J* **34**, 2391–2392 (2015).
344. Martinez, J. *et al.* Molecular characterization of LC3-associated phagocytosis reveals distinct roles for Rubicon, NOX2 and autophagy proteins. *Nat Cell Biol* **17**, 893–906 (2015).
345. Huang, J. *et al.* Activation of antibacterial autophagy by NADPH oxidases. *Proc Natl Acad Sci U S A* **106**, 6226–6231 (2009).
346. Romao, S. *et al.* Autophagy proteins stabilize pathogen-containing phagosomes for prolonged MHC II antigen processing. *J Cell Biol* **203**, 757–766 (2013).
347. Keller, C. W. *et al.* ATG-dependent phagocytosis in dendritic cells drives myelin-specific CD4+ T cell pathogenicity during CNS inflammation. *Proc Natl Acad Sci U S A* **114**, E11228–E11237 (2017).
348. Arbogast, F. *et al.* ATG5 is required for B cell polarization and presentation of particulate antigens. *Autophagy* **15**, 280–294 (2019).
349. Münz, C. Non-canonical Functions of Macroautophagy Proteins During Endocytosis by Myeloid Antigen Presenting Cells. *Front Immunol* **9**, 2765 (2018).
350. Dice, J. F. Chaperone-Mediated Autophagy. *Autophagy* **3**, 295–299 (2007).
351. Deffit, S. N. & Blum, J. S. A central role for HSC70 in regulating antigen trafficking and MHC class II presentation. *Mol Immunol* **68**, 85–88 (2015).
352. Pérez, L. *et al.* LAMP-2C Inhibits MHC Class II Presentation of Cytoplasmic Antigens by Disrupting Chaperone-Mediated Autophagy. *J Immunol* **196**, 2457–2465 (2016).
353. Malnati, M. S. *et al.* Processing pathways for presentation of cytosolic antigen to MHC class II-restricted T cells. *Nature* **357**, 702–704 (1992).
354. Comber, J. D., Robinson, T. M., Siciliano, N. A., Snook, A. E. & Eisenlohr, L. C. Functional macroautophagy induction by influenza A virus without a contribution to major histocompatibility complex class II-restricted presentation. *J Virol* **85**, 6453–6463 (2011).
355. Miller, M. A., Ganesan, A. P. V., Luckashenak, N., Mendonca, M. & Eisenlohr, L. C. Endogenous antigen processing drives the primary CD4+ T cell response to influenza. *Nat Med* **21**, 1216–1222 (2015).
356. Rajagopal, D., Bal, V., Mayor, S., George, A. & Rath, S. A role for the Hsp90 molecular chaperone family in antigen presentation to T lymphocytes via major histocompatibility complex class II molecules. *Eur J Immunol* **36**, 828–841 (2006).

357. Houlihan, J. L., Metzler, J. J. & Blum, J. S. HSP90alpha and HSP90beta isoforms selectively modulate MHC class II antigen presentation in B cells. *J Immunol* **182**, 7451–7458 (2009).
358. Tsuji, T. *et al.* Heat shock protein 90-mediated peptide-selective presentation of cytosolic tumor antigen for direct recognition of tumors by CD4(+) T cells. *J Immunol* **188**, 3851–3858 (2012).
359. LeibundGut-Landmann, S. *et al.* Mini-review: Specificity and expression of CIITA, the master regulator of MHC class II genes. *Eur J Immunol* **34**, 1513–1525 (2004).
360. Cebulla, C. M., Miller, D. M. & Sedmak, D. D. Viral inhibition of interferon signal transduction. *Intervirology* **42**, 325–330 (1999).
361. Goodbourn, S., Didcock, L. & Randall, R. E. Interferons: cell signalling, immune modulation, antiviral response and virus countermeasures. *J Gen Virol* **81**, 2341–2364 (2000).
362. Hegde, N. R., Chevalier, M. S. & Johnson, D. C. Viral inhibition of MHC class II antigen presentation. *Trends Immunol* **24**, 278–285 (2003).
363. Ting, J. P.-Y. & Trowsdale, J. Genetic control of MHC class II expression. *Cell* **109 Suppl**, S21–33 (2002).
364. Abendroth, A. *et al.* Modulation of major histocompatibility class II protein expression by varicella-zoster virus. *J Virol* **74**, 1900–1907 (2000).
365. Leonard, G. T. & Sen, G. C. Effects of adenovirus E1A protein on interferon-signaling. *Virology* **224**, 25–33 (1996).
366. Gotoh, B., Komatsu, T., Takeuchi, K. & Yokoo, J. Paramyxovirus strategies for evading the interferon response. *Rev Med Virol* **12**, 337–357 (2002).
367. Miller, D. M. *et al.* Human cytomegalovirus inhibits major histocompatibility complex class II expression by disruption of the Jak/Stat pathway. *J Exp Med* **187**, 675–683 (1998).
368. Le Roy, E., Mühlethaler-Mottet, A., Davrinche, C., Mach, B. & Davignon, J. L. Escape of human cytomegalovirus from HLA-DR-restricted CD4(+) T-cell response is mediated by repression of gamma interferon-induced class II transactivator expression. *J Virol* **73**, 6582–6589 (1999).
369. Li, D. *et al.* Down-regulation of MHC class II expression through inhibition of CIITA transcription by lytic transactivator Zta during Epstein-Barr virus reactivation. *J Immunol* **182**, 1799–1809 (2009).
370. Balan, N., Osborn, K. & Sinclair, A. J. Repression of CIITA by the Epstein-Barr virus transcription factor Zta is independent of its dimerization and DNA binding. *J Gen Virol* **97**, 725–732 (2016).
371. Lin, J.-H. *et al.* Epstein-Barr virus LMP2A suppresses MHC class II expression by regulating the B-cell transcription factors E47 and PU.1. *Blood* **125**, 2228–2238 (2015).
372. Cai, Q. *et al.* IRF-4-mediated CIITA transcription is blocked by KSHV encoded LANA to inhibit MHC II presentation. *PLoS Pathog* **9**, e1003751 (2013).
373. Thakker, S. *et al.* Kaposi's Sarcoma-Associated Herpesvirus Latency-Associated Nuclear Antigen Inhibits Major Histocompatibility Complex Class II Expression by Disrupting Enhanceosome Assembly through Binding with the Regulatory Factor X Complex. *J Virol* **89**, 5536–5556 (2015).
374. Schmidt, K., Wies, E. & Neipel, F. Kaposi's sarcoma-associated herpesvirus viral interferon regulatory factor 3 inhibits gamma interferon and major histocompatibility complex class II expression. *J Virol* **85**, 4530–4537 (2011).
375. Zuo, J., Hislop, A. D., Leung, C. S., Sabbah, S. & Rowe, M. Kaposi's Sarcoma-Associated Herpesvirus-Encoded Viral IRF3 Modulates Major Histocompatibility Complex Class II (MHC-II) Antigen Presentation through MHC-II Transactivator-Dependent and -Independent Mechanisms: Implications for Oncogenesis. *J Virol* **87**, 5340–5350 (2013).
376. Lee, A. W. *et al.* Human cytomegalovirus decreases constitutive transcription of MHC class II genes in mature Langerhans cells by reducing CIITA transcript levels. *Mol Immunol* **48**, 1160–1167 (2011).
377. Kanazawa, S., Okamoto, T. & Peterlin, B. M. Tat competes with CIITA for the binding to P-TEFb and blocks the expression of MHC class II genes in HIV infection. *Immunity* **12**, 61–70 (2000).
378. Amigorena, S. *et al.* Invariant chain cleavage and peptide loading in major histocompatibility complex class II vesicles. *J Exp Med* **181**, 1729–1741 (1995).
379. Cresswell, P. Invariant chain structure and MHC class II function. *Cell* **84**, 505–507 (1996).
380. Neumann, J., Eis-Hübinger, A. M. & Koch, N. Herpes simplex virus type 1 targets the MHC class II processing pathway for immune evasion. *J Immunol* **171**, 3075–3083 (2003).
381. Zuo, J. *et al.* Epstein-Barr Virus Evades CD4+ T Cell Responses in Lytic Cycle through BZLF1-mediated Downregulation of CD74 and the Cooperation of vBcl-2. *PLoS Pathog* **7**, e1002455 (2011).
382. Li, P. *et al.* Disruption of MHC class II-restricted antigen presentation by vaccinia virus. *J Immunol* **175**, 6481–6488 (2005).
383. Yao, Y. *et al.* Vaccinia virus infection induces dendritic cell maturation but inhibits antigen presentation by MHC class II. *Cellular Immunology* **246**, 92–102 (2007).

384. Rehm, K. E. *et al.* Vaccinia virus decreases major histocompatibility complex (MHC) class II antigen presentation, T-cell priming, and peptide association with MHC class II. *Immunology* **128**, 381–392 (2009).
385. Wang, N., Weber, E. & Blum, J. S. Diminished Intracellular Invariant Chain Expression after Vaccinia Virus Infection. *The Journal of Immunology* **183**, 1542–1550 (2009).
386. Rehm, K. E., Connor, R. F., Jones, G. J. B., Yimbu, K. & Roper, R. L. Vaccinia virus A35R inhibits MHC class II antigen presentation. *Virology* **397**, 176–186 (2010).
387. Forsyth, K. S. & Eisenlohr, L. C. Giving CD4+ T cells the slip: viral interference with MHC class II-restricted antigen processing and presentation. *Curr Opin Immunol* **40**, 123–129 (2016).
388. Stumptner-Cuvelette, P. *et al.* HIV-1 Nef impairs MHC class II antigen presentation and surface expression. *Proc Natl Acad Sci U S A* **98**, 12144–12149 (2001).
389. Toussaint, H. *et al.* Human immunodeficiency virus type 1 nef expression prevents AP-2-mediated internalization of the major histocompatibility complex class II-associated invariant chain. *J Virol* **82**, 8373–8382 (2008).
390. Tomazin, R. *et al.* Cytomegalovirus US2 destroys two components of the MHC class II pathway, preventing recognition by CD4+ T cells. *Nat Med* **5**, 1039–1043 (1999).
391. Hegde, N. R. *et al.* Inhibition of HLA-DR assembly, transport, and loading by human cytomegalovirus glycoprotein US3: a novel mechanism for evading major histocompatibility complex class II antigen presentation. *J Virol* **76**, 10929–10941 (2002).
392. Odeberg, J., Plachter, B., Brandén, L. & Söderberg-Nauclér, C. Human cytomegalovirus protein pp65 mediates accumulation of HLA-DR in lysosomes and destruction of the HLA-DR alpha-chain. *Blood* **101**, 4870–4877 (2003).
393. Quinn, L. L. *et al.* The Missing Link in Epstein-Barr Virus Immune Evasion: the BDLF3 Gene Induces Ubiquitination and Downregulation of Major Histocompatibility Complex Class I (MHC-I) and MHC-II. *J Virol* **90**, 356–367 (2016).
394. Sievers, E. *et al.* Glycoprotein B from strain 17 of herpes simplex virus type I contains an invariant chain homologous sequence that binds to MHC class II molecules. *Immunology* **107**, 129–135 (2002).
395. Zuo, J. & Rowe, M. Herpesviruses Placating the Unwilling Host: Manipulation of the MHC Class II Antigen Presentation Pathway. *Viruses* **4**, 1335–1353 (2012).
396. Orvedahl, A. *et al.* HSV-1 ICP34.5 confers neurovirulence by targeting the Beclin 1 autophagy protein. *Cell Host Microbe* **1**, 23–35 (2007).
397. Verpooten, D., Ma, Y., Hou, S., Yan, Z. & He, B. Control of TANK-binding Kinase 1-mediated Signaling by the  $\gamma$ 134.5 Protein of Herpes Simplex Virus 1. *Journal of Biological Chemistry* **284**, 1097–1105 (2009).
398. Weidberg, H. & Elazar, Z. TBK1 Mediates Crosstalk Between the Innate Immune Response and Autophagy. *Sci. Signal.* **4**, (2011).
399. Gannagé, M. *et al.* Matrix protein 2 of influenza A virus blocks autophagosome fusion with lysosomes. *Cell Host Microbe* **6**, 367–380 (2009).
400. Borel, S. *et al.* HIV-1 viral infectivity factor interacts with microtubule-associated protein light chain 3 and inhibits autophagy. *AIDS* **29**, 275–286 (2015).
401. Kyei, G. B. *et al.* Autophagy pathway intersects with HIV-1 biosynthesis and regulates viral yields in macrophages. *J Cell Biol* **186**, 255–268 (2009).
402. Alfaisal, J. *et al.* HIV-1 Vpr inhibits autophagy during the early steps of infection of CD4 T cells. *Biol Cell* **111**, 308–318 (2019).
403. Spriggs, M. K. *et al.* The extracellular domain of the Epstein-Barr virus BZLF2 protein binds the HLA-DR beta chain and inhibits antigen presentation. *J Virol* **70**, 5557–5563 (1996).
404. Mullen, M. M., Haan, K. M., Longnecker, R. & Jardetzky, T. S. Structure of the Epstein-Barr virus gp42 protein bound to the MHC class II receptor HLA-DR1. *Mol Cell* **9**, 375–385 (2002).
405. Rensing, M. E. *et al.* Epstein-Barr virus gp42 is posttranslationally modified to produce soluble gp42 that mediates HLA class II immune evasion. *J Virol* **79**, 841–852 (2005).
406. Rensing, M. E. *et al.* Interference with T cell receptor-HLA-DR interactions by Epstein-Barr virus gp42 results in reduced T helper cell recognition. *Proc Natl Acad Sci U S A* **100**, 11583–11588 (2003).
407. Alzhanova, D. *et al.* T cell inactivation by poxviral B22 family proteins increases viral virulence. *PLoS Pathog* **10**, e1004123 (2014).
408. Richetta, C. *et al.* Sustained Autophagy Contributes to Measles Virus Infectivity. *PLoS Pathog* **9**, e1003599 (2013).
409. Petkova, D. S. *et al.* Distinct Contributions of Autophagy Receptors in Measles Virus Replication. *Viruses* **9**, 123 (2017).
410. Orvedahl, A. *et al.* Autophagy Protects against Sindbis Virus Infection of the Central Nervous System. *Cell Host & Microbe* **7**, 115–127 (2010).

411. Viret, C., Duclaux-Loras, R., Nancey, S., Rozières, A. & Faure, M. Selective Autophagy Receptors in Antiviral Defense. *Trends in Microbiology* **29**, 798–810 (2021).
412. Shi, J. *et al.* Cleavage of sequestosome 1/p62 by an enteroviral protease results in disrupted selective autophagy and impaired NFκB signaling. *Autophagy* **9**, 1591–1603 (2013).
413. Mohamad, Y. *et al.* CALCOCO2/NDP52 and SQSTM1/p62 differentially regulate coxsackievirus B3 propagation. *Cell Death Differ* **26**, 1062–1076 (2019).
414. Shi, J., Fung, G., Piesik, P., Zhang, J. & Luo, H. Dominant-negative function of the C-terminal fragments of NBR1 and SQSTM1 generated during enteroviral infection. *Cell Death Differ* **21**, 1432–1441 (2014).
415. Corona, A. K., Saulsbery, H. M., Corona Velazquez, A. F. & Jackson, W. T. Enteroviruses Remodel Autophagic Trafficking through Regulation of Host SNARE Proteins to Promote Virus Replication and Cell Exit. *Cell Reports* **22**, 3304–3314 (2018).
416. Waisner, H. & Kalamvoki, M. The ICP0 Protein of Herpes Simplex Virus 1 (HSV-1) Downregulates Major Autophagy Adaptor Proteins Sequestosome 1 and Optineurin during the Early Stages of HSV-1 Infection. *J Virol* **93**, e01258-19 (2019).
417. Leymarie, O. *et al.* Influenza virus protein PB1-F2 interacts with CALCOCO2 (NDP52) to modulate innate immune response. *Journal of General Virology* **98**, 1196–1208 (2017).
418. Chen, M. *et al.* TRIM14 Inhibits cGAS Degradation Mediated by Selective Autophagy Receptor p62 to Promote Innate Immune Responses. *Molecular Cell* **64**, 105–119 (2016).
419. Jin, S. *et al.* Tetherin Suppresses Type I Interferon Signaling by Targeting MAVS for NDP52-Mediated Selective Autophagic Degradation in Human Cells. *Molecular Cell* **68**, 308–322.e4 (2017).
420. Du, Y. *et al.* LRRC25 inhibits type I IFN signaling by targeting ISG15-associated RIG-I for autophagic degradation. *EMBO J* **37**, 351–366 (2018).
421. Wu, Y. *et al.* Selective autophagy controls the stability of transcription factor IRF3 to balance type I interferon production and immune suppression. *Autophagy* **17**, 1379–1392 (2021).
422. Xie, W. *et al.* Selective autophagy controls the stability of TBK1 via NEDD4 to balance host defense. *Cell Death Differ* **29**, 40–53 (2022).
423. Zeng, Y. *et al.* The PB1 protein of influenza A virus inhibits the innate immune response by targeting MAVS for NBR1-mediated selective autophagic degradation. *PLoS Pathog* **17**, e1009300 (2021).
424. Sui, C. *et al.* SARS-CoV-2 NSP13 Inhibits Type I IFN Production by Degradation of TBK1 via p62-Dependent Selective Autophagy. *The Journal of Immunology* **208**, 753–761 (2022).
425. Poiesz, B. J. *et al.* Detection and isolation of type C retrovirus particles from fresh and cultured lymphocytes of a patient with cutaneous T-cell lymphoma. *Proc Natl Acad Sci U S A* **77**, 7415–7419 (1980).
426. Yoshida, M., Miyoshi, I. & Hinuma, Y. Isolation and characterization of retrovirus from cell lines of human adult T-cell leukemia and its implication in the disease. *Proc Natl Acad Sci U S A* **79**, 2031–2035 (1982).
427. Gessain, A. & Mahieux, R. Tropical spastic paraparesis and HTLV-1 associated myelopathy: Clinical, epidemiological, virological and therapeutic aspects. *Revue Neurologique* **168**, 257–269 (2012).
428. Kannian, P. & Green, P. L. Human T Lymphotropic Virus Type 1 (HTLV-1): Molecular Biology and Oncogenesis. *Viruses* **2**, 2037–2077 (2010).
429. Martin, J., Maldonado, J., Mueller, J., Zhang, W. & Mansky, L. Molecular Studies of HTLV-1 Replication: An Update. *Viruses* **8**, 31 (2016).
430. Hanon, E. *et al.* High Frequency of Viral Protein Expression in Human T Cell Lymphotropic Virus Type 1-Infected Peripheral Blood Mononuclear Cells. *AIDS Research and Human Retroviruses* **16**, 1711–1715 (2000).
431. Hoxie, J. A., Matthews, D. M. & Cines, D. B. Infection of human endothelial cells by human T-cell leukemia virus type I. *Proc Natl Acad Sci U S A* **81**, 7591–7595 (1984).
432. Koyanagi, Y. *et al.* In vivo infection of human T-cell leukemia virus type I in non-T cells. *Virology* **196**, 25–33 (1993).
433. Macatonia, S. E., Cruickshank, J. K., Rudge, P. & Knight, S. C. Dendritic Cells from Patients with Tropical Spastic Paraparesis Are Infected with HTLV-1 and Stimulate Autologous Lymphocyte Proliferation. *AIDS Research and Human Retroviruses* **8**, 1699–1706 (1992).
434. Doi, K. *et al.* Preferential selection of human T-cell leukemia virus type I provirus integration sites in leukemic versus carrier states. *Blood* **106**, 1048–1053 (2005).
435. Derse, D., Hill, S. A., Princler, G., Lloyd, P. & Heidecker, G. Resistance of human T cell leukemia virus type 1 to APOBEC3G restriction is mediated by elements in nucleocapsid. *Proc. Natl. Acad. Sci. U.S.A.* **104**, 2915–2920 (2007).
436. Lee, T. H. *et al.* Human T-cell leukemia virus-associated membrane antigens: identity of the major antigens recognized after virus infection. *Proc. Natl. Acad. Sci. U.S.A.* **81**, 3856–3860 (1984).
437. Nam, S. H., Kidokoro, M., Shida, H. & Hatanaka, M. Processing of gag precursor polyprotein of human T-cell leukemia virus type I by virus-encoded protease. *J Virol* **62**, 3718–3728 (1988).

438. Paine, E., Gu, R. & Ratner, L. Structure and expression of the human T-cell leukemia virus type 1 envelope protein. *Virology* **199**, 331–338 (1994).
439. Larocca, D., Chao, L. A., Seto, M. H. & Brunck, T. K. Human T-cell Leukemia Virus minus strand transcription in infected T-cells. *Biochemical and Biophysical Research Communications* **163**, 1006–1013 (1989).
440. Gaudray, G. *et al.* The Complementary Strand of the Human T-Cell Leukemia Virus Type 1 RNA Genome Encodes a bZIP Transcription Factor That Down-Regulates Viral Transcription. *J Virol* **76**, 12813–12822 (2002).
441. Cann, A. J., Rosenblatt, J. D., Wachsman, W., Shah, N. P. & Chen, I. S. Y. Identification of the gene responsible for human T-cell leukaemia virus transcriptional regulation. *Nature* **318**, 571–574 (1985).
442. Felber, B. K., Paskalis, H., Kleinman-Ewing, C., Wong-Staal, F. & Pavlakis, G. N. The pX Protein of HTLV-I Is a Transcriptional Activator of Its Long Terminal Repeats. *Science* **229**, 675–679 (1985).
443. Inoue, J., Yoshida, M. & Seiki, M. Transcriptional (p40x) and post-transcriptional (p27x-III) regulators are required for the expression and replication of human T-cell leukemia virus type I genes. *Proc. Natl. Acad. Sci. U.S.A.* **84**, 3653–3657 (1987).
444. Leung, K. & Nabel, G. J. HTLV-1 transactivator induces interleukin-2 receptor expression through an NF-kappa B-like factor. *Nature* **333**, 776–778 (1988).
445. Mulloy, J. C. *et al.* Human T-Cell Lymphotropic/Leukemia Virus Type 1 Tax Abrogates p53-Induced Cell Cycle Arrest and Apoptosis through Its CREB/ATF Functional Domain. *J. Virol.* **72**, 8852–8860 (1998).
446. Ressler, S., Morris, G. F. & Marriott, S. J. Human T-cell leukemia virus type 1 Tax transactivates the human proliferating cell nuclear antigen promoter. *J Virol* **71**, 1181–1190 (1997).
447. Schmitt, I., Rosin, O., Rohwer, P., Gossen, M. & Grassmann, R. Stimulation of Cyclin-Dependent Kinase Activity and G<sub>1</sub> to S-Phase Transition in Human Lymphocytes by the Human T-Cell Leukemia/Lymphotropic Virus Type 1 Tax Protein. *J Virol* **72**, 633–640 (1998).
448. Kashanchi, F. & Brady, J. N. Transcriptional and post-transcriptional gene regulation of HTLV-1. *Oncogene* **24**, 5938–5951 (2005).
449. Nerenberg, M., Hinrichs, S. H., Reynolds, R. K., Khoury, G. & Jay, G. The *tat* Gene of Human T-Lymphotropic Virus Type 1 Induces Mesenchymal Tumors in Transgenic Mice. *Science* **237**, 1324–1329 (1987).
450. Tanaka, A. *et al.* Oncogenic transformation by the tax gene of human T-cell leukemia virus type I in vitro. *Proc. Natl. Acad. Sci. U.S.A.* **87**, 1071–1075 (1990).
451. Grassmann, R. *et al.* Role of human T-cell leukemia virus type 1 X region proteins in immortalization of primary human lymphocytes in culture. *J Virol* **66**, 4570–4575 (1992).
452. Robek, M. D. & Ratner, L. Immortalization of CD4<sup>+</sup> and CD8<sup>+</sup> T Lymphocytes by Human T-Cell Leukemia Virus Type 1 Tax Mutants Expressed in a Functional Molecular Clone. *J Virol* **73**, 4856–4865 (1999).
453. Ross, T. M., Narayan, M., Fang, Z.-Y., Minella, A. C. & Green, P. L. Human T-Cell Leukemia Virus Type 2 Tax Mutants That Selectively Abrogate NFkB or CREB/ATF Activation Fail To Transform Primary Human T Cells. *J Virol* **74**, 2655–2662 (2000).
454. Sun, S.-C. & Yamaoka, S. Activation of NF-kB by HTLV-I and implications for cell transformation. *Oncogene* **24**, 5952–5964 (2005).
455. Zhang, W. *et al.* Morphology and ultrastructure of retrovirus particles. *AIMS Biophysics* **2**, 343–369 (2015).
456. Lingwood, D., Kaiser, H.-J., Levental, I. & Simons, K. Lipid rafts as functional heterogeneity in cell membranes. *Biochemical Society Transactions* **37**, 955–960 (2009).
457. Inlora, J., Collins, D. R., Trubin, M. E., Chung, J. Y. J. & Ono, A. Membrane Binding and Subcellular Localization of Retroviral Gag Proteins Are Differentially Regulated by MA Interactions with Phosphatidylinositol-(4,5)-Bisphosphate and RNA. *mBio* **5**, e02202-14 (2014).
458. Demirov, D. G. & Freed, E. O. Retrovirus budding. *Virus Research* **106**, 87–102 (2004).
459. Le Blanc, I. *et al.* HTLV-1 structural proteins. *Virus Research* **78**, 5–16 (2001).
460. Fan, N. *et al.* Infection of peripheral blood mononuclear cells and cell lines by cell-free human T-cell lymphoma/leukemia virus type I. *J Clin Microbiol* **30**, 905–910 (1992).
461. Igakura, T. *et al.* Spread of HTLV-I Between Lymphocytes by Virus-Induced Polarization of the Cytoskeleton. *Science* **299**, 1713–1716 (2003).
462. Nejmeddine, M., Barnard, A. L., Tanaka, Y., Taylor, G. P. & Bangham, C. R. M. Human T-lymphotropic Virus, Type 1, Tax Protein Triggers Microtubule Reorientation in the Virological Synapse. *Journal of Biological Chemistry* **280**, 29653–29660 (2005).
463. Kfoury, Y. *et al.* The Multifaceted Oncoprotein Tax. in *Advances in Cancer Research* vol. 113 85–120 (Elsevier, 2012).
464. Burton, M., Upadhyaya, C. D., Maier, B., Hope, T. J. & Semmes, O. J. Human T-Cell Leukemia Virus Type 1 Tax Shuttles between Functionally Discrete Subcellular Targets. *J Virol* **74**, 2351–2364 (2000).

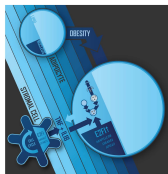


465. Gatza, M. L. & Marriott, S. J. Genotoxic Stress and Cellular Stress Alter the Subcellular Distribution of Human T-Cell Leukemia Virus Type 1 Tax through a CRM1-Dependent Mechanism. *J Virol* **80**, 6657–6668 (2006).
466. Lavorgna, A. & Harhaj, E. W. Regulation of HTLV-1 tax stability, cellular trafficking and NF- $\kappa$ B activation by the ubiquitin-proteasome pathway. *Viruses* **6**, 3925–3943 (2014).
467. Grassmann, R., Aboud, M. & Jeang, K.-T. Molecular mechanisms of cellular transformation by HTLV-1 Tax. *Oncogene* **24**, 5976–5985 (2005).
468. Harhaj, E. & Harhaj, N. Mechanisms of Persistent NF- $\kappa$ B Activation by HTLV-I Tax. *IUBMB Life (International Union of Biochemistry and Molecular Biology: Life)* **57**, 83–91 (2005).
469. Ducasa, N. *et al.* Autophagy in Human T-Cell Leukemia Virus Type 1 (HTLV-1) Induced Leukemia. *Front. Oncol.* **11**, 641269 (2021).
470. Sun, S.-C., Elwood, J., Beraud, C. & Greene, W. C. Human T-Cell Leukemia Virus Type I Tax Activation of NF- $\kappa$ B/Rel Involves Phosphorylation and Degradation of I $\kappa$ B $\alpha$  and RelA (p65)-Mediated Induction of the c-rel Gene. *MOL. CELL. BIOL.* **14**, (1994).
471. Xiao, G. Retroviral oncoprotein Tax induces processing of NF- $\kappa$ B2/p100 in T cells: evidence for the involvement of IKK $\alpha$ . *The EMBO Journal* **20**, 6805–6815 (2001).
472. Harhaj, E. W. & Sun, S.-C. IKK $\gamma$  Serves as a Docking Subunit of the I $\kappa$ B Kinase (IKK) and Mediates Interaction of IKK with the Human T-cell Leukemia Virus Tax Protein. *Journal of Biological Chemistry* **274**, 22911–22914 (1999).
473. Chu, Z.-L., Shin, Y.-A., Yang, J.-M., DiDonato, J. A. & Ballard, D. W. IKK $\gamma$  Mediates the Interaction of Cellular I $\kappa$ B Kinases with the Tax Transforming Protein of Human T Cell Leukemia Virus Type 1. *Journal of Biological Chemistry* **274**, 15297–15300 (1999).
474. Jin, D.-Y., Giordano, V., Kibler, K. V., Nakano, H. & Jeang, K.-T. Role of Adapter Function in Oncoprotein-mediated Activation of NF- $\kappa$ B. *Journal of Biological Chemistry* **274**, 17402–17405 (1999).
475. Good, L. & Sun, S.-C. Persistent Activation of NF- $\kappa$ B/Rel by Human T-Cell Leukemia Virus Type 1 Tax Involves Degradation of I $\kappa$ B $\alpha$ . *J. VIROL.* **70**, (1996).
476. Higuchi, M. *et al.* Cooperation of NF- $\kappa$ B2/p100 Activation and the PDZ Domain Binding Motive Signal in Human T-Cell Leukemia Virus Type 1 (HTLV-1) Tax1 but Not HTLV-2 Tax2 Is Crucial for Interleukin-2-Independent Growth Transformation of a T-Cell Line. *J Virol* **81**, 11900–11907 (2007).
477. Lamsoul, I. *et al.* Exclusive Ubiquitination and Sumoylation on Overlapping Lysine Residues Mediate NF- $\kappa$ B Activation by the Human T-Cell Leukemia Virus Tax Oncoprotein. *Mol Cell Biol* **25**, 10391–10406 (2005).
478. Nasr, R. *et al.* Tax ubiquitylation and sumoylation control critical cytoplasmic and nuclear steps of NF- $\kappa$ B activation. *Blood* **107**, 4021–4029 (2006).
479. Peloponese, J.-M. *et al.* Ubiquitination of Human T-Cell Leukemia Virus Type 1 Tax Modulates Its Activity. *J Virol* **78**, 11686–11695 (2004).
480. Kfoury, Y. *et al.* Ubiquitylated Tax targets and binds the IKK signalosome at the centrosome. *Oncogene* **27**, 1665–1676 (2008).
481. Huang, J., Ren, T., Guan, H., Jiang, Y. & Cheng, H. HTLV-1 Tax Is a Critical Lipid Raft Modulator That Hijacks I $\kappa$ B Kinases to the Microdomains for Persistent Activation of NF- $\kappa$ B. *Journal of Biological Chemistry* **284**, 6208–6217 (2009).
482. Journo, C. *et al.* NRP/Optineurin Cooperates with TAX1BP1 to potentiate the activation of NF- $\kappa$ B by human T-lymphotropic virus type 1 tax protein. *PLoS Pathog* **5**, e1000521 (2009).
483. Chun, A. C. *et al.* Coiled-coil motif as a structural basis for the interaction of HTLV type 1 Tax with cellular cofactors. *AIDS Res Hum Retroviruses* **16**, 1689–1694 (2000).
484. Chin, K.-T., Chun, A. C. S., Ching, Y.-P., Jeang, K.-T. & Jin, D.-Y. Human T-cell leukemia virus oncoprotein tax represses nuclear receptor-dependent transcription by targeting coactivator TAX1BP1. *Cancer Res* **67**, 1072–1081 (2007).
485. Iha, H. *et al.* Inflammatory cardiac valvulitis in TAX1BP1-deficient mice through selective NF- $\kappa$ B activation. *EMBO J* **27**, 629–641 (2008).
486. Shembade, N. *et al.* The E3 ligase Itch negatively regulates inflammatory signaling pathways by controlling the function of the ubiquitin-editing enzyme A20. *Nat Immunol* **9**, 254–262 (2008).
487. Shembade, N., Parvatiyar, K., Harhaj, N. S. & Harhaj, E. W. The ubiquitin-editing enzyme A20 requires RNF11 to downregulate NF- $\kappa$ B signalling. *EMBO J* **28**, 513–522 (2009).
488. Shembade, N., Pujari, R., Harhaj, N. S., Abbott, D. W. & Harhaj, E. W. The kinase IKK $\alpha$  inhibits activation of the transcription factor NF- $\kappa$ B by phosphorylating the regulatory molecule TAX1BP1. *Nat Immunol* **12**, 834–843 (2011).
489. Schwob, A. *et al.* SQSTM-1/p62 potentiates HTLV-1 Tax-mediated NF- $\kappa$ B activation through its ubiquitin binding function. *Sci Rep* **9**, 16014 (2019).

490. Bangham, C. R. M. CTL quality and the control of human retroviral infections: Highlight. *Eur. J. Immunol.* **39**, 1700–1712 (2009).
491. Vine, A. M. *et al.* The Role of CTLs in Persistent Viral Infection: Cytolytic Gene Expression in CD8+ Lymphocytes Distinguishes between Individuals with a High or Low Proviral Load of Human T Cell Lymphotropic Virus Type 1. *The Journal of Immunology* **173**, 5121–5129 (2004).
492. Goon, P. K. C. *et al.* Human T Cell Lymphotropic Virus (HTLV) Type-1-Specific CD8<sup>+</sup> T Cells: Frequency and Immunodominance Hierarchy. *J INFECT DIS* **189**, 2294–2298 (2004).
493. Goon, P. K. C. *et al.* High frequencies of Th1-type CD4<sup>+</sup> T cells specific to HTLV-1 Env and Tax proteins in patients with HTLV-1-associated myelopathy/tropical spastic paraparesis. *Blood* **99**, 3335–3341 (2002).
494. Goon, P. K. C. *et al.* Human T Cell Lymphotropic Virus Type I (HTLV-I)-Specific CD4<sup>+</sup> T Cells: Immunodominance Hierarchy and Preferential Infection with HTLV-I. *The Journal of Immunology* **172**, 1735–1743 (2004).
495. Bangham, C. R. M. Human T Cell Leukemia Virus Type 1: Persistence and Pathogenesis. *Annu Rev Immunol* **36**, 43–71 (2018).
496. Vine, A. M. *et al.* Polygenic control of human T lymphotropic virus type I (HTLV-I) provirus load and the risk of HTLV-I-associated myelopathy/tropical spastic paraparesis. *J Infect Dis* **186**, 932–939 (2002).
497. Jeffery, K. J. M. *et al.* HLA alleles determine human T-lymphotropic virus-I (HTLV-I) proviral load and the risk of HTLV-I-associated myelopathy. *Proc. Natl. Acad. Sci. U.S.A.* **96**, 3848–3853 (1999).
498. Jeffery, K. J. *et al.* The influence of HLA class I alleles and heterozygosity on the outcome of human T cell lymphotropic virus type I infection. *J Immunol* **165**, 7278–7284 (2000).
499. Sabouri, A. H. *et al.* Impaired function of human T-lymphotropic virus type 1 (HTLV-1)-specific CD8<sup>+</sup> T cells in HTLV-1-associated neurologic disease. *Blood* **112**, 2411–2420 (2008).
500. Kattan, T. *et al.* The Avidity and Lytic Efficiency of the CTL Response to HTLV-1. *The Journal of Immunology* **182**, 5723–5729 (2009).
501. Masaki, A. *et al.* Human T-cell lymphotropic/leukemia virus type 1 (HTLV-1) Tax-specific T-cell exhaustion in HTLV-1-infected individuals. *Cancer Sci* **109**, 2383–2390 (2018).
502. Toulza, F. *et al.* FoxP3<sup>+</sup> regulatory T cells are distinct from leukemia cells in HTLV-1-associated adult T-cell leukemia. *Int J Cancer* **125**, 2375–2382 (2009).
503. Nascimento, C. R. *et al.* Monocytes from HTLV-1-infected patients are unable to fully mature into dendritic cells. *Blood* **117**, 489–499 (2011).
504. Makino, M., Shimokubo, S., Wakamatsu, S. I., Izumo, S. & Baba, M. The role of human T-lymphotropic virus type 1 (HTLV-1)-infected dendritic cells in the development of HTLV-1-associated myelopathy/tropical spastic paraparesis. *J Virol* **73**, 4575–4581 (1999).
505. Makino, M., Wakamatsu, S., Shimokubo, S., Arima, N. & Baba, M. Production of Functionally Deficient Dendritic Cells from HTLV-I-Infected Monocytes: Implications for the Dendritic Cell Defect in Adult T Cell Leukemia. *Virology* **274**, 140–148 (2000).
506. Shimoyama, M. Diagnostic criteria and classification of clinical subtypes of adult T-cell leukaemia-lymphoma. A report from the Lymphoma Study Group (1984-87). *Br J Haematol* **79**, 428–437 (1991).
507. Rizkallah, G. *et al.* Dendritic cell maturation, but not type I interferon exposure, restricts infection by HTLV-1, and viral transmission to T-cells. *PLoS Pathog* **13**, e1006353 (2017).
508. Koralnik, I. J., Lemp, J. F., Gallo, R. C. & Franchini, G. In vitro infection of human macrophages by human T-cell leukemia/lymphotropic virus type I (HTLV-I). *AIDS Res Hum Retroviruses* **8**, 1845–1849 (1992).
509. Alais, S., Mahieux, R. & Dutartre, H. Viral Source-Independent High Susceptibility of Dendritic Cells to Human T-Cell Leukemia Virus Type 1 Infection Compared to That of T Lymphocytes. *J Virol* **89**, 10580–10590 (2015).
510. Ali, A. *et al.* Dendritic cells infected in vitro with human T cell leukaemia/lymphoma virus type-1 (HTLV-1); enhanced lymphocytic proliferation and tropical spastic paraparesis. *Clin Exp Immunol* **94**, 32–37 (1993).
511. Al-Dahoodi, Z. M., Takemoto, S., Kataoka, S. & Taguchi, H. Dysfunction of Dendritic and T Cells as the Cause of Immune Suppression in HTLV-I Infected Individuals. *J Clin Exp Hematopathol* **43**, 43–48 (2003).
512. Mostoller, K., Norbury, C. C., Jain, P. & Wigdahl, B. Human T-cell leukemia virus type I Tax induces the expression of dendritic cell markers associated with maturation and activation. *J Neurovirol* **10**, 358–371 (2004).
513. Jain, P. *et al.* Modulation of dendritic cell maturation and function by the Tax protein of human T cell leukemia virus type 1. *J Leukoc Biol* **82**, 44–56 (2007).
514. Ren, T. *et al.* HTLV-1 Tax deregulates autophagy by recruiting autophagic molecules into lipid raft microdomains. *Oncogene* **34**, 334–345 (2015).
515. Tang, S.-W., Chen, C.-Y., Klase, Z., Zane, L. & Jeang, K.-T. The Cellular Autophagy Pathway Modulates Human T-Cell Leukemia Virus Type 1 Replication. *J Virol* **87**, 1699–1707 (2013).

516. Lotteau, V. *et al.* Intracellular transport of class II MHC molecules directed by invariant chain. *Nature* **348**, 600–605 (1990).
517. Pissani, F. & Streeck, H. Emerging concepts on T follicular helper cell dynamics in HIV infection. *Trends Immunol* **35**, 278–286 (2014).
518. Bevan, M. J. Helping the CD8+ T-cell response. *Nat Rev Immunol* **4**, 595–602 (2004).
519. Cenerenti, M., Saillard, M., Romero, P. & Jandus, C. The Era of Cytotoxic CD4 T Cells. *Front. Immunol.* **13**, 867189 (2022).
520. Nuchtern, J. G., Biddison, W. E. & Klausner, R. D. Class II MHC molecules can use the endogenous pathway of antigen presentation. *Nature* **343**, 74–76 (1990).
521. Kirkin, V. History of the Selective Autophagy Research: How Did It Begin and Where Does It Stand Today? *J Mol Biol* **432**, 3–27 (2020).
522. vogt, A. B., Moldenhauer, G., Hämmerling, G. J. & Kropshofer, H. HLA-DM stabilizes empty HLA-DR molecules in a chaperone-like fashion. *Immunol Lett* **57**, 209–211 (1997).
523. Lightstone, L. *et al.* In the absence of the invariant chain, HLA-DR molecules display a distinct array of peptides which is influenced by the presence or absence of HLA-DM. *Proc Natl Acad Sci U S A* **94**, 5772–5777 (1997).
524. Neeffes, J., Jongasma, M. M. L. & Berlin, I. Stop or Go? Endosome Positioning in the Establishment of Compartment Architecture, Dynamics, and Function. *Trends Cell Biol* **27**, 580–594 (2017).
525. Johnson, D. E., Ostrowski, P., Jaumouillé, V. & Grinstein, S. The position of lysosomes within the cell determines their luminal pH. *Journal of Cell Biology* **212**, 677–692 (2016).
526. Ferrante, A. & Gorski, J. A Peptide/MHCII conformer generated in the presence of exchange peptide is substrate for HLA-DM editing. *Sci Rep* **2**, 386 (2012).
527. Margiotta, A. *et al.* Invariant chain regulates endosomal fusion and maturation through an interaction with the SNARE Vti1b. *Journal of Cell Science* jcs.244624 (2020) doi:10.1242/jcs.244624.
528. Bruchez, A. *et al.* MHC class II transactivator CIITA induces cell resistance to Ebola virus and SARS-like coronaviruses. *Science* **370**, 241–247 (2020).
529. David, V., Hochstenbach, F., Rajagopalan, S. & Brenner, M. B. Interaction with newly synthesized and retained proteins in the endoplasmic reticulum suggests a chaperone function for human integral membrane protein IP90 (calnexin). *J Biol Chem* **268**, 9585–9592 (1993).
530. Ou, W. J., Cameron, P. H., Thomas, D. Y. & Bergeron, J. J. Association of folding intermediates of glycoproteins with calnexin during protein maturation. *Nature* **364**, 771–776 (1993).
531. Myhill, N. *et al.* The subcellular distribution of calnexin is mediated by PACS-2. *Mol Biol Cell* **19**, 2777–2788 (2008).
532. Lakkaraju, A. K. *et al.* Palmitoylated calnexin is a key component of the ribosome-translocon complex: Palmitoylated calnexin is a key component of the RTC. *The EMBO Journal* **31**, 1823–1835 (2012).
533. Forgac, M. Vacuolar ATPases: rotary proton pumps in physiology and pathophysiology. *Nat Rev Mol Cell Biol* **8**, 917–929 (2007).
534. Iha, H. *et al.* Inflammatory cardiac valvulitis in TAX1BP1-deficient mice through selective NF-kappaB activation. *EMBO J* **27**, 629–641 (2008).
535. Kourjian, G. *et al.* HIV Protease Inhibitor-Induced Cathepsin Modulation Alters Antigen Processing and Cross-Presentation. *The Journal of Immunology* **196**, 3595–3607 (2016).
536. Vaithilingam, A. *et al.* A simple methodology to assess endolysosomal protease activity involved in antigen processing in human primary cells. *BMC Cell Biol* **14**, 35 (2013).
537. Segev, N. Ypt and Rab GTPases: insight into functions through novel interactions. *Curr Opin Cell Biol* **13**, 500–511 (2001).
538. Rink, J., Ghigo, E., Kalaidzidis, Y. & Zerial, M. Rab conversion as a mechanism of progression from early to late endosomes. *Cell* **122**, 735–749 (2005).
539. Yoshimura, S., Bondeson, J., Foxwell, B. M. J., Brennan, F. M. & Feldmann, M. Effective antigen presentation by dendritic cells is NF-κB dependent: coordinate regulation of MHC, co-stimulatory molecules and cytokines. *International Immunology* **13**, 675–683 (2001).
540. Lee, K.-W., Lee, Y., Kim, D.-S. & Kwon, H.-J. Direct role of NF-κB activation in Toll-like receptor-triggered HLA-DRA expression. *Eur. J. Immunol.* **36**, 1254–1266 (2006).
541. Hang, D. T. T., Song, J.-Y., Kim, M.-Y., Park, J.-W. & Shin, Y.-K. Involvement of NF-κB in changes of IFN-γ-induced CIITA/MHC-II and iNOS expression by influenza virus in macrophages. *Molecular Immunology* **48**, 1253–1262 (2011).
542. Forlani, G., Abdallah, R., Accolla, R. S. & Tosi, G. The MHC-II transactivator CIITA, a restriction factor against oncogenic HTLV-1 and HTLV-2 retroviruses: similarities and differences in the inhibition of Tax-1 and Tax-2 viral transactivators. *Front Microbiol* **4**, 234 (2013).

543. Mogensen, T. H. IRF and STAT Transcription Factors - From Basic Biology to Roles in Infection, Protective Immunity, and Primary Immunodeficiencies. *Front Immunol* **9**, 3047 (2018).
544. Johnson, J. M. *et al.* Free Major Histocompatibility Complex Class I Heavy Chain Is Preferentially Targeted for Degradation by Human T-Cell Leukemia/Lymphotropic Virus Type 1 p12<sup>1</sup> Protein. *J Virol* **75**, 6086–6094 (2001).
545. Zhao, T. *et al.* Human T-cell leukemia virus type 1 bZIP factor selectively suppresses the classical pathway of NF-kappaB. *Blood* **113**, 2755–2764 (2009).
546. Marshall, R. S., Hua, Z., Mali, S., McLoughlin, F. & Vierstra, R. D. ATG8-Binding UIM Proteins Define a New Class of Autophagy Adaptors and Receptors. *Cell* **177**, 766–781.e24 (2019).
547. Verlhac, P. *et al.* Autophagy receptor NDP52 regulates pathogen-containing autophagosome maturation. *Cell Host Microbe* **17**, 515–525 (2015).
548. Mandell, M. A. *et al.* TRIM Proteins Regulate Autophagy and Can Target Autophagic Substrates by Direct Recognition. *Developmental Cell* **30**, 394–409 (2014).
549. Kimura, T. *et al.* TRIM-mediated precision autophagy targets cytoplasmic regulators of innate immunity. *Journal of Cell Biology* **210**, 973–989 (2015).
550. Nisole, S., Stoye, J. P. & Saïb, A. TRIM family proteins: retroviral restriction and antiviral defence. *Nat Rev Microbiol* **3**, 799–808 (2005).
551. Sarraf, S. A. *et al.* Loss of TAX1BP1-Directed Autophagy Results in Protein Aggregate Accumulation in the Brain. *Molecular Cell* **80**, 779–795.e10 (2020).



## TAX1BP1 a novel player in antigen presentation

Gabriela Sarango, Bénédicte Manoury & Arnaud Moris

To cite this article: Gabriela Sarango, Bénédicte Manoury & Arnaud Moris (2022): TAX1BP1 a novel player in antigen presentation, Autophagy, DOI: [10.1080/15548627.2022.2153570](https://doi.org/10.1080/15548627.2022.2153570)

To link to this article: <https://doi.org/10.1080/15548627.2022.2153570>



Published online: 06 Dec 2022.



Submit your article to this journal [↗](#)



Article views: 103



View related articles [↗](#)



View Crossmark data [↗](#)

## TAX1BP1 a novel player in antigen presentation

Gabriela Sarango<sup>a</sup>, Bénédicte Manoury<sup>b</sup>, and Arnaud Moris <sup>a</sup>

<sup>a</sup>Institute for Integrative Biology of the Cell (I2BC), Université Paris-Saclay, CEA, CNRS, Gif-sur-Yvette, France; <sup>b</sup>Institut Necker Enfants Malades, INSERM U1151-CNRS UMR 8253, Faculté de médecine Necker, Université de Paris, Paris, France

**KEYWORDS** Antigen presentation; autophagy receptors; calnexin; HLA-DM; immunopeptidome; interactome; invariant chain; MHC; T cells; TAX1BP1  
**ARTICLE HISTORY** Received 21 November 2022; Revised 24 November 2022; Accepted 26 November 2022

CD4<sup>+</sup> T lymphocytes play a major role in establishing and maintaining antiviral immunity. They are activated by antigenic peptides derived from extracellular or newly synthesized (endogenous) proteins presented by the MHC-II molecules. Little is known about the mechanisms leading to endogenous MHC-II-restricted antigen presentation. We recently revealed a novel function of the macroautophagy/autophagy receptor (AR), TAX1BP1, in the presentation of endogenous viral antigens to CD4<sup>+</sup> T cells. In this punctum, we will focus on MHC-II-restricted endogenous antigen presentation and the involvement of TAX1BP1 in the biology of MHC-II molecules.

CD4<sup>+</sup> T cells govern the quality of antibody responses and provide help to mount long-lasting cytotoxic CD8<sup>+</sup> T cell responses. However, it is also clear that CD4<sup>+</sup> T cells can exert a direct cytotoxic effect on virus-infected cells and can also infiltrate tumors. It is generally assumed that peptide presented by MHC-II molecules are solely derived from extracellular viral proteins that are captured by phagocytosis or receptor-mediated endocytosis. However, since the eighties, we know that MHC-II molecules can present newly synthesized self- and virus-derived peptides after lysosomal proteolysis. More recently, it was shown that CD4<sup>+</sup> T cell responses to influenza virus are mainly driven by peptides derived from intracellular antigens within antigen presenting cells (APCs). The pathways leading to the loading of MHC-II molecules with endogenous antigens remain poorly characterized. One unresolved issue is how cytosolic antigens are transported into MHC-II-loading compartments (MIIC) that are ill-defined late endo-lysosomal intracellular vesicles.

The pathways of autophagy are obvious candidates that can potentially feed the MIIC with endogenous peptides. The characterization of the MHC-II immunopeptidome, meaning the repertoire of peptides presented by MHC-II molecules, revealed that macroautophagy (herein referred to as autophagy) contributes to the processing of cytoplasmic and nuclear antigens. Using *in vivo* models, several labs established that autophagy participates in the generation of endogenous MHC-II-restricted antigenic peptides and strongly influences thymic selection of auto-reactive CD4<sup>+</sup> T cells. Further evidence that autophagy plays a role in endogenous antigen

presentation comes from *in vitro* studies using APCs transfected with mRNAs or cDNAs encoding tumor or viral antigens targeted to phagophores. However, overall, there are few examples showing endogenous degradation of native tumor or viral antigens to be dependent on autophagy. In fact, autophagy effectors may directly or indirectly affect MHC-II-restricted antigen presentation by regulating, for instance, the delivery of proteases into the MIIC. The molecular links between autophagy and MHC-II-restricted antigen presentation, in particular the mechanisms allowing the delivery of autophagy-degraded antigens to the MIIC, remain poorly defined.

In our recent work [1], we hypothesized that the ARs may contribute at various, so far unknown, levels to MHC II-restricted viral antigen presentation. ARs, in particular CALCOCO2/NDP52, OPTN, SQSTM1/p62, NBR1 and TAX1BP1, target intracellular compounds (e.g., mitochondria, bacteria) or protein aggregates into phagophores, the precursors to autophagosomes, in a process called selective autophagy. In addition, some ARs also regulate signaling pathways and the maturation/trafficking of intracellular vesicles. TAX1BP1, CALCOCO2 and OPTN, for instance, are required for the maturation of autophagosomes whereas TAX1BP1, CALCOCO2, and SQSTM1/p62 orchestrate the maturation of early endosomes into late endosomes.

To study the role of ARs in endogenous presentation, we used siRNA targeting CALCOCO2, OPTN, SQSTM1/p62 and TAX1BP1. Solely silencing TAX1BP1 leads to dramatic reduction of antigen-specific CD4<sup>+</sup> T cell activation. Further highlighting that ARs exert multiple redundant but also exclusive roles. We used a variety of native viral (e.g., HIV-Gag and pp65 proteins from HIV-1 and HCMV, respectively) and model antigens targeted or not to phagophores (HIV-Gag fused to LC3 or LC3<sup>G120A</sup>, respectively) and highlighted that TAX1BP1 affects antigens whose processing is dependent on or independent of autophagy degradation (Figure 1). To get a broader view on the influence of TAX1BP1 on the peptide repertoire bound to MHC-II molecules, we used an MS-based immunopeptidomic approach and showed that TAX1BP1 expression has a major influence on the diversity but also on the affinity of MHC-II ligands. Interestingly, a functional

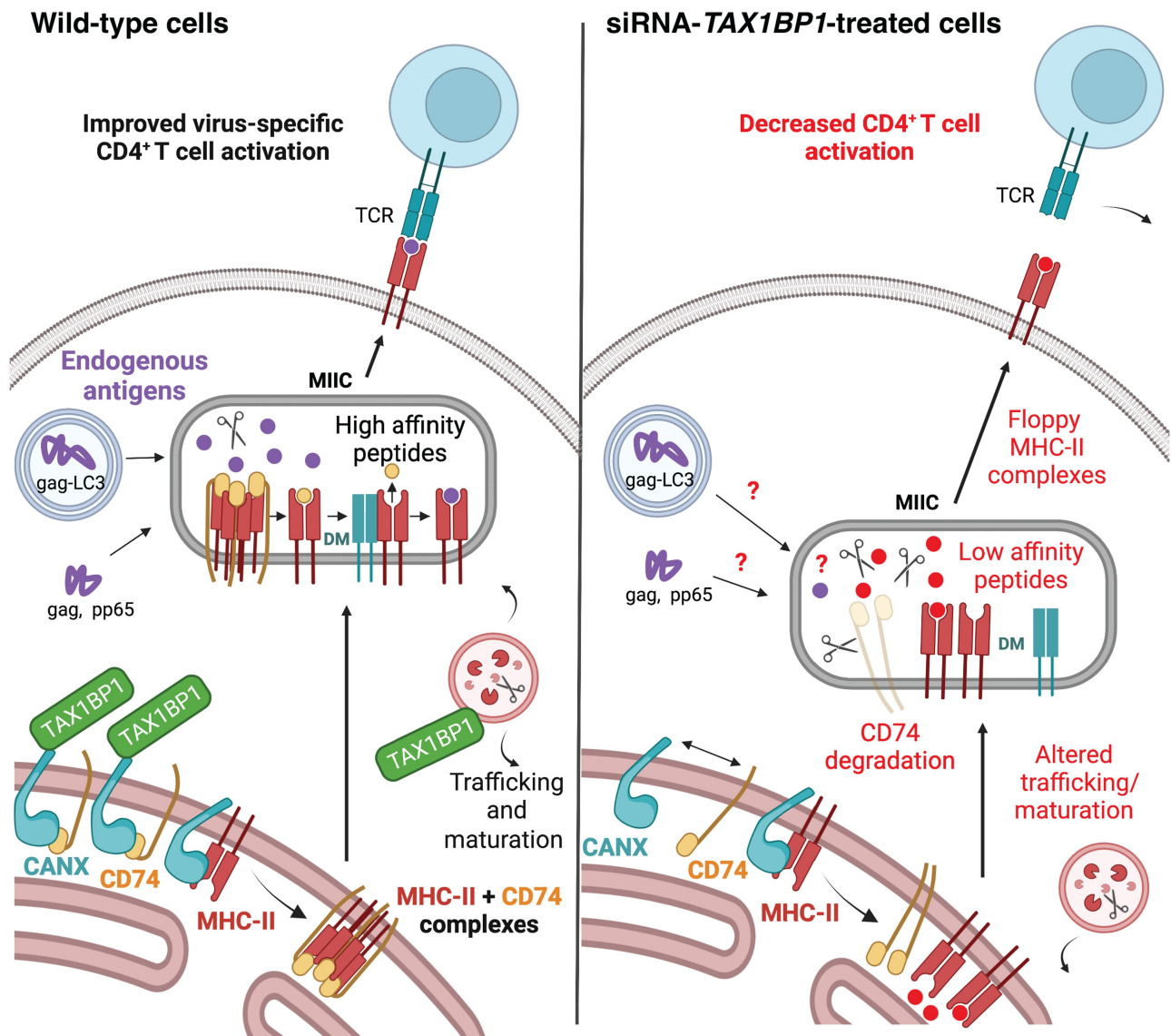


**Figure 1.** The autophagy receptor TAX1BP1 stabilizes the invariant chain (CD74) and regulates MHC-II trafficking, thereby favoring the presentation of high-affinity peptides to virus-specific CD4<sup>+</sup> T cells: 1) TAX1BP1 loss prevents the activation of HIV- and HCMV-specific CD4<sup>+</sup> T cell clones; 2) TAX1BP1 expression affects the quality and the diversity of peptides presented by MHC-II molecules; 3) TAX1BP1 interacts with the cytoplasmic tail of CANX to favor MHC-II molecule chaperoning by the invariant chain (CD74); 4) in the absence of TAX1BP1, CD74 is degraded; 5) CANX silencing replicates TAX1BP1 deficiency by decreasing CD4<sup>+</sup> T cell activation and exacerbating CD74 degradation.

enrichment analysis of the identified peptides did not reveal a major influence of TAX1BP1 silencing on the cellular distribution of the source protein of MHC-II ligands. Overall, these results suggested that the selective targeting of antigens to phagophores by TAX1BP1 is probably not at play.

To decipher the underlying molecular mechanisms, in TAX1BP1-silenced cells, we then analyzed various steps of MHC-II molecule trafficking, loading and functions. We revealed that TAX1BP1-silencing induces an exacerbated degradation of the invariant chain (CD74/Ii), which might at least partially explain the perturbation of the immunopeptidome. CD74 is indeed a major actor in the biology of MHC-II molecules dictating the folding of the  $\alpha\beta$ MHC-heterodimer, their trafficking to late endosomes and the affinity of peptides loaded onto MHC-II molecules (Figure 1). Importantly, the stability of CD74 is itself

regulated by the ER chaperone CANX (calnexin). Consequently, we performed imaging of intracellular vesicles (in particular MHC-II<sup>+</sup> compartments) and we studied the fate of molecules (HLA-DM, CD74/Ii) involved in MHC-II molecule loading and trafficking. We observed that TAX1BP1 silencing influences  $\alpha\beta$ MHC heterodimer stability, the positioning of late endosomes (including MHC<sup>+</sup> HLA-DM<sup>+</sup> vesicles), lysosomes and autophagosomes (Figure 1). Importantly, in an MS-based interactome, we identified CANX as a binding-partner of TAX1BP1. Thereafter, because CANX is also known to bind CD74, we decided to focus on the role of CANX, to provide insights on one of the mechanisms of action of TAX1BP1. We readily demonstrate, that TAX1BP1 interacts with CANX in various APCs and binds its cytosolic tail (Figure 1). Finally, we provide the first direct

demonstration that in human cells CANX-silencing induces CD74 degradation and inhibits MHC-II-restricted antigen presentation, thus replicating the functional consequences of TAX1BP1 silencing.

In summary, we identified TAX1BP1 as a key player in MHC-II-restricted antigen presentation and CD4<sup>+</sup> T cell immunity. Our study opens new avenues for research, both in the functions of ARs in MHC-II biology and in the study of viruses that might target ARs to escape immune recognition by CD4<sup>+</sup> T cells.

### Disclosure statement

No potential conflict of interest was reported by the author(s).

### Funding

This work was supported by Agence Nationale de la Recherche [AutoVirim (ANR-14-CE14-0022)]; Agence Nationale de la Recherche sur le Sida et les Hépatites Virales [ECTZ74132]; Université Paris-Saclay [PhD-salary for GS]; Sidaction [17-1-AEQ-11102-1]

### ORCID

Arnaud Moris  <http://orcid.org/0000-0002-5052-1678>

### Reference

- [1] Sarango G, Richetta C, Pereira M, et al. The autophagy receptor TAX1BP1 (T6BP) improves antigen presentation by MHC-II molecules. *EMBO Rep.* 2022;e55470. DOI:10.15252/embr.202255470.



## **Appendix 2: List of attended congresses**

8ème Colloque Annuel du LabEx LERMIT : short talk

XXIIIème Journées Francophones de Virologie 2021 : short talk

Club Francophone de l'Autophagie (CFATG) édition 2021 : short talk

VI European Congress of Immunology 2021 edition: short talk

Necker Institute retreat 2021: poster

XXIVème Journées Francophones de Virologie 2022 : poster

Keystone Symposia on Positive-Strand RNA viruses 2022: poster

**Résumé :** Les lymphocytes T CD4<sup>+</sup> jouent un rôle majeur dans l'établissement et le maintien de l'immunité antivirale. Ils sont activés par des peptides antigéniques dérivés de pathogènes ou de tumeurs présentés par les molécules du complexe majeur d'histocompatibilité de classe II (CMH-II). Le CMH-II est exprimé par des cellules présentatrices d'antigènes (CPA) professionnelles, telles que les lymphocytes B et les cellules dendritiques, et par des CPA non professionnelles en conditions inflammatoires. Le CMH-II présente des peptides antigéniques dérivés de sources extra- et intracellulaires, correspondant à la présentation exogène et endogène, respectivement. Les antigènes sont ensuite acheminés aux compartiments de chargement du CMH-II (MIIC) où ils sont progressivement dégradés par les protéases endo-lysosomales, telles que les cathepsines, en peptides pouvant être chargés sur les molécules du CMH-II naissantes. Parmi les différentes voies de dégradation des antigènes, l'autophagie contribue au traitement des antigènes cytosoliques et nucléaires. De nombreux virus modulent cette voie d'auto-dégradation en ciblant ses nombreux récepteurs. Dans la première partie de cette étude, nous émettons l'hypothèse que les récepteurs de l'autophagie sélective (RAS) participent à diverses étapes, jusqu'à présent inconnues, de la présentation d'antigènes viraux par le CMH-II. En utilisant des siRNA, nous montrons que NDP52, OPTN et p62 n'affectent pas de manière significative la présentation d'un antigène viral aux lymphocytes T CD4<sup>+</sup>, tandis que TAX1BP1 influence à la fois la présentation d'un antigène viral dépendant et indépendant de l'autophagie par le CMH-II. En analysant l'immunopeptidome des molécules du CMH-II, en présence ou en l'absence de TAX1BP1, nous montrons que TAX1BP1 affecte dramatiquement le répertoire et la qualité des peptides présentés. L'extinction de TAX1BP1 induit une relocalisation périmoléculaire du MIIC, une diminution de la stabilité des complexes CMH-II-peptides et une dégradation rapide de la chaîne invariante I $\alpha$  (CD74), facteur clé du trafic cellulaire des molécules du CMH-II et de leur chargement. Nous avons ensuite déterminé l'interactome de TAX1BP1 et identifié la protéine chaperonne du RE, Calnexine (CANX), comme partenaire de TAX1BP1. Nous démontrons dans différentes CPAs que TAX1BP1 interagit avec CANX via sa queue cytosolique, connue pour réguler les fonctions de CANX dans le RE. De manière importante, nous montrons que l'extinction de CANX entraîne également une dégradation exacerbée de I $\alpha$  et une diminution de l'activation des lymphocytes T CD4<sup>+</sup>. Dans la deuxième partie de cette étude, nous avons utilisé l'oncoprotéine Tax du HTLV-1, connue pour recruter TAX1BP1, OPTN et p62 dans l'activation prolongée de NF- $\kappa$ B induite par le virus. Nous nous demandons si les virus pourraient cibler les RAS pour échapper aux réponses immunitaires antivirales. Nous montrons que l'expression de Tax inhibe la présentation d'un antigène viral par le CMH-II et affecte le répertoire des peptides présentés ainsi que leur abondance relative sans influencer leur affinité prédite aux molécules du CMH-II. Nous observons que Tax induit la relocalisation du MIIC et affecte sa maturation. De plus, nous suggérons que l'expression de Tax modifie l'activité des cathepsines lysosomales sans influencer la dégradation de I $\alpha$ . Après évaluation du rôle des RAS dans l'inhibition de l'activation des lymphocytes T CD4<sup>+</sup> médiée par Tax, nous montrons que l'OPTN est nécessaire pour l'inhibition de la présentation d'antigènes par le CMH-II médiée par Tax. De plus, en utilisant des mutants d'ubiquitination de Tax, nous montrons qu'une ubiquitination spécifique de Tax est nécessaire pour son interaction avec OPTN. Dans l'ensemble, nous caractérisons TAX1BP1 en tant qu'acteur majeur de la présentation d'antigènes par le CMH-II et proposons OPTN comme cible du HTLV-1 pour échapper à la présentation d'antigènes par le CMH-II et à l'activation des cellules T CD4<sup>+</sup>.